



Aalborg Universitet

AALBORG UNIVERSITY
DENMARK

Experimental Investigations of Tension Piles in Sand Subjected to Static and Cyclic Loading

Thomassen, Kristina

DOI (link to publication from Publisher):
[10.5278/vbn.phd.engsci.00056](https://doi.org/10.5278/vbn.phd.engsci.00056)

Publication date:
2016

Document Version
Publisher's PDF, also known as Version of record

[Link to publication from Aalborg University](#)

Citation for published version (APA):
Thomassen, K. (2016). *Experimental Investigations of Tension Piles in Sand Subjected to Static and Cyclic Loading*. Aalborg Universitetsforlag. <https://doi.org/10.5278/vbn.phd.engsci.00056>

General rights

Copyright and moral rights for the publications made accessible in the public portal are retained by the authors and/or other copyright owners and it is a condition of accessing publications that users recognise and abide by the legal requirements associated with these rights.

- Users may download and print one copy of any publication from the public portal for the purpose of private study or research.
- You may not further distribute the material or use it for any profit-making activity or commercial gain
- You may freely distribute the URL identifying the publication in the public portal -

Take down policy

If you believe that this document breaches copyright please contact us at vbn@aub.aau.dk providing details, and we will remove access to the work immediately and investigate your claim.

**EXPERIMENTAL INVESTIGATIONS OF
TENSION PILES IN SAND SUBJECTED
TO STATIC AND CYCLIC LOADING**

**BY
KRISTINA THOMASSEN**

DISSERTATION SUBMITTED 2016



AALBORG UNIVERSITY
DENMARK

Experimental Investigations of Tension Piles in Sand Subjected to Static and Cyclic Loading

PhD Thesis
Kristina Thomassen

Thesis submitted January 2016

Thesis submitted: January 10, 2016

PhD supervisor: Prof. Lars Bo Ibsen
Aalborg University

Assistant PhD supervisor: Assoc. Prof. Lars Vabbersgaard Andersen
Aalborg University

PhD committee: Associate Professor Benjamin Nordahl Nielsen (chair.)
Aalborg University

Technical Director Ole Hededal
COWI A/S

Professor Martin Achmus
Leibniz University Hannover

PhD Series: Faculty of Engineering and Science, Aalborg University

ISSN (online): 2246-1248
ISBN (online): 978-87-7112-467-5

Published by:
Aalborg University Press
Skjernvej 4A, 2nd floor
DK – 9220 Aalborg Ø
Phone: +45 99407140
aauf@forlag.aau.dk
forlag.aau.dk

© Copyright: Kristina Thomassen

Printed in Denmark by Rosendahls, 2016

Preface

The work presented in this PhD thesis is funded by the Danish Advanced Technology Foundation via the program “Cost-effective deep water foundations for large offshore wind turbines”. The financial support is sincerely acknowledged.

I would like to thank Professor Lars Bo Ibsen for the opportunity to write this PhD thesis. Lars Bo Ibsen and Lars Vabbersgaard Andersen have supervised the PhD work. Their guidance and support are greatly appreciated.

A great amount of work was carried out in the laboratory at Aalborg University. So, I would like to express my appreciation to the entire technical staff for discussions and help to overcome the problems related to the test setup and for lightening the mood when nothing seemed to be working. A special thanks to Kim Borup, responsible for the test setup, and to the student workers who took the job of preparing the soil prior to each test.

Last but not least, I would like to express my gratitude to my family for their many hugs and moral support. A special thanks to my mother for giving me a well-intentioned kick in the pants at the right time and to Kasper and Benjamin for taking care of our home in the last few months.

Kristina Thomassen
Aalborg University, January 10, 2016

Curriculum Vitae

Kristina Thomassen



Higher education

June 2010 M.Sc. Civil Engineering, Aalborg University

June 2008 B.Sc. Civil Engineering, Aalborg University

Professional Experience

May 2011 – PhD student at the Department of Civil Engineering, Aalborg University
Dec. 2015

Aug. 2010 – Research Assistant at the Department of Civil Engineering, Aalborg University
Apr. 2011

Teaching Experience

Postgraduate level	Advanced Geotechnical Engineering: Upper and lower bound solutions.
Undergraduate level	Foundation and Earth Pressure: Groundwater flow and groundwater lowering, piled foundations. Supervision of 1 st and 5 th semester student project including foundation methods.

Scientific Publications

Journal papers	<p>Thomassen, K., Ibsen, L.B. and Andersen, L.V. "Laboratory Test Setup for Cyclic Axially Loaded Piles in Sand," Submitted to <i>Geotechnical Testing Journal</i> Apr. 2015, under review.</p> <p>Thomassen, K., Andersen, L.V. and Ibsen, L.B. "Static Tension Tests on Axially Loaded Pile Segments in Sand," Submitted to <i>Journal of Geotechnical and Geoenvironmental Engineering</i> Dec. 2015.</p> <p>Thomassen, K., Andersen, L.V. and Ibsen, L.B. "Axial Cyclic Loading Tests on Pile Segments in Sand," Submitted to <i>Journal of Ocean and Wind Energy</i> Jan. 2016.</p>
Conference papers	<p>Thomassen, K., Andersen, L.V. and Ibsen, L.B., 2012, "Comparison of Design Methods for Axially Loaded Driven Piles in Cohesionless Soil," <i>Proc. 22nd Int. Offshore and Polar Engineering Conf. (ISOPE2012)</i>, International Society of Offshore and Polar Engineers, pp. 705-712.</p> <p>Thomassen, K., Ibsen, L.B. and Andersen, L.V., 2012, "Case Study of CPT-based Design Methods for Axial Capacity of Driven Piles in Sand," <i>Proc. 16th Nordic Geotechnical Meeting (NGM2012)</i>, Vol. 1, Danish Geotechnical Society, pp. 463-470.</p>

Roesen, H.R., Thomassen, K., Ibsen, L.B. and Sørensen, S.P.H., 2011, "Evaluation of Small-Scale Laterally Loaded Monopiles in Sand," *Symp. Proc. 64th Canadian Geotech. Conf. and 14th Pan-American Conf. on Soil Mechanics and Engineering, 5th Pan-American Conf. on Teaching and Learning of Geotech. Eng.*, Canadian Geotechnical Society and the International Society for Soil Mechanics and Geotechnical Engineering.

Thomassen, K., Roesen, H.R., Ibsen, L.B. and Sørensen, S.P.H., 2011, "Small-Scale Testing of Laterally Loaded Monopiles in Sand," *Symp. Proc. 64th Canadian Geotech. Conf. and 14th Pan-American Conf. on Soil Mechanics and Engineering, 5th Pan-American Conf. on Teaching and Learning of Geotech. Eng.*, Canadian Geotechnical Society and the International Society for Soil Mechanics and Geotechnical Engineering.

Technical reports

Vaitkunaite, E., Thomassen, K. and Borup, K., 2015, "Safety Instructions in the AAU Geotechnical Laboratory (Large Yellow Box)," *DCE Technical Report No. 197*, Aalborg University, Department of Civil Engineering.

Thomassen, K., 2015, "Test Procedure for Axially Loaded piles in Sand," *DCE Technical Report No. 196*, Aalborg University, Department of Civil Engineering.

Thomassen, K., 2015, "Test Setup for Axially Loaded piles in Sand," *DCE Technical Report No. 19*, Aalborg University, Department of Civil Engineering.

Christensen, H.R., Thomassen, K. and Kofoed, J.P., 2009, "Guide to Mildsim," *DCE Technical Report No. 73*, Aalborg University, Department of Civil Engineering.

Contract
reports

Thomassen, K. and Ibsen, L.B., 2015, "Test of Gravel to South Leg - Siri Platform," *DCE Contract Report No. 175*, Aalborg University, Department of Civil Engineering.

Ibsen, L.B., Madsen. S., Petersen, L.B., Roesen, H.R., Sørensen, S.P.H. and Thomassen, K., 2010, "SWEEP Project RAT : Geotechnical Analyses Stage 1," *DCE Contract Report No. 106*, Aalborg University, Department of Civil Engineering.

Abstract

For offshore wind turbines, the design criterion regarding tolerated deflection of the wind turbine structure is important in order to maintain the desired energy production. Unwanted permanent deflections of the wind turbine are usually caused by poor design regarding the effect of repeated, cyclic loading occurring from wind and waves. Due to the growing demand on renewable energy, many wind farms are planned for construction in the near future. With limited space for additional onshore and near-shore installations, these wind farms will be located on sites further offshore and with deeper water depths greater than existing wind farms. This implies new requirements for the foundations and support structures.

Previously, the monopile has been the most commonly used type of foundation, but with increased water depths other foundation concepts such as the jacket pile foundation have become popular. The jacket pile foundation is widely used in the offshore oil and gas industry, in which the piles are mainly loaded in compression. However, wind turbines have relatively low self weight compared to the forces from wind and waves which provide great overturning moments. Hence, tension regularly occurs in one or more of the piles within a jacket structure supporting an offshore wind turbine. Over time, repeated cyclic tension in the piles can lead to accumulated displacement upward, resulting in critical permanent tilt of the turbine. The current design methods do not adequately account for the cyclic loading effects on the bearing capacity and the accumulated displacements.

This thesis presents a state-of-the-art review concerning the shaft capacity of piles installed in sand. The review shows the factors influencing the pile shaft capacity and the methods that have been used to find and analyze these factors. The most commonly used methods for evaluating the shaft capacity are small-scale pile load tests. However, the current design methods are based on rather few full-scale pile load tests.

This study presents a new laboratory test setup for conducting pile load tests and analyzing the effect of cyclic loading on the pile shaft capacity and permanent displacements of a pile in tension. The tests were conducted with an open-ended pile segment installed in dense sand. The pile segment had a diameter of 0.5 m and a length of 1 m. The large diameter was chosen in order to reduce the scaling effects on the pile–soil interface behavior. The short length of the pile and application of a surcharge at the sand surface enabled modeling of 1 m pile segments at different stress levels corresponding to different depths within the seabed.

Static tension tests and one-way cyclic tension tests with varying mean load and loading amplitude provided results comparable to the results of previous research found in the literature. The results of the static tests were compared to the predictions of current design methods. Moreover, there is a proposition for a relation between the CPT cone resistance and the unit shaft friction for the test results. The results of the cyclic loading tests showed great consistency with other research. The conclusion was that different variations of the mean load and loading amplitude had different effects on the pile capacity. Low amplitudes can actually increase the capacity while high amplitudes can lead to rapid degradation of the shaft capacity. Hence, the importance of the loading conditions on the pile capacity is evident from the tests, and jacket pile foundations should be designed accordingly.

Resumé

For havvindmøller er designkriteriet for den acceptable hældning af vindmøllekonstruktionen vigtig i forhold til opretholdelse af den ønskede energiproduktion. Uønsket permanent hældning af vindmøllen er ofte en følge af dårligt design i forhold til indflydelsen af gentagen cyklisk belastning fra vind og bølger. På grund af den voksende efterspørgsel på vedvarende energi, planlægges der opførelse af mange nye vindmølleparker i den nærmeste fremtid. Med den begrænsede plads til flere vindmølleparker på land eller i nærkystområder, vil disse nye parker blive opført længere fra kysten på større vanddybder end de eksisterende havvindmølleparker. Dette indebærer nye betingelser for vindmøllernes fundamenter og substrukturer.

Tidligere var monopæle den mest brugte funderingsmetode, men med større vanddybde har andre fundamentstyper som f.eks. pælefunderede jackets vundet indpas. Pælefunderede jacketløsninger er meget brugt i offshore olie- og gasindustrien, hvor pælene som regel er belastede i tryk. Imidlertid har vindmøller en relativt lav egenvægt i forhold til kræfterne fra vind og bølger, som leverer store væltningmomenter. Det vil sige, at der ofte vil opstå træk i en eller flere af pælene i jackets brugt til havvindmøller. Med tiden kan gentagen cyklisk træk i pælene medføre en opadrettet flytning af den enkelte pæl og dermed resultere i en kritisk hældning af vindmøllekonstruktionen. De nuværende dimensioneringsmetoder tager ikke på tilfredsstillende vis højde for den cykliske belastningseffekt på bæreevnen og de akkumulerede flytninger.

Denne afhandling præsenterer en gennemgang af den nyeste forskning omhandlende overflademodstanden af pæle installerede i sand. Gennemgangen angiver de faktorer, der har indflydelse på pælens overflademodstand, og de metoder, der har været brugt til at analysere disse faktorer. De mest brugte metoder til analyse af disse faktorer er pæleforsøg udført i lille målestok. Dog er de nuværende dimensioneringsmetoder baseret på forholdsvis få pæleforsøg i fuld skala.

Dette studie præsenterer en ny forsøgsopstilling i laboratorie til udførelse af pæleforsøg og analyserer effekten af cyklisk belastning på pælebæreevnen og på den permanente flytning af en pæl i træk. Forsøgene blev udført med et segment af en hul pæl med åben ende installeret i sand med en høj lejringstæthed. Pælesegmentet havde en diameter på 0.5 m og en længde på 1 m. Den store diameter blev valgt for at reducere skaleringseffekter på opførslen i berøringsfladen mellem pæl og jord. Den korte pælelængde og påføring af en belastning på sandets overflade gjorde det muligt at analysere 1 m pæl ved forskellige spændingsniveauer svarende til forskellige jorddybder under havbunden.

Statiske trækforsøg og envejscykliske trækforsøg med varierende middellast og lastamplitude producerede resultater, som var sammenlignelige med tidligere forskningsresultater fundet i litteraturen. Resultaterne af de statiske forsøg blev sammenlignet med resultaterne af de nuværende dimensioneringsmetoder. Desuden blev der opstillet en relation mellem CPT spidsmodstanden og overflademodstanden. Resultaterne af de cykliske forsøg viste stor overensstemmelse med anden forskning. Variationen af middellasten og lastamplituden havde forskellige effekter på pælebæreevnen. Små lastamplituder kan faktisk forøge bæreevnen, mens store lastamplituder kan medføre hurtig degradering af bæreevnen. Lastforholdene har altså en stor betydning for pælebæreevnen, og pæle, der bruges til jackets, bør derfor dimensioneres i henhold til dette.

Contents

Preface	iii
Curriculum Vitae	v
Abstract	ix
Resumé	xi
1 Introduction	1
1.1 Prospects of Offshore Wind Energy	1
1.2 Loading Conditions	2
1.3 Foundation Concepts	3
1.4 Design of Jacket Pile Foundation	4
1.5 Motivation and Research Aims	5
1.6 Overview of the Thesis	6
2 State-of-the-Art	7
2.1 Current Design Practice	7
2.2 Factors Influencing Shaft Capacity	8
2.2.1 Stress Conditions and Stress Changes	9
2.3 Methods for Evaluating the Influencing Factors	11
2.3.1 Full-Scale Pile Testing	11
2.3.2 Small-Scale Pile Testing	12
2.3.3 Laboratory Testing	16
2.3.4 Numerical Modeling	17
2.4 Analyses of Influencing Factors	18
2.4.1 Pile installation	18
2.4.2 Pile Ageing	18
2.4.3 Interface Properties	19
2.4.4 Cyclic Loading	21
2.5 Design Methods for Unit Skin Friction	23
2.5.1 API-00	23

2.5.2	NGI-05	24
2.5.3	ICP-05	25
2.5.4	Fugro-05	27
2.5.5	UWA-05	28
2.5.6	Simplified ICP and Offshore UWA	29
2.5.7	Basis for the Terms in the Design Methods	30
2.5.8	Evaluation of the Methods	32
2.6	Total Pile Capacity	34
2.7	Concluding Remarks	36
3	Scope of the Thesis	37
3.1	Main Findings of State-of-the-Art	37
3.2	Aim and Objectives of the Thesis	38
4	Test Setup and Test Procedure for Pile Load Tests	41
4.1	Considerations for the Test Setup and Test Procedure	41
4.1.1	Pile Design	41
4.1.2	Sand Preparation and Pile Installation	42
4.1.3	Vertical Effective Stress	43
4.1.4	Horizontal Effective Stress	44
4.1.5	Stress Changes	46
4.2	Summary of Paper A	47
4.2.1	Main Findings	49
4.3	Recommended Improvements	50
5	Analysis of Pile Load Test Results	53
5.1	Summary Paper B	53
5.1.1	Main Findings	54
5.2	Test Program	54
5.3	Considerations for Interpretation of Static Tests	55
5.4	Summary of Paper C	55
5.4.1	Main Findings	57
5.5	Considerations for Interpretation of Cyclic Test	58
5.6	Summary of Paper D	59
5.6.1	Main findings	59
5.7	Recommendations for Future Research	62
6	Conclusions and Recommendations for Future Research	63
6.1	Conclusions	63
6.2	Recommendations for Future Work	65
6.2.1	Recommendations for the Test Setup	65
6.2.2	Proposed Research	66
	References	67

Contents

A	Static Tension Tests on Axially Loaded Pile Segments in Sand	77
B	Comparison of Design Methods for Axially Loaded Driven Piles in Cohesionless Soil	99
C	Static Tension Tests on Axially Loaded Pile Segments in Sand	119
D	Axial Cyclic Loading Tests on Pile Segments in Sand	143
E	Force Sensors	161
F	Static Test Results	167
G	Cyclic Test Results	191

Chapter 1

Introduction

1.1 Prospects of Offshore Wind Energy

For years researchers have warned about the observed climate changes that are a product of the industrial revolution and the growing emission of greenhouse gasses. In recent years, politicians, especially in the industrialized countries, have had the environmental issues on the agenda when discussing national and international politics. The European Commission has decided on targets for reduction of greenhouse gas emissions, for share of renewable energy of the energy consumption, and for improvements in energy efficiency for the membership countries (European Commission 2010, 2014). Compared to 1990, the greenhouse gas emission should be reduced by 20 % in 2020 and 40 % in 2030 while the energy efficiency should be improved by 20 % in 2020 and 25 % in 2030. As for the share of renewable energy it should be 20 % of the energy consumption by 2020 and 27 % in 2030.

Wind energy is one of the renewable energy industries which has experienced a massive growth over the last 30 years. At the end of 2014, the installed wind power capacity could produce enough energy to cover 10.2 % of the energy consumption in the EU corresponding to 128.8 GW installed wind power capacity. Of this capacity, onshore installations account for approximately 120.6 GW and offshore installations accounts for 8 GW (EWEA 2015). The European Wind Energy Association (EWEA) has a 2020 target of 40 GW offshore wind power capacity which seems realistic as offshore wind energy projects of 100 GW in total were already proposed by 2009 (EWEA 2009).

The offshore energy potential is enormous. The offshore wind conditions are better compared to the onshore wind conditions and it is possible to build very large wind turbines. However, some of the challenges of building

offshore wind farms are the cost of the soil investigations, installation and maintenance; these are much more challenging than onshore especially because of the weather conditions. These challenges negatively affect the price of a kWh from offshore wind energy. The Danish part of the North Sea is one of the most cost-effective areas of the North Sea to install wind turbines due to the wind and subsoil conditions (Vindmølleindustrien 2015). Nevertheless, it is necessary to reduce the costs of the different steps involved in installation and maintenance of an offshore wind farm in order to make the industry sustainable. In this process, it is also necessary to bring down the cost of the wind turbine structure and substructure itself. A large part of this budget originates from the cost of the wind turbine foundations, and thus it is of interest reducing its costs.

1.2 Loading Conditions

An offshore wind turbine is subject to environmental loads from wind, waves, and currents. Moreover, it is affected by the loads from the structure. The actual load conditions for the wind turbines are a combination of these loads and the interaction that these loads induce. The loads can be divided in four categories: Quasi-static, cyclic, stochastic, and transient (Böker 2009)

The North Sea does not freeze according to Sørensen & Sørensen (2011) and, therefore, the above-mentioned four categories of loads include the following: The quasi-static loads include the self-weight of the structure, the mean wind, and currents. The cyclic loading emerges from the rotational speed of the blades, mass imbalance, blades passing the wind turbine tower, and regular waves. The stochastic loads emerge from wind turbulence and irregular sea states. The transient loads come from the turbine start and stop, gusts, and breaking waves.

In the design phase, the target value for the natural frequency of an offshore wind turbine is usually chosen in the range between $1P$ and $3P$ (Figure 1.1). $1P$ defines the rotor rate that is in the range 0.17-0.33 Hz. $3P$ defines the frequency at which the blades pass the wind turbine tower. For a large, modern, three-bladed wind turbine, this frequency is in the range 0.5-1 Hz. This provides a so-called “soft-stiff” structure which sets criteria for the stiffness of the foundation. The energy rich wind turbulence frequencies lie below 0.1 Hz, and the turbulent wind field is normally modeled using the von-Karman or the Kaimal spectrum. The energy rich waves normally lie in the range 0.05-0.5 Hz while the extreme waves occur in the range 0.07-0.14 Hz. The wave field in the North Sea is determined by the JONSWAP (Joint European North Sea Wave Project) spectrum.

1.3. Foundation Concepts

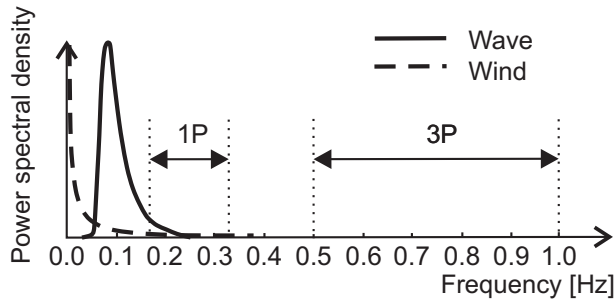


Figure 1.1: Excitation ranges for an offshore wind turbine (LeBlanc 2009).

The very low self-weight of the wind turbine structure compared to the wind and wave induced loads results in a very high moment load at the seabed level. Therefore, the offshore wind turbine foundation must be designed according to this load condition. The commonly used foundation concepts are briefly described in the following section.

1.3 Foundation Concepts

Two general types of substructure concepts for offshore wind turbines are mono-foundations and poly-foundations. A mono-foundation consists of a single foundation element while the multi-foundation consists of more foundation elements, typically three or four.

Monopiles and monobuckets are mono-foundations. Classical gravity-based foundations belong to this class as well and transfer horizontal loads and overturning moment to the ground by contact pressure and friction at the base of the foundation. A monopile foundation is the most widely used foundation concept, and here the loads are transferred to the ground by lateral soil pressure along the pile shaft; this requires large diameter piles (up to 8 m or more for so-called XL monopiles). These foundation concepts are limited to relatively low water depths due to the large overturning moment. A relatively new concept of mono-foundations is the monobucket where the loads are transferred both by contact pressure between the seabed and the bucket lid and by lateral soil pressure along the bucket shaft.

For water depths above 30 m, it is preferred to use poly-foundations such as tripods and lattice structures fixed to the subsoil by open-ended steel pipe piles or buckets. The piles or buckets for these foundation types are mainly loaded axially in tension or compression, and the load is transferred to the

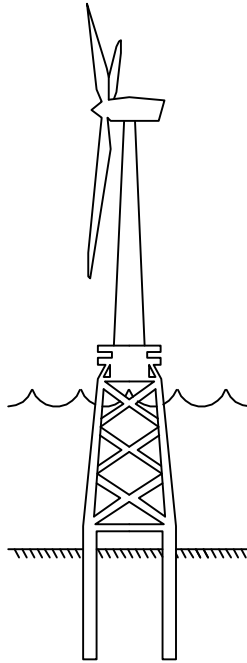


Figure 1.2: Offshore wind turbine on jacket pile foundation.

ground primarily by skin friction and base resistance.

Because of the growing demand on offshore wind turbines, construction sites at deeper waters than 30 m are adopted. This means that the most popular foundation concept, the monopile, is no longer applicable and other foundation concepts must be used. One of the used concepts is lattice structure fixed to the subsoil by three or four piles called the jacket pile foundation (cf. Figure 1.2). The current study is motivated by observation regarding this specific foundation concept as described later in this introduction. Thus, the following section about foundation design is limited to jacket pile foundations.

1.4 Design of Jacket Pile Foundation

The offshore standard DNV (2010) gives the following guidelines for design of offshore jacket pile foundations. First of all, the limit states to be considered are the following:

- Ultimate limits state (ULS) regarding the ultimate load carrying resistance and failure due to cyclic loading.

1.5. Motivation and Research Aims

- Serviceability limit state (SLS) regarding tolerance criteria applicable to normal use (e.g. deflections of the foundation).

For jacket pile foundations the two cases to be considered in ULS are axial loading and combined lateral and moment loading. The capacity of each pile must be verified for these two cases when the structure is subjected to extreme load conditions. This verification can be based on a combined analysis of the substructure and the foundation piles. Usually the Winkler model approach is used for pile design. In this approach the pile is modeled as a beam element on an elastic foundation. The pile–soil interaction is modeled as a series of uncoupled springs. The stiffness of these springs is governed by p - y , t - z and Q - z curves. The p - y curves define the lateral soil response; the t - z curves define the axial soil response along the pile shaft and Q - z the axial soil response at the pile base.

The design in SLS must ensure that the deflection tolerances given in the design basis for the wind turbine structure are not exceeded. The load conditions considered for this limit state must be chosen as the conditions which will cause permanent deformations of the soil and, thus, result in displacements of the foundation piles, possibly resulting in a permanent tilt of the support structure. In this aspect it is necessary to account for the cumulative deformations of the soil due to cyclic loading. For axially loaded piles, the deflection is usually determined using the t - z and Q - z curve methods. The cumulative displacement of the piles depends on the mean load and especially on the cyclic loading amplitude.

1.5 Motivation and Research Aims

The oil and gas industry has successfully used lattice structures with piles as foundation method for offshore platforms for a long period of time. The platforms are heavy structures, and the foundation piles are most commonly loaded in compression. This load condition is widely analyzed in the literature and the design methods are well documented. However, when this foundation concept is applied for offshore wind turbines—very light structures—the piles are sometimes mainly loaded in tension because of the large overturning moment. An observed but not documented effect of tension piles in dense to very dense sand at locations in the North Sea is that they move upwards because of cyclic loading effects. That this phenomenon is observed must mean that the design methods for piles in tension are not documented well enough and that the effect of cyclic loading does not reflect correctly in the design codes.

The literature shows that quite a lot of research has been conducted in the field of axially loaded piles to give a better understanding of the mechanisms during loading. This research includes both physical modeling—such as full-scale and small-scale pile load tests—and numerical modeling. However, the findings are not yet validated to a state where it is adopted in the design codes. As such, further research within the subject is still needed.

The aim of the research presented in this thesis was first of all to design a laboratory test setup where the scaling effects caused by the ratio between the pile diameter and the grain size are reduced and the soil–pile interface is comparable to full-scale tests. Static tension tests were conducted with this new laboratory setup to state the validity of the test setup by showing that it could produce repeatable and reliable test results. The results of the static tests also formed the basis for the load conditions applied in the cyclic loading tests. The effect of one-way cyclic loading on the pile capacity and accumulated displacements was analyzed.

1.6 Overview of the Thesis

Following this introduction, the thesis consists of the following chapters:

- **Chapter 2** presents a state-of-the-art review of topics related to the capacity of axially loaded piles used in offshore foundation concepts.
- **Chapter 3** contains the scope of the thesis, starting with a short summary of the state-of-the-art review leading to the methods for conducting laboratory tests and analyzing the results used in this thesis.
- **Chapter 4** describes the background for the choices made when constructing the test setup, a summary of the journal paper introducing the test setup, and the pros and cons for the test setup as well as things that could have been done to improve the test setup and thus the test results
- **Chapter 5** includes summaries of papers concerning the design methods for determining the pile shaft capacity, analyzes of static loading tests, and analyzes of cyclic loading tests. Moreover, the chapter presents some considerations for the analyzes as well as recommendations for future work.
- **Chapter 6** provides the overall conclusions of the research project and recommendations for future work.

Chapter 2

State-of-the-Art

As stated in the introduction, this research project concerns tension piles in dense sand subjected to static and cyclic loading. Therefore, this state-of-the-art only treats research done about the shaft capacity of axially loaded piles in sand. This chapter presents the current design practice for offshore axially loaded piles. The following sections introduce the factors influencing the pile shaft capacity, the methods for analyzing these factors as well as the current design methods for finding the unit skin friction.

2.1 Current Design Practice

DNV (2010) and API (2011) provide guidelines for the design of offshore foundations including design of axially loaded piles. Figure 2.1 shows a schematic overview of the design flow for axially loaded piles subjected to cyclic loading as recommended by the design codes. Load and in-situ soil conditions are found for the specific site, and preliminary choice of the pile characteristics is made based on these conditions. In-situ tests, laboratory testing and experimental data from model and field tests constitute the effect of cyclic loading on the soil and soil–pile interface properties. The most commonly used approach for analyzing the pile shaft capacity and accumulated displacements is the Winkler model approach in which the pile is modeled as a beam and the pile–soil interaction is modeled as uncoupled springs governed by t - z curves. The t - z curves are dependent on the unit skin friction which is influenced by the factors described in Section 2.2.

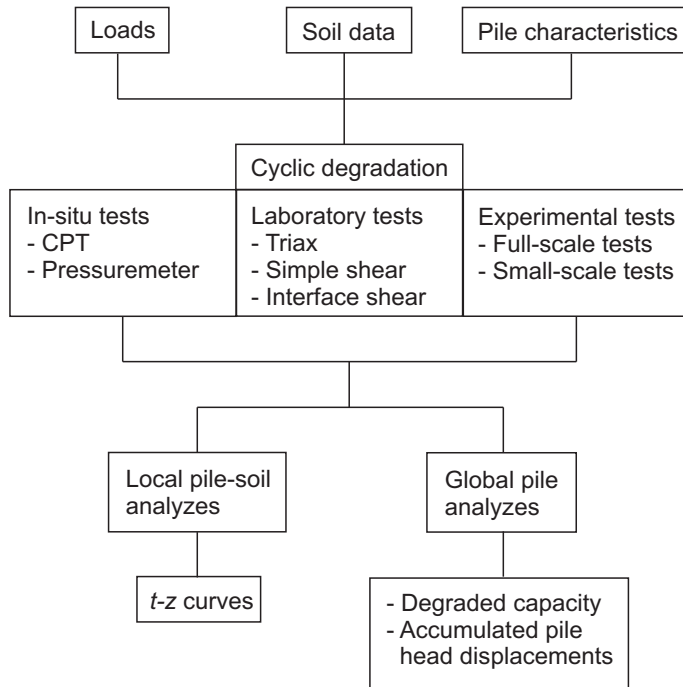


Figure 2.1: Flow chart for design of axially loaded piles used in offshore foundations.

2.2 Factors Influencing Shaft Capacity

The capacity and the accumulated displacement of axially loaded piles depend on the in-situ soil conditions, pile design, and stress changes due to installation, time after installation, and load history.

The in-situ soil conditions:

- Soil type (sand, clay, silt, etc.)
- Relative density
- Deformation properties
- Grain distribution and grain shape

Pile design:

- Geometry (pipe piles, open- or closed-ended, length, diameter, wall thickness)
- Interface properties between pile and soil

Stress conditions and stress changes:

2.2. Factors Influencing Shaft Capacity

- In-situ stresses
- Stress changes due to installation (friction fatigue, pore pressure build up, dilation or contraction in the pile soil interface)
- Time after installation (ageing, equalization)
- Loading

Load conditions:

- Types of loads (quasi-static, cyclic (mean load, amplitude, frequency, and number of repetitions), stochastic, and transient)
- Magnitude, duration, direction and combination of loads

2.2.1 Stress Conditions and Stress Changes

Figure 2.2 shows the life cycle of a driven pile in sand, and the stress changes during this life cycle is shortly described in the following (Randolph & Gourvenec 2011). The shaft friction is governed by Coulomb's law; thus, the unit skin friction, f_s , can be determined from the radial stress at failure, σ'_{rf} , and the interface friction angle, δ .

Stress Changes During Installation

During installation of the pile, the soil at the pile tip experiences a radial displacement in order to make room for the pile. This results in an increase of the radial effective stress at the pile tip. The magnitude of this stress increase is dependent in the design of the pile tip: Open- or closed-ended or plugging of the open-ended pile during installation. The penetration resistance and, thus, the radial stress increase of a closed-ended pile is of course higher than for an open-ended pile. Full plugging of an open-ended pile seldom happens during installation because of inertia of the soil plug. A partially plugged pile results in radial stress increases between the two extremes.

The hammer blows during pile driving causes shearing back and forth in the pile soil interface resulting in contraction of the sand. This means a reduction of the horizontal stresses and, thereby, also of the unit shaft friction along the pile shaft. The stress reduction at a certain depth increases as the distance, h , to the pile tip increases. This effect is called friction fatigue.

Stress Changes After Installation

If the pile is not loaded right after installation, the radial stresses increase. The phenomenon—called set-up—is not well examined for piles in sand, but it is believed to be caused by two different effects: Dissipation of excess pore water pressure emerging from pile driving and ageing. The capacity increase

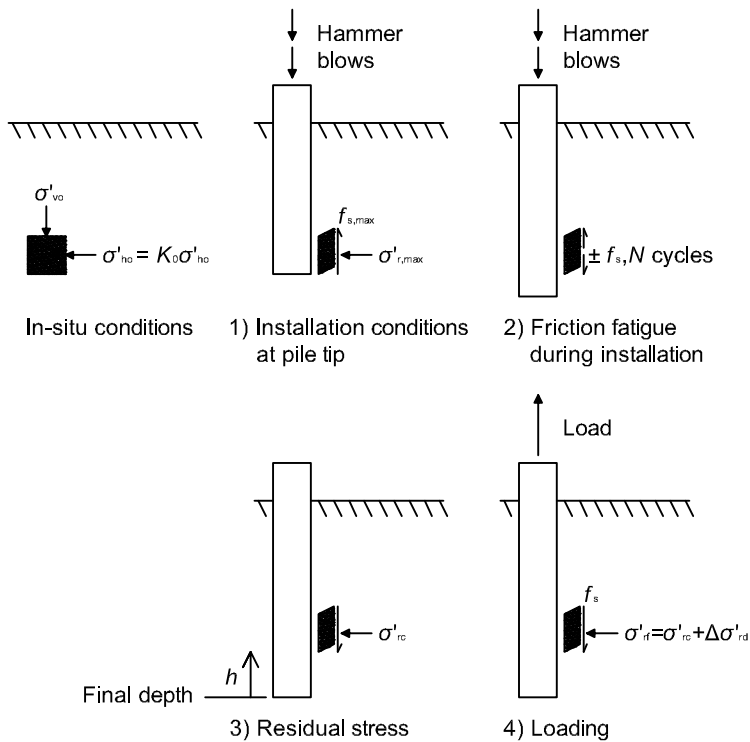


Figure 2.2: Stress changes for a driven pile in sand, after Randolph & Gourvenec (2011).

due to ageing depends on changes in the soil skeleton characteristics, changes in the stress regime surrounding the pile, and changes of the pile–soil interaction (Augstenesen 2006).

Stress Changes During Loading

During loading, the radial stress, σ'_r , slightly changes because of Poisson's ratio for the pile and the dilation of the soil close to the pile. Because of the Poisson effect, the pile expands towards the adjacent soil under compression loading leading to an increase of σ'_r . Under tension loading, the pile contracts away from the adjacent soil leading to a decrease in σ'_r (Jardine et al. 2005). Due to the relative roughness of the pile–soil interface, dilation happens during loading leading to an increase of the radial effective stress, $\Delta\sigma'_{rd}$. The dilation effect is dependent on the sand grain size and shape, the roughness of the pile surface and on the pile diameter. Open-ended piles usually fail plugged even though the installation was unplugged. This is because the internal unit skin friction due to arching at the pile tip is much higher than the external unit shaft friction.

2.3 Methods for Evaluating the Influencing Factors

Experimental data from full- and small-scale pile tests as well as laboratory tests and numerical models are used for assessment of the factors influencing the shaft resistance. This section presents different types of these tests and their advantages and limitations.

2.3.1 Full-Scale Pile Testing

Full-scale pile testing may seem to be the optimal way of testing pile capacity and accumulated displacements. The results are not influenced by any scaling effects and the soil conditions are realistic. However, there are some drawbacks of full-scale testing. Firstly, the cost of conducting such tests is very high. This has resulted in a scarcity of full-scale testing (especially for offshore conditions). Thus, all possible types of soil conditions and pile designs are of course not explored to the full extent. That means that the results of specific conditions are few and very site specific and that the analyses of the test results must be extrapolated to conditions outside the databases. Secondly, most of the full-scale testing conducted so far suffers from the lack of instrumentation making it impossible to separate the shaft resistance and the base resistance for piles in compression or cyclic loading. Thirdly, the tests are limited to the given soil profile at the test site which is seldom homogeneous with depth.

At the test site in Dunkerque, France, Chow (1997) conducted field tests with the Imperial College Pile (ICP) which is a closed-ended steel pipe pile instrumented to measure pore pressures, radial total stresses, local shear stresses, and temperatures at the pile shaft. The piles were 102 mm in diameter and were installed by jacking to embedded depths between 6 and 20 m. The soil conditions were shelly medium-sized, marine sand with relative densities varying from dense to very dense. At the same test site in Dunkerque, Jardine & Standing (2000) conducted tests on open-ended full-scale piles with a diameter of 456 mm. Two piles were 19 m long and six piles were 10 m long. Jardine & Standing (2012) report cyclic loading tests on the same piles. Lehane et al. (1993) conducted static field tests with the ICP installed by jacking at Labenne, France. The sand at Labenne was medium-sized dune sand varying from loose to medium dense (Lehane et al. 1993).

Baeßler et al. (2013) report the establishment of a test site near Berlin, Germany, for testing full-scale piles subjected to static and cyclic loading. Ten tubular piles with a diameter of 0.711 m and embedded lengths of 17.7 m are installed by driving at a site mainly consisting of different sand layers.

2.3.2 Small-Scale Pile Testing

Small-scale pile testing has the advantages of being cheaper to conduct than full-scale testing, enables analyses of the different influencing factors separately, and has the possibility of instrumenting both pile specimen and the surrounding soil to detect the stress changes in the interface and in the soil during loading. The disadvantages of small-scale testing are scaling effects and the challenge of modeling free field stress conditions is a challenging task in small-scale modeling as testing at low stress levels does not provide realistic results. In addition to these things, the boundary conditions will influence the results in most laboratory test setups. Calibration chambers are the most widely used laboratory test setup for small-scale pile testing even though centrifuge tests are also conducted.

Different types of calibration chambers have been used to investigate the behavior of axially loaded piles. The Grenoble 3SR Laboratory Calibration Chamber is a calibration chamber with a height of 1.5 m and a diameter of 1.2 m. The vertical chamber walls are either rigid, lined with a latex membrane to reduce the friction between soil and wall, or three neoprene membranes that can be individually induced with pressure are placed along the chamber walls. Pressurized neoprene membranes are also used to apply vertical surcharge loads at the soil surface. Rimoy (2013), Silva et al. (2013), Tsuha et al. (2012), Jardine et al. (2009), Zhu et al. (2009) used this calibration chamber to test the effects of static and cyclic loading on the shaft and base resistance as well as to investigate the soil stresses during loading. The pile specimen was a closed-ended, stainless steel pile with a diameter of $D = 36$ mm and length of $L = 980$ mm. The sand used in the tests was air-pluviated into the chamber to obtain the wanted relative densities.

Chan & Hanna (1980) used a calibration chamber with rigid vertical boundaries where the wall friction was reduced by grease. The bottom boundary was rigid as well while surcharge was applied at the top surface. The pile specimen was a close-ended aluminum pile with $D = 19$ mm and $L = 570$ mm. The tests were conducted in medium dense, dry sand.

Another type of calibration chambers are, in general, designed as a triaxial apparatus in the way of introducing vertical and horizontal stresses to the soil element. Le Kouby et al. (2004) used this type of calibration chamber with a height of 700 mm and diameter of 520 mm to conduct tests in dry sand on a metallic, closed-ended pile specimen with $D = 20$ mm and $L = 500$ mm. Thomas & Kempfert (2011) used a calibration chamber with a height in the range of 80-100 mm and a diameter of 50 mm. The steel pile specimen was lead through the soil element with the tip into a cavity to analyze the skin

2.3. Methods for Evaluating the Influencing Factors

friction only. The tests were conducted in both dry and wet sands.

De Nicola & Randolph (1999) conducted centrifuge tests to analyze the installation processes and effect of static compression and tension loading on open- and closed-ended piles in dry sand. The applied acceleration level was 100 g allowing a scaling of 1/100 of pile length and diameter of a prototype. The pile specimen was made of aluminum but coated with epoxy to protect the seven axial strain gauges placed on the outside pile wall. The pile diameter was 18 mm, the embedded length was in the range 50-180 mm and the pile wall thickness was 0.55 mm. Both open- and closed-ended piles were tested. The relative density of the fine grained silica sand was in the range 70-100 %. Christenson & Scott (1993) conducted centrifuge tests in dry and wet sands on closed-ended piles with a diameter of 13 mm and embedded lengths of 552 and 594 mm. The piles were installed in a centrifuge chamber with a diameter of 152 mm and depth of 617 mm and loaded in tension and compression. Li et al. (2012) conducted cyclic loading tests on piles in sand in a centrifuge at 50 g. The closed-ended pile had a diameter of 10 mm and an embedded length of 180 mm. The diameter of the chamber was 850 mm and the depth was 400 mm. The pile was jacked into sand with a relative density of 83 %.

Scaling Effects

A surcharge can be applied to the soil sample in a calibration chamber. However, the calibration chamber only models a specific soil depth instead of the gradual increase in stresses which is present along the pile shaft in full-scale tests. Another scaling problem is the difference in pile-soil interface properties between small- and full-scale testing. This difference shows in the increased dilation effects for small-scale tests assumed given by $4G\Delta r/D$ (Jardine et al. 2005). G is the soil shear modulus and Δr the radial displacement in the interface dependent on the pile surface roughness. The formulation shows that decreasing the pile diameter without decreasing the pile surface roughness leads to a high contribution of dilation to the radial stresses compared to full-scale testing. This effect is often seen reduced in small-scale tests by choosing a pile specimen with a smooth surface, but attention must be paid to this when deciding on a test setup and dilation effects must be taken into account when analyzing model test results.

The advantage of centrifuge testing is that the effective stress increase with depth is modeled almost correctly (Leth et al. 2008). This means correct scaling of the pile length and diameter. For installation and load studies of axially loaded piles, this also results in correct replication of the shaft response and the soil plug stresses during driving (De Nicola & Randolph 1999). In

Table 2.1: Possible boundary conditions for laboratory tests in calibration chambers.

Boundary conditions	Horizontal	Vertical
BC1	$\sigma_h = \text{constant}$	$\sigma_v = \text{constant}$
BC2	$\epsilon_h = 0$	$\epsilon_v = 0$
BC3	$\sigma_h = \text{constant}$	$\epsilon_v = 0$
BC4	$\epsilon_h = 0$	$\sigma_v = \text{constant}$
BC5 (free-field simulator)	Constant lateral stiffness	$\sigma_v = \text{constant}$

principle, the grain size should be scaled as well; however, by choosing finer grained sand the material properties will change and not provide the wanted test results. Thus, the original material is often used and the influence of the grain size must be taken into consideration when analyzing the test results. When conducting tests that involve water in the sand, it is necessary to change the flow properties of the soil. As the grain size and hydraulic conductivity remain the same, a fluid with increased viscosity must be used.

Effects of Boundary Conditions

The boundary conditions are important to consider when analyzing results from laboratory tests in both calibration chambers and centrifuges. Both the horizontal and vertical boundary conditions have an impact on the test results. Table 2.1 shows the possible boundary conditions for laboratory tests in pressure chambers.

The mentioned boundary conditions have been used in various laboratory tests on piles subjected to cyclic loading. Le Kouby et al. (2004) used BC1, Silva et al. (2013) employed BC4, and Rimoy (2013) conducted tests with both BC3 and BC5. Only Rimoy (2013) discussed the effect of the boundary conditions on results of two-way cyclic loading tests in calibration chamber with BC3 and BC5 boundary conditions. During the tests, radial, vertical and hoop stresses were measured within $2 < R_{\text{chamber}}/R_{\text{pile}} < 8$ range of the pile. The sensors all showed stress reductions which were slightly higher for tests with BC3 than BC5. The stress degradation was higher in the early stages of cycling than after 100s or 1000s of cycles.

The impact of the vertical boundary conditions on penetration resistance is discussed for several penetration tests conducted in pressure chambers. Salgado et al. (1998) studied the chamber size effects on penetration resistance in sand and reported that BC1 and BC4 generate almost the same values of penetration resistance, which are lower than results found for free-field conditions. The lower penetration resistance emerges from the fact that the stress at the vertical boundary is constant during the tests. At the same time, the stress is applied by means of a membrane allowing the soil to yield at the

2.3. Methods for Evaluating the Influencing Factors

boundary. Because the stress at the membrane is held constant, a reduction in confining pressure takes place and results in decrease of the penetration resistance compared to free-field conditions. The BC2 and BC3 ideally have no strain at the lateral boundary, but in reality this is seldom the case. Many pressure chambers have flexible walls which are almost impossible to make perfectly rigid meaning that small straining can take place. Salgado et al. (1998) report that BC2 and BC3 generate almost the same penetration resistance which is overestimated compared to free-field results. To make room for the pile, a contraction of the elastic zone and maybe crushing of the grains around the pile to a much greater extent than in the free field will take place because of the rigid boundaries. Salgado et al. (1998) recommend BC1 and BC4 rather than BC2 and BC3 conditions to be adopted in laboratory testing because the chamber size effects are better known and can be accounted for. The boundary effects depend on the compressibility of the sand, i.e. its mineralogy, granulometry and grain shape (Schmertmann 1978, Robertson & Campanella 1983, Lunne et al. 1997).

Various researchers have tried to overcome the problems of the underestimation of the penetration resistance found for BC1 and BC4 conditions by controlling the stress at the vertical boundary during a test. Foray (1991) and Ghionna & Jamiolkowski (1991) made calibration chambers in which the stress could be adjusted during the test to simulate field conditions. However, the stress was still the same over the entire vertical boundary as only one membrane was used. Huang & Hsu (2005) built a calibration chamber where the lateral boundary consisted of several membrane rings, where each of the rings could be brought to an individual stress value, making it possible to vary the lateral stress in the chamber with depth. This free-field simulation is referred to as BC5.

Schnaid & Houlsby (1991) state that the horizontal stress conditions have more influence on the penetration resistance than the vertical stress conditions. The distribution of the applied vertical stress depends on arching which again depends on the following parameters: 1) Value of applied overburden pressure, 2) chamber dimensions, 3) roughness of the chamber walls, 4) soil void ratio, 5) soil type, and 6) over-consolidation ratio (Al Douri et al. 1993). Al Douri et al. (1993) investigated the effect of first three parameters on both silica and calcareous sands. Different overburden pressures were applied to soil in three different sized pressure chambers in which the wall roughness was varied from rough to smooth wall. The vertical stress at the bottom of the pressure chamber reduced when the roughness of the wall increased. The same tendencies were observed when reducing the D/L ratios of the chamber.

Effects of Saturation

Most small-scale tests on piles in sand are conducted in dry sand under the assumption that excess pore pressure would not develop in saturated clean sand. However, tests in soils with lower permeability may be strongly affected by pore pressure development (Tsuha et al. 2012).

Thomas & Kempfert (2011) conducted undrained one- and two-way cyclic loading tests on piles in sand and measured pore pressure development near the pile. The excess pore pressure had a negative effect on the pile capacity. No comments were given on whether the results would have been different had the tests been undrained.

Bellotti et al. (1988) conducted penetration tests in a calibration chamber on dry Ticino sand and on sand saturated by three different methods involving CO₂ and vacuum. The sleeve friction was much lower in the saturated sand than in the dry sand, while the cone resistance was only 10-15 % lower in the saturated than in the dry sand. Bellotti et al. (1988) did not give an explanation for the observation. Christenson & Scott (1993) observed similar results in centrifuge tests of axial static tension and compression loaded piles where the total capacity of the piles were reduced when conducting the tests in saturated sand compared to tests conducted in dry sand.

Coyle & Sulaiman (1967) analyzed the effect of saturation on the shaft resistance of a pile specimen installed in poorly graded silty sand. Drained as well as undrained tests showed increases of the shaft resistance compared to tests in a dry sand sample. The undrained test showed the highest shaft resistance; however, it decreased after a peak at a small displacement while, for the drained test, the shaft resistance continued to increase and eventually reach the same value as the undrained test. Coyle & Sulaiman (1967) suggested that water flow away from the pile in the drained tests led to the increase while water flow towards the pile-soil interface in the undrained tests resulted in decrease of the shaft resistance.

2.3.3 Laboratory Testing

Besides small-scale pile testing, other types of laboratory testing such as direct shear tests are used to examine for example the pile-soil interface properties. Usually, direct shear tests are conducted with constant normal load (CNL) or constant volume (CV), but constant normal stiffness (CNS) interface shear tests have been considered appropriate to model the constrained interface dilation. The constant normal stiffness was assumed to be $K = \Delta\sigma'_{rd}/\Delta r = 4G/D = 2G/R$ (Johnston et al. 1987, Lehane et al. 1993,

2.3. Methods for Evaluating the Influencing Factors

Jardine et al. 2005). However, as G varies with the relative density, the shear strain and the stress level, the stiffness is not constant. Thus, the true pile-soil interface behavior lies somewhere between the behavior of CNL and CNS shear tests.

Interface ring shear tests introduce the possibility of modeling the effect of shearing over a long distances. Thus, installation effects of the interface can be analyzed (Ho et al. 2011, Jardine et al. 2005). Effects of both static and cyclic displacements can be modeled with the direct shear tests and the ring shear tests.

2.3.4 Numerical Modeling

Physical modeling is restrained in the way that it is not possible to analyze all types of load conditions, soil conditions and pile characteristics. However, the results of physical models give good insight into the influencing parameters of a given problem. These results can be used to propose constitutive models to be used in various numerical models. Numerical modeling gives the possibility of calibration to tests of a physical model and then extrapolating to other conditions for the load, soil, and pile and, thereby, analyze the effect of these changes. However, numerical models for determination of cyclic capacity of axially loaded piles are still scarce.

Abdel-Rahman & Achmus (2011) and Abdel-Rahman et al. (2014) made finite element models in ABAQUS of a full-scale pile subjected to cyclic loading to find the number of cycles to failure and the accumulated displacements to derive interaction diagrams for different soil conditions, pile characteristics, and load conditions. The models were based on a simple expression for the interface volume contraction found from cyclic simple shear tests on sand conducted by Silver & Seed (1971). Loria et al. (2015) used results of a static centrifuge pile test to validate a finite element model. The pile was considered elastic while the pile-soil interface was modeled elasto-plastic based on the Mohr-Coulomb criterion. The finite element model showed good agreement to the centrifuge test results. However, it was noted that the choice of the interface parameters was very important for the output; especially the interface friction and dilation angles had a great impact on the results.

Prai-ai (2013) modeled the interface direct tests in a 2D plain strain model in Plaxis2D using the embedded Mohr-Coulomb criterion to model the interface behavior. For dense sand, the numerical models of monotonic CNL tests did not include the softening behavior seen in the laboratory tests; however, for loose sand the numerical model provided results close to the laboratory results. For modeling monotonic CNS, more advanced material models should

be used. Peng et al. (2014) modeled the dilatant behavior of a pile-soil interface with a distinct element model of a shear box to investigate the parameters controlling shaft resistance. The analysis was conducted as CNS, CNL, and constant volume (CV) tests. The influence of the initial normal stress, the void ratio, the normal stiffness, and the loading-unloading history was investigated. The size and shape of the soil particles was not modeled.

2.4 Analyses of Influencing Factors

2.4.1 Pile installation

The radial effective stress during installation decreases as the distance of a given soil horizon to the pile tip, h , increases. White & Lehane (2004) suggest that the degradation depends on the installation method, pile shape and sand properties. Jardine et al. (2005) consider the interaction causes to depend on three things: 1) Pile installation induces extreme stresses at the pile tip which decreases with distance to the pile tip, 2) the effect of cyclic installation loading accumulates, and 3) circumferential arching develops above the pile tip. However, the reduction reaches a quasi-constant limit at a so-called critical depth. Lehane et al. (1993) analyzed pile tests and found that the radial effective stress reduced with h/R . For open-ended piles the decay of the radial effective stress was more rapid and the factor R^* was introduced (Chow 1997). R^* is the radius of a solid pile with the same cross-sectional area as the open-ended pile.

Lehane et al. (2005a) assumes the reduction of the radial effective stress is dependent on the magnitude and type of cycles during installation based on findings of White & Lehane (2004). Thus, less decay was observed for jacked piles that induce few one-way cycles during installation compared to driven piles that induced many two-way cycles during installation. White and White & Lehane (2004) found that the decay increases with higher levels of radial stiffness ($4G/D$). Hence, in sand with the same shear modulus the radial stress in a given soil horizon reduces if the pile diameter is increased. On the basis of these two observations and the fact that the hammer selection for pile driving is usually proportional to the pile slenderness ratio, L/D , Lehane et al. (2005a) propose the radial effective stress to be dependent on h/D with a quasi-constant limit at a critical depth.

2.4.2 Pile Ageing

The design methods for axially loaded piles in sand do not account for the effect of time after installation on the capacity, even though some of the methods indicate at what time after installation, the methods apply. Different tests

2.4. Analyses of Influencing Factors

have confirmed that ageing has an effect on the pile capacity e.g. (Chow et al. 1998, Jardine et al. 2006). The investigations showed that piles experience increase of capacity with time even after the equalization of pore pressures is over (Chow et al. 1998, Jardine et al. 2006).

The literature proposes possible explanations for the ageing effect. Chow et al. (1998) considered the following three mechanisms to contribute to the ageing effect: Changes in the stress regime surrounding the pile, increased interface dilation, and increased interface roughness due to chemical corrosion (White & Zhao 2006). The main contribution to the ageing effects was thought to be caused by increase in the radial effective stresses due to relaxation of the circumferential arching formed under the pile installation (Chow et al. 1998, White & Bolton 2004, White et al. 2005). Axelsson (2000) performed load tests on concrete piles driven into loose and medium-dense sand and found that the interface dilation gave a more significant contribution to the increase in radial stresses than stress changes due to relaxation. Gavin et al. (2012) reported load tests on driven open-ended pipe piles in dense sand used to study the effect of ageing. The preliminary results suggested that the increase in radial effective stress is a combination of relaxation, increased dilation and sand bonding to the pile surface.

2.4.3 Interface Properties

The conditions in the interface are dependent on the normal stress on the interface, the relative density of the sand, the sand granulometry and the relative interface roughness (depending both on grain size and pile surface roughness).

Interface friction angle

Both direct shear tests and ring shear tests show that the constant volume interface friction angle, δ_{cv} but dependent on the relative interface roughness and the mean grain size, d_{50} (Kishida & Uesugi 1987, Jardine et al. 1992, Ho et al. 2011). Jardine et al. (1992) conducted constant normal direct interface shear tests with steel plate roughness of 6-10 μm which showed that δ_{cv} is independent of the initial relative density and it increases with the relative roughness of the interface. The tests showed that $22^\circ < \delta_{cv} < 36^\circ$ decreasing with increasing d_{50} (cf. Figure 2.3). Direct shear tests performed by UK Ltd showed less variation of the interface friction angle: $28^\circ < \delta_{cv} < 30^\circ$ (cf. Figure 2.3). While CUR (2001) recommends a constant $\delta_{cv} = 29^\circ$ (cf. Figure 2.3) as pile driving tests in dense sand are found to reduce the relative interface roughness due to abrading of the steel surface and crushing of sand grains. Jardine et al. (2005) performed ring shear tests that showed reduction of the

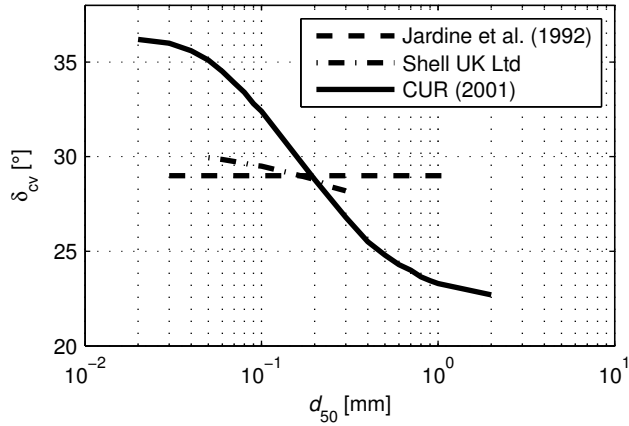


Figure 2.3: Interface friction in sand illustrative trends from direct shear interface tests after Jardine et al. (2005).

dependency of the initial particle size. However, White & Bolton (2004) observed that finer grains tend to mitigate from the interface shear zone during pile installation. For coarse grained soils, this could lead to lower δ_{cv} than found in interface ring shear tests. Ho et al. (2011) conducted interface ring shear tests with monotonic displacements and found δ_{cv} to be independent of the initial relative density of the sand. The analyses also revealed that the dependency of the main grain sizes decreased when the displacements increased.

Interface Dilation or Contraction

CNL and CNS interface shear tests with a high relative roughness and dense sand showed dilation within the first few millimeters of displacement where after the interface shear strength decreased to a residual value (Prai-ai 2013, Mortara et al. 2007, Boulon 1989, Uesugi & Kishida 1986). Dilatation takes place as a radial displacement, Δr , in the interface shear zone develops for slip to occur. The displacement must be in the magnitude of the average peak-to-trough roughness of the pile surface $2R_{cla}$. The change in radial effective stress increases with the shear modulus of the sand, G , but is inversely proportional to the pile diameter and may be estimated by the cavity expansion equation $2G\Delta r/R$ e.g. (Jardine et al. 2005). Thus, the contribution to the unit skin friction may be negligible for piles with $D > 1$ m, but important for medium scale piles and dominant for small-scale piles.

Kelly (2001) conducted a two-way cyclic test that began with 110 mm mono-

2.4. Analyses of Influencing Factors

tonic shearing, followed by 10 displacement controlled cycles, and ended with 100 monotonic shearing cycles. The first phase showed dilation at the interface. Low-level cycles resulted in interface contractions while high-level cycles led to hysteretic “butterfly wings” (volumetric changes with contraction, phase transformation and dilation within each cycle). The last loading phase introduced further contraction.

Particle Crushing

Interface ring shear tests under monotonic displacement up to 8 m showed large-scale particle crushing (Yang et al. 2010, Ho et al. 2011). Ho et al. (2011) reported that the crushed materials were localized in a shear band which grew under monotonic shearing to large displacements from between 4 to 15 times the mean grain size of the sands with an upper limit of 5 mm in tests involving 8 m shear displacement under maximum normal effective stress of 800 kPa.

2.4.4 Cyclic Loading

The piles in a foundation for an offshore wind turbine are subjected to cyclic loading both in the installation face where the pile is driven into the soil and in the serviceability mode due to waves, wind, and rotation of the wind turbine blades. Cyclic loading can lead to either decrease or increase of the pile capacity. Two things cause degradation of the unit skin friction during cyclic loading: In the shear band at the pile–soil interface, the cyclic loading leads to densification of the soil and thus to stress relief and reduction of the shear resistance (Silva et al. 2013). Moreover, cyclic loading can cause excess pore pressure build-up which also reduces the effective stresses and thus the shear resistance. This degradation is most significant in cohesive soils, cemented calcareous soils, and silt whereas it is must less significant in coarse grained cohesionless soils. In some load cases, depending on the mean load and cyclic loading amplitude, the ultimate shaft capacity of pile in coarse grained cohesionless soils might even increase e.g. (Jardine & Standing 2012, Jardine et al. 2006, Le Kouby et al. 2004). Beside the capacity of the single piles in the foundation in ULS, pile group effects must be accounted for as well.

Typical storm loading consists of a series of waves of increasing magnitude, but decreasing number, with the peak design loading usually occurring only once. Instead of modeling the complete load series, offshore design normally uses an equivalent number of cycles of the peak design loading to represent the cumulative damage that occurs during the full sequence. Four different types of cyclic stress regimes: i) Symmetric two-way (relatively rare, but the most commonly applied in laboratory testing programs), ii) asymmetric two-

way, iii) ideal one-way, and iv) biased one-way (Randolph 2012).

One-way cyclic loading with small amplitudes lead to minimal accumulated displacements and increased pile capacity (Jardine & Standing 2000, 2012, Chan & Hanna 1980, Le Kouby et al. 2004, Rimoy 2013, Thomas & Kempfert 2011). Silva et al. (2013) explain the capacity gains with densification at the pile-soil interface leading to more marked dilation during further loading and thus shaft capacity gains. Increasing the cyclic amplitude can have a negative effect i.e. decrease the number of cycles to failure (Thomas & Kempfert 2011, Chan & Hanna 1980). Thomas & Kempfert (2011) report a possible beneficial effect of increasing the mean load. The cyclic stiffness varies with cyclic loading amplitude and remains constant until beginning of failure (Rimoy 2013).

Two-way cyclic loading is more damaging than one-way cyclic loading (Randolph 2012). Two-way cyclic loading with high cyclic amplitude leads to radial stress reductions in the interface resulting in rapidly accumulated displacements and failure (Silva et al. 2013, Jardine & Standing 2000, 2012, Thomas & Kempfert 2011). Increasing the mean load have decreases the number of load cycles before failure (Thomas & Kempfert 2011).

Chan & Hanna (1980) found that a stable test can become unstable after several thousands of cycles, indicating that the number of cycles affects the results of cyclic loading and that the definition of a stable state of no failure or large accumulation of displacements after 1000 cycles may not be true for situations of many loading cycles.

Karlsruud et al. (1986), Poulos (1988), Jardine & Standing (2000, 2012), Tsuha et al. (2012) proposed interactions diagrams predicting the response of the pile depending on the mean load and loading amplitude relative to the static capacity of the pile. The interaction diagrams predict whether a pile will be stable, meta-stable or unstable (these definitions are given below) for the given loading conditions. Puech (2013) proposes including interaction diagrams in the preliminary design of offshore foundations to predict the effect of cyclic loading. Jardine & Standing (2012) defined the stable, meta-stable, and unstable conditions for their stability diagram as:

- Stable (S) cyclic load behavior: The pile has not failed after 1000 load cycles, not experienced loss of shaft capacity, and the displacement rates are very low.
- Meta-stable (MS) cyclic load behavior: The pile can sustain up to 1000 load cycles but experiences loss of pile capacity and a moderate displacement rate.

2.5. Design Methods for Unit Skin Friction

- Unstable (US) cyclic load behavior: The pile fails within 100 load cycles.

The proposed interaction diagrams are based on the findings of small-scale and full-scale pile tests with one-way and two-way cyclic loading. The interaction diagrams are based on rather few tests on a limited number of soil conditions, pile characteristics, and load conditions. Abdel-Rahman et al. (2014) proposed a finite element model accounting for interface contraction due to cyclic loading to derive stability diagrams for a variety of soil conditions, pile characteristics, and load conditions. However, the authors suggested further studies on using a less simple material law for the soil as well as adjusting the initial stress conditions.

2.5 Design Methods for Unit Skin Friction

The method is only applicable for open-ended steel pipe piles in cohesionless siliceous soils. The internal unit skin friction is assumed equal to the external unit skin friction which is a conservative assumption because of arching of the soil column in the pile which is assumed to lead to a higher internal skin friction. No distinction is made between shaft capacity for piles loaded in tension and piles loaded in compression. Moreover, the piles are assumed installed by impact driving into significant depths, which means that the piles in general are driven unplugged. However, the piles can act plugged during static loading. The unit skin friction is based on earth pressure theory and follows a Coulomb criterion:

2.5.1 API-00

$$f_s = \beta \sigma'_{v0} = K_f \tan \delta \sigma'_{v0} < f_{s,\text{lim}} \quad (2.1)$$

where

σ'_{v0}	vertical effective stress at the point in question,
β	shaft friction factor ($\beta = K_f \tan \delta$),
K_f	coefficient of lateral earth pressure,
δ	interface friction angle,
$f_{s,\text{lim}}$	limiting shaft friction.

Table 2.2 provides guidelines for values of β if no other data is available. For long piles, f_s may not increase linearly with the overburden pressure. In such cases, it may be appropriate to use the limiting values of f_s given in Table 2.2.

Table 2.2: API-00 design parameters for cohesionless siliceous soil (API 2011).

D_r [%]	Soil	β (open-ended) [-]	β (closed-ended) [-]	$\tau_{f,lim}$ [kPa]
0-15	Sand			
15-35	Sand			
15-35	Sand-silt	N/A	N/A	N/A
35-65	Silt			
65-85	Silt			
35-65	Sand-silt	0.29	0.36	67
35-65	Sand			
65-85	Sand-silt	0.37	0.46	81
65-85	Sand			
85-100	Sand-silt	0.46	0.57	96
85-100	Sand	0.56	0.70	115

API-00 Database

The last revision of API-00 was based on 34 tests on steel pipe piles with diameters in the range 0.2-0.9 m and lengths in the range 3.3-21.3 m (Olson & Al-Shafei 1988). Only four of these piles were open-ended. The rest were closed-ended. Of the open-ended piles, three were loaded in tension and the last in compression. For the closed-ended piles, seven were loaded in tension and the rest were loaded in compression.

2.5.2 NGI-05

Clausen et al. (2005) proposed the NGI-05 method where the unit skin friction is based on results of piles loaded in tension, because only the total pile capacity was recorded for most of the piles loaded in compression. The method was based on the assumptions that the skin friction in homogeneous soil layers has a triangular distribution with depth. Moreover, the unit skin friction in compression was assumed to be a constant multiplied by the unit skin friction in tension. The internal unit shaft friction is assumed three times higher than the external shaft friction due to arching at the pile tip. The external unit skin friction is given by

$$f_s = \frac{z}{z_{tip}} p_a F_{load} F_{tip} F_{mat} F_{sig} F_{Dr} > 0.1 \sigma'_{v0} \quad (2.2)$$

$$F_{sig} = \left(\frac{\sigma'_{v0}}{p_a} \right)^{0.25} \quad (2.3)$$

$$F_{Dr} = 2.1 (D_r - 0.1)^{1.7} \quad (2.4)$$

2.5. Design Methods for Unit Skin Friction

$$D_r = 0.4 \ln \left(\frac{q_c}{22 (\sigma'_{v0} p_a)^{0.5}} \right) \quad (2.5)$$

where

z	depth below ground surface,
z_{tip}	pile tip depth,
p_a	atmospheric pressure (100 kPa),
F_{load}	1.0 for tension, 1.3 for compression,
F_{tip}	1.0 if driven open-ended, 1.6 if driven closed-ended,
F_{mat}	1.0 for steel, 1.2 for concrete,
F_{sig}	accounts for the variation of the vertical effective stresses at the point in question,
F_{D_r}	accounts for the relative density of the sand,
D_r	relative density (values larger than one should be accepted),
q_c	cone resistance at a given depth,
σ'_{v0}	vertical effective stress at the point in question.

NGI-05 Database

The method is based on 85 load tests at 35 different locations. The database included concrete piles as well as open- and closed-ended steel piles. The majority of the piles had an installation depth of 2-35 m and installed in sand with a relative density within the range 20-70 %. However, the database also included a few piles with embedded depths up to 90 m installed in sand with relative densities below 20 %, and some piles installed at sites with relative densities up to 100 %. For 56 of the test sites, CPT data was available while for the rest of the tests, SPT data was available. The SPT results were converted to corresponding CPT cone resistances. However, the predicted capacities for the piles with CPT data showed better agreement with the load test measurements than the predicted capacities with the converted SPT data (Clausen et al. 2005).

2.5.3 ICP-05

Jardine et al. (2005) provided the ICP-05 method that applies to silica sands, piles with circular cross-sections, and capacities available in 'first-time' slow maintained loading tests conducted about ten days after driving. The unit

skin friction follows a Coulomb failure criterion as

$$f_s = \sigma'_{rf} \tan \delta_{cv} = a (b\sigma'_{rc} + \Delta\sigma'_{rd}) \tan \delta_{cv} \quad (2.6)$$

$$\sigma'_{rc} = 0.029q_c \left(\frac{\sigma'_{v0}}{p_c} \right)^{0.13} \left(\max \left[\frac{h}{R^*}, 8 \right] \right)^{-0.38} \quad (2.7)$$

$$\Delta\sigma'_{rd} = 2G \frac{\Delta r}{R} \quad (2.8)$$

$$G = G_0 = q_c \left(0.0203 + 0.00125\eta - 1.21 \cdot 10^{-5}\eta^2 \right)^{-1} \quad (2.9)$$

$$\eta = \frac{q_c}{(\sigma'_{v0} p_a)^{0.5}} \quad (2.10)$$

where

σ'_{rf}	radial effective stress at failure,
σ'_{rc}	radial effective stress after installation and equalization,
δ_{cv}	constant volume interface friction angle,
$\Delta\sigma'_{rd}$	change in radial stress due to loading stress path (dilation),
a	0.9 for open-ended piles in tension, 1 for open-ended piles in compression, 1 for closed-ended piles in both tension and compression,
b	1 for piles in compression, 0.8 for piles in tension,
q_c	cone resistance at a given depth,
σ'_{v0}	vertical effective stress at depth z ,
p_a	atmospheric pressure (100 kPa),
h	distance above the pile tip = pile length – depth z ,
R	outside radius of a pile,
R_i	inside radius of a pile,
R^*	equivalent radius = $(R^2 - R_i^2)^{0.5}$,
G	sand shear modulus taken as the small strain shear modulus G_0 ,
Δr	interface dilation estimated to be 0.02 mm for lightly rusted piles.

2.5. Design Methods for Unit Skin Friction

ICP-05 Database

The method is based on the full-scale tests on open-ended pipe piles that were conducted in the dense to very dense sand at Dunkerque, France (Jardine & Standing 2000). Moreover, the method is based on the field tests with the closed-ended steel pipe Imperial College Pile (ICP) that were conducted in the dense to very dense sand at Dunkerque, France (Chow 1997) and in loose to medium dense sand at Labenne, France (Lehane et al. 1993). The installation method for the ICP was jacking.

2.5.4 Fugro-05

Kolk et al. (2005) suggested the Fugro-05 method for steel pipe piles in silica sands. (According to API (2000), the formulation given in Kolk et al. (2005) is incorrect; however, Lehane et al. (2005b) give the correct formulation). In compression, the unit skin friction is given by

$$f_s = 0.08q_c \left(\frac{\sigma'_{v0}}{p_a} \right)^{0.05} \left(\frac{h}{R^*} \right)^{-0.9} \quad \text{for } \frac{h}{R^*} \geq 4 \quad (2.11)$$

$$f_s = 0.08q_c \left(\frac{\sigma'_{v0}}{p_a} \right)^{0.05} 4^{-0.9} \left(\frac{h}{4R^*} \right) \quad \text{for } \frac{h}{R^*} < 4 \quad (2.12)$$

In tension, the unit skin friction is given by

$$f_s = 0.045q_c \left(\frac{\sigma'_{v0}}{p_a} \right)^{0.15} \left(\max \left[\frac{h}{R^*}, 4 \right] \right)^{-0.85} \quad (2.13)$$

where

- q_c cone resistance at a given depth,
- σ'_{v0} vertical effective stress at depth z ,
- p_a atmospheric pressure (100 kPa),
- h distance above the pile tip = pile length – depth z ,
- R outside radius of a pile,
- R_i inside radius of a pile,
- R^* equivalent radius = $(R^2 - R_i^2)^{0.5}$,

Fugro-05 Database

The method is based on 45 pile load tests on steel pipe piles driven open- or closed-ended on sites with siliceous sand. The used load test data includes 24 tension and 21 compression tests.

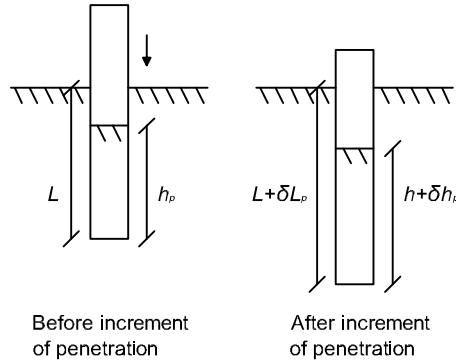


Figure 2.4: Definition of the incremental filling ratio IFR , after (Randolph & Gourvenec 2011).

2.5.5 UWA-05

The method applies to driven steel pipe piles installed in silica sand 10-20 days after installation Lehane et al. (2005a). The unit skin friction follows a Coulomb failure criterion as

$$f_s = \sigma'_{rf} \tan \delta_{cv} = \frac{f}{f_c} (\sigma'_{rc} + \Delta\sigma'_{rd}) \tan \delta_{cv} \quad (2.14)$$

$$\sigma'_{rc} = 0.03q_c A_{r,eff}^{0.3} \left(\max \left[\frac{h}{D}, 2 \right] \right)^{-0.5} \quad (2.15)$$

$$A_{r,eff} = 1 - IFR \left(\frac{D_i^2}{D^2} \right) \quad (2.16)$$

$$IFR = \frac{\delta h_p}{\delta L} \approx \min \left[1, \left(\frac{D_i}{1.5} \right)^{0.2} \right] \quad (2.17)$$

$$\Delta\sigma'_{rd} = 2G \frac{\Delta r}{R} \quad (2.18)$$

$$G = 185q_c q_{cN1}^{-0.7} \quad (2.19)$$

$$q_{cN1} = \frac{q_c / p_a}{(\sigma'_{v0} / p_a)^{0.5}} \quad (2.20)$$

2.5. Design Methods for Unit Skin Friction

where

σ'_{rf}	radial effective stress at failure,
σ'_{rc}	radial effective stress after installation and equalization,
δ_{cv}	constant volume interface friction angle,
$\Delta\sigma'_{rd}$	change in radial stress due to loading stress path (dilation),
f/f_c	0.9 1 for compression and 0.75 for tension,
h	distance above the pile tip = pile length –depth z ,
$A_{r,eff}$	effective area ratio,
D	outside diameter of a pile,
D_i	inside diameter of a pile,
IFR	incremental filling ratio defining the plugged/unplugged condition of the pile,
$\delta h_p,$ δL	defined in Figure 2.4. $IFR = 0$ corresponds to plugged penetration. $IFR = 1$ corresponds to unplugged penetration, while a value of IFR between 0 and 1 corresponds to partial plugging. Near the pile tip, it is σ'_{rc} difficult to measure and it is considered constant over the last $2D$ of the length above the pile tip,
G	sand shear modulus,
Δr	interface dilation estimated to be 0.02 mm for lightly rusted piles.

UWA-05 Database

The UWA-05 design method is based on 74 pile load tests with appurtenant CPT-data on sites with siliceous sand. Thus, this method is based on the largest database compared to other CPT-based methods suggested. The tested piles were both steel pipe piles and concrete piles. In order to analyze the database and develop a new design method, the database was divided into four sub-databases: Closed-ended piles in tension, closed-ended piles in compression, open-ended piles in tension, and open-ended piles in compression. Despite the relatively large number of large-scale tests, the number of adequate tests is rather low when dividing the databases into subsets. Moreover, the databases do not include enough tests on piles with the dimensions used offshore Lehane et al. (2005b).

2.5.6 Simplified ICP and Offshore UWA

Offshore piles typically act plugged during static loading i.e. $IFR = 1$. Moreover, $\Delta\sigma'_{rd}$ tends to zero. API (2011) gives the following simplified methods of the ICP-05 and UWA-05 with the values given by Table 2.3. Lehane et al.

Table 2.3: Values for Equation (2.21).

Method	a	b	c	d	u	v
Simplified ICP:						
Compression	0.1	0.2	0.4	1.0	0.023	$4\sqrt{A_r}$
tension	0.1	0.2	0.4	1.0	0.016	$4\sqrt{A_r}$
Offshore UWA:						
Compression	0.0	0.3	0.5	1.0	0.030	2
tension	0.0	0.3	0.5	1.0	0.022	2

(2005b) are the instigators of the offshore UWA method.

$$f_s = uq_c \left(\frac{\sigma'_{v0}}{p_a} \right)^a A_r^b \left(\max \left[\frac{L-z}{D}, v \right] \right)^{-c} (\tan \delta_{cv})^d \quad (2.21)$$

$$A_r = 1 - \left(\frac{D_1^2}{D^2} \right) \quad (2.22)$$

2.5.7 Basis for the Terms in the Design Methods

Soil relative density

- **NGI:** The relative density of the sand is determined from q_c . The relationship between the two parameters is based on the diagrams shown in Fig. 5.47 of Lunne et al. (1997).
- **ICP, Fugro, UWA:** Uses q_c directly in the methods as an expression for the sand relative density.

Effective vertical stress

- **NGI, ICP, Fugro:** All define the unit skin friction as dependent on the in-situ vertical effective stress.
- **UWA:** Includes a dependency of the in-situ vertical effective stress in the term expressing dilation in the pile–soil interface.

Friction fatigue

- **NGI:** The friction fatigue effect reducing f_s as the distance to the pile tip increases is expressed by the term z/z_{tip} .
- **ICP:** The friction fatigue effect is accounted for in the term h/R^* that has a quasi-constant limit at a critical depth. Based on the Labenne and Dunkerque pile load tests, the decay was suggested to be a power law with the power -0.38.

2.5. Design Methods for Unit Skin Friction

- **Fugro:** The method accounts for the friction fatigue effect in the same way as ICP; however, a lower limit of the reduction is not included.
- **UWA:** Lehane et al. (2005a) accounts for the radial effective stress change by the term h/D with a quasi-constant limit at a critical depth. Jardine et al. (2005) suggested the friction fatigue effect to decay with the power -0.38; however, this number was based on results of jacked piles. Lehane et al. (2005a) suggest -0.5 for driven piles, which is the installation method commonly used offshore.

Soil displacement during installation

- **NGI:** Introduces with no further explanation F_{tip} that accounts for an open- or closed-ended pile.
- **ICP, Fugro:** Introduction of R^* which is the radius of a solid pile with the same cross-sectional area as the open-ended pile.
- **UWA:** Introduction of an effective area ratio, A_{rs}^* , that is unity for closed ended piles. For open-ended pipe piles, A_{rs}^* depends on the area of the pile material and the area of the soil plug inside the pile if the pile experiences partial or full plugging during installation. The incremental filling ratio (*IFR*) introduces the soil displacement at the pile tip due to plugging and depends on installation method, pile wall thickness, inner pile diameter, soil layering, plug densification or dilation.

Interface friction angle

- **NGI:** The method does not apply an interface friction angle but does introduce a material factor, F_{mat} , accounting for higher unit skin friction for concrete piles than for steel piles.
- **ICP:** δ_{cv} depends on grain size, shape, and mineralogy of the sand as well as on the roughness of the pile surface. Jardine et al. (2005) highly recommend site specific interface shear tests to find the interface friction angle.
- **Fugro:** Uesugi et al. (1989) analyzed pile load tests and laboratory interface shear tests that indicated changes of sand grading and steel roughness leading to a constant interface friction angle of 29° .
- **UWA:** If site specific tests are not available, the trendline found by Jardine et al. (1992) is recommended for $d_{50} > 0.2$ mm, while for $d_{50} < 0.2$ mm an upper limit of $\tan \delta_{cv} = 0.55$ is recommended corresponding to the CUR (2001) recommendations (cf. Figure 2.3).

Dilation

- **NGI:** The method does not account for dilation.

- **ICP:** Increase of the radial effective stress due to constrained dilation in the interface. A radial displacement, Δr , in the interface shear zone develops for slip to occur. The displacement must be in the magnitude of the average peak-to-trough roughness of the pile surface $2R_{\text{cla}}$. The change in radial effective stress increases with the shear modulus of the sand, G , but is inversely proportional to the pile diameter and may be estimated by the cavity expansion equation $2G\Delta r/R$ e.g. (Jardine et al. 2005). Thus, the contribution to the unit skin friction may be negligible for piles with $D > 1$ m, but important for medium scale piles and dominant for small-scale piles.
- **Fugro:** The method applies to full-scale offshore piles and dilation effects are considered negligible.
- **UWA:** The ICP recommendations are adopted in the UWA method except a modification of the equation for finding the shear modulus G .

Tension or compression loading

- **NGI:** The factor F_{load} defines a higher unit skin friction for compression than for tension loading.
- **ICP:** The development of the radial effective stress is smaller in tension than compression due to rotation of the principal stress and radial contraction of the pile during loading (elongation of the pile). The radial contraction is more pronounced for open-ended pipe piles than for closed-ended piles; this is accounted for in the method.
- **Fugro:** The unit skin friction is considered higher for compression than for tension loading. In the expression for the unit skin friction for compression loading, the method also introduces a reduction near the pile tip as suggested by finite element analyses (De Nicola & Randolph 1993).
- **UWA:** For the reasons given for the ICP method, the unit skin friction tension is less than the compression capacity. However, the distinction between this reduction in unit skin friction for closed- and open-ended piles is not taken into account in the UWA method.

2.5.8 Evaluation of the Methods

Lehane et al. (2005b) assessed the performance of the API method and the four CPT based methods by comparing the predictions of the methods to the UWA database. The performance of each method was examined by reviewing the ratios of the calculated capacities, Q_c , and the measured capacities, Q_m . The Q_c/Q_m ratios were plotted against the pile tip depth, the pile diameter, the slenderness ratio, and the average relative density along the pile shaft, respectively. However, no distinction was made between steel pipe

2.5. Design Methods for Unit Skin Friction

piles and concrete piles and the cross-sectional design (square, circular etc.). Lehane et al. (2005*b*) derived the following tendencies for the methods.

For closed-ended piles in compression, API-00 predicted the lowest and most conservative capacities. Furthermore, API-00 predictions tended to under-predict the capacity of short piles in dense sands and over-predict the capacity of long piles in loose sand. Contrary to API-00, the four CPT methods (UWA-05, ICP-05, NGI-99, Fugro-05) did not show any strong bias with pile length, pile aspect ratio, and average sand relative densities. UWA-05 and ICP-05 methods displayed the lowest COV for Q_c/Q_m .

For closed-ended piles in tension, API-00 showed a clear tendency to over-predict the pile capacity in loose sands. The CPT-based methods did not show a systematic bias for Q_c/Q_m to vary with relative density. The small database for these types of tests made evaluation of bias for the CPT-based methods relatively subjective. NGI-99 had significantly higher COV for Q_c/Q_m for this sub-database than for the other sub-databases. Again, UWA-05 had the lowest COV for Q_c/Q_m .

For open-ended piles in compression, API-00 showed the highest COV for Q_c/Q_m . Fugro-05 showed a more distinct trend to under-predict capacities at large L/D values than for closed-ended piles in compression. UWA-05 had the lowest COV for Q_c/Q_m .

For open-ended piles in tension, again API-00 showed the highest and UWA-05 the lowest COV for Q_c/Q_m . The performance of the CPT-based methods was broadly similar and all methods perform significantly better than API-00.

It is not sufficient to base the reliability of a method on its performance against a given database. Instead the differences between the methods need to be considered when assessing the reliability of each method. It should be noted that these CPT-based methods can give significantly different results (Lehane et al. 2005*b*). A sufficient design method should consider the primary physical processes controlling the capacity of a pile before extrapolating from a database analysis to offshore piles (Lehane et al. 2005*b*). Some complications of interpretation of the axial static pile capacity databases are as follows: i) Separating base and shaft capacity as many tests are conducted on un-instrumented piles, ii) the tests are conducted relatively shortly after installation, thus not accounting for ageing, and iii) detecting the effect of cyclic loading both from pile driving and in-service stages.

2.6 Total Pile Capacity

The Winkler model approach is one of the most widely used methods for evaluating the pile capacity and displacements. The pile is modeled as a beam and the soil response to the axial pile displacement is modeled as uncoupled springs (Figure 2.5). The spring stiffness is governed by the t - z curves which again depend on the unit skin friction and all the influencing factors described in the previous sections.

API (2011) recommends the t - z curve for sand given in Table 2.4 if no other formulation is provided. However, the literature does propose a number of empirical t - z curves based on full-scale or model pile tests. This section presents four of these t - z curve formulations where the following symbols are used: t is the mobilized unit skin friction, z is the local axial pile displacement, t_{\max} is the maximum unit skin friction with the corresponding pile displacement $z_{t_{\max}}$, t_{res} is the residual unit skin friction over a post-peak displacement Δz_{res} , t_{post} is the residual unit skin friction at a post-peak displacement Δz , and η_{res} is a softening parameter.

The API (2011) provides the t - z curve formulation for sand given in Table 2.4. The method does not account for strain softening after the peak value of the unit skin friction but stays constant at the maximum value.

Table 2.4: t - z curve formulation in API (2011).

z/z_{\max}	t/t_{\max}
0.00	0.00
0.16	0.30
0.31	0.50
0.57	0.75
0.80	0.90
1.00	1.00
2.00	1.00
inf	1.00

The following three methods all include strain softening to a residual value of t . Randolph & Gourvenec (2011) suggest a parabolic function for t - z curves:

$$t_{\text{ini}} = t_{\max} \left(2 \frac{z}{z_{t_{\max}}} - \left(\frac{z}{z_{t_{\max}}} \right)^2 \right) \quad (2.23)$$

$$t_{\text{post}} = t_{\max} - 1.1 (t_{\max} - t_{\text{res}}) \left(1 - \exp \left(-2.4 \left(\frac{\Delta z}{\Delta z_{\text{res}}} \right)^{\eta_{\text{res}}} \right) \right) \quad (2.24)$$

2.6. Total Pile Capacity

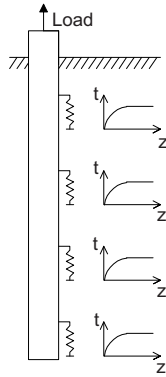


Figure 2.5: Winkler model approach for axially loaded pile in tension.

Fellenius (2013) gives the following formulation for the 80 % function:

$$t = \frac{\sqrt{z}}{C_1 z + C_2} \quad (2.25)$$

$$C_1 = \frac{1}{2t_{\max}\sqrt{z_{t_{\max}}}} \quad (2.26)$$

$$C_2 = \frac{\sqrt{z_{t_{\max}}}}{2t_{\max}} \quad (2.27)$$

Zhang & Zhang (2012) propose the following formulations for t - z curves from tests on bored piles:

$$t = \frac{z(a + cz)}{(a + cz)^2} \quad (2.28)$$

$$t_{\max} = \frac{1}{4(b - c)} \quad (2.29)$$

$$z_{t_{\max}} = \frac{a}{b - 2c} \quad (2.30)$$

$$a = (b - 2c) z_{t_{\max}} \quad (2.31)$$

$$b = \frac{1 - \sqrt{1 - \beta_s}}{2\beta_s} \frac{1}{t_{\max}} \quad (2.32)$$

$$c = \frac{2 - \beta_s - 2\sqrt{1 - \beta_s}}{4\beta_s} \frac{1}{t_{\max}} \quad (2.33)$$

$$\beta_s = \frac{t_{\text{res}}}{t_{\max}} \quad (2.34)$$

2.7 Concluding Remarks

This chapter provided a literature review of the factors influencing the shaft capacity of an axially loaded pile in tension subjected to both static and cyclic loading. The review presented the current design approaches and the methods for identifying some of the factors influencing the pile shaft capacity. A lot of research concerning axially loaded piles installed in sand is available, but more is still needed to extrapolate the current design methods to a larger variety of the soil conditions, load combination, and pile characteristics found offshore. Chapter 3 presents the main findings of this state-of-the-art review relevant for the current PhD study.

Chapter 3

Scope of the Thesis

The state-of-the-art review clearly shows that there is a lot of research regarding the capacity of axially loaded piles in sand. However, research is still needed in order to expand the basis for the existing design methods for the unit skin friction and to include the use of interaction diagrams in the currently used design flow. This chapter summarizes the main findings of the state-of-the-art and describes the objectives of the present PhD thesis as well as its contribution to the research of axially loaded piles.

3.1 Main Findings of State-of-the-Art

The state-of-the-art study revealed the factors influencing the shaft capacity of an axially loaded pile. Many of these influencing factors have been observed, analyzed and discussed based on both pile and laboratory tests by researchers. With the CPT-based methods introduced in 2005 for prediction of the unit skin friction, most of the observed influencing factors are accounted for one way or another. However, these methods are developed based on different pile test databases and laboratory tests and, thus, they can provide different predictions of the capacity. Nevertheless, the overall agreement is that these CPT-based methods give much better predictions of the shaft capacity than the traditional design methods. Two of the contributions to stress changes for an axially loaded pile during its life cycle, namely setup due to ageing and cyclic loading, are not accounted for in any of the methods.

The analysis of the cyclic loading effects on the pile capacity involves in-situ tests, laboratory tests as well as full- and small-scale pile tests. There are no full-scale offshore pile tests, and even full-scale tests on onshore piles analyzing the effect of cyclic loading on the pile capacity are scarce. Small-scale pile tests conducted in calibration chambers and centrifuges suffer from scaling

and boundary effects that must be taken into consideration when analyzing the test results. Some of the cyclic loading tests underlie proposed interaction diagrams predicting the effect of given cyclic load conditions on the pile behavior. These interaction diagrams are based on very few tests; thus, the tested soil conditions and pile parameters are limited. The diagrams are not yet included in the recommended design flow for axially loaded offshore piles even though they could provide help with predicting the cyclic loading behavior of the foundation.

3.2 Aim and Objectives of the Thesis

The motivation for the thesis was the observed—but not documented—large accumulated upward displacements of tension piles in jacket pile foundations for offshore wind turbines located at sites with dense sand. These displacements must be avoided because they can lead to tilting of the entire wind turbine structure exceeding the design criteria. Based on this observation and the main findings of the state-of-the-art study, the conclusion was there is a need for more tests within the field of tension piles in dense sand.

To conduct pile load tests a new laboratory test setup was built. One objective was to make a sand box and pile specimen where scaling-effects were reduced so as to get correct pile-soil interface properties. Thus, the test setup was designed to accommodate an open-ended steel pipe pile with a diameter close to full-scale piles. However, the possible size of the test setup sets limitations of the length of the pile specimen. As described, the aim was to analyze the behavior of tension piles subjected to cyclic loading and, thus, the work involves conducting static and cyclic tension tests in the new test setup. The results of the static tension tests are compared to the design methods for prediction of the unit shaft friction. Moreover, t - z curves obtained from the results are compared to existing formulations.

The cyclic tests were performed as series of load cycles with constant mean load and cyclic amplitude for duration of two days. Several tests were conducted with different values of the mean load and cyclic amplitude in order to analyze the effect of changing these two parameters on the pile capacity, accumulated displacements and cyclic stiffness. The present thesis discusses the results and compares these with findings of other researchers.

The scientific outcome of the studies is reflected in the enclosed papers:

- **Paper A:** Laboratory Test Setup for Cyclic Axially Loaded Piles in Sand

3.2. Aim and Objectives of the Thesis

- **Paper B:** Comparison of Design Methods for Axially Loaded Driven Piles in Cohesionless Soil
- **Paper C:** Static Tension Tests on Axially Loaded Pile Segments in Sand
- **Paper D:** Axial Cyclic Loading Tests on Pile Segments in Sand

Chapter 4

Test Setup and Test Procedure for Pile Load Tests

As stated in Scope of the Thesis, the objective of the test setup was to analyze the effect of static and cyclic tension load on a pile segment with a diameter close to full-scale piles to model the interface properties correctly. This chapter is mainly based on Paper A regarding the test setup. However, prior to a summary of Paper A there is a discussion of the considerations for pile design, soil preparation, installation method, and stress conditions not explained to full extent in the paper. The last section provides recommendations for improving the test setup.

4.1 Considerations for the Test Setup and Test Procedure

The design of the sand box and the pile was determined before any tests were made. However, some modifications to the soil processing procedure were made after the first tests. When analyzing the test results, some additional questions regarding the stress conditions in the sand box came up and demanded further considerations. This section presents the preliminary choices, the following modifications, and the considerations of the stress conditions.

4.1.1 Pile Design

Figure 4.1 shows the pile specimen and Figure 4.2 shows the laboratory test setup. The pile diameter of 0.5 m was much closer to full-scale piles than the pile specimens normally used in calibration chamber tests. Field tests were



Figure 4.1: The pile segment.

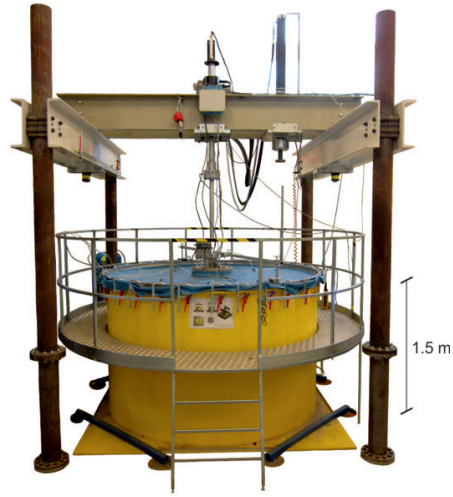


Figure 4.2: Laboratory test setup.

not an option and the size of the laboratory sand box limited the length of the pile specimen to 1 m. The pile wall thickness was very small (3 mm) for decreasing the possible end bearing in the one-way cyclic loading tests described and analyzed in Paper D. However, the wall thickness was large enough to avoid instability of the pile during installation and loading. Because of the short length and the rigidity of the pile specimen, straining was assumed not to occur in the pile specimen under loading. Thus, the pile was compared to a pile segment of 1 m length, and the unit skin friction reported in Paper C was based solely on the measured loads of the static loading tests. Besides the choice of a large diameter to reduce scaling effects, the pile segment was made of steel and the use resulted in a lightly rusted pile. Hence, the pile–soil interface properties were very similar to the ones found for offshore full-scale piles.

4.1.2 Sand Preparation and Pile Installation

The sand used in the tests and the soil processing procedure were adopted from tests on small-scale monopiles and monobuckets conducted in other test setups at Aalborg University, Denmark e.g. (Foglia et al. 1991, Thomassen et al. 2011). The sand was prepared by saturating the sand and using a rod vibrator to ensure the wanted relative density of the sand prior to installation of the test specimen. Hedegaard & Borup (1993) and Ibsen et al. (1994) investigated the properties of the sand through laboratory testing. Larsen (2008) described the custom-made CPT device at Aalborg University and provided the correlation between the CPT cone resistance and the friction angle, dila-

4.1. Considerations for the Test Setup and Test Procedure

tion angle, and the relative density of the sand deposited in the test setup. The soil processing procedure in these earlier conducted tests provided repeatable soil conditions for the tests.

The same preparation procedure was tried out for the tests described in this thesis. In the first tests, the pile segment was pushed into the sand by means of a hydraulic piston after soil vibration. However, the pile segment plugged during installation and the hydraulic system was not powerful enough to complete the installation. It was necessary to pull out the pile segment a few centimeters of the sand and thereafter continue the installation. This “pull-out and continue” installation procedure was needed several times in each installation. The result of the installation procedure was that the effect of the installation was completely unknown. Moreover, the installation could not be conducted identically in all the tests. To avoid the effects of this unreliable installation, it was decided to install the pile segment before the soil vibration. Thereby, the installation did not affect the test results presented by Paper A, Paper C and Paper D—only the soil processing affected them.

4.1.3 Vertical Effective Stress

The short pile length made it possible to individually model one meter pile segments. To model the stress variation along the pile shaft of a longer pile, it was necessary to find a method to increase the vertical effective stress. The most commonly used method for increasing the effective stress in model tests in calibration chambers is to use a rigid plate concealing the soil surface and placing a water-filled membrane under this rigid plate, which induces different pressures in this membrane providing a surcharge at the soil surface. The large diameter of the sand box used for the tests in this thesis and the open-ended pile segment complicated the use of such a system for applying an overburden pressure. Instead the membrane–vacuum system used by Foglia et al. (1991) was adopted. Figure 4.3 shows the membrane placed on the soil surface and sealed at the sand box edge and at pile head. A vacuum pump was connected to the membrane through hoses and quick couplings as described in Paper A. 70 kPa was the maximum applied suction that could remain stable for a longer period of time (more than two days). The suction level provided an increase of the effective stresses equivalent to an applied overburden pressure of the same size cf. Figure 4.4. When applying suction, the water was sucked out of the sand box leaving the sand with a very low degree of saturation.

It was not discovered whether insufficient sealing at the pile and sand box edge or air trapped in the water or both things were the cause of the water being sucked out of the system. After the tests with applied suction, the sand

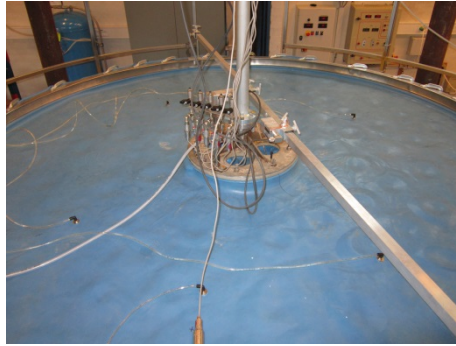


Figure 4.3: Membrane–vacuum system used to increase the vertical effective stress in the sand box.

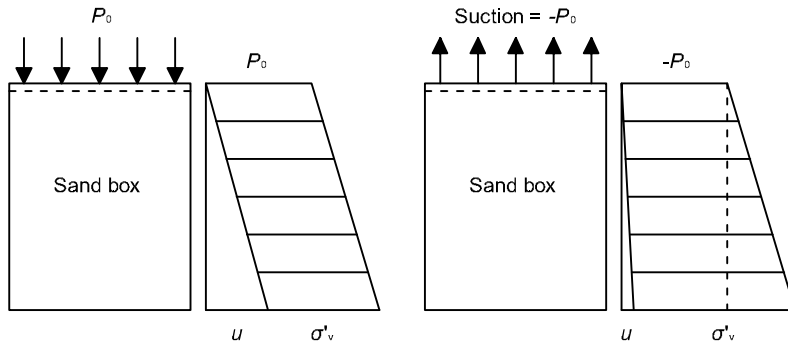


Figure 4.4: Increase of the vertical effective stress in saturated sand by applying an overburden pressure (left) and by applying suction to the membrane and sucking the water out of the sand box (right).

looked like a sponge, cf. Figure 4.5. The holes were probably the effect of expansion of the air trapped in the sand and subjected to vacuum. The effect on the test results of this observation is not further discussed.

4.1.4 Horizontal Effective Stress

Two things concerning the horizontal effective stress were affecting the test results. First of all, the small ratio of five between the sand box diameter and the pile diameter almost certainly affects the test results especially as the vertical boundaries of the sand box were rigid. Rimoy (2013) conducted cyclic tests on a model pile in a calibration chamber with BC3 and BC5 boundary conditions that showed stress changes in the soil at least within a range of $R_{\text{chamber}}/R_{\text{pile}} = 8$ from the pile. Paper A provides a more detailed description of these boundary conditions, but BC3 includes rigid vertical boundaries,

4.1. Considerations for the Test Setup and Test Procedure



Figure 4.5: Sand structure after tests with applied suction.

while BC5 provides vertical boundaries simulating free field conditions. Salgado et al. (1998) made penetration tests in a calibration chamber and found that rigid vertical boundaries (BC2 and BC3) have a constraining effect leading to higher penetration resistances than would be observed in free field conditions. Thus, the boundary conditions of the test setup most likely affected the tests results of the tests presented in Paper C and Paper D.

The other thing concerning the horizontal effective stress was the consolidation ratio of the sand. Paper C presents a comparison of the static test results to results of a simple axis-symmetric finite element model. The comparison indicated that the sand in the sand box was not normally consolidated but instead heavily over-consolidated as it was necessary to use high coefficients of lateral earth pressure at rest, K_0 , in the models. $K_0 = 3$ was used when applying overburden pressures of $P_0 = 0$ and 35 kPa, and $K_0 = 5$ for $P_0 = 70$ kPa to achieve pile capacities resembling those measured in the tests. Gaydazhiev et al. (2015) attempted to find K_0 , in the sand box by means of flat dilatometer tests (DMT). Eight test sequences were made, each with DMT measurements at depths of 0.30, 0.45, 0.6, 0.75, and 0.9 m with no suction applied. However, the values for a depth of 0.3 m varied between $K_0 = 0$ and $K_0 = 0.6$, while for a depth of 0.9 m the values varied between 0.3 and 3.4. Thus, the dispersion of the results was too large to conclude a specific K_0 -value. Mayne (1992) proposed correlations between K_0 , q_c , and the over-consolidation ratio, OCR .

$$OCR = 5.04K_0^{1.54} \quad (4.1)$$

$$K_0 = \frac{(p_a/\sigma'_v)(q_c/p_a)^{1.6}}{145 \exp\left(\left(\frac{(q_c/p_a)(p_a/\sigma'_v)^{0.5}}{12.2OCR^{0.18}}\right)^{0.5}\right)} \quad (4.2)$$

where p_a is a reference stress (100 kPa), and σ'_v is the vertical effective stress.

However, for the test presented in this thesis, test specific q_c was only found in the saturated sand before each test in order to find the relative density, D_r . With the current test setup it was not possible to have the pile installed, increase the effective vertical stress, and then make CPTs that could reflect the true conditions for the tests. Gaydazhiev et al. (2015) conducted CPTs at different levels of vertical stress increases without a test specimen installed in the sand in the same sand box and with the same sand as the pile load test discussed in this thesis. CPTs were conducted in the sandbox before applying suction to determine the relative density of the sand under the same conditions as it was determined before the pile load tests. The CPTs conducted before applying suction showed average relative densities in the range 82-90 %. Puech & Foray (2002) proposed that for a sand profile with constant relative density, q_c would reach a quasi-stationary value at a critical depth. Gaydazhiev et al. (2015) used this in the interpretation of the CPTs conducted with applied suction as each of the conducted CPTs showed a quasi-stationary value. These values were plotted against the effective vertical stress, and an expression for q_c depending on the vertical effective stress was proposed:

$$q_{c,\text{fitted}} = 5324.1\text{kPa} \left(\frac{\sigma'_v}{1\text{kPa}} \right)^{0.3998} \quad (4.3)$$

Figure 4.6 shows the K_0 and OCR from the CPT as well as the DMT results. The DMT results suggest that the over-consolidation increases with the depth in the sand box perhaps as a result of the soil processing procedure. The CPT results imply that the over-consolidation decreases with increasing vertical effective stresses. This is in contradiction with the findings of the comparison of test results to the finite element model results. Overall, the results do not provide clear conclusions, and a new and more comprehensive study is recommended for future testing in the sand box.

4.1.5 Stress Changes

Measurements of the horizontal stress changes were desirable in the sand box to analyze both the effect of application of suction and to study the stress changes during loading of the pile segment. Measurements should include stress changes at the pile–soil interface, in the sand at different positions away from the pile and at the sand box boundaries. The pile wall was as described very thin and it was not possible to embed normal force transducers or strain gauges in the surface. Moreover, the sand processing procedure made it impossible to place soil stress sensors in the sand. An attempt was made to obtain the horizontal effective stresses directly by means of five FlexiForces force sensors from Tekscan (2010) mounted on an aluminum bar at different

4.2. Summary of Paper A

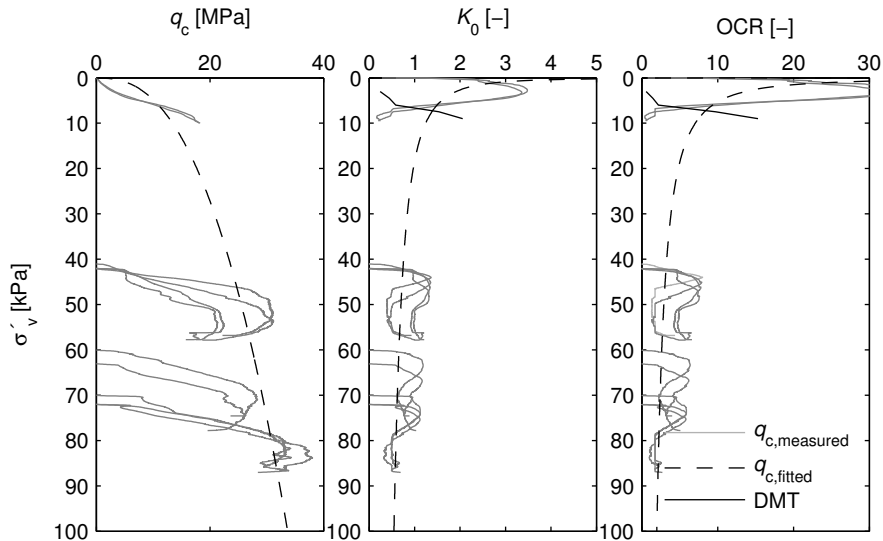


Figure 4.6: q_c from the CPTs conducted with suction applied and from the equation fitted to the results. K_0 and OCR determined from CPT and DMT results.

levels (Figure 4.7). The bar was pressed into the sand before soil preparation. After soil preparation, suction was applied and the corresponding horizontal stress was measured (Figure 4.7). However, the output from the sensors was poor. First of all, the sensors were nearly impossible to calibrate as the output varied from time to time when applying the same load. Secondly, the sensors were very slow in obtaining a steady value and drifted with time, which would make them very difficult to use during cyclic testing where the stress path would change in accordance with the applied load cycles. Due to the insufficiency of the sensors and time constraint in the laboratory, the project of measuring the stresses with the FlexiForce sensors was terminated. Appendix E provides a thorough description of the attempt. No further attempts were made to measure the stress changes.

4.2 Summary of Paper A

Paper A “Laboratory Test Setup for Cyclic Axially Loaded Piles in Sand” presents in detail the chosen test setup and test procedures for conducting static and cyclic loading tests on a pile in tension. The tests were conducted with an open-ended pipe pile segment made of steel with a diameter of 0.5 m almost resembling the pile diameter sizes used offshore. The pile segment length was 1 m which enabled analysis of local interface friction.

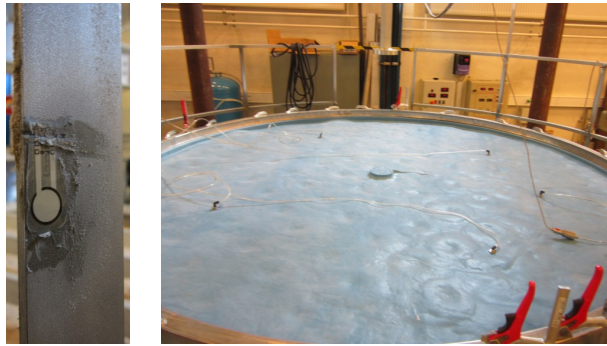


Figure 4.7: FlexiForce sensor attached to the bar (left) and the bar installed in the sand under the membrane with applied suction (right).

The inner dimensions of the sand box in which the tests were conducted was $D_{\text{box}} = 2.5$ m and $H_{\text{box}} = 1.5$ m. The sand layer was 1.2 m deep and consisted of the uniformly graded Aalborg University Sand No. 1. At the bottom of the box was a drainage system consisting of a piping system and 0.3 m of gravel. The pipes were connected to a water inlet, water outlet and an ascension pipe. A felt cloth covered the gravel layer to prevent sand from the superjacent sand layer to enter the drainage system. The drainage system was an important part of the setup as it enabled saturation of the sand which was necessary due to the chosen preparation procedure. An upward hydraulic gradient through the drainage system loosened the sand between tests and enabled installation of the pile segment prior to each test. Vibration of the sand with a rod vibrator after the installation ensured an average relative density of 85 % with depth. This relative density resembled the very dense sand found at some sites of offshore wind turbine farms in the North Sea. The elastic rubber membrane placed on the sand surface, sealed at the sand box edge and the pile head, and connected to a vacuum pump increased the effective vertical stress at the sand surface. With this system, tests with 0, 35, and 70 kPa suction were conducted. During tests with applied suction, nearly all the water was sucked out of the sand leaving the sand layer almost unsaturated. However, this was not thought to affect the results much since the tests were run at slow displacement rate for the static tests and low frequencies for the cyclic tests assumedly preventing any pore pressure build-up if the sand had been saturated.

The test program consisted of both displacement-controlled static tests and load-controlled one-way cyclic loading tests, thus, the load equipment was chosen in order to make these test varieties possible. The static tests were conducted at displacement rates of 0.002 mm/s and stopped when a dis-

4.2. Summary of Paper A

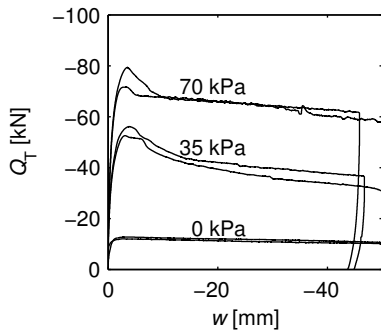


Figure 4.8: Load–displacement curves for the six static tests with surcharges of 0, 35, and 70 kPa.

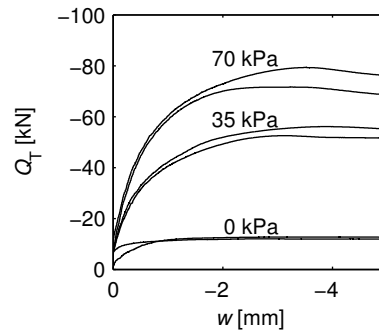


Figure 4.9: Initial part of the load–displacement curves for the six static tests.

placement of 0.05 m was reached. The mean load and load amplitude of the cyclic loading tests were based on the maximum force found from the static tests. The load frequency of the cyclic tests was 0.1 Hz and there was 17,280 applied load cycles corresponding to two days. Each of the cyclic tests was followed by a displacement controlled static tension test if a displacement of 0.05 m was not reached before the cyclic loading sequence ended. The paper presents the results of six static tests conducted with suction level of 0, 35, and 70 kPa as well as two one-way cyclic loading tests conducted without applied suction.

4.2.1 Main Findings

Figures 4.8 and 4.9 present the results of the six static tests and show that the test setup produced repeatable test results and that the shaft capacity increased when the vertical effective stress was increased.

Figures 4.10 and 4.11 present the test results of two cyclic tests conducted at 0 kPa overburden pressure and with different mean load and amplitude. The results showed that the choices of the mean load and load amplitude had great effect on the test outcome. A high mean load and amplitude can result in unstable tests where the failure criterion is reached after only a fraction of the planned load cycles, whereas a small mean load and amplitude can increase the shaft capacity of the pile segment, according to results of post-cyclic static tests. These findings are consistent with findings of, for example, Jardine & Standing (2012), Jardine et al. (2006), Le Kouby et al. (2004), Chan & Hanna (1980).

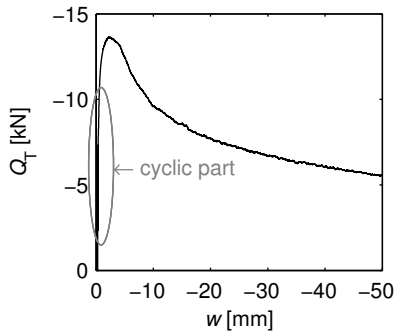


Figure 4.10: Load–displacement curve for a cyclic test at 0 kPa with $Q_{\text{mean}} = 0.4Q_{\text{max static}}$ and $Q_{\text{cyclic}} = 0.2Q_{\text{max static}}$.

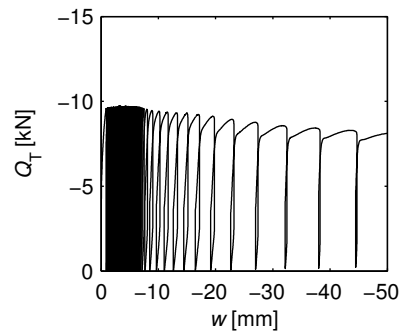


Figure 4.11: Load–displacement curve for a cyclic test at 0 kPa with $Q_{\text{mean}} = 0.4Q_{\text{max static}}$ and $Q_{\text{cyclic}} = 0.4Q_{\text{max static}}$.

4.3 Recommended Improvements

In a novel test setup such as the one presented here, it is possible to make many improvements getting a better understanding of the soil conditions both in-situ and during pile load tests as well as a better understanding of stress changes at the pile–soil interface, in the sand at different positions from the pile, and at the vertical boundaries of the sand box.

To improve the soil conditions and remove some of the uncertainties of the present setup the following studies are proposed

- Determining the relative density of the sand from the cone resistance showed that the soil conditions were the same from one position to another in the sand box. However, it also showed that the relative density varied from around 60 % to almost 100 % with depth. A vibration study is proposed where the vibration penetration rate for the upper part of the sand layer is decreased and for the lower part of the sand layer is increased. This way it may be possible to get a more homogeneous relative density with depth.
- Test specific CPT results for the tests with applied suction could be obtained by making a couple of CPT inlets in the membrane used when the test specimen is installed.
- The sand in the test setup was not replaced at any time during the tests reported in Paper A, Paper C and Paper D, and the assumption was that the sand grains in the soil–pile interface was replaced before each new test due to the sand preparation procedure. Beside the sieve analysis made from sand stuck to the pile wall after eight static tests—reported in Paper C—that showed no changes of the sand grain distribution, no

4.3. Recommended Improvements

investigations were made to support this assumption. It is proposed to conduct a study where sieve analyzes, triaxial tests and examination of the particle shapes are made to analyze the sand characteristics after some rounds of vibration. A study like this will display if the sand should be changes after a certain number of tests to ensure the same soil characteristic for all tests.

- An analysis of the reason for the water being sucked out of the system (problems with sealing or air in the water) should be made. If it is possible to run tests in saturated sand, the pore pressure could be measured in the tests with applied suction and the uncertainties of the effects of nearly saturated soil would be avoided.

To improve the understanding of what happens in the pile–soil interface, the following is suggested:

- Radial and shear stresses could be measured at the pile shaft, in the sand at different distances from the pile and at sand box edge.
- Another attempt to find the coefficient of lateral earth pressure should be made. This could be done with a second round of DMT tests or by measuring the horizontal stress changes.
- Boundary effects could be reduced by applying other boundary conditions. Free field conditions could be simulated in accordance with Huang & Hsu (2005) by using rings of water-filled membranes with the possibility of changing the pressure in the membranes.
- Interface shear tests could be conducted to find the test specific friction angle for the analyzes of the test results.

However, as the main conclusion it should be emphasized that the preliminary test results show that the presented test setup can produce repeatable results and that the results are consistent with other researchers' findings.

Chapter 4. Test Setup and Test Procedure for Pile Load Tests

Chapter 5

Analysis of Pile Load Test Results

This chapter is based on three papers. The first, Paper B (Thomassen et al. 2012), presents a case study for comparison of some of the design methods for the unit skin friction listed in API (2000). Paper C provides the results of the static loading tests and the comparison of the results to some of the existing design methods for offshore driven piles in sand. Paper D presents the results of the cyclic loading tests and an analysis of the results mainly consisting of the influence of mean load and cyclic loading amplitude on the pile behavior. Before the summaries of Paper C and Paper D, some considerations for the analyses of the test results are given. The last section of this chapter lists suggestions for further research with the described test setup.

5.1 Summary Paper B

Paper B “Comparison of Design Methods for Axially Loaded Driven Piles in Cohesionless Soil” (Thomassen et al. 2012) presents three methods for design of driven piles in sand and a comparison of the predictions of these methods based on two uniform soil profiles with different relative densities. The three design methods are the traditional API-00 that is the recommended design method by API (2000) and DNV (2010) and the two CPT-based methods NGI-05 and UWA-05 developed by Clausen et al. (2005) and Lehane et al. (2005*b*), respectively. In 2007 the two CPT-based methods were included in the commentary of API (2000). The general opinion is that the API-00 method gives bad predictions of the capacity for all soil conditions and pile properties and that the CPT-based methods are more reliable because they consider more of the factors influencing the pile capacity. However, the CPT-based

methods are based on rather few onshore pile load tests with very specific site conditions and pile characteristics. Thus, API (2000) recommends carefulness when using the CPT-based methods and extrapolation to conditions for which they are not developed.

The predictions of the three design methods are compared by calculating the capacities of open-ended steel pipe piles with diameters of 1, 2, and 3 m and lengths of 5-85 m. The diameter to wall thickness ratio was 40 for all piles. The relative density, D_r , of the two homogeneous soil profiles was 50 % and 80 %, respectively. The CPT cone resistance, q_c , for the two profiles was computed from the relation between D_r and q_c given by Jamiolkowski et al. (2003). Both the tension and the compression capacity were determined and the results were compared to the database studies of Lehane et al. (2005a).

5.1.1 Main Findings

The results are, not surprisingly, consistent with the results of Lehane et al. (2005a) if the results of API-00 and NGI-05 methods are compared to the predictions of UWA-05 method, which may be the most reliable method because it is based on the largest pile test database and includes most of the factors influencing the pile capacity. For tension piles with a diameter of 1 m installed in dense sand, API-00 predicts lower capacity of short piles (< 20 m) than UWA-05 and DNV-05. DNV-05 predicts the highest capacities of the three methods while UWA predicts capacities that are only about two-thirds of the NGI-05 capacity.

5.2 Test Program

The test setup presented in Paper A was used to perform ten static and eleven cyclic tension tests. The aim of the static tests was to compare the tension capacity to CPT-based design methods and to provide basis for choice of the mean load and cyclic loading amplitude for the one-way cyclic loading tests. The objective of the cyclic loading test program was to analyze the effect of cyclic loading on the shaft capacity and to study which load conditions that are appropriate for jacket pile foundations for offshore wind turbines to comply with the requirements for maximum deflection of the structure. Table 5.1 states the test program that covers different effective vertical stress levels (surcharges) and for the cyclic loading covers variations of mean load and cyclic loading amplitude as well. Appendices F and G show the results of all the conducted tests.

5.3. Considerations for Interpretation of Static Tests

Table 5.1: Test program for static and cyclic loading tests and measured maximum tension force in static tests.

Static tests	Surcharge [kPa]	Q_{max} [kN]	Cyclic tests	Q_{mean} [kN]	Q_{cyclic} [kN]	Surcharge [kPa]	$Q_{max,pc}$ [kN]
T1S0	0	10.2 ¹⁾	T11C0	-4.84	-4.84	0	- ⁴⁾
T2S0	0	13.5	T12C70	-30.12	-30.12	70	-101.5
T3S0	0	11.6	T13C0	-4.84	-2.42	0	-12.4
T4S20	20	31.4	T14C35	-21.66	-21.66	35	-57.2
T5S35	35	- ²⁾	T15C35	-21.66	-10.83	35	-64.8
T6S0	0	11.6 ³⁾	T16C70	-30.12	-15.06	70	-104.3
T7S35	35	56.0	T17C0	-4.84	-2.42	0	-13.7
T8S70	70	79.3	T18C70	-45.18	-30.12	70	- ⁴⁾
T9S70	70	71.2	T19C70	-45.18	-15.06	70	-101.6
T10S35	70	52.3	T20C70	-60.24	-15.06	70	-87.56
			T21C70	-60.24	-22.59	70	- ⁴⁾

Notes:

¹⁾ No distinct peak, not used in the analyses.

²⁾ Membrane broke before termination of test and no result was obtained.

³⁾ The displacement of the pile segment was not recorded, not used in the analyses.

⁴⁾ Pull-out during cyclic loading sequence.

5.3 Considerations for Interpretation of Static Tests

Comparison of the unit skin friction found in the tests to the CPT-based design methods is a difficult task as the CPT-based methods among other things account for the friction fatigue effect emerging from pile installation by driving or jacking. The terms provide a reduction of the radial stress at the pile shaft at a given soil depth as the pile moves further into the ground. This effect was not present in the tests as the soil was processed around the pile after installation. In the comparison of the test results to the two offshore methods, simplified ICP, and offshore UWA, the friction fatigue term is removed from the expressions. However, the test results show much lower values of the unit skin friction than the predictions of these CPT-based methods, which suggests that the radial stress for the test setup is less than the radial stress for a pile segment subjected to installation.

5.4 Summary of Paper C

Paper C “Static Tension Tests on Axially Loaded Pile Segments in Sand” presents the analyses of results of seven static tension tests conducted in the test setup and with the pile segment presented in Paper A. The aim of the tests was to find a unit skin friction at the given vertical effective stress levels from the load-displacement curves and to find an expression linking the cone resistance, q_c , to the found unit skin frictions. Moreover, the unit skin

friction should be compared to the prediction of the unit skin friction given in some of the design methods. From the unit skin friction t - z curves for the tests were determined and compared to existing t - z curve formulations.

A short review of other research showed that it could be expected that when increasing the effective vertical stress in the sand, the tension capacity of the pile segment would increase. It was also expected that dilation at the pile-soil interface would show in the load displacement curves both because of the high relative density with an average value of 85 % and because of the high relative pile-soil interface roughness e.g. (Prai-ai 2013, Mortara et al. 2007). The soil preparation procedure in which the sand was processed by vibration after the installation removed installation effects and could result in a peak and subsequent declination of the load-displacement curves as seen for pile load tests on buried piles Le Kouby et al. (2013). Moreover, the rigid vertical boundaries could cause higher capacities than free field tests on the same pile segment Salgado et al. (1998).

Figure 5.1 presents the comparison of the results to simple finite element models of the tests that indicated that the sand was heavily over-consolidated. This over-consolidation may emerge from the vibration procedure. The finite element models showed that the soil plug inside the pile moved up with the pile in the beginning of the loading sequence and that a cone shaped part of the lower part of the soil plug stopped moving when the displacement of the pile continued. The observation after the tests was that the soil inside the pile segment had moved around 3 cm up during the tests. Thus, the pile segment partially plugged during loading. Through a discussion of these findings, the unit skin friction was determined from the assumption of a fully plugged pile. Thus, only the outer shaft friction was included in the calculations.

Figure 5.2 shows The unit skin friction determined from the test results compared to the traditional design method for finding the unit skin friction, the API-00 method, and also to the CPT-based methods, simplified ICP, and offshore UWA methods developed for offshore design (API 2011). The CPT-based expressions resulted in an expression for the unit skin friction of the presented test results.

Finally, the test results were reformulated to t - z curves and compared to t - z curves found in the literature (Figures 5.3 and 5.4). The t - z curve formulations used in the interpretation were the curve recommended in API (2011), a parabolic function (Randolph & Gourvenec 2011), the Zhang function (Zhang & Zhang 2012), and the 80 % function (Fellenius 2013). The two first are recommended for driven piles in silica sand, while the next is based on pile load tests with various soil conditions such as sand, silt, and clay.

5.4. Summary of Paper C

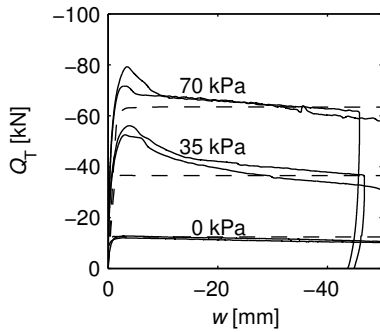


Figure 5.1: Dashed lines are Plaxis results with $K_0 = 3$ for surcharges of 0 and 35 kPa, and with $K_0 = 5$ for a surcharge of 70 kPa. The solid lines are the test results.

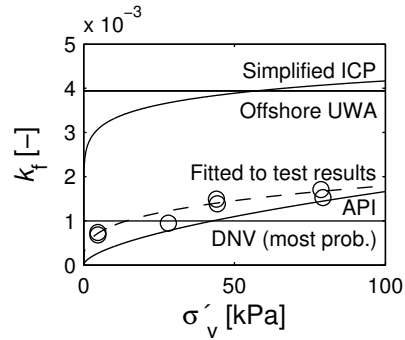


Figure 5.2: k_f factors determined based on the test results, the CPT-based methods, and the API method.

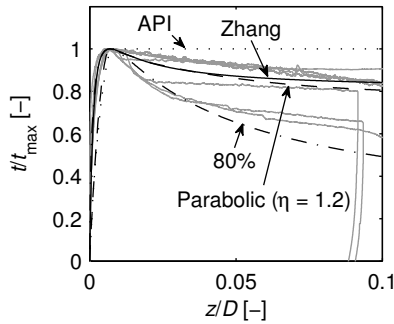


Figure 5.3: t - z curve formulations compared to the t - z curves obtained from the test results (gray).

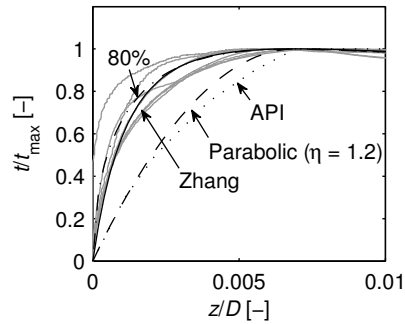


Figure 5.4: Initial part of the t - z curves.

5.4.1 Main Findings

The measured load-displacement curves are in agreement with the expected results of dilation at the interface since the curves for suction levels of 35 and 70 kPa show a distinct peak and all tests show a post peak declination.

Comparison of the test results to results of finite-element models indicated a high over-consolidation of the sand probably due to the soil processing procedure between tests.

Based on the observations during and after the tests, the pile plugged during loading. This behavior is the same as expected for offshore piles and, for example, in the offshore UWA method this mechanism is a premise for the

expression of the unit skin friction.

The unit skin friction shows best correlation with the predictions of the API-00 method even though this method is commonly thought to underestimate the shaft capacity of short pile in dense sand. The Simplified ICP and Offshore UWA gave predictions more than two times higher than the unit skin friction found from the test results. The predictions would have been even higher if the dilation term of the original expressions for ICP-05 and UWA-05 (Jardine et al. 2005, Lehane et al. 2005b) were included as it should have been as the pile diameter was below 1 m.

An expression for the unit skin friction as a function of the CPT cone resistance was suggested based on the expressions for the Simplified ICP and Offshore UWA. As the installation effects were eliminated in the current test setup, the friction fatigue term was removed leaving an expression depending on the effective vertical stress, the end condition of the pile, and the interface friction angle. The effect of dilation was not accounted for in the expression even though the expressions for dilation given by Jardine et al. (2005), Lehane et al. (2005b) suggested a great contribution from dilation due to the soil conditions and pile diameter.

From the analysis of the t - z curves the conclusion was that the Zhang formulation gave the best fit to the curves found from the test results even though this formulation was based on bored piles in various soil conditions.

5.5 Considerations for Interpretation of Cyclic Test

The design codes API (2011) and DNV (2010) state that the effect of cyclic loading should be taken into account for example by using laboratory tests like triaxial tests and direct shear tests. Puech (2013) suggests that interaction diagrams such as proposed by Jardine & Standing (2012) are used in the preliminary design to estimate if a chosen foundation design will be stable for the given soil and load conditions. This particular interaction diagram is based on rather few field tests and small-scale tests in calibration chambers on piles installed in dense sand. Poulos (1988) and Karlsrud et al. (1986) proposed interactions/stability diagrams for other soil conditions. However, the number of cyclic loading tests is scarce, and only a small number of soil conditions and pile parameters have been studied in cyclic pile load tests so far.

5.6 Summary of Paper D

Paper D, “Axial Cyclic Loading Tests on Pile Segments in Sand”, presents the results of eleven one-way cyclic tension tests on the pile segment. The background for the tests was the observation of tilt of offshore wind turbines with jacket pile foundations because of accumulated upward displacements of piles in tension subjected to cyclic loading. The objective of the tests was to analyze the effect of varying mean load and cyclic load amplitude on the shaft capacity, on the accumulated displacements, and on the cyclic unloading and reloading stiffness.

The eleven one-way cyclic loading tests were run at surcharge levels of 0, 35, and 70 kPa. The aim was to conduct both stable and unstable tests at each surcharge level in accordance with the interaction diagram proposed by Jardine & Standing (2012). The mean loads and cyclic loading amplitudes were based on the maximum load of the static tension tests presented by Paper C. Each test sequence consisted of two days of load controlled cycling at a frequency of 0.1 Hz. If the pile segment had not reached the chosen limiting displacement of 60 mm within the two days of cyclic loading, a subsequent displacement controlled test was performed till the limiting value of the displacement was obtained. Figures 5.5 and 5.6 shows the load–displacement curves for a meta-stable and a stable cyclic loading test. The soil was prepared between each test by the soil processing procedure described in Paper A. Thus, none of the tests were influenced by previous loading.

The load, the pile head displacement, the pore pressure (for the tests without surcharge), and the suction level (for the tests with applied surcharge) were measured during the tests. These measurements enabled analyses of the effect of the mean load and cyclic loading amplitude on the shaft capacity, accumulated displacements, and the cyclic stiffness. Moreover, the outcome of the tests was compared to the interaction diagram.

5.6.1 Main findings

The measurements of the pore pressure in the tests without surcharge showed that there was no excess pore pressure during the stable cyclic loading (Figure 5.7). However, the last few cycles of the meta-stable tests ending with large incremental displacements showed pore pressure build-up (Figure 5.8).

The effects on the shaft capacity and the accumulated displacement of varying the cyclic amplitude and the mean load were as follows:

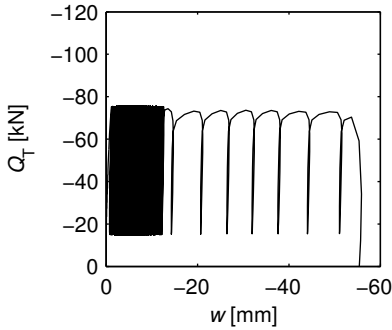


Figure 5.5: Load–displacement curve for Test T19C70.

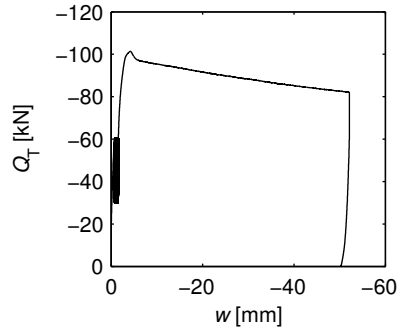


Figure 5.6: Load–displacement curve for Test T18C70.

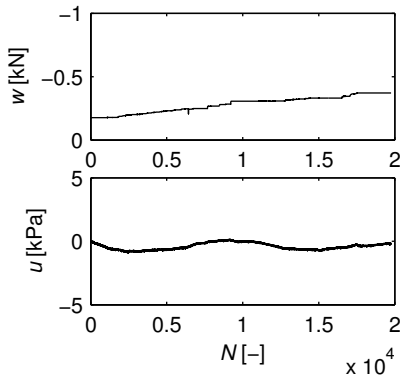


Figure 5.7: Pore pressure measured during the stable test T17C0.

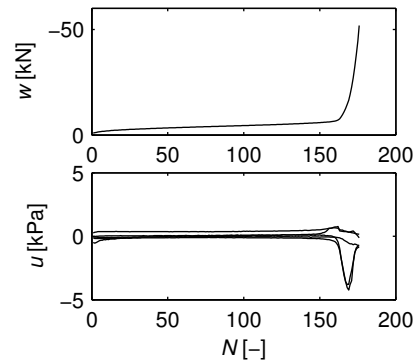


Figure 5.8: Pore pressure measured during the meta-stable test T11C0.

- Both stable and meta-stable conditions—as defined by Jardine & Standing (2012)—where the pile was not pulled out during the cyclic sequence, resulted in shaft capacity gains.
- Small cyclic amplitudes resulted in shaft capacity gain and very small accumulated displacements. This is consistent with findings of Jardine & Standing (2012) and Thomas & Kempfert (2011).
- Increasing the mean load had a negative effect on the accumulated displacements and eventually led to unstable conditions (Figure 5.9).
- Increase of the load amplitude led to more rapid degradation of the shaft capacity and faster accumulation of displacements than a similar increase of the mean load (Figure 5.9). These findings match the observations of Thomas & Kempfert (2011) and Chan & Hanna (1980).

5.6. Summary of Paper D

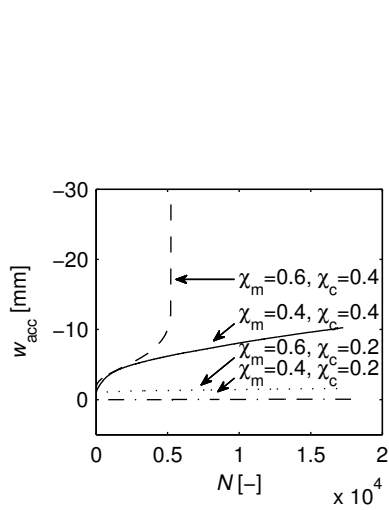


Figure 5.9: Accumulated displacements during the cyclic load sequences of tests T12C70 ($\chi_m = 0.4$, $\chi_c = 0.4$), T16C70 ($\chi_m = 0.4$, $\chi_c = 0.2$), T18C70 ($\chi_m = 0.6$, $\chi_c = 0.4$) and T19C70 ($\chi_m = 0.6$, $\chi_c = 0.2$).

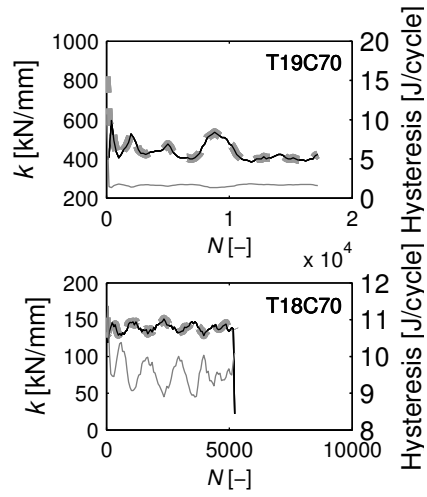


Figure 5.10: Unloading stiffness, k_{un} , (dashed gray line), reloading stiffness, k_{re} , (solid black line), and hysteresis (solid gray line) for the stable test T19C70 and the meta-stable test T18C70.

The cyclic stiffness was evaluated based on the secant stiffness of the unloading and reloading curves. Except for the first few cycles in all the tests and the last few cycles in the meta-stable tests, the unloading and reloading stiffness were nearly identical and remained constant during the tests. In the meta-stable tests, the unloading stiffness remained constant throughout the test but the reloading stiffness decreased drastically in the last few cycles with large displacements in each cycle. The stiffness varied with cyclic loading amplitude which is consistent with observations of Rimoy (2013). The hysteresis of the load cycles increased when the stiffness decreased. Figure 5.10 displays the variations of the stiffness and hysteresis during a stable and a meta-stable test.

Comparison to the interaction diagram proposed by Jardine & Standing (2012) suggested that the maximum static tension load used as preference for the chosen cyclic loading sequences should have been found from static tests with preliminary cyclic loading to simulate the influence of the serviceability load condition on the shaft capacity. If the maximum load from the pre-cyclic static tests were used in the comparison of test results to the interaction diagram, the results matched the limits for stable, meta-stable, and unstable conditions fairly well.

5.7 Recommendations for Future Research

From the analyses of the static loading tests, it was evident that the friction fatigue term included in the CPT based design methods for the unit skin friction complicated the comparison to the test results. The term accounts for the effect of pile installation by driving (UWA-05) or jacking (ICP-05). In the comparison, the term was excluded from the design methods, but if the maximum value of the h/D ratio given in UWA-05 is used, the method provides shaft capacities closer to the test results than if the term is disregarded. This suggests that the soil processing procedure used in the tests has a more negative effect on the interface shear strength than pile driving. However, it is unknown whether this is the cause for the low capacities in the test results compared to the design methods, and an analysis of the interface conditions within the test setup is recommended.

The pore pressure measurements in the meta-stable cyclic loading tests conducted without surcharge showed pore pressure build-up in the last few cycles with large incremental displacements. If it was possible to improve the test setup in such a way that the water is not sucked out of the sand box in the tests with surcharge, it would be interesting to analyze the effect of the pore pressure build up.

It would be interesting with a study revealing the effect of the number of cycles on the shaft capacity, as would a study with varying cyclic amplitudes and mean loads through a load series to simulate a true load sequence. The effect of the cyclic frequency is another interesting study.

Chapter 6

Conclusions and Recommendations for Future Research

Planning of future offshore wind farms on sites with deeper waters leads to an increasing use of jacket pile foundations for wind turbines. An observation of tilt of offshore wind turbines installed in dense sand indicates that the design of piles in tension for this soil condition and subjected to cyclic loading is not examined well enough. The aim of this thesis was to analyze the effect of cyclic loading on the pile shaft capacity by conducting pile load tests in a laboratory test setup. The objective of the test setup was to model the pile-soil interface as close to reality as possible to reduce some of the scale effects normally seen in calibration chamber or centrifuge tests.

6.1 Conclusions

A test setup following the requirements stated in Scope of the Thesis was successfully constructed. The following criteria were met:

- The open-ended pipe pile had a diameter of 0.5 m that is much closer to full-scale pile diameters than diameters of pile specimens normally used in calibration chamber pile load tests.
- The sand box size limited the pile length to 1 m. However, only tension load tests were conducted and, thus, the contribution from the end bearing of the pile segment was negligible.
- The membrane–vacuum system made it possible to increase the vertical effective stress to different levels. With the short pile diameter the test

results could be interpreted as results of 1 m pile segment at different soil depths.

- The loading system enabled variation of the loading conditions (load and displacement controlled tests, rate of penetration or load, cyclic loading with different mean load, load amplitude, and frequency).
- Most importantly the test results showed that the test setup could produce repeatable results.

The load–displacement curves obtained in the static displacement-controlled tension tests showed the following:

- A peak occurring in the load–displacement curve after few millimeters of displacement indicated dilation at the pile–soil interface during loading. Dilation was expected because of the dense sand and the high relative roughness of the interface.
- Because of the rigidity of the pile specimen, the unit skin friction was found directly from the measured tension force. The unit skin frictions from the tests were found to be much lower than the predictions of the CPT–based design methods. This could be caused by the fact that the friction fatigue term was removed from the design method expressions in the analysis providing the largest possible prediction of the unit skin friction for the comparison. This implies that the sand processing procedure used after installation of the pile segment provides a rather weak pile–soil interface.
- t - z curves were found for all tests and compared to existing formulations. The test results showed more consistency with formulation based on tests on bored piles in different soil conditions than with formulations for driven piles in sand.

The one-way cyclic loading tests were load–controlled with the same mean load and cyclic load amplitude applied for a period of two days with a cyclic frequency of 1 Hz. The mean load and the amplitude were based on the maximum tension force measured in the static tests. The following observations were made from the cyclic tests:

- Low cyclic amplitudes led to increase of the static pull-out capacity of the pile segment. Increase of the mean load or the load amplitude reduced the number of cycles to failure and increased the accumulated displacement. Increase of the amplitude led to more rapid degradation than an equivalent increase of the mean load.
- The unloading and reloading stiffness were almost identical throughout the tests. However, the reloading stiffness dropped drastically with the last few cycles of the meta-stable tests ending with pull-out where the incremental displacements were high. The stiffness was dependent on

6.2. Recommendations for Future Work

the load amplitude—lower amplitudes gave higher stiffness—and was almost constant throughout the tests. The hysteresis of each load cycle increased as the stiffness decreased.

- The meta-stable tests conducted at surcharge levels of 0 kPa in fully saturated sand showed pore pressure build-up in the last few cycles with large incremental displacements.
- Comparison of the behavior of the tests (stable, meta-stable, and unstable) was not entirely consistent with the Jardine & Standing (2012) interaction diagram.

6.2 Recommendations for Future Work

The following is divided in recommendations for future work with the test setup used in this thesis and in recommendations for other types of research that can be conducted to improve the understanding of axially loaded piles.

6.2.1 Recommendations for the Test Setup

A new test setup has limitations and a number of improvements can be suggested:

- As the sand is not replaced between tests, the soil conditions should be monitored more closely by means of e.g. sieve analyzes and triaxial tests so as to see the effect of soil vibration and pile load testing and to determine if it is necessary to replace the sand more frequently.
- Investigation of the effect of saturation could be made, but this requires development of a method for avoiding the water to get sucked out of the sand box prior to tests with applied suction.
- To improve the understanding and analysis of the test results, measurements of the stress changes at the pile-soil interface, at the sand box boundary, and in the soil at different distances from the pile would provide information about boundary conditions, the coefficient of lateral earth pressure, dilation in the interface, and installation effects.
- The boundary conditions could be changed to enable simulation of free-field conditions (BC5) with any degree of over-consolidation.
- Interface shear test would provide test specific values of the interface friction angle.

If the above recommendations are followed, the test setup provides good potential for analyzes of the following:

- Effect on the shaft capacity of the number of load cycles, cyclic frequency, and load sequences with varying mean load and loading amplitude.

- Tests with other soil types (requires laboratory tests to determine new correlation between the CPT cone resistance and the relative density, friction angle, and dilation angle).
- Investigation of conditions inside the pile regarding plugging and outside the pile regarding arching.

6.2.2 Proposed Research

The state-of-the-art review revealed that even though quite a lot of research within the field of axially loaded piles has been carried out, more research is still needed to cover more soil types, in situ stresses before and after installation, pile characteristics, and load conditions. Especially more research about the effect of cyclic loading and ageing is required in order to improve the design methods. The following research would improve the understanding of the pile shaft capacity:

- Full-scale tests on instrumented piles to provide information about effects of installation, ageing, and load conditions. The piles should be instrumented to enable separation of the end bearing and shaft capacity, and to provide stress and strain measurements at different levels of the pile.
- Different interface shear tests could provide more information on the interface friction angle and volume changes under various characteristics of soil, surface, and load.
- The results of interface shear tests could be used to develop constitutive models for the pile-soil interface behavior. These models could be used in either analytical or numerical models to analyze the bearing capacity, displacement, and stiffness of a jacket pile foundation.
- More research involving numerical modeling is needed to extrapolate the current knowledge to other soil, pile, and load conditions.

The above recommendations and suggestions could end up in interaction diagrams that account for various design conditions. These diagram would be a powerful tool in the preliminary design of offshore wind turbine foundations.

References

- Abdel-Rahman, K. & Achmus, M. (2011), Behavior of foundation piles of offshore wind energy plants under axial cyclic loading, *in* 'SIMULIA Customer Conference'.
- Abdel-Rahman, K., Achmus, M. & Kuo, Y.-S. (2014), A numerical model for the simulation of pile capacity degradation under cyclic axial loading, *in* 'Numerical Methods in Geotechnical Engineering (NUMGE2014)', Hicks, M.A and Brinkgreve, R.B.J. and Rohe, A., CRC Press, Taylor & Francis Group, pp. 563–568.
- Al Douri, R., Hull, T. & Poulos, H. (1993), 'Influence of test chamber boundary conditions', *Geotechnical Testing Journal* **16**(4), 550–562.
- API (2000), *Recommended Practice for Planning, Designing and Constructing Fixed Offshore Platforms – Working Stress Design*, American Petroleum Institute.
- API (2011), *Geotechnical and Foundation Design Considerations*, API RP 2GEO, 1. ed. edn, American Petroleum Institute.
- Augustesen, A. (2006), *The Effects of Time on Soil Behaviour and Pile Capacity*, PhD Thesis, Aalborg University.
- Axelsson, G. (2000), Set-up of driven piles in sand: The effect of constrained dilatancy on the shaft behaviour during loading, *in* 'Proceedings of the International Conference on Geotechnical and Geological Engineering (Geo-Eng2000)'.
- Baeßler, M., Rücker, W., Cuéllar, P., Georgi, S. & Karbeliov, K. (2013), 'Large-scale testing facility for cyclic axially loaded piles', *Steel Construction* **6**(3), 200–206.
- Bellotti, R., Crippa, V., Pedroni, S. & Ghionna, V. N. (1988), Saturation of sand specimen for calibration chamber tests, *in* 'Proceedings of the International Symposium on Penetration Testing (ISOPT-1)', pp. 661–672.

- Böker, C. (2009), *Load simulation and local dynamics of support structures for offshore wind turbines*, PhD Thesis, Leibnitz Universität Hannover.
- Boulon, M. (1989), 'Basic features of soil structure interface behaviour', *Computers and Geotechnics* **7**, 115–131.
- Chan, S.-F. & Hanna, T. (1980), 'Repeated loading on single piles in sand', *Journal of the Geotechnical Engineering Division* **106**(2), 171–188.
- Chow, F. (1997), *Investigations into displacement pile behaviour for offshore foundations*, PhD Thesis, University of London, Imperial College.
- Chow, F., Jardine, R., Brucy, F. & Nauroy, J. (1998), 'Effects of time on capacity of pipe piles in dense marine sands', *Journal of Geotechnical and Geoenvironmental Engineering* **124**(3), 254–264.
- Christenson, J. & Scott, F. (1993), *Axially-loaded centrifuge pile tests.*, OSAPR Project 13, American Petroleum Institute.
- Clausen, C., Aas, P. & Karlsrud, K. (2005), Bearing capacity of driven piles in sand, the NGI approach, in S. Gourvenec & M. Cassidy, eds, 'Proceedings of the International Symposium on Frontiers in Offshore Geotechnics (ISFOG 2005)', Taylor & Francis Group, p. 677–681.
- Coyle, H. & Sulaiman, I. (1967), 'Skin friction for steel piles in sand', *Journal of the Soil Mechanics and Foundation Division* pp. 261–278.
- CUR (2001), *Bearing capacity of steel pipe piles.*, Report 2001-8, Centre for Civil Engineering Research and Codes.
- De Nicola, A. & Randolph, M. (1993), 'Tensile and compressive shaft capacity of piles in sand', *Journal of Geotechnical Engineering* **119**(12), 1952–1973.
- De Nicola, A. & Randolph, M. (1999), 'Centrifuge modelling of pipe piles in sand under axial loads', *Géotechnique* **49**(3), 295–318.
- DNV (2010), *DNV-OS-J101–Design of offshore structures*, Det norske Veritas Classification A/S.
- European Commission (2010), *COMMUNICATION FROM THE COMMISSION TO THE EUROPEAN PARLIAMENT, THE COUNCIL, THE EUROPEAN ECONOMIC AND SOCIAL COMMITTEE AND THE COMMITTEE OF THE REGIONS. Energy 2020 A strategy for competitive, sustainable and secure energy. COM(2010) 639 final*, European Commission.
- European Commission (2014), *COMMUNICATION FROM THE COMMISSION TO THE EUROPEAN PARLIAMENT, THE COUNCIL, THE EUROPEAN ECONOMIC AND SOCIAL COMMITTEE AND THE COMMITTEE*

References

- OF THE REGIONS. *A policy framework for climate and energy in the period from 2020 to 2030*. COM(2014) 015 final, European Commission.
- EWEA (2009), *Oceans of Opportunity - Harnessing Europe's largest domestic energy resource*, European Wind Energy Association.
- EWEA (2015), *WIND IN POWER: 2014 EUROPEAN STATISTICS*, European Wind Energy Association.
- Fellenius, B. (2013), 'Discussion on Zhang, Q.Q. and Zhang, Z.M. (2012). "A simplified non-linear approach for single pile settlement analysis."', *Canadian Geotechnical Journal* **50**(6), 685–687.
- Foglia, A., Ibsen, L. & Andersen, L. (1991), An innovative physical model for testing bucket foundations, in 'Proceedings of the 16th Nordic Geotechnical Meeting', Copenhagen, Denmark, p. 323–330.
- Foray, P. (1991), Scale and boundary effects on calibration chamber pile tests, in 'Proceeding of the 1st International Symposium on Calibration Chamber Testing (ISOCCT1)', Elsevier, p. 147–160.
- Gavin, K., Igoe, D. & Kirwan, L. (2012), 'The effect of ageing on the axial capacity of piles in sand', *Geotechnical Engineering* **166**(GE2), 122–130.
- Gaydazhiev, D., Puscasu, I., Vaitkunaite, E. & Ibsen, L. (2015), Investigation of dense sand properties in shallow depths using CPT and DMT, in 'Proceedings of the 3rd International Conference on the Flat Dilatometer', International Society for Soil Mechanics and Geotechnical Engineering, p. 223–230.
- Ghionna, V. & Jamiolkowski, M. (1991), A critical appraisal of calibration chamber testing of sands, in 'Proceedings of the 1st International Symposium on Calibration Chamber Testing/ISOCCT1', Elsevier, p. 13–39.
- Hedegaard, J. & Borup, M. (1993), *Klassifikationsforsøg med Baskarp Sand No. 15*, Aalborg University, Denmark.
- Ho, T., Jardine, R. & Anh-Minh, N. (2011), 'Large-displacement interface shear between steel and granular media', *Géotechnique* **61**(3), 221–234.
- Huang, A.-B. & Hsu, H.-H. (2005), 'Cone penetration tests under simulated field conditions', *Géotechnique* **55**(5), 345–354.
- Ibsen, L., Hanson, M., Hjort, T. & Thaarup, M. (1994), *Baskarp Sand No. 15*, Data Report 9301, Aalborg University, Denmark.

- Jamiolkowski, M., Lo Presti, D. & Manassero, M. (2003), Evaluation of relative density and shear strength of sands from CPT and DMT, in 'Soil Behaviour and Soft Ground Construction: Geotechnical Special Publication No. 119', ASCE 2003, pp. 201–238.
- Jardine, R., Bitang, Z., Foray, P. & Dalton, C. (2009), 'Experimental arrangements for investigation of soil stresses developed around a displacement piles', *Soils and Foundations* 49(5), 661–673.
- Jardine, R., Chow, F., Overy, R. & Standing, J. (2005), *ICP design methods for driven piles in sands and clays*, Thomas Telford.
- Jardine, R., Lehane, B. & Everton, S. (1992), Friction coefficients for piles in sands and silts, in 'Proceedings of the International Conference on Off-shore Site Investigation and Foundation Behaviour', Society for Underwater Technology, Springer Netherlands, p. 661–677.
- Jardine, R. & Standing, J. (2000), *Pile load testing performed for HSE cyclic loading study at Dunkirk, France. Volume 1 & 2.*, Offshore Technology Report OTO 2000 007, Health and Safety Executive, London, UK.
- Jardine, R. & Standing, J. (2012), 'Field axial cyclic loading experiments on piles driven in sand', *Soils and Foundations* 52(4), 723–736.
- Jardine, R., Standing, J. & Chow, F. (2006), 'Some observations of the effect of time on the capacity of piles driven in sand', *Géotechnique* 56(4), 227–244.
- Johnston, I., Lam, T. & Williams, A. (1987), 'Constant normal stiffness direct shear testing for socketed pile design in weak rock', *Géotechnique* 37, 83–89.
- Karlsrud, K., Nadim, F. & Haugen, T. (1986), Piles in clay under cyclic axial loading: field test and computational modelling, in 'Proceedings of the 3rd International Conference on Numerical Methods in Offshore Piling', pp. 165–190.
- Kelly, R. (2001), *Development of a Large Diameter Ring Shear Apparatus and its use for Interface Testing*, PhD Thesis, University of Sydney.
- Kishida, H. & Uesugi, M. (1987), 'Tests of the interface between sand and steel in the simple shear apparatus', *Géotechnique* 37(1), 45–52.
- Kolk, H., Baaijens, A. & Senders, M. (2005), Design criteria for pipe piles in silica sands, in S. Gourvenec & M. Cassidy, eds, 'Proceeding of the International Symposium on Frontiers in Offshore Geotechnics (ISFOG 2005)', Taylor & Francis Group, p. 711–716.

References

- Larsen, K. (2008), *Static Behaviour of Bucket Foundations, Vol. 2: Static Behaviour of Bucket Foundations : test results from laboratory tests*, PhD Thesis, Aalborg University.
- Le Kouby, A., Canou, C. & Dupla, J. (2004), Behaviour of model piles subjected to cyclic axial loading, in 'Proceedings of the International Conference Cyclic Behaviour of Soils and Liquefaction Phenomena', Taylor & Francis Group, London, UK, p. 159–166.
- Le Kouby, A., Dubla, J., Canou, J. & Francis, R. (2013), 'Pile response in sand: experimental development and study', *International Journal of Physical Modelling in Geotechnics* **13**(4), 122–137.
- LeBlanc, C. (2009), *Design of Offshore Wind Turbine Support Structures: Selected topics in the field of geotechnical engineering*, PhD Thesis, Aalborg University.
- Lehane, B., Jardine, R., Bond, A. & Frank, R. (1993), 'Mechanisms of shaft friction on sand from instrumented pile tests', *Journal of Geotechnical Engineering* **119**(1), 19–35.
- Lehane, B., Schneider, J. & Xu, X. (2005a), *A Review of Design Methods for Offshore Driven Piles in Siliceous Sand*, The University of Western Australia.
- Lehane, B., Schneider, J. & Xu, X. (2005b), The UWA-05 method for prediction of axial capacity of driven piles in sand, in S. Gourvenec & M. Cassidy, eds, 'Proceeding of the International Symposium on Frontiers in Offshore Geotechnics (ISFOG 2005)', Taylor & Francis Group, p. 661–667.
- Leth, C., Krogsbøll, A. & Hededal, O. (2008), Centrifuge facilities at Technical University of Denmark, in 'Proceedings of the Nordic Geotechnical Meeting No. 15', Norwegian Geotechnical Society, Sandefjord, Norway.
- Li, Z., Bolton, M. & Haigh, S. (2012), 'Cyclic axial behaviour of piles and pile groups in sand', *Canadian Geotechnical Journal* **49**, 1074–1087.
- Loria, A., Orellana, F., Minardi, A., Fürbringer, J.-M. & Laloui, L. (2015), 'Predicting the axial capacity of piles in sand', *Computers and Geotechnics* **96**, 485–495.
- Lunne, T., Robertson, P. & Powell, J. (1997), *Cone Penetration Testing in Geotechnical Practice*, Blackie Academic and Professional.
- Mayne, P. (1992), Tentative method for estimating σ'_{h0} from q_c data in sands, in 'Proceedings of the International Symposium on Calibration Chamber Testing', Potsdam, New York, p. 249–256.

- Mortara, G., Mangiola, A. & Ghionna, V. (2007), 'Cyclic shear stress degradation and post-cyclic behaviour from sand-steel interface direct shear tests', *Canadian Geotechnical Journal* **44**, 739–752.
- Olson, R. & Al-Shafei, K. (1988), Axial load capacities of steel pipe piles in sand, in 'Proceedings of the 2nd International Conference on Case Histories in Geotechnical Engineering', p. 1731–1738.
- Peng, S., NG, C. & Zheng, G. (2014), 'The dilatant behaviour of sand-pile interface subjected to loading and stress relief', *Acta Geotechnica* **9**, 425–437.
- Poulos, H. (1988), 'Cyclic stability diagram for axially loaded piles', *Journal of Geotechnical and Geoenvironmental Engineering* **114**(8), 877–895.
- Prai-ai, S. (2013), *Behaviour of soil-structure interfaces subjected to a large number of cycles. Application to piles*, PhD Thesis, University of Grenoble.
- Puech, A. (2013), Advances in axial cyclic pile design: Contribution of the SOLCYP project, in 'Proceedings of TC 209 Workshop - 18th ICSMGE', Paris, France, pp. 45–57.
- Puech, A. & Foray, P. (2002), Refined model for interpreting shallow penetration cpts in sands, in 'Offshore Technology Conference', Houston, Texas USA.
- Randolph, M. (2012), Offshore design approaches and model tests for sub-failure cyclic loading of foundations, in C. Di Prisco & D. Wood, eds, 'Mechanical Behaviour of Soils Under Environmentally Induced Cyclic Loads', Springer Wien New York, pp. 441–480.
- Randolph, M. & Gourvenec, S. (2011), *Offshore Geotechnical Engineering*, Spon Press.
- Rimoy, S. (2013), *Ageing and Axial Cyclic Loading Studies of Displacement Piles in Sand*, PhD Thesis, Imperial College London.
- Robertson, P. & Campanella, R. (1983), 'Interpretation of cone penetrometer test: Part I: Sand', *Canadian Geotechnical Journal* **20**(4), 718–733.
- Salgado, R., Mitchell, J. & Jamiolkowski, M. (1998), 'Calibration chamber size effects on penetration resistance in sand', *Journal of Geotechnical and Geoenvironmental Engineering* **124**(9), 878–887.
- Schmertmann, J. (1978), *Guidelines for Cone Penetration Test, Performance and Design*, FHWA-TS-78-209, US Federal Highway Administration.
- Schnaid, F. & Houlsby, G. (1991), 'An assessment of chamber size effects on the calibration of in situ tests in sand', *Géotechnique* **41**(3), 437–445.

References

- Silva, M., Foray, P., Rimoy, S., Jardine, R., Tshusa, C. & Yang, Z. (2013), Influence of cyclic axial loads on the behaviour of piles driven in sand, in 'Proceedings of TC 209 Workshop – 18th ICSMGE, Paris September 4th 2013, Design for cyclic loading: Piles and other foundations', Paris, France, pp. 81–84.
- Silver, L. & Seed, B. (1971), 'Volume changes in sands during cyclic loading', *Proc. of the American Society of Civil Engineers* **97**(SM9), 1171–1182.
- Sørensen, J. & Sørensen, J., eds (2011), *Wind energy systems - Optimising design and construction for safe and reliable operation*, Woodhead Publishing.
- Tekscan (2010), *Tekscan FlexiForce® Sensor User Manual*, Tekscan.
- Thomas, S. & Kempfert, H.-G. (2011), 'Untersuchung des Pfahltragverhaltens infolge zyklischer axialer Einwirkungen in einer Spannungszelle', *Pfahl-Symposium 2011* **94**, 139–158.
- Thomassen, K., Andersen, L. & Ibsen, L. (2012), Comparison of design methods for axially loaded driven piles in cohesionless soil, in 'Proceedings of the 22nd International Offshore and Polar Engineering Conf. (ISOPE2012)', International Society of Offshore and Polar Engineers, Rhodes, Greece, pp. 705–712.
- Thomassen, K., Roesen, H., Sørensen, S. & Ibsen, L. (2011), Small-scale testing of laterally loaded monopiles in sand, in 'Symposium Proceedings: 64th Canadian Geotechnical Conference and 14th Pan-American Conference on Soil Mechanics and Eng., 5th Pan-American Conference on Teaching and Learning of Geotechnical Engineering', Pan-AM CGS Geotechnical Conference, Toronto, Ontario, Canada.
- Tsuhua, C., Foray, P., Jardine, R., Yang, Z., Silva, M. & Rimoy, S. (2012), 'Behaviour of displacement piles in sand under cyclic axial loading', *Soils and Foundations* **52**(3), 393–410.
- Uesugi, M. & Kishida, H. (1986), 'Influential factors of friction between steel and dry sand', *Soils and Foundations* **26**(2), 33–46.
- Uesugi, M., Kishida, H. & Tsubakihara, Y. (1989), 'Friction between sand and steel under repeated loading', *Soils and Foundations* **29**(3), 127–137.
- Vindmølleindustrien (2015), 'Energipolitik og planlægning. Offshore.', http://www.windpower.org/da/energipolitik_og_planlaegning/offshore.html.
- White, D. & Bolton, M. (2004), 'Displacement and strain paths during plane-strain model pile installation in sand', *Géotechnique* **54**(6), 375–397.

- White, D. & Lehane, B. (2004), 'Friction fatigue on displacement piles in sand', *Géotechnique* **54**(10), 645–658.
- White, D., Schneider, J. & B.M., L. (2005), The influence of effective area ratio on shaft friction displacement piles in sand, *in* 'Proceedings of the 1st International Symposium on Frontiers in Offshore Geotechnics (ISFOG)', p. 741–747.
- White, D. & Zhao, Y. (2006), A model-scale investigation into 'set-up' of displacement piles in sand, *in* '6th International Conference on Physical Modelling in Geotechnics', Hong Kong, China.
- Yang, Z., Jardine, R., Zhu, B., Foray, P. & Tsuha, C. (2010), 'Sand grain crushing and interface shearing during displacement pile installation in sand', *Géotechnique* **60**(6), 469–482.
- Zhang, Q. & Zhang, Z. (2012), 'A simplified non-linear approach for single pile settlement analysis', *Canadian Geotechnical Journal* **49**(11), 1256–1266.
- Zhu, B., Jardine, R. & Foray, P. (2009), 'The use of miniature stress measuring cells in laboratory applications involving stress reversals', *Soils and Foundations* **49**(5), 675–688.

APPENDIX

Appendix A

Laboratory Test Setup for Cyclic Axially Loaded Piles in Sand

Kristina Thomassen
Lars Bo Ibsen
Lars Vabbersgaard Andersen

The paper has been submitted and is under review for
Geotechnical Testing Journal
April, 2015

The layout has been revised.

Abstract

This paper presents a comprehensive description and the considerations regarding the design of a new laboratory test setup for testing cyclic axially loaded piles in sand. The test setup aims at analyzing the effect of axial one-way cyclic loading on pile capacity and accumulated displacements. Another aim was to test a large diameter pile segment with dimensions resembling full-scale piles to model the interface properties between pile and sand correctly. The pile segment was an open-ended steel pipe pile with a diameter of 0.5 m and a length of 1 m. The sand conditions resembled the dense sand conditions found several places in the North Sea. To simulate various vertical effective stress states, an elastic rubber membrane was placed on the soil surface and connected to a vacuum system, thus, increasing the effective stresses in the sand. A custom-made CPT device was used to confirm equal soil conditions for all tests. For verifications purposes six static tension tests conducted at three different vertical effective stress levels of 0, 35 and 70 kPa. The load-displacement curves showed that the test setup provides repeatable test results. A preliminary comparison between the unit shaft friction determined from the API RP 2GEO standard and from the test results indicated overconsolidation of the sand. Two initial one-way cyclic loading tests provided results of effects on pile capacity and accumulated displacements in agreement with other researchers' test results.

A.1 Introduction

Because of today's focus on the need for renewable energy, several offshore wind farms are under construction and more are planned for future installation. Much activity of this kind can be seen in the North Sea near the coasts of Denmark, Germany and Great Britain. For many of the existing and future sites, the soil conditions are dense to very dense sands. Some of these offshore wind turbines are installed on three or four legged jacket structures. The oil and gas industry have used jacket foundations for a long time and the design methods for piles loaded in compression are well examined. These design methods are now used when determining the bearing capacity of offshore wind turbine foundations. However, wind turbines are very light structures which can result in piles loaded in tension. The situation of piles cyclically loaded in tension is not well examined and pull-out of the piles may be a risk for the wind turbines. Pull-out of some of the piles in a foundation may result in irrecoverable tilt of the wind turbine. Therefore, it is of great interest to examine the behavior of piles cyclically loaded in tension.

The effect of cyclic loading on axially loaded piles in sand has been studied by means of both full-scale and small-scale testing. Jardine & Standing (2000, 2012) as well as Baeßler et al. (2013) performed full-scale cyclic loading tests.

Small-scale testing is less expensive than full-scale testing and, thus, has been conducted to a greater extent than full-scale testing. Amongst others, Chan & Hanna (1980), Le Kouby et al. (2004), and Thomas & Kempfert (2011) used calibration chamber tests to study the effect of one-way and two-way cyclic loading with different mean loads and load amplitudes on the pile capacity. The common characteristics of these test setups are the size and design of the test segments more similar to a CPT device than to a full-scale open-ended pipe pile. Moreover, the tests are conducted at 1G with an overburden pressure applied to the sand surface to increase the effective stresses by means of water or air filled pressurized membranes under fixed plates. At Aalborg University another type of test setup is used for small-scale testing at 1G. Instead of applying an overburden pressure, an elastic rubber membrane is placed on the soil surface and suction is applied. Foglia et al. (1991) and Vaitkunaite et al. (2014) used this method for experimental testing of horizontally and axially loaded suction buckets, respectively.

The intention was to construct and use a similar test setup to conduct medium-scale testing of an axially, cyclically loaded pile segment to investigate the pile-soil interaction at one-way cyclic tension loading. Medium scale implies a pile segment with a diameter of 0.5 m, close to the diameter of full-scale piles. As the test setup cannot accommodate a full pile with this diameter, the segment was only 1 m long. By simulating one meter of soil and pile at a time, it was an aim to enable analysis of a distinct t - z curve for each simulated depth.

This paper focuses on a detailed description of the test setup and test procedures. The following section presents the factors influencing the axial pile capacity when conducting small-scale testing. A discussion of these factors leads to argumentation for the chosen design. The result sections present the results of six static tests and two cyclic loading tests to verify the usability of the test setup. Advantages and limitations of the test setup are discussed. Finally, conclusions are drawn and recommendations for future work with the test setup are given.

A.2 Objectives of Test Setup

Design of a proper test setup necessitates discussion of the factors influencing the targeted test results. For small-scale testing of axially cyclically loaded piles, the influencing factors include:

- Scaling effects.
- Pile design (dimensions, material).

A.3. Pile Segment

- Test setup design (boundary effects, stress variation).
- Soil conditions (soil characteristics, relative density, saturation).
- Installation method.
- Load conditions (compression/tension, two-way and one-way cyclic loading, load/displacement controlled, amplitude, mean load, frequency, number of cycles).

The objective of the test setup described in the following was to enable investigation of the effect of cyclic loading on the pile shaft resistance of a pile segment which has a diameter comparable to full-scale, i.e. a diameter of at least 0.5 m, at conditions corresponding to service mode of an offshore wind turbine. Thus, at the time of testing, the pile segment should be unaffected by the installation procedure e.g. by preparation of the soil to match the targeted soil properties after installation. A pile segment with a length of 1 m was considered and as such, the principle in the test is not to model the full pile but only part of it. By increasing the effective stresses within the soil in the test setup, the idea was to simulate 1 m pile at different soil depths. Moreover, it should be possible to run both load and displacement controlled tests. During the tests, the applied loads, the pile head displacement and the effective stresses at the soil surface should be recorded.

A.3 Pile Segment

The pile segment illustrated in Figure A.1 had the dimensions $L_{\text{pile}} = 1$ m and $D_{\text{pile}} = 0.5$ m. According to Randolph & Gourvenec (2011) the smallest offshore piles have a diameter of around 0.76 m and vary in diameter to wall thickness ratios between 25 and 100. Thus, the diameter of the pile segment was much closer to full scale than piles normally used in small-scale tests. The pile segment was made of steel, which resulted in a corroded surface of the pile, thus, giving realistic properties of the pile roughness and, thereby, the pile-soil interface friction. With a wall thickness, $t_{\text{pile}} = 3$ mm, the diameter to wall thickness ratio was 167.

The wall thickness was as thin as possible without risk of instability and buckling of the segment to reduce any pile base resistance that may occur during cyclic loading even though only one-way cyclic tension tests were planned.

The pile lid, which was used to connect the pile segment to the hydraulic piston, had four large holes, so the pile acted as a pipe pile during tests. Five pore pressure transducers placed on the pile wall, measured the pore

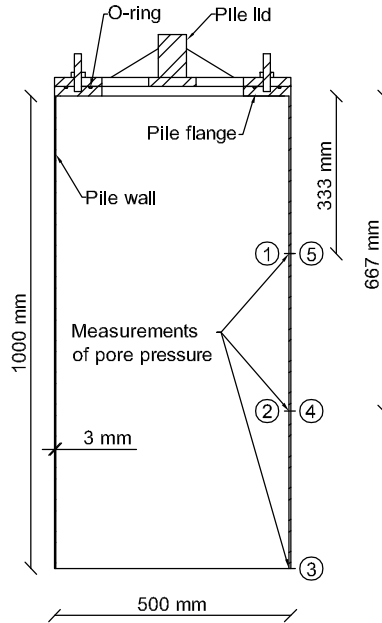


Figure A.1: Cross-sectional view of the pile segment.

pressure at positions of $1/3$ and $2/3 L_{\text{pile}}$ inside and outside the pile wall as well as at the pile tip.

A.4 Test Setup

Figure A.2 shows the test setup whose main features is the sand box in which the pile segment was installed and a load frame where the loading equipment was attached.

Figure A.3a shows the test setup layout while Figure A.3b and Figure A.3c show cross-sectional views of the test setup. The inner dimensions of the sand box were $D_{\text{box}} = 2.5$ m and $H_{\text{box}} = 1.5$ m. The sand layer had the thickness $H_{\text{sand}} = 1.2$ m with a subjacent layer of gravel serving as a part of a drainage system. The system consisted of perforated pipes placed in 0.3 m gravel covered by a felt cloth ensuring homogenous water flow in the sand and preventing sand from getting into the drainage system. The system was coupled to a water outlet, a water tank and an ascension pipe. The water tank placed above the sand container allowed introduction of a hydraulic gradient which was monitored by means of the ascension pipe.

A.4. Test Setup

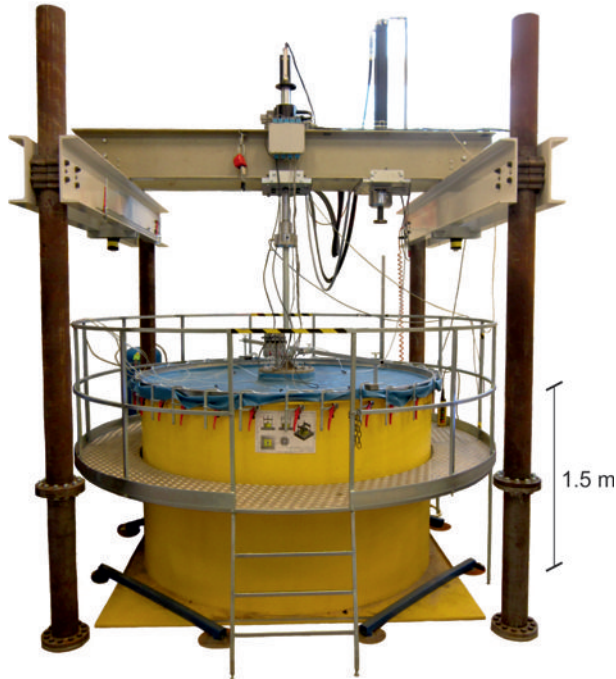


Figure A.2: Sand box and load beam system of the test setup.

A.4.1 Loading system

Two hydraulic pistons were attached to the load frame and could be moved in the longitudinal direction of the load beam. The 250 bars hydraulic piston to the right was used to install the pile and to conduct CPTs (Figure A.3b). The pump pressure was regulated according to the displacement rate of the piston which is measured by an ASM WS10ZG position transducer. The manually operated hydraulic piston was displacement controlled. A 250 kN load cell of the type HBM U10M measured the load. An ASM WS17KT displacement transducer with a range of 2500 mm measured the displacement of the piston. The equipment was connected to a HBM Spider 8 and measurements were recorded with the HBM program Catman Professional with a sample rate of 1 Hz.

The hydraulic piston in the middle was used when running tests (Figure A.3b). This hydraulic system can be both displacement and load controlled and is operated through the computer program MOOG Integrated Test Suite. A 250 kN load cell of the type HBM U10M measured the load during displacement controlled tests and controlled the pressure in the hydraulic cylinder during load controlled tests. By means of this setup it was possible to make

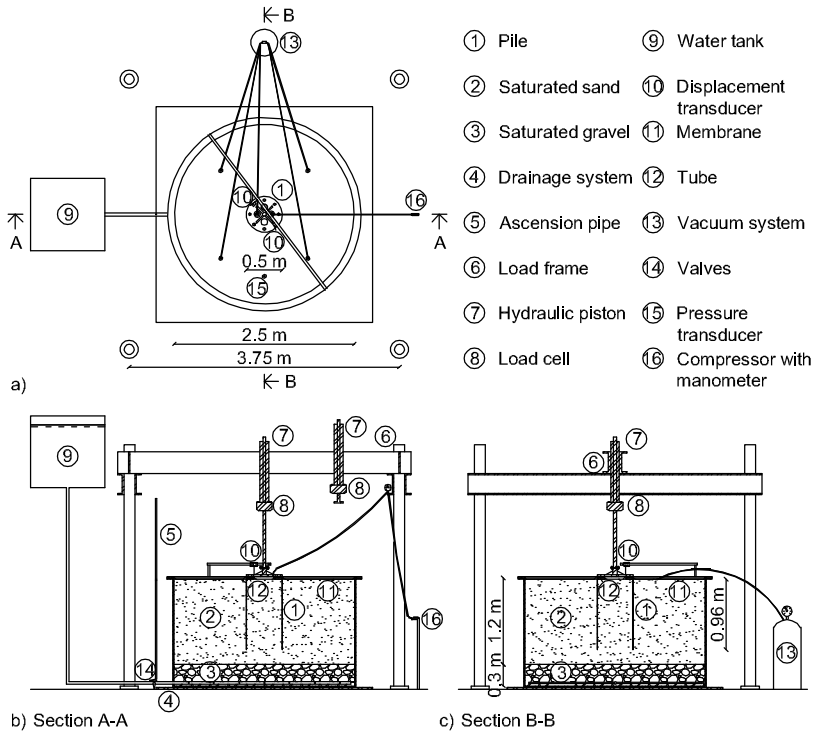


Figure A.3: (a) Layout of the test setup; (b) Section A-A cross-sectional view of the test setup; (c) Section B-B cross-sectional view of the test setup.

a variety of tests, such as: Displacement or load controlled tests; static tests; and cyclic tests with different mean loads, cyclic amplitudes, wave shapes, and frequency. Two ASM WS10 displacement transducers with a 0-125 mm range placed opposite each other on the pile lid 50 mm from the pile edge measured the pile head displacement. The equipment was connected to an HBM MGC Plus and recorded by Catman Professional with a sample rate of 2 Hz.

A.4.2 Boundary Conditions

The effects of the boundary conditions on the results of laboratory tests depend on the ratio between the chamber radius and the pile radius, $R_{\text{chamber}}/R_{\text{pile}}$. Rimoy (2013) reported results of two-way cyclic loading test in a calibration chamber with $R_{\text{chamber}}/R_{\text{pile}} = 33$. During the tests, radial, vertical and hoop stresses were measured within $2 < R_{\text{chamber}}/R_{\text{pile}} < 8$ range of the pile. The sensors all showed stress reductions under sustained loading.

A.4. Test Setup

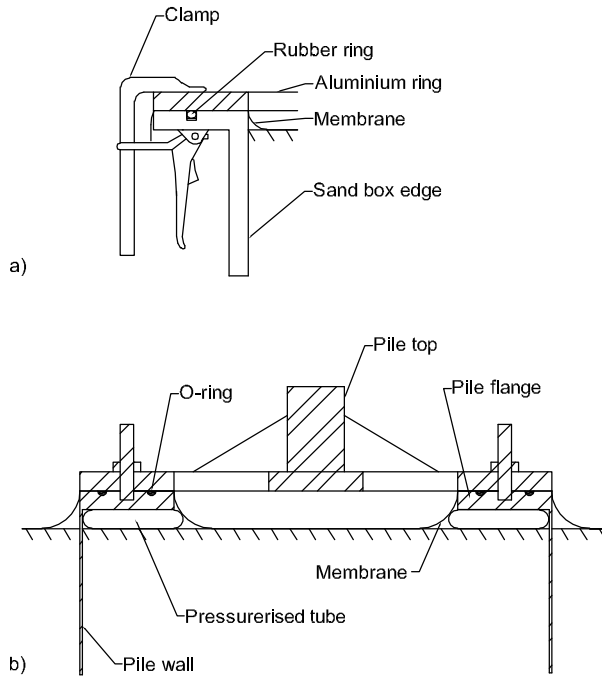


Figure A.4: (a) Sealing of membrane at sand box edge; (b) sealing of membrane at pile flange.

Neither soil stresses nor the stresses at the boundary were measured in the presented test setup. Because $R_{\text{chamber}}/R_{\text{pile}} = 6$ it must be assumed that stress reductions may take place during the cyclic loading tests. However, the effect of the boundary could not be analyzed with the present test setup.

A.4.3 Increase of Effective Stresses

At low stress levels the soil parameters vary strongly with the stresses. This is a problem when conducting tests at 1G. To avoid this in the present test setup, the effective vertical stress was increased by an elastic rubber membrane placed on the sand surface, sealed at the sand box edge and at the pile (Figure A.4), and connected to a vacuum pump. Common practise for increasing the effective vertical stress in calibration chamber tests is to use a rigid plate on the soil surface. By not using a rigid plate in the present test setup, the soil failure at the soil surface was not restricted.

The vacuum system was attached to the membrane by means of hoses and five quick couplings-four at the soil surface outside the pile and one on the soil surface inside the pile. As part of the vacuum system, a 200 L water tank collected the water outflow emerging as air trapped in the system expanded

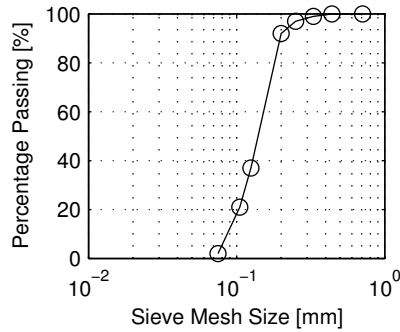


Figure A.5: Sieve analyses for Aalborg University Sand No. 1 (Hedegaard & Borup 1993).

during suction and pressed the water out through the hoses. A felt cloth placed between the membrane and the sand surface restricted the sand from being sucked into the hoses and ensured a homogeneous distribution of the suction on the soil surface. A pressurized tube placed under the pile flange prevented the membrane from being sucked underneath the pile flange and get torn or unwantedly stretched. The excess pressure in the tube is of the same magnitude as the suction on the membrane so that the pressure on the soil surface under the pile flange was the same as on the remaining soil surface. A LISAB-NS-5B pressure sensor (0-5 bar) measured the suction on the membrane.

The membrane and vacuum system is not used for tests without increase of the vertical effective stress. However, the remaining setup was the same as for test with increase of the vertical effective stress.

A.5 Sand Specifications

Aalborg University Sand No. 1 is used when doing laboratory testing of offshore foundations at Aalborg University. The material properties of the sand are well-defined from classification tests and triaxial tests at Aalborg University (Hedegaard & Borup 1993, Ibsen et al. 1994). Figure A.5 presents the grain size distribution which shows a uniform grading making it possible to get a homogeneous compaction of the sand. Table A.1 presents the material properties of the sand found from the classification tests. e_{\max} and e_{\min} were found according to Danish practice (Lund et al. 2001).

A.6. Soil Preparation

Table A.1: Material properties for Aalborg University Sand No. 1 (Hedegaard & Borup 1993).

d_s [g/cm ³]	e_{\max} [-]	e_{\min} [-]	d_{50} [-]	$c_u = d_{60}/d_{10}$ [-]
2.64	0.854	0.549	0.14	1.78

A.6 Soil Preparation

At many wind farm locations in the North Sea, very dense sand is found in the upper soil layers, and it is at these sites the shake-up problem is observed. Existing tests were mostly conducted in medium dense to dense sands e.g. (Chan & Hanna 1980, Le Kouby et al. 2004, Jardine et al. 2009). Thus, tests in very dense sand are desirable; therefore, the sand in the presented study should reach a relative density, D_r , of around 85%. A relative density of around 85% was achieved by using the following soil processing procedure which is similar to that used by Foglia et al. (1991) and Vaitkunaite et al. (2014). Initial soil preparation before any tests:

1. Sand was placed in the sand box.
2. The sand was loosened by a hydraulic gradient.
3. The sand was vibrated with a rod vibrator.
4. Cone penetration tests (CPTs) were conducted and the was calculated from the CPT cone resistance
5. Step 2-4 were repeated until the average relative density converged at $D_r = 85\%$.

Soil preparation between each test (the sand is not replaced between tests):

1. The sand was loosened by a hydraulic gradient.
2. The pile segment was installed while the hydraulic gradient is still applied.
3. The sand outside and inside the pile was vibrated with a rod vibrator.
4. CPTs were conducted to verify and average relative density of 85%.

A.6.1 Hydraulic Gradient

The applied hydraulic gradient loosened the sand and enabled vibration with a rod vibrator and installation of the pile segment. The hydraulic gradient had the magnitude $i = 0.9i_{\text{crit}}$ to avoid piping channels in the sand. The gradient was monitored by observing the water level in the ascension pipe.

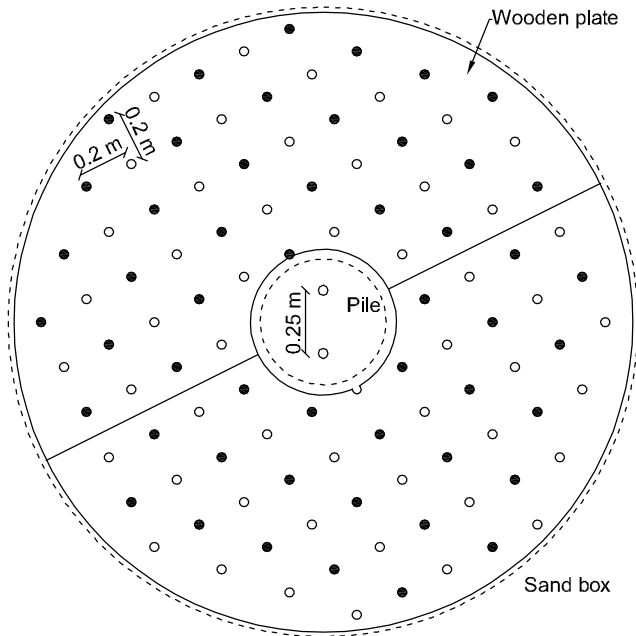


Figure A.6: Sketch of the wooden plate (top view), the black and white circles indicate the holes vibrated before every second test.

A.6.2 Soil Vibration

The water level was 5 cm above the sand surface to avoid air flow into the sand during vibration. The vibration was done with a Wacker Neuson IRFU45 rod vibrator. A wooden plate with equally spaced holes ensured a uniform compaction of the sand by leading the rod vibrator through these holes (Figure A.6). The wooden plate was placed in brackets 10 cm above the sand surface and had no influence on the achieved soil conditions.

In the initial soil preparation phase, every hole of the wooden plate was vibrated once before conducting CPTs and reapplying the hydraulic gradient. The rod vibrator was lead 1.1 m into the sand and pulled up again in approximately 1 min at a constant speed. A vibration study established that the desired relative density could be reached by vibrating every second hole instead of every hole. This vibration procedure was therefore adopted between tests. Before a test every second vibration hole (marked with black) was vibrated and before the next test the other holes (white) were vibrated and so on for the following tests. The sand was vibrated at two positions inside the pile.

A.6. Soil Preparation

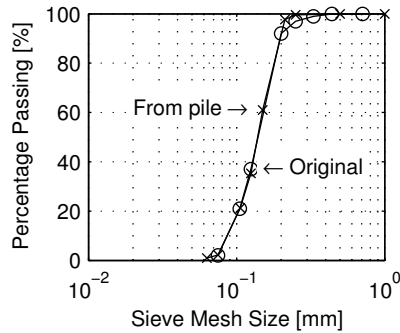


Figure A.7: Sieve analyses conducted on the unused sand prior to the tests and sand scraped off the pile wall after eight static tests.

The loosening and vibration procedures relocated the sand grains preventing the same sand grains to be polished or crushed in all tests and, thereby, avoiding changes of the soil characteristics. Sieve analyses of sand stuck to the pile wall after eight static tests support this assumption as it shows no changes in grain distribution compared to sieve analyses conducted on a sample of sand prior to any tests (cf. Figure A.7).

A.6.3 Installation

During pile installation, the surrounding soil experiences failure. Over time however, set-up will result in soil capacity gain. When conducting cyclic tests it is necessary to account for set-up or any other change in load history on the results. One way is to install the pile in a sand sample by jacking or pushing and then find the static capacity of the pile right before and right after a cyclic test, whereby, it is possible to compare these values of the capacity to one another e.g. (Tsuha et al. 2012). Another way is to deposit the sand around the pile, this way any effects of installation are avoided e.g. (Le Kouby et al. 2004). An objective of the herein presented test setup was to model a pile in service mode; hence, at a time after installation where maximum set-up was achieved. Thus, the soil was prepared to the desired relative density after pile installation. The pile was installed to an embedded depth of 0.96 m—leaving room for the pressurized tube under the pile flange—with an installation rate of 5 mm/s while applying the hydraulic gradient. Even though the soil was very loose during installation, plugging of the segment is observed during installation. Thus, indicating that plugging is likely to occur during tests as well.

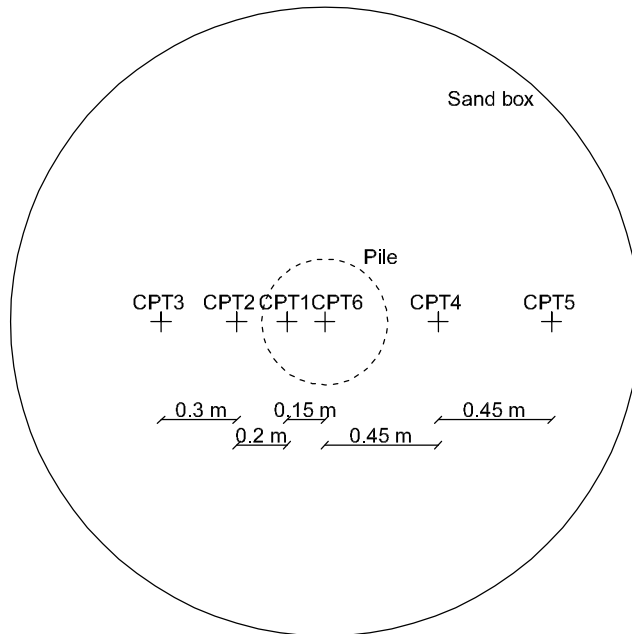


Figure A.8: (Position of the six CPTs (top view) conducted prior to each test.

A.6.4 Analyses of Soil Conditions

CPTs were conducted after vibration with a penetration rate of 5 mm/s at the six positions in the sand box illustrated in Figure A.8. The CPTs validated that the sand is approximately homogeneous throughout the box and that the density was identical from test to test. The CPT device was custom-made with a cone diameter of 15 mm and a cone inclination of 60° . The CPTs were conducted in the saturated sand before the tests; thus, the soil conditions for the CPTs were the same whether or not the following test was made with applied suction. The CPT penetration depth was 1000 mm i.e. the distance from the CPT cone to the gravel layer was 200 mm with an additional distance of 300 mm to the rigid bottom boundary. The cone resistance was therefore not affected by the rigid boundary.

An iterative procedure involving the following equations determines the friction angle, dilation angle, relative density, and effective unit weight from the CPT cone resistance. The expressions for the internal angle of friction and the dilation angle are based on results from triaxial tests on Aalborg University Sand No. 1 (Ibsen et al. 2009, 1994). Figure A.9 shows the parameters achieved from the CPT results. The relative density varies between 60-100% with depth but this variation was repeatable from test to test. The mean

A.6. Soil Preparation

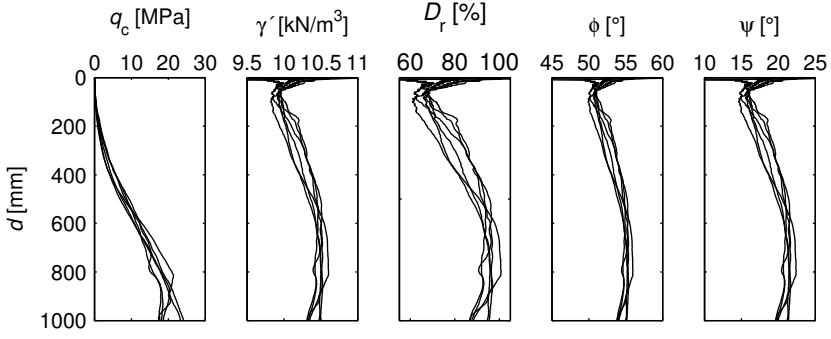


Figure A.9: Example of CPT cone resistances and the determined values of γ' , D_r , φ_{tr} , and ψ_{tr} versus penetration depth prior to a test.

value of the relative density for the first twelve tests—nine static and three cyclic—was 85.9% with a standard deviation between tests of 1.7%. The relative density showed no systematic increase or decrease.

$$\gamma' = \frac{d_s - 1}{1 + e_{\text{in-situ}}} \gamma_w \quad (\text{A.1})$$

$$\sigma'_1 = \gamma' d \quad (\text{A.2})$$

$$D_r = c_2 \left(\frac{\sigma'_1 / \sigma'_{1,\text{ref}}}{(q_c / q_{c,\text{ref}})^{c_1}} \right)^{c_3} \quad (\text{A.3})$$

$$D_r = \frac{e_{\text{max}} - e_{\text{in-situ}}}{e_{\text{max}} - e_{\text{min}}} \quad (\text{A.4})$$

where γ' is the effective unit weight of soil, $e_{\text{in-situ}}$ is the in-situ void ratio, γ_w is the unit weight of water, σ'_1 is the effective vertical stress, d is the depth below soil surface, D_r is the relative density, $\sigma'_{1,\text{ref}}$ is the reference effective vertical stress, 1 MPa, $(c_1, c_2, c_3) = (0.75, 0.0514, -0.42)$, is the CPT cone resistance, $q_{c,\text{ref}}$ is the reference CPT cone resistance, here chosen as 1 MPa.

$$\varphi_{tr} = a_1 D_r + a_2 \left(\sigma'_3 / \sigma'_{3,\text{ref}} \right)^{-0.2807} + a_3 \quad (\text{A.5})$$

$$\psi_{tr} = b_1 D_r + b_2 \left(\sigma'_3 / \sigma'_{3,\text{ref}} \right)^{-0.09764} + b_3 \quad (\text{A.6})$$

where φ_{tr} is the friction angle, $(a_1, a_2, a_3)=(15.2^\circ, 27.39^\circ, 23.21^\circ)$, D_r is the relative density, σ'_3 is the confining pressure, $\sigma'_{3,ref}$ is the reference effective horizontal stress, 1 kPa, ψ_{tr} is the dilation angle, $(b_1, b_2, b_3)=(19.5^\circ, 14.86^\circ, 9.946^\circ)$.

The Federal Highway Administration (FHWA) standard for interpretation of cone penetration tests, FHWA (1992) provides methods to analyze D_r from q_c . However, the methods provide values between -20% and 150% for the q_c profile in Figure A.9 which does not seem realistic. Thus, the method outlined in this paper which is calibrated for the specific sand and CPT device is used in the analysis of soil properties.

A.7 Test Results

Results of six static loading tests conducted at three different surcharge levels—0, 35, and 70 kPa—are given in the following. Moreover, two examples of cyclic loading tests without membrane are given.

The tests with applied suction were saturated throughout the test. For the tests with applied suction, the vacuum system sucked out most of the water leaving the sand almost unsaturated during the tests. Most calibration chamber tests were conducted in dry sand under the assumption of drained conditions and the effect of saturation is, therefore, negligible e.g. (Tsuha et al. 2012). Thomas & Kempfert (2011) reports excess pore pressure build-up in saturated sand and observed a negative effect of the bearing capacity for piles in saturated sand compared to dry sand. The effect was higher for two-way than one-way cyclic loading. However, the tests were run at a relatively high frequency of 1 Hz. The frequency of the herein presented tests was 0.1 Hz and it was assumed, that no excess pore pressure would build-up at this frequency.

The applied suction (surcharge) level has the same effect on the vertical effective stress as an applied overburden pressure. In the following the surcharge level is defined positive. The total measure tension force, Q_T , is defined negative and so is the upward displacement of the pile segment, w .

A.7.1 Results of Static Tests

The purpose of the tests was to examine the sleeve friction of an axially loaded pile, thus, only tension tests were conducted to avoid influence of the tip resistance on the bearing capacity. Another desired outcome of the static tests was the maximum load necessary to pull out the pile. The maxi-

A.7. Test Results

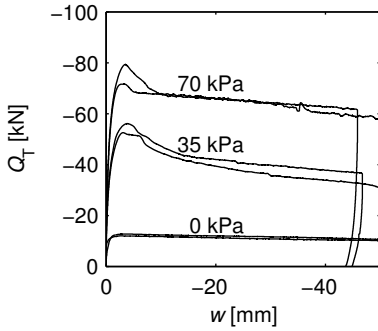


Figure A.10: Load–displacement curves for six static tests with surcharges of 0, 35, and 70 kPa, respectively.

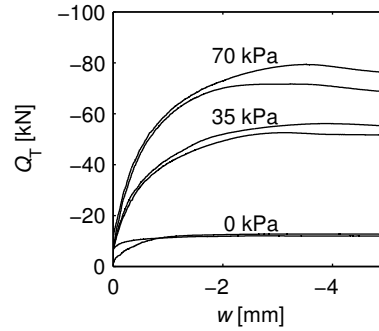


Figure A.11: Load–displacement curves for six static tests with surcharges of 0, 35, and 70 kPa, respectively.

imum force was then used to determine the mean value and amplitude of the subsequent cyclic loading tests. The static tests were displacement controlled and performed at a velocity of 0.002 mm/s to ensure drained conditions. A total displacement of 50 mm of the pile top was applied for the static tests. Figures A.10 and A.11 shows the load-displacement curves for six static tests conducted at surcharges of 0, 35, and 70 kPa, respectively. The graphs show that the load needed to move the pile segment increased with increasing suction on the membrane, as expected. Furthermore, they show that the maximum loads were reached at displacements of 3-4 mm.

Because of the short length of the pile segment the unit skin friction, f_s , is calculated directly from Q_T . Soil surface elevation of approximately 30 mm was observed inside the pile after the tests which means that the pile plugged during loading. Hence, f_s is calculated as

$$f_s = \frac{Q_T - W_{\text{pile}} - W_{\text{plug}}}{A_o} \quad (\text{A.7})$$

where W_{pile} is the weight of the pile segment and equipment below the load cell, W_{plug} is the plug weight, and A_o is the outer pile shaft area.

Figure A.12 shows f_s versus the pile displacement while Figure A.13 displays the maximum unit skin friction plotted against the effective vertical stress in sand half way down the pile shaft. API (2011) recommends the following determination of f_s :

$$f_s = \beta \sigma'_v \quad (\text{A.8})$$

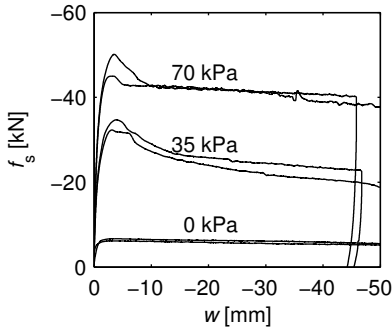


Figure A.12: Unit skin friction for the six static tests with surcharges of 0, 35, and 70 kPa, respectively.

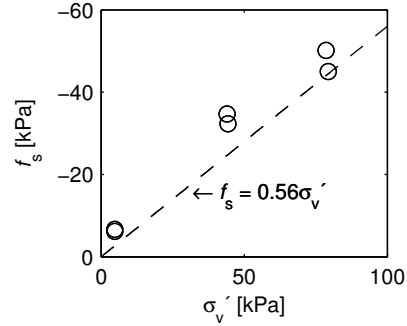


Figure A.13: Maximum unit skin friction, $f_{s,max}$, (circles) versus effective vertical stress at the middle of the pile shaft compared to the API (2011) recommendations.

where β is the shaft friction factor which is 0.56 for very dense sand ($D_r > 85\%$), and σ'_v is the effective vertical stress at the depth in question. f_s from the test results are a bit higher than f_s determined from the API method. This is in good agreement with pile test database studies showing that the API method under-predicts the tension capacity of short piles in dense sand (Lehane et al. 2005).

A.7.2 Results of Cyclic Tests

The cyclic tests were conducted after the described soil preparation procedure. Thus, no previous static or cyclic loading tests influenced the test results. The cyclic tests were constructed of three steps: Firstly, the mean load was reached with the same speed as was found from the load-time curve of the static tests. Secondly, cyclic loading was performed for two days with a frequency of 0.1 Hz. Thirdly, if the pile had not failed after the two days, a static test ran in continuation of the cyclic loading to a total displacement of the pile top of 50 mm. This was done to examine the effect of the cyclic loading on the static bearing capacity of the pile segment. The test was terminated if the displacement of 50 mm was reached before the second day of cyclic loading.

Figures A.14 and A.15 show the results of two cyclic loading tests conducted without membrane. The mean load, Q_{mean} , and the cyclic amplitude, Q_{cyclic} , illustrated by Figure A.16 are chosen based on the average maximum pull-out force, $Q_{max\ static} = 12.1$ kN, obtained from the static tests. The first test illustrated, had a mean load of $0.4Q_{max\ static}$ and cyclic amplitude of $0.2Q_{max\ static}$. The cyclic loading did not result in accumulated displacement

A.7. Test Results

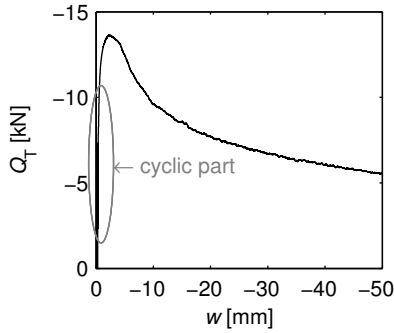


Figure A.14: Load–displacement curve for cyclic test at 0 kPa with $Q_{\text{mean}} = 0.4Q_{\text{max static}}$ and $Q_{\text{cyclic}} = 0.2Q_{\text{max static}}$.

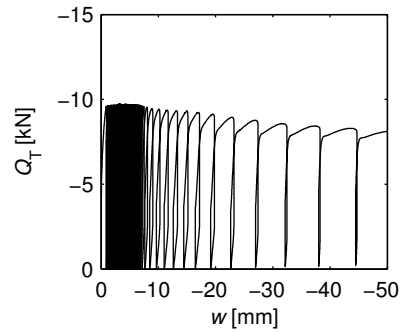


Figure A.15: Load–displacement curve for cyclic test at 0 kPa with $Q_{\text{mean}} = 0.4Q_{\text{max static}}$ and $Q_{\text{cyclic}} = 0.4Q_{\text{max static}}$.

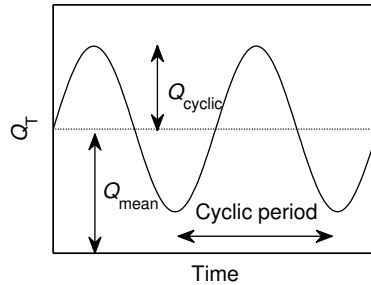


Figure A.16: Illustration of the cyclic loading parameters.

and the maximum static pull-out force reached in the pre-cyclic static test was 13.7 kN. Thus, the cyclic loading resulted in a bearing capacity gain of 13% compared to results of the static tests with no prior cyclic loading. Figure A.16 displays the result of a test with a mean load of $0.4Q_{\text{max static}}$ and cyclic amplitude of $0.2Q_{\text{max static}}$. The graph shows that the maximum displacement of 50 mm was reached before the two days of cyclic loading ended, after no more than 177 cycles.

These preliminary results resemble findings of other researchers well. For one-way cyclic loading tests, small amplitudes can increase the static capacity (Jardine & Standing 2012, Jardine et al. 2006, Le Kouby et al. 2004). Increase of the cyclic amplitude decreases the number of cycles to failure (Thomas & Kempfert 2011, Chan & Hanna 1980).

A.8 Advantages and Disadvantages of the Test Setup

One of the advantages of the described test setup is that the design of the pile segment, such as the pile diameter and that it is open-ended, gives a much closer resemblance to full-scale piles compared to the pile segments usually used in laboratory testing. Hence, the scaling of the sand grains compared to the pile surface roughness is not an issue when interpreting the test results.

Because of the short length of the pile, the conditions are relatively homogeneous for the entire length and the test results can be interpreted as a single t - z curve along a pile at the depth corresponding to the increase of the effective stresses in the soil. A disadvantage of the short length is that the influence of the base resistance increases. However, only one-way cyclic loading test of piles in tension were conducted and the base resistance are in these cases negligible.

Because of the size of the sandbox and the way of saturating the sand it is not possible to completely avoid air presence in the sand. Due to the applied suction, the air expands and presses the water out through the suction tubes. Thus, the water level drops to about 0.9 m below the sand surface leaving the sand only partially saturated. The effect of saturated, partially saturated or dry sand on the cyclic axial capacity of piles in sand was not explored. It is assumed that the tests are carried out at a frequency preventing excess pore water pressure development and, therefore, it is assumed that the saturation degree of the sand has no impact on the test results.

A.9 Conclusion and Recommendations

This paper presented a new laboratory test setup for testing axially loaded piles in sand. The purpose of the test setup was to gain knowledge about the behavior of piles used in jacket foundations for offshore wind turbines which, due to the low self-weight of the structure, are often loaded in tension. Therefore, the test setup was constructed to examine piles subjected to one-way cyclic axial tension loading. The diameter of the test segment was close to that of full-scale piles. The pile wall thickness was small to reduce the influence of base resistance to a minimum. The length of the pile segment was 1 m which enabled analysis of the skin friction at a given depth below the soil surface. To simulate different soil depths, the effective stresses in the sand were increased by placing a rubber membrane on the sand surface and applying a maximum of 70 kPa suction to the sand box.

A.10. Acknowledgments

The static tests showed that the test setup produces repeatable test results. The preliminary cyclic test results showed good agreement with results found in the literature. The static test results are currently being analyzed and compared to the CPT-based methods suggested by API (2011), while more cyclic tests are being conducted and analyzed. Recommendations for improvements of the test setup include strain or stress measurements at the rigid vertical boundary of the sand box to monitor the stress changes and estimate the boundary effects.

Another improvement would be to refine the vibration procedure to ensure a more uniform sand deposit with depth. In the presented sand preparation procedure, the rod vibrator moved with a constant speed both up and down. Perhaps a more uniform deposit could have been made by a slower penetration rate in the top of the sand layer and a faster rate at the bottom.

A.10 Acknowledgments

The research is funded by the Danish Advanced Technology Foundation via the program “Cost-effective deep water foundations for large offshore wind turbines”. The financial support is sincerely acknowledged.

References

- API (2011), *Geotechnical and Foundation Design Considerations*, API RP 2GEO, 1. ed. edn, American Petroleum Institute.
- Baeßler, M., Rücker, W., Cuéllar, P., Georgi, S. & Karbeliov, K. (2013), ‘Large-scale testing facility for cyclic axially loaded piles’, *Steel Construction* **6**(3), 200–206.
- Chan, S.-F. & Hanna, T. (1980), ‘Repeated loading on single piles in sand’, *Journal of the Geotechnical Engineering Division* **106**(2), 171–188.
- FHWA (1992), *The cone penetrometer test*, FHWA-SA-91-043, U.S. Federal Highway Administration.
- Foglia, A., Ibsen, L. & Andersen, L. (1991), An innovative physical model for testing bucket foundations, in ‘Proceedings of the 16th Nordic Geotechnical Meeting’, Copenhagen, Denmark, p. 323–330.
- Hedegaard, J. & Borup, M. (1993), *Klassifikationsforsøg med Baskarp Sand No. 15*, Aalborg University, Denmark.

- Ibsen, L., Hanson, M., Hjort, T. & Thaarup, M. (1994), *Baskarp Sand No. 15.*, Data Report 9301, Aalborg University, Denmark.
- Ibsen, L., Hanson, M., Hjort, T. & Thaarup, M. (2009), *MC-Parameter Calibration of Baskarp Sand No. 15.*, DCE Technical Report No. 62, Department of Civil Engineering, Aalborg University, Denmark.
- Jardine, R., Bitang, Z., Foray, P. & Dalton, C. (2009), 'Experimental arrangements for investigation of soil stresses developed around a displacement piles', *Soils and Foundations* **49**(5), 661–673.
- Jardine, R. & Standing, J. (2000), *Pile load testing performed for HSE cyclic loading study at Dunkirk, France. Volume 1 & 2.*, Offshore Technology Report OTO 2000 007, Health and Safety Executive, London, UK.
- Jardine, R. & Standing, J. (2012), 'Field axial cyclic loading experiments on piles driven in sand', *Soils and Foundations* **52**(4), 723–736.
- Jardine, R., Standing, J. & Chow, F. (2006), 'Some observations of the effect of time on the capacity of piles driven in sand', *Géotechnique* **56**(4), 227–244.
- Le Kouby, A., Canou, C. & Dupla, J. (2004), Behaviour of model piles subjected to cyclic axial loading, in 'Proceedings of the International Conference Cyclic Behaviour of Soils and Liquefaction Phenomena', Taylor & Francis Group, London, UK, p. 159–166.
- Lehane, B., Schneider, J. & Xu, X. (2005), *A Review of Design Methods for Offshore Driven Piles in Siliceous Sand*, The University of Western Australia.
- Randolph, M. & Gourvenec, S. (2011), *Offshore Geotechnical Engineering*, Spon Press.
- Thomas, S. & Kempfert, H.-G. (2011), 'Untersuchung des Pfahltragverhaltens infolge zyklischer axialer Einwirkungen in einer Spannungszelle', *Pfahl-Symposium 2011* **94**, 139–158.
- Tsuha, C., Foray, P., Jardine, R., Yang, Z., Silva, M. & Rimoy, S. (2012), 'Behaviour of displacement piles in sand under cyclic axial loading', *Soils and Foundations* **52**(3), 393–410.
- Vaitkunaite, E., Ibsen, L. & Nielsen, B. (2014), New medium-scale laboratory testing of bucket foundation capacity in sand, in 'Proceedings of the 24th International Ocean and Polar Engineering Conference', Busan, South Korea, p. 514–520.

Appendix B

Comparison of Design Methods for Axially Loaded Driven Piles in Cohesionless Soil

Kristina Thomassen
Lars Vabbersgaard Andersen
Lars Bo Ibsen

The paper has been published in the
*Proceedings of the Twenty-second (2012) International Offshore and Polar
Engineering Conference*, pp. 705–712, 2012.

***Proceedings of the Twenty-second (2012) International Offshore and Polar
Engineering Conference***

Rhodes, Greece, June 17–22, 2012

***Copyright © 2012 by the International Society of Offshore and Polar Engi-
neers (ISOPE)***

ISBN 978-1-880653-94-4 (Set); ISSN 1098-6189 (Set)

The layout has been revised.

Abstract

For offshore wind turbines in deeper waters, a jacket sub-structure supported by axially loaded piles is thought to be the most suitable solution. The design method recommended by API and two CPT-based design methods are compared for two uniform sand profiles. The analysis shows great contrast in the predictions of bearing capacities calculated by means of the three methods for piles loaded in both tension and compression. This implies that further analysis of the bearing capacity of axially loaded piles in sand should be conducted.

KEY WORDS: Piles; capacity; offshore; sand.

B.1 Introduction

The increased focus on renewable energy sources has resulted in the development of large offshore wind farms in the North Sea. As the interest for offshore wind farms increases, locations with deeper water are included as possible sites for the wind farms. At water depths greater than approximately 25 m, current technology implies that the most suitable foundation solution for the wind turbine is a jacket substructure supported by axially loaded piles. For this jacket solution, the large overturning moment capacity is ensured by the axial capacity of the piles in compression and tension.

The recommended design method for the axial capacity of the offshore driven piles in cohesionless soil is the so-called β -method, suggested by API (2000), in which the effective overburden pressure at the depth in question is used. However, comparisons between the capacity calculated using the API β -method and full-scale measurements show that the β -method under-predicts the capacity of short piles (length less than 20 m) in dense sand, over-estimates the capacity of long piles in loose sand, and gives a shaft capacity less conservative for piles in tension than for piles in compression (Lehane et al. 2005a, Schneider et al. 2008).

The API method is developed for predictions of pile capacities for piles used in the oil and gas industry. For this type of construction, the selfweight is so great that the piles are loaded in compression at all times. The conservatism in API-00 for short piles is not of high importance for the oil and gas industry. This is because it is crucial that an oil platform does not fail and as the companies only build one offshore platform at a time, the extra cost of a longer pile is less than the cost of optimising the design. For an offshore wind farm with jacket sub-structures however, a large amount of piles is to be installed and the cost of the piles is very important, indicating that an optimisation of

the piles is in place. As the piles can be loaded in tension, the prediction of the tension capacity of the piles should not be less conservative than the prediction of the compression capacity. Thus, it is important to develop methods that give a more accurate prediction of the pile capacities than the β -method.

Onshore field investigations have shown strong correlation between the local shaft friction and the CPT cone resistance. Therefore, the recommended design method for onshore driven piles in cohesionless soil is a CPT-based approach. Several CPT-based methods have been proposed for the design of offshore driven piles, e.g. the UWA-05, the ICP-05, and the NGI-99 method. These methods are based on static loading tests on piles with dimensions smaller than the ones used offshore. However, the database studies performed in Lehane et al. (2005a) and Schneider et al. (2008) indicate that the CPT-based methods perform better against the database than the β -method, hereafter referred to as the API-00 method. The analyses also show that UWA-05 performs slightly better than the other CPT-based methods, probably due to the fact that UWA-05 takes more of the main factors influencing the pile capacity into account.

The CPT-based methods have been included in the commentary of API (API 2007). However, none of the methods are recommended for routine design because too few load tests on piles with the dimensions used offshore have been conducted to verify the predictions of the CPT-based methods. DNV (2010) does not include or even mention the CPT-based methods.

The three methods are described in the following and then used to calculate the capacity of piles with the dimensions used offshore. The calculations are conducted based on uniform sand profiles with dense and loose sand, respectively. The predictions of the methods are then compared.

B.2 Design Methods

The total bearing capacity Q_t is calculated from Equation (B.1) as the sum of the shaft capacity and the end bearing capacity.

$$Q_t = Q_s + Q_b = \int A_s \tau_f dz + A_b q_{b0,1} \quad (\text{B.1})$$

where Q_s (kN) is the shaft capacity, Q_b (kN) is the base capacity, A_s (m^2/m) is the external shaft area, A_b (m^2) is the base area, τ_f (kPa) is the local shaft friction at failure at depth z (m), $q_{b0,1}$ (kPa) is the end bearing capacity at a pile tip displacement of $0.1D$ for API-00 and UWA-05 and at a pile head displacement of $0.1D$ for NGI-99. The difference between these two definitions

B.2. Design Methods

of the displacement at failure is whether the axial deformation of the pile is taken into account. The difference is small for short piles in loose sand but increases with increasing pile length and/or relative density of the sand.

The shaft capacity is influenced by many factors. The main factors are: Relative density of the soil; soil displacement and/or plugging depending on the pile type; friction between the pile and soil; friction fatigue emerging from the installation method; dilation of the sand during shear; and whether the pile is loaded in compression or tension.

In API-00, the shaft capacity calculation is based only on the relative density and the vertical effective stress. Thus, API-00 reflects few of the main influencing factors. The CPT-based methods allow for better predictions of the relative density, compressibility, and stress level of the soil by using the CPT cone resistance q_c in the expression for the pile capacity.

B.2.1 API-00 Design Method

According to API (2000), the local shaft friction is given by:

$$\tau_f = K_f \tan \delta \sigma'_{v0} = \beta \sigma'_{v0} \quad (\text{B.2})$$

where K_f is the coefficient of lateral earth pressure, δ is the interface friction angle, σ'_{v0} is the vertical effective stress at the point in question, and β is the shaft friction factor ($\beta = K_f \tan \delta$).

The unit end bearing capacity is given by:

$$q_{b0,1} = N_q \sigma'_{v0} \quad (\text{B.3})$$

where N_q is the bearing capacity factor and σ'_{v0} is the vertical effective stress at the pile tip level.

The parameters listed in Table B.1 can be used as guidelines when detailed information such as CPT data, strength tests on high quality samples, model tests, or pile driving performance are not available. For long piles, τ_f and $q_{b0,1}$ may not increase linearly with the overburden pressure, and it may be appropriate to use the limiting values given in Table B.1.

The total capacity for a pile loaded in compression is dependent on the smallest of the plugged and the unplugged resistance i.e. the least of the total internal shaft friction and the end bearing of the soil plug. The internal local

Table B.1: Design parameters for cohesionless siliceous soil, after (API 2007).

D_r [%]	Soil [description]	β [-]	$\tau_{i,lim}$ [kPa]	N_q [-]	$q_{b0,1,lim}$ [MPa]
0-15	Sand				
15-35	Sand				
15-35	Sand-silt	— ¹	— ¹	— ¹	— ¹
35-65	Silt				
65-85	Silt				
35-65	Sand-silt	0.29	67	12	3
35-65	Sand				
65-85	Sand-silt	0.37	81	20	5
65-85	Sand				
85-100	Sand-silt	0.46	96	40	10
85-100	Sand	0.56	115	50	12

¹It is recommended to use CPT-based methods for these soils.

shaft friction is considered equal to the external local shaft friction. API (2007) does not give any recommendations for a pile loaded in tension. However, from static calculations, it is assumed that the total capacity is dependent on the smallest of the plugged and the unplugged resistance, i.e. the least of the total internal shaft friction and the submerged weight of the soil plug.

The method is only applicable for cohesionless siliceous soils, i.e. not applicable for carbonate sands and gravels. The piles are assumed to be open-ended steel pipe piles of uniform outer diameter. Still, no distinction is made between shaft capacity for piles loaded in tension and piles loaded in compression. Moreover, the piles are assumed installed by impact driving into significant depths, which means that the piles in general are driven unplugged. However, the piles can act plugged during static loading. For piles driven fully plugged or closedended, the values of β may be assumed 25% higher than for unplugged piles.

B.2.2 NGI-99 Design Method

The NGI-99 design method is based on 56 pile load tests at sites with CPT or SPT data. The expression for the relative density is based on the CPT cone resistance q_c and thus, a correlation between the SPT blow count and q_c was used for developing the design method. The piles were installed in sand with relative densities of 0.2 to 0.7. Most of the piles had a pile length between approximately 5 m and 25 m (Clausen et al. 2005).

The local shaft friction is given by:

$$\tau_f = \frac{z}{z_{tip}} p_a F_{load} F_{tip} F_{mat} F_{sig} F_{Dr} > 0.1 \sigma'_{v0} \quad (\text{B.4})$$

B.2. Design Methods

where z is the depth below ground surface, z_{tip} is the pile tip depth, p_a is the atmospheric pressure (100 kPa), F_{load} is 1.0 for tension and 1.3 for compression, F_{tip} is 1.0 if driven open-ended and 1.6 if driven closed-ended, F_{mat} is 1.0 for steel and 1.2 for concrete. F_{sig} is given by:

$$F_{\text{sig}} = \left(\frac{\sigma'_{v0}}{p_a} \right)^{0.25} \quad (\text{B.5})$$

where σ'_{v0} (kPa) is the vertical effective stress at the point in question. Finally, F_{D_r} (-) is given by:

$$F_{D_r} = 2.1 (D_r - 0.1)^{1.7} \quad (\text{B.6})$$

D_r is the relative density given by:

$$D_r = 0.4 \ln \left(\frac{q_c}{22 (\sigma'_{v0} p_a)^{0.5}} \right) \quad (\text{B.7})$$

where q_c is the cone resistance at a given depth. Values of D_r larger than one should be accepted.

The expression for τ_f reflects some of the influencing factors on the shaft capacity. At a given depth, τ_f is reduced as the pile is driven deeper into the ground increasing the distance to the pile tip. This reduction is called friction fatigue and is expressed by the term z/z_{tip} . For piles in compression, τ_f is assumed to be a constant times τ_f for piles in tension, as given by the factor F_{load} . The influence of the pile end condition is given by F_{tip} . F_{sig} describes the dependency on the vertical effective stresses, though τ_f is found to be more dependent on the relative density which is taken into account by the factor F_{D_r} .

For open-ended piles, the end bearing capacity is taken as the smallest of the unplugged and the plugged base resistance in the same manner as for API-00. However, the internal local shaft friction is taken as three times the external value. This ratio is based on observations in the field and assumed to emerge from the soil displacement at pile tip during installation. Two plain strain models are made in order to make a simple comparison of the normal stresses inside and outside the pile wall during installation. One is a model of a horizontal cross-section of the soil plug exposed to a lateral displacement corresponding to half the pile wall thickness. The other is a model of the soil surrounding the pile also exposed to a lateral displacement corresponding

to half the pile wall thickness. If Poisson's ratio of the soil is set to 1/3, the ratio between the normal stresses in the soil for the two models becomes exactly three. Even though the models are very simple, this ratio indicates that assuming the internal local shaft friction three times the external value is in agreement with the physical processes in the soil during installation.

The unit annular end bearing is calculated assuming a stress against the pile wall of $q_{c,tip}$. The plugged unit end bearing is calculated from:

$$q_{b0.1} = \frac{0.7q_{c,tip}}{1 + 3D_f^2} \quad (B.8)$$

NGI-99 can also be used for closed-ended piles. In this case, the unit end bearing capacity is given by:

$$q_{b0.1,closed-ended} = \frac{0.8q_{c,tip}}{1 + D_f^2} \quad (B.9)$$

B.2.3 UWA-05 Design Method

The UWA-05 design method is based on 74 pile load tests with appurtenant CPT data on sites with silicious sand. Thus, this method is based on a larger database than the other CPT-based methods suggested. The tested piles were both steel pipe piles and concrete piles. To analyse the database and develop a new design method, the database was divided into four sub-categories: closed-ended piles in tension, closed-ended piles in compression, open-ended piles in tension, and open-ended piles in compression. As the load tests were performed on sites with siliceous sand, the method is not applicable for piles in carbonate sands and gravels.

The local shaft friction follows a Coulomb failure criterion as given by:

$$\tau_{i,e} = \sigma'_{rf} \tan \delta_{cv} = \frac{f}{f_c} (\sigma'_{rc} + \Delta\sigma'_{rd}) \tan \delta_{cv} \quad (B.10)$$

where σ'_{rf} is the radial effective stress at failure, δ_{cv} is the constant volume interface friction angle, f/f_c is 1 for compression and 0.75 for tension, σ'_{rc} is the radial effective stress after installation and equalization, and $\Delta\sigma'_{rd}$ is the change in radial stress due to the loading stress path (dilation).

δ_{cv} depends on the grain size, shape and mineral type of the soil as well as on the roughness of the pile. Ideally, δ_{cv} is measured in laboratory interface

B.2. Design Methods

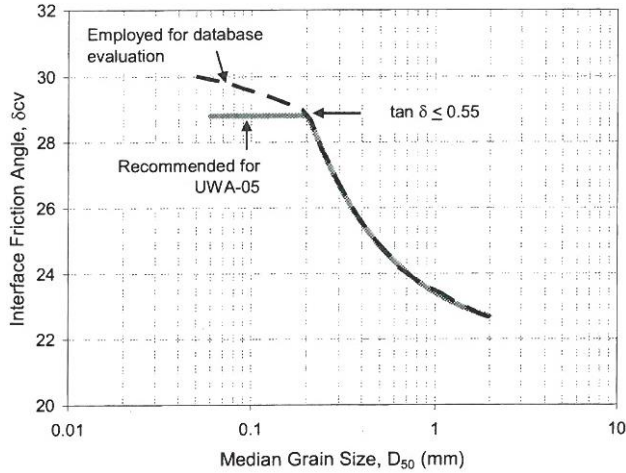


Figure B.1: Variation of the interface friction angle with the median grain size (modified by from ICP-05 guidelines) (Lehane et al. 2005a).

shear tests; however, it can be estimated as a function of the mean effective particle diameter, d_{50} , as shown in Figure B.1. Because of crushing the sand into fine grains during loading, δ_{cv} tends to be a constant value of approximately 29° .

The radial effective stress after installation σ'_{rc} depends on several factors: The relative density of the soil, the relative depth to the pile tip, h , and the degree of soil displacement during installation. The dependency on the relative density is expressed in terms of the CPT cone resistance q_c . A dependency on the relative depth to the pile tip derives from friction fatigue and emerges from the installation method and the diameter of the pile. The friction fatigue is described in terms of h/D . The lateral displacement of the soil during installation is given by the area ratio A_r which depends on the incremental filling ratio IFR . IFR is an expression for the plugged/unplugged condition of the pile:

$$IFR = \frac{\delta h_p}{\delta L} \quad (\text{B.11})$$

where δh_p and δL are defined in Figure B.2. $IFR = 0$ corresponds to plugged penetration. $IFR = 1$ corresponds to unplugged penetration, while a value of IFR between 0 and 1 corresponds to partial plugging. A simplified ap-

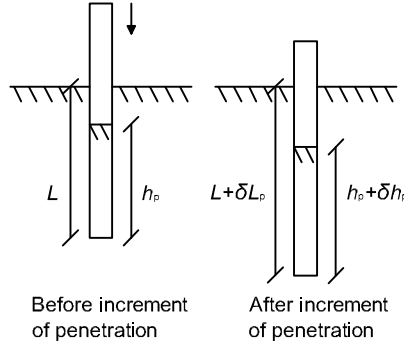


Figure B.2: Definition of the parameters used for defining the incremental filling ratio IFR as given by Equation (B.11), after (Randolph & Gourvenec 2011).

proximation of IFR averaged is given by:

$$IFR = \min \left[1, \left(\frac{D_i}{1.5} \right)^{0.2} \right] \quad (B.12)$$

Near the pile tip, it is difficult to measure σ'_{rc} and it is considered constant over the last $2D$ of the length above the pile tip. Based on these considerations, the radial effective stress after installation and equalization is given by:

$$\sigma'_{rc} = 0.03q_c A_r^{0.3} \left(\max \left[\frac{h}{D}, 2 \right] \right)^{-0.5} \quad (B.13)$$

where h is the distance above the pile tip = pile length – depth z , D is the outer diameter of the pile. A_r is the effective area ratio given by:

$$A_r = 1 - IFR \left(\frac{D_i^2}{D^2} \right) \quad (B.14)$$

where D_i is the inner diameter of the pile.

The change in radial stress $\Delta\sigma'_{rd}$ is an expression for the dilation of the soil during loading given by:

$$\Delta\sigma'_{rd} = 4G \frac{\Delta r}{D} \quad (B.15)$$

B.2. Design Methods

where G is the shear modulus and Δr is the dilation assumed to be 0.02 mm. A detailed expression for G can be found in Lehane et al. (2005b).

For piles with $D > 1$ m, $\Delta\sigma'_{rd}$ may contribute with less than 5% of the total bearing capacity. This means that for offshore piles, $\Delta\sigma'_{rd}$ is negligible and not taken into account in the expression for the local shaft friction. UWA-05 considers offshore piles driven unplugged but failing plugged during static loading ($IFR = 1$). This assumption sound plausible as the soil in the pile-soil interface must be disturbed during pile driving and not able to mobilise the friction necessary for the pile to plug. However, after installation the disturbed soil will restore its strength and the pile may fail plugged.

The expression for the local shaft friction for offshore piles is then given by:

$$\tau_{t,e} = \frac{f}{f_c} 0.03 q_c A_r^{0.3} \left(\max \left[\frac{h}{D}, 2 \right] \right)^{-0.5} \tan \delta_{cv} \quad (\text{B.16})$$

The unit end bearing capacity is given by:

$$q_{b0.1,w} = q_{b0.1,p} = \bar{q}_c (0.15 + 0.45 A_r) \quad (\text{B.17})$$

where \bar{q}_c is the average cone resistance averaged using the Begemann procedure described by Schmertmann (1978).

B.2.4 Results of database studies

The CPT-based methods are developed based on load tests on piles with the majority of the pile lengths less than 30 m and diameters less than 1 m. Database analyses of the described design methods have been performed by Lehane et al. (2005a) and Schneider et al. (2008). These databases are primarily the same as the database on which UWA-05 is based. However, the databases suffer from a shortage of piles with the dimensions used offshore. Therefore, the capacity prediction of offshore piles cannot be judged solely on the performance of the design methods against the databases. The methods must also be assessed by how many of the main influencing factors on the capacity of a pile they account for when extrapolating the method to offshore piles (Lehane et al. 2005a).

UWA-05 gives slightly better predictions than the other CPT-based methods compared to the database piles, most likely due to the more detailed formulation compared to e.g. NGI-99. Because of the detailed expressions for the physical processes, UWA-05 should also provide better predictions of the

capacity of offshore piles. The factors taken into account by UWA-05 are: the dependency of the shaft friction and the base resistance on the CPT cone resistance q_c ; the reduction of the local shaft friction with the distance h from the pile tip; the dependency of the capacity on the soil displacement; variation of the coefficient of friction between pile and soil; increase of the friction due to dilation in the pile-soil interface; the effect on the base capacity from the variation of q_c near the pile tip.

Analysis of piles in uniform sand profiles performed by Lehane et al. (2005a) show the following tendencies for the API-00 predictions compared to the UWA-05 predictions; API-00 under-estimates capacities of short piles in dense sand. For loose sands, API-00 overestimates the capacity of long piles and may over or under-estimate the capacity of short piles.

B.3 Comparison of Design Methods

In order to compare the three methods, predictions of pile capacities of piles installed in soil profiles of dense and loose sands, respectively, are calculated. The relative density is assumed to be 80% for the dense sand and 50% for the loose sand. A relative density of 50% is the lower limit of what is to expect offshore. The piles have diameters of 1 m, 2 m, and 3 m and a diameter wall thickness ratio of 40 while the pile lengths are varied from 5-85 m.

UWA-05 assumes unplugged installation and plugged failure mode. Meanwhile, API-00 and NGI-99 determines whether the piles should be considered plugged or unplugged from static considerations. Thus, if the end bearing capacity exceeds the total internal shaft friction, the pile is assumed to fail in an unplugged manner. In API-00, the internal friction is considered equal to the external friction, while the internal friction is taken as three times the external value in NGI-99. The difference in the methods means that for a given pile geometry and soil conditions, API-00 may determine the axial capacity based on an unplugged calculation while NGI-99 will use a plugged calculation.

B.3.1 Soil Conditions

Uniform soil conditions are used to examine the design methods. Soil profiles are established for relative densities, D_r , of 50% and 80%, respectively. From these relative densities, values of the CPT cone resistance, q_c , are computed by means of the relation given by Jamiolkowski et al. (2003). This relation gives a variation of q_c as shown in Figure B.3. In the calculations, q_c is averaged over 0.5 m intervals.

B.3. Comparison of Design Methods

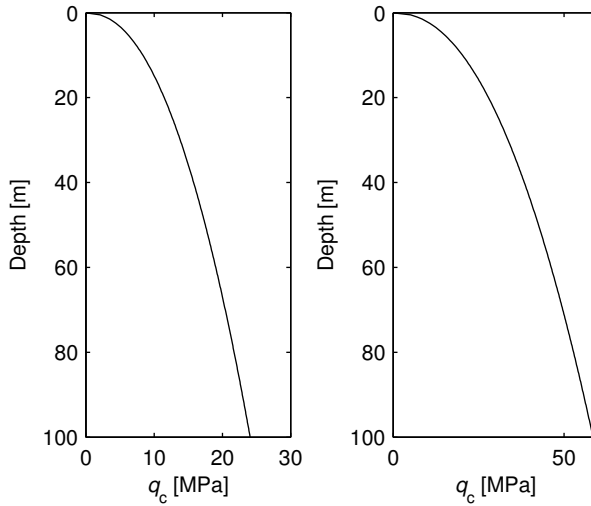


Figure B.3: To the left: The CPT cone resistance q_c for a relative density of 50%. To the right: The CPT cone resistance q_c for a relative density of 80%.

B.3.2 Dense Sand, Piles in Tension

Figures B.4a to B.4c shows the predictions of the tension capacity for piles in dense sand. In this case, all three methods assume plugged calculation.

The tendencies of NGI-99 and API-00 are the same for all three pile diameters and all pile lengths. Though, NGI-99 predicts slightly higher capacities than API-00. For piles with a diameter of 1 m, UWA-05 predicts higher capacities than API-00 for pile lengths less than 20 m. For longer piles, UWA predicts capacities increasingly lower than API-00. For piles with a diameter of 2 m and lengths less than 40 m, UWA-05 predicts higher capacities than API-00. For piles with diameters of 3 m, the three methods predict capacities relatively close to each other.

The difference between the predictions of UWA-05 and NGI-99 for the piles with a diameter of 1 m is surprising, because the CPT-based methods are developed based on load test databases where the majority of the pile lengths are less than 25 m and diameters less than 1 m. An explanation to these differences could be that little attention has been paid to developing an accurate method for piles in tension as the piles used in the oil and gas industry are always loaded in compression. However, the three methods predict rather similar results for piles with diameters of 3 m.

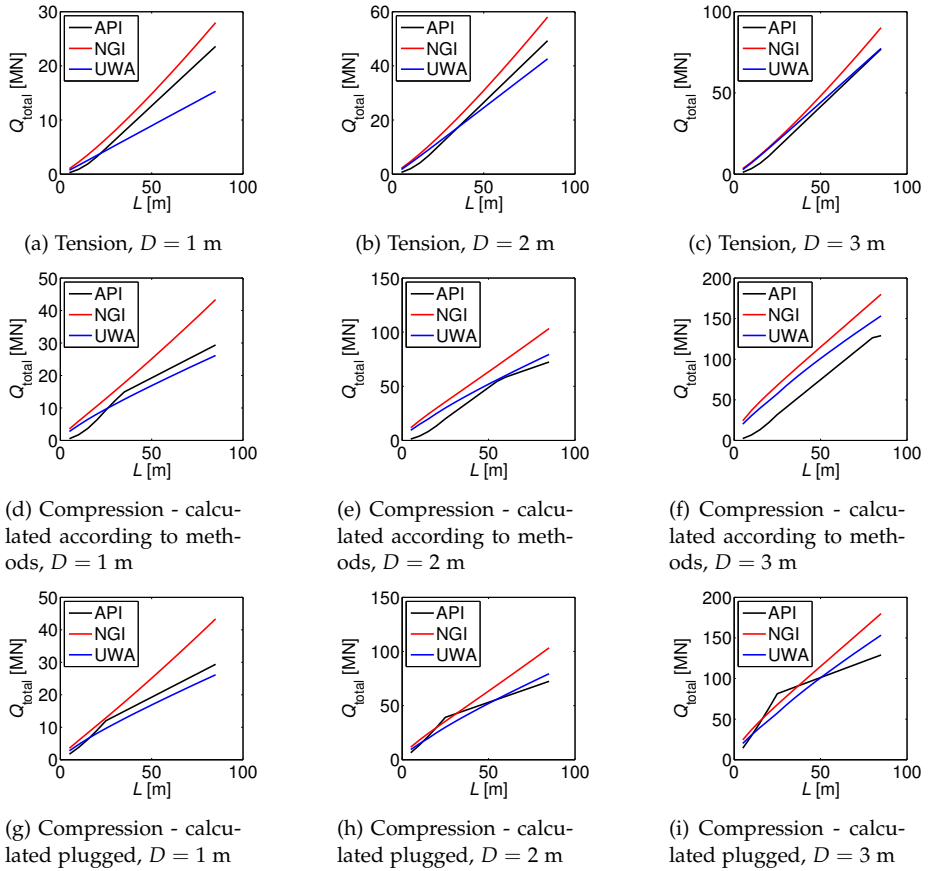
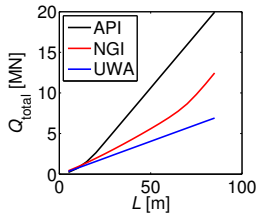
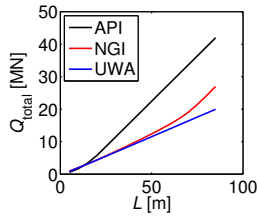


Figure B.4: Calculated capacities for piles in tension and compression in dense sands.

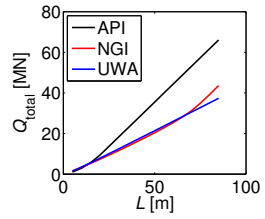
B.3. Comparison of Design Methods



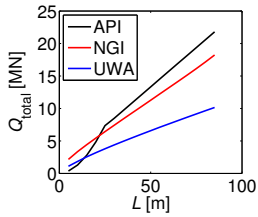
(a) Tension, $D = 1$ m



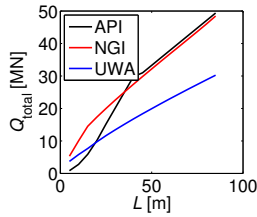
(b) Tension, $D = 2$ m



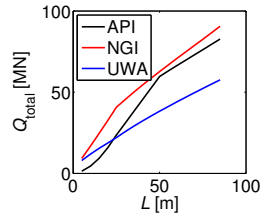
(c) Tension, $D = 3$ m



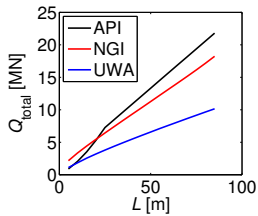
(d) Compression - calculated according to methods, $D = 1$ m



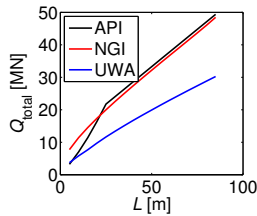
(e) Compression - calculated according to methods, $D = 2$ m



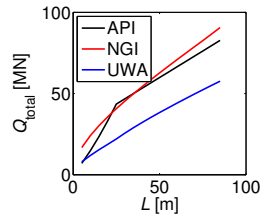
(f) Compression - calculated according to methods, $D = 3$ m



(g) Compression - calculated plugged, $D = 1$ m



(h) Compression - calculated plugged, $D = 2$ m



(i) Compression - calculated plugged, $D = 3$ m

Figure B.5: Calculated capacities for piles in tension and compression in loose sands.

If a pile with a diameter of 1 m were to be designed for a design load of approximately 10 MN, NGI-99 would predict a pile length of 35 m while UWA-05 would predict a pile length of 55 m. This is a great difference that can have a large economic effect when designing piles for an offshore wind farm.

B.3.3 Dense Sand, Piles in Compression

Figures B.4d to B.4f shows the predictions of the compression capacity for piles in dense sand. For the given soil conditions, API-00 is calculated unplugged for $L < 35$ m for $D = 1$ m, $L < 60$ m for $D = 2$ m, and $L < 85$ m for $D = 3$ m, respectively. The predictions of the bearing capacity for these cases are conservative compared to the predictions given by NGI-99 and UWA-05. NGI-99 only calculates unplugged for a pile diameter of 1 m and length less than 10 m.

NGI-99 predicts the highest capacities for piles with $D = 1$ m. The difference between the NGI-99 predictions and the predictions of API-00 and UWA-05 becomes more distinct as the pile length increases. The capacities predicted by NGI-99 increases from being 30% higher than the predictions of UWA-05 to being 60% higher for the longer piles. API-00 predicts lower capacities than UWA-05 for piles shorter than 25 m. For piles where API-00 assumes plugged failure mode, API-00 and UWA-05 shows the same incremental increase in capacity.

For a pile diameter of 2 m, NGI-99 predicts capacities approximately 25% higher than UWA-05. API-00 predicts much lower capacities for $L < 60$ m than the CPT-based methods except for piles longer than 60 m where API-00 calculates plugged failure mode and gives results similar to those of UWA-05.

As for piles in tension, the distinction between the capacities predicted by NGI-99 and UWA-05 decreases when the pile diameter increases. NGI-99 predicts capacities 15% higher than UWA-05 for a pile diameter of 3 m. For this pile diameter, API-00 gives lower capacities than the CPT-based methods for all pile lengths.

Figures B.4g to B.4i shows predictions of the bearing capacity if the piles are assumed to fail in a plugged manner for all three design methods. As expected, the predicted API-00 capacities increase for the piles where the method due to the static considerations would assume unplugged failure mode. For a pile diameter of 1 m, API-00 gives lower capacities than UWA-05 for piles shorter than 15 m. For the two other examined pile diameters, API-00 over-estimates the capacity compared to UWA-05 for pile lengths between

B.4. Conclusion

10 m and 60 m. Moreover, API-00 predicts capacities higher than NGI-99 for pile lengths between 20 m and 30 m for a pile diameter of 2 m and between 20 m and 40 m for a pile diameter of 3 m.

B.3.4 Loose Sand, Piles in Tension

Figures B.5a to B.5c shows the predictions of the tension capacity for piles in loose sand. The predictions for the three methods are very different. NGI-99 and UWA-05 give similar results for short piles with a diameter of 1 m. The similarity between the predictions of the two CPT-based methods amplifies with increasing diameter. Compared to UWA-05, API-00 heavily over-estimates the bearing capacity.

B.3.5 Loose Sand, Piles in Compression

Figures B.5d to B.5f shows that the three methods give very different predictions of the compression capacity for piles in loose sand. API-00 assumes unplugged failure mode for $L < 30$ m for $D = 1$ m, $L < 40$ m for $D = 2$ m, and $L < 50$ m for $D = 3$ m, respectively, for the given soil condition. The method under-estimates the bearing capacity for short piles, but heavily over-predicts the capacity for long piles compared to UWA-05.

NGI-99 assumes unplugged failure mode for pile lengths less than 15 m and 30 m for pile diameters of 2 m and 3 m, respectively. The method over-estimates the capacity for all the examined pile lengths and pile diameters compared to UWA-05. NGI-99 predicts capacities approximately 70% higher than UWA-05 for $D = 1$ m and 60% higher for $D = 2$ m and $D = 3$ m.

Using a plugged failure mode for NGI-99 makes no significant difference in the predictions of the capacity. For API-00, however, using plugged failure mode increases the capacities which then are further over-estimated compared to UWA-05 as shown in Figures B.5g to B.5i. However, the predictions of API-00 for piles longer than 25 m come closer to the predictions of NGI-99.

B.4 Conclusion

From the comparison of the methods, the three described design methods are seen to predict very different bearing capacities. The differences may occur because of the fact that the methods are developed based on pile load test on piles with lengths less than 30 m and diameters less than 1 m for the majority of the piles. UWA-05 is thought to be the most reliable method when extrapolating to the pile dimension offshore because it takes many of the physical

processes into account.

Comparing the predictions of API-00 to the predictions of UWA-05 provide conclusions similar to those in Lehané et al. (2005a). API-00 under-estimates the capacity of short piles in dense sand, over-estimates the capacity of long piles in loose sand. For piles in dense sand, API-00 gives a shaft capacity less conservative for piles in tension than for piles in compression. The capacity increases if the piles which are normally calculated unplugged are considered plugged. For piles in dense sand, API-00 over-predicts instead of under-predicting the capacity except for short piles. For piles in loose sand, API-00 overpredicts the capacity compared to UWA-05, for short piles as well as for long piles when assuming plugged failure.

Comparing the predictions of NGI-99 to the predictions of UWA-05 provides the following conclusions: NGI-00 over-predicts capacities in dense sands for piles in compression. NGI-99 and UWA-05 give similar capacities for pile diameters of 3 m for piles in dense sands loaded in tension. NGI-99 over-predicts capacities for pile diameters of 1 m and 2 m for piles in dense sands loaded in tension. NGI-99 overpredicts capacities of piles in loose sand.

The variations in the prediction of the capacity of long piles in tension for the three methods indicate that little attention has been paid to developing an exact expression. Due to the low self-weight of the wind turbine structure, the tension capacity may determine the pile design. Therefore, it is important to develop a reliable design method for piles in tension. The predictions of the three methods vary a lot depending on pile lengths, pile diameters and relative density of the soil both for piles loaded in tension and in compression. In order to develop a reliable design method for offshore axially loaded piles, further analyses of the shaft friction are necessary.

Further analyses could include collection of more data of pile load tests for piles with the dimensions used offshore and with appurtenant CPT data for sites with varying soil relative densities. Furthermore, smallscale testing—or full-scale testing if possible—should be conducted so as to get an improved understanding of the shaft friction for both tension and compression loading.

Besides improved knowledge of how a pile acts during static loading, the effect of cyclic loading should also be examined to a wider extent. As described in the introduction, offshore wind turbines are very light structures compared to an offshore platform. This means that the piles in the foundation will change between compression and tension loading. The effect of this phenomenon and additional cyclic wave loading on the interface friction is very uncertain. To analyse this effect, laboratory cyclic loading test

B.5. Acknowledgement

should be conducted. During the tests, the pile should be statically loaded in either tension or compression and subjected to a series of load cycles with different amplitudes corresponding to an offshore wave situation. Additional tests where the static load shifts between compression and tension should be conducted as well to see the effect on the interface friction.

B.5 Acknowledgement

This research is funded by the Danish Advanced Technology Foundation via the programme “Cost-effective deep water foundations for large offshore wind turbines”. The financial support is sincerely acknowledged.

References

- API (2000), *Recommended Practice for Planning, Designing and Constructing Fixed Offshore Platforms – Working Stress Design*, American Petroleum Institute.
- API (2007), *Recommended Practice for Planning, Designing and Constructing Fixed Offshore Platforms – Working Stress Design. Errata and supplement 3*, American Petroleum Institute.
- Clausen, C., Aas, P. & Karlsrud, K. (2005), Bearing capacity of driven piles in sand, the NGI approach, in S. Gourvenec & M. Cassidy, eds, ‘Proceedings of the International Symposium on Frontiers in Offshore Geotechnics (ISFOG 2005)’, Taylor & Francis Group, p. 677–681.
- DNV (2010), *DNV-OS-J101–Design of offshore structures*, Det norske Veritas Classification A/S.
- Jamiolkowski, M., Lo Presti, D. & Manassero, M. (2003), Evaluation of relative density and shear strength of sands from CPT and DMT, in ‘Soil Behaviour and Soft Ground Construction: Geotechnical Special Publication No. 119’, ASCE 2003, pp. 201–238.
- Lehane, B., Schneider, J. & Xu, X. (2005a), *A Review of Design Methods for Offshore Driven Piles in Siliceous Sand*, The University of Western Australia.
- Lehane, B., Schneider, J. & Xu, X. (2005b), The UWA-05 method for prediction of axial capacity of driven piles in sand, in S. Gourvenec & M. Cassidy, eds, ‘Proceeding of the International Symposium on Frontiers in Offshore Geotechnics (ISFOG 2005)’, Taylor & Francis Group, p. 661–667.
- Randolph, M. & Gourvenec, S. (2011), *Offshore Geotechnical Engineering*, Spon Press.

- Schmertmann, J. (1978), *Guidelines for Cone Penetration Test, Performance and Design*, FHWA-TS-78-209, US Federal Highway Administration.
- Schneider, J., Xu, X. & Lehane, B. (2008), 'Database assessment of CPT-based design methods for axial capacity of driven piles in siliceous sands', *Journal of Geotechnical and Geoenvironmental Engineering* **134**(9), 1227–1244.

Appendix C

Static Tension Tests on Axially Loaded Pile Segments in Sand

Kristina Thomassen
Lars Vabbersgaard Andersen
Lars Bo Ibsen

The paper has been submitted to
Journal of geotechnical and Geoenvironmental Engineering
November, 2015

The layout has been revised.

Abstract

This paper provides laboratory test results of static axially loaded piles in sand. With a newly developed test setup, the pile-soil interface friction was investigated by using an open-ended steel pile segment with a diameter of 0.5 m. Use of a pile length of 1 m enabled the pile-soil interface friction to be analyzed at a given soil horizon while increasing the vertical effective stress in the sand. Test results obtained by this approach can be analyzed as single t-z curves and compared to predictions of unit shaft friction from current design methods for offshore foundations. The test results showed best agreement with the traditional design method given in the American Petroleum Institute (API) design code. When t-z curves obtained from the test results were compared to t-z curve formulations found in the literature, the Zhang formulation gave good predictions of the initial and post-peak parts of the t-z curves found in the test results.

C.1 Introduction

When the water depth exceeds 30 m, a jacket foundation with three or four legs becomes appropriate as the foundation for offshore wind turbines. Due to the light weight of wind turbine structures, one or more of these piles are sometimes loaded in tension. This situation has not been well examined because the primary use of pile foundations offshore has been in the oil and gas industry. In these applications, the weight of the structures is high compared to the horizontal loads from wind and waves, resulting in piles loaded in compression. Thus, research is needed within the field of axially loaded piles in tension.

Due to the expense, few full-scale tests have been conducted on offshore piles e.g. (Jardine & Standing 2012, Baeßler et al. 2013). Instead, pile behavior has been examined on the small scale in calibration chambers e.g. citepChan1980,Jardine2009,LeKouby2004 by using closed-ended piles of stainless steel or aluminum. The pile roughness was reduced to minimize scaling effects due to the relatively small size of the sand grains compared to the diameter of the pile.

The present research analyzed the resistance against pull-out of an axially loaded pile in dense to very dense sand, resembling the soil conditions found at specific wind park locations in the North Sea. The test setup attempted to model the pile-soil interface friction accurately, by using an open-ended steel pile segment with a diameter of 0.5 m, which is close to the diameter of the full-scale pile. Use of a pile length of 1 m enabled the pile-soil interface friction to be analyzed at a given soil horizon while increasing the effective stress

in the sand. Hence, t - z curves for different vertical effective stress levels could be determined and analyzed. The aim of the research was to determine the pull-out resistance of a pile in the serviceability mode (i.e., when the effect of the installation on the bearing capacity is reduced because of setup over time). Instead of installing the pile and leaving it in the test setup for a period of time before testing, the sand was processed after pile installation to a state thought to resemble the serviceability mode conditions.

Short descriptions of the test setup and test procedure are given, followed by the test results in the form of the measured bearing capacity of the pile segment. The results are compared to the unit skin friction determined from current design methods. Moreover, t - z curves are obtained from the test results and compared to expressions from the literature.

C.2 Methodology and Test Program

C.2.1 Test setup

Figures C.1 and C.2 show the test setup that consisted of a box of 2.5 m in diameter with a layer of dense sand of 1.2 m in depth. The hydraulic cylinder on the right was used to install the pile segment and to conduct cone penetration tests (CPTs). The hydraulic cylinder on the left was used during tests. The test sand was Aalborg University Sand No. 1 with the material properties given in Table C.1. Comprehensive descriptions of the test setup and sand processing procedure are provided by Thomassen et al. "Laboratory Test Setup for Cyclic Axially Loaded Piles in Sand," submitted, Aalborg University, Denmark.

The pile segment used in the tests had an outer diameter of $D_{\text{pile}} = 0.5$ m, pile wall thickness of $t_{\text{pile}} = 0.003$ m, and embedded length of $L_{\text{pile}} = 0.96$ m. The segment was made of steel, which resulted in a corroded pile surface to obtain the correct pile-soil interface properties. To minimize any contribution from base resistance in the planned cyclic loading tests, the wall thickness was chosen to be as small as possible without risking instability problems during pile installation. The idea of using a pile with a length of 0.96 m was to enable laboratory tests on a large-diameter pile, while increasing the vertical effective stress in the soil to simulate pile segments at different soil depths. The vertical effective stress in the soil was increased by using a membrane-vacuum system. An elastic rubber membrane was placed on the soil surface and tightened at the sandbox edge to create an airtight system coupled to a vacuum pump. The vertical effective stress was increased by applying suction to the sandbox through five quick couplings placed on the membrane.

C.2. Methodology and Test Program

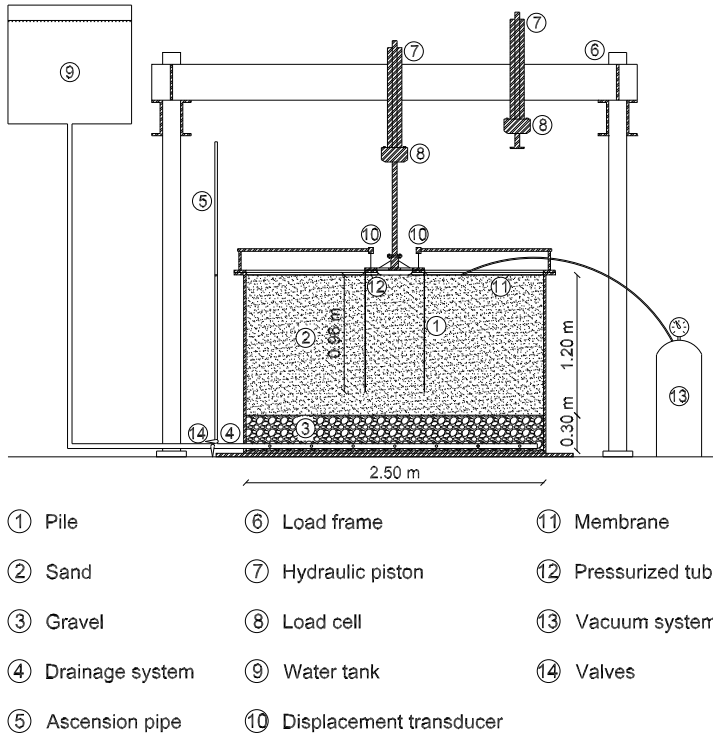


Figure C.1: Schematic illustration of the test setup.

Table C.1: Material Properties of Aalborg University Sand No. 1 Hedegaard & Borup (1993).

d_s [g/cm ³]	e_{\max} [-]	e_{\min} [-]	d_{50} [-]	$c_u = d_{60}/d_{10}$ [-]
2.64	0.854	0.549	0.14	1.78

C.2.2 Test Procedure

Sand in the sandbox was not replaced between tests. Instead, it was loosened by a hydraulic gradient, $i = 0.9i_{\text{crit}}$, to rehomogenize the soil after the previous test. The pile segment was then installed in the sand, which was then prepared to the desired relative density by a rod vibrator. The relative density of sand before the tests was approximately 85%. During a test, sand very close to the interface was affected by shearing, which might lead to grain crushing. The soil loosening and vibrating steps were assumed to rearrange the grains, resulting in new and undamaged interface conditions for each test. Thus, the bearing capacity of the pile segment was not influenced by any installation mechanism.



Figure C.2: Setup for a test with applied suction.

Seven static tension tests were conducted at suction levels of 0, 20, 35, and 70 kPa. These displacement-controlled tests were conducted at a displacement rate of 0.002 mm/s. During the tests, the pile head displacement, resulting load, and suction level were measured.

C.2.3 Expected Results

Test results are affected by the conditions of the test setup and test specimen, such as the pile-soil interface properties, installation method, pile segment dimensions, and boundary conditions. Effects of these parameters have been examined for different test setups in the literature. Interface conditions are affected by the relative density of the sand, relative interface roughness, sand grain properties (e.g., shape and size), and normal stress on the interface. Shear box tests under conditions of constant normal load and constant normal stiffness have revealed that, in the case of dense sand and high relative interface roughness, dilation occurs within the first few millimeters of displacement, with a subsequent decrease to a residual value of interface shear

C.3. Test Results

strength (Prai-ai 2013, Mortara et al. 2007, Boulon 1989, Uesugi & Kishida 1986). Dilatant behavior at the pile-soil interface induces a radial stress change that is dependent on the pile diameter (Boulon & Foray 1986) and may be significant for piles with $D < 1$ m (Jardine et al. 2005). Angular sand grains lead to a higher interface shear strength compared to rounded sand grains. Increased normal stresses on the interface will increase the interface shear strength. A virgin pile-soil interface, with sand prepared around the test pile, may show a peak followed by a decrease in shaft friction due to sand grain rearrangements during loading (Le Kouby et al. 2013). During pile installation, the grains are rearranged and likely crushed, which may affect the load-displacement curve such that no peak load occurs (Le Kouby et al. 2013).

The effect of the lateral boundary conditions has mostly been examined by penetration tests (Huang & Hsu 2005, Salgado et al. 1998, Schnaid & Houlsby 1991, Foray 1991, Ghionna & Jamiolkowski 1991). In a calibration chamber with rigid lateral boundaries, no lateral displacement occurs at the boundaries. When sand at the boundary is affected by pile loading, the pull-out resistance might be higher than the results of similar tests in free field (Salgado et al. 1998).

The above-mentioned effects on pile test results lead to some expected effects for the present study. For example, an increase of the vertical effective stress in the sand would lead to increases in the horizontal stress and the pull-out capacity of the pile segment. Dilation was expected because of the high relative density of the sand and high relative interface roughness. Moreover, the pile-soil interface was thought to have properties comparable to those of a virgin interface, due to the soil processing procedure. As a result, the shaft friction may peak and subsequently decline. Finally, due to the rigid lateral boundaries, higher capacities may be found in the present tests compared to tests conducted in free field.

C.3 Test Results

The following sections present the load-displacement curves obtained in the tests, as well as observations made during and after the tests. Tension load and resulting upward displacements of the pile are defined as negative. As suction is assumed to increase the effective stress to the same extent as an applied overburden pressure, the applied suction is defined as positive. Test results are compared to results obtained in a Plaxis model of the test setup.

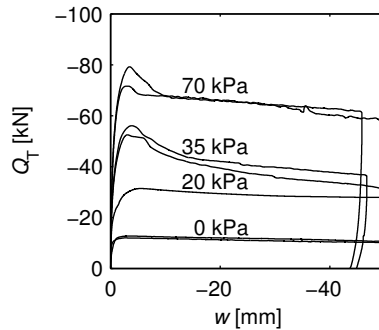


Figure C.3: Measured pull-out force versus pile head displacement. Surcharge is indicated in each test.

C.3.1 Recorded Load-Displacement Curves

Figure C.3 displays the load–displacement curves for all tests. All curves show the expected peak load. However, peaks of curves for tests at suction levels (surcharges) of 35 and 70 kPa are much more distinct than peaks at 0 and 20 kPa. Partial plugging was observed in all tests because the surface inside the pile was elevated approximately 30 mm compared to the outside sand surface.

In tests with the membrane, as not 100% hermetically sealed. This meant that most of the water was sucked out of the system before the test. Thus, sand was only partly saturated during tests with the membrane and applied suction. In these tests, sand near the pile–soil interface was stuck to the piles (Figure C.4). In tests without applied suction, the sand was saturated throughout the test and did not stick to the pile during pull-out.

Figure C.5 shows the uninstillation of the pile after a test with applied suction. The sand was not saturated before uninstillation and remained stuck to the upper one third of the pile shaft when the pile was pulled out of the sand. These observations implied that part of the failure happened in the sand and not at the pile–soil interface. This fact may have an increasing effect on the difference between the peak and residual values of the measured force during the tests, because a sand–sand shear band experiences greater dilation than a soil–plate interface (Lehane et al. 1993). Another explanation of the distinct peaks may be that part of the soil plug stopped moving along with the pile at some point during the tests.



Figure C.4: After tests with applied suction, sand in the interface is stuck to the pile.

C.3.2 Comparison to Finite Element Models

Tests at 0, 35, and 70 kPa were modelled as axisymmetric models in PLAXIS 2D AE to get a better understanding of the test mechanisms. To model the change in vertical effective stress obtained by applying suction to the sandbox, a surface load, P_0 , of the same magnitude was applied in the PLAXIS models. In these models, the sand was considered unsaturated. In the model without overburden pressure, the sand was saturated.

Table C.2 shows the material properties, which were chosen to resemble the conditions in the real test setup. Friction and dilation angles were determined from the results of CPTs conducted before each test by the method described in Ibsen et al. (2009). The constant volume interface friction angle, δ_{cv} , was chosen to be 28.8° . Ho et al. (2011) suggested a dependency of δ_{cv} on d_{50} and the interface displacement. For $d_{50} = 0.14$ (Aalborg University Sand No. 1), δ_{cv} is very close to the value of 28.8° recommended for CPT-based methods (Jardine et al. 2005, API 2011, Jardine et al. 1992). Table C.3 gives the material properties of the pile, which are the same as for the pile segment used in the test setup.

To obtain force values that were similar to the residual values of forces measured in the physical tests, high values of the coefficient of lateral earth pressure at rest, K_0 , had to be used in the models (i.e., $K_0 = 3$ for $P_0 = 0$ or 35 kPa, and $K_0 = 5$ for $P_0 = 70$ kPa). Figure C.6 shows the comparison between the test results and the Plaxis calculations. The large values of K_0 may be reasonable, as flat dilatometer tests conducted in the sandbox by Gaydadjzhiev et al. (2015) showed that K_0 values vary between 0.5 and 5. Soil processing with the rod vibrator may have introduced a large degree of overconsolidation. To reach the peak values from the tests in the PLAXIS models, either much higher values of K_0 or higher interface friction values must be applied.



Figure C.5: Uninstallation of the pile after a test with applied suction. Sand is not resaturated before uninstallation, and some sand is stuck to the upper one third of the pile.

Even if the residual force was obtained in the PLAXIS models, the displacement of the soil plug was smaller than the displacement observed in the tests. However, during the first part of the loading in PLAXIS, the soil moved up along with the pile (although soil may not have moved at the same rate as the pile). As loading continued, the bottom part of the soil plug stopped moving. This implies that the force measured in the laboratory tests included the weight of the entire soil plug at the beginning of the test. As the test proceeded, this weight was reduced to around two thirds of the total soil plug weight. These observations may explain the observed large peak force. Of course, the explanation implies that an internal friction along the pile shaft was not activated when the soil plug stopped moving.

C.3.3 Shaft Friction

Due to partial plugging, it was difficult to determine the contribution of the internal skin friction on the pile segment wall to the skin friction resistance, Q_s . The contribution can be assumed to range between no contribution (fully plugged) and complete contribution (unplugged). This relationship can be expressed as follows:

C.3. Test Results

Table C.2: Material Properties of the Sand and Interfaces.

Parameter	Unit	Sand (0 kPa)	Sand (35 kPa)	Sand (70 kPa)	gravel
General					
Material Model	-	MC	MC	MC	MC
Type of material behaviour	-	Drained	Drained	Drained	Drained
Soil unit weight above phreatic level, γ_{unsat}	kN/m ³	17	17	17	18
Soil unit weight below phreatic level, γ_{sat}	kN/m ³	20	20	20	20
Parameters					
Young's modulus, E'	kN/m ²	13400	17000	23600	45000
Poisson's ratio, ν'	-	0.23	0.23	0.23	0.3
Cohesion (constant), c'_{ref}	kN/m ²	0.1	0.1	0.1	0.1
Friction angle, ϕ'	°	53.0	51.0	48.1	45
Dilation angle, ψ'	°	19.0	18.7	17.8	15
Interface friction angle, δ_{cv}	°	28.8	28.8	28.8	-
$R_{\text{inter}} (\tan \delta_{\text{cv}} / \tan \phi')$	-	0.41	0.45	0.49	-

Table C.3: Material Properties of the Pile (Shell).

Parameter	Unit	Pile
Material type	-	Elastic, isotropic
Axial stiffness, EA	kN/m	630000
Flexural rigidity, EI	kN·m ² /m	0.4725
Specific weight, w	kN/m/m	0.52
Poisson's ratio, ν	-	0.3

$$Q_{s,\text{plugged}} = Q_T - W_{\text{pile}} - W_{\text{plug}} \quad (\text{C.1})$$

$$Q_{s,\text{unplugged}} = Q_T - W_{\text{pile}} \quad (\text{C.2})$$

where W_{pile} is the weight of the pile segment and equipment under the load cell, and W_{plug} is the weight of the soil plug.

Figure C.7 shows the difference between Equations (C.1) and (C.2), using a test conducted at 70 kPa as an example. However, even the situation of a fully plugged pile during the first millimeters of displacement and a fully unplugged pile for the remainder of the test does not explain the distinct peak of the load-displacement curve. Therefore, the skin friction resistance,

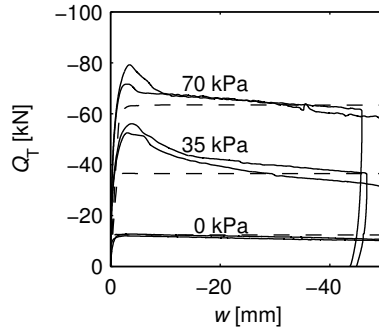


Figure C.6: Plaxis results versus test results. Dashed lines are Plaxis results with $K_0 = 3$ for surcharges of 0 and 35 kPa, and with $K_0 = 5$ for a surcharge of 70 kPa.

Q_s , is given as

$$Q_s = A_s \int_0^{L_{\text{pile}}} f_s dz \quad (\text{C.3})$$

where A_s is the pile area per unit length of the pile, L_{pile} is the pile tip depth, and f_s is the unit shaft friction at depth z . For the plugged case, A_s is the external pile area. For the unplugged case, A_s is both the internal and external pile area. Figure C.8 displays the unit shaft friction for these two conditions, for a test conducted at 70 kPa.

In the next section, the unit skin friction obtained from the test results is compared to the results from current design methods. Moreover, t - z curves are derived from the test results and compared to expressions for t - z curves given in the literature.

C.4 Comparison to Existing Design Methods

The test results were compared to the traditional design methods given by the American Petroleum Institute (API) (API 2011) and to CPT-based design methods. The desired outcome was a formulation of f_s expressed as an empirical coefficient, k_f , relating the average cone resistance, q_c , at depth z to the skin friction, f_s , such as:

$$f_s = k_f q_c \quad (\text{C.4})$$

k_f factors were found for the design methods and compared to those of the test results.

C.4. Comparison to Existing Design Methods

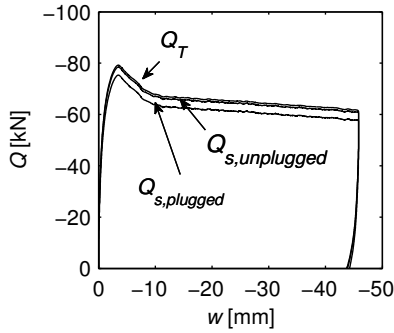


Figure C.7: Difference between fully plugged and unplugged determinations of Q_s for a test conducted at 70 kPa.

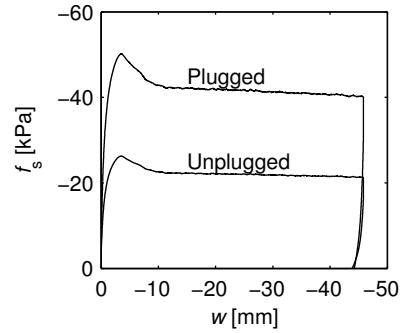


Figure C.8: Unit shaft friction versus pile head displacement for the plugged and unplugged cases, for a test conducted at 70 kPa.

C.4.1 CPT Cone Resistance

To find the k_f factors, the CPT cone resistance in the sandbox had to be known. Before each test, CPTs were performed to determine the relative density of the sand. CPT results could only be used for tests without applied suction; a CPT could not be conducted when the pile segment was installed and a membrane was placed on the sand surface. Therefore, no q_c measurements relating directly to each test were available. However, Gaydadjhiev et al. (2015) conducted CPTs in the sandbox at different stress levels without any test specimens installed.

The empirical relationship between the effective vertical stress, σ'_v , and the CPT cone resistance, q_c , had the form:

$$q_{c,\text{fitted}} = 5324.1\text{kPa} \left(\frac{\sigma'_v}{1\text{kPa}} \right)^{0.3998} \quad (\text{C.5})$$

Figure C.9 shows q_c as a function of σ'_v based on Equation (C.5) and the q_c values from CPTs conducted before tests without applied suction. Although the q_c profiles are different, the $\int q_c$ results from tests without applied suction do not differ substantially. Thus, results from the fitted profile were used in the comparison of all tests. For tests without applied suction, σ'_v was calculated by assuming that the sand was saturated throughout the test. For tests with a membrane and applied suction, σ'_v was calculated by assuming unsaturated sand, because most of the water was sucked out of the sandbox before the test.

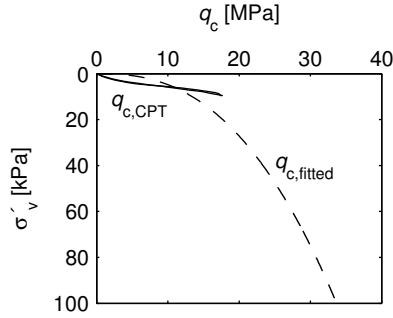


Figure C.9: Cone resistance based on CPTs conducted before tests without suction and on the fitted expression given by Equation (C.5) versus the vertical effective stress.

C.4.2 Traditional Design Method

The API (2011) suggests the following definition of the unit shaft friction:

$$f_s = \beta \sigma'_v = K \tan(\delta) \sigma'_v \quad (\text{C.6})$$

where β is a dimensionless shaft friction factor, σ'_v is the effective vertical stress at a given depth, K is the coefficient of lateral earth pressure, and δ is the interface friction angle. As K was unknown, the recommendations given in API (2011) for $D_r = 0.85$ were followed; hence, $\beta = 0.56$.

C.4.3 CPT-based Methods

The Det norske Veritas (DNV 1992) proposed the simplest form of a CPT-based method, in which k_f is given in terms of a most probable value (0.001) and a highest expected value (0.003). More advanced CPT-based methods include the ICP-05, UWA-05, and NGI-05 methods, which all account for the stress state, pile dimensions and material, as well as installation effects (Jardine et al. 2005, Lehane et al. 2005b, Clausen et al. 2005).

The ICP-05 and UWA-05 methods follow the Coulomb criterion,

$$f_s = \sigma'_{rf} \tan \delta_{cv} = (\sigma'_{rc} + \Delta \sigma'_{rd}) \tan \delta_{cv} \quad (\text{C.7})$$

where σ'_{rf} is the radial effective stress at failure, δ_{cv} is the constant volume interface friction angle, σ'_{rc} is the radial effective stress after installation and equalization, and $\Delta \sigma'_{rd}$ is the change in radial stress due to the loading stress path (dilation). Expressions for σ'_{rc} and $\Delta \sigma'_{rd}$ vary for the ICP-05 and UWA-05

C.4. Comparison to Existing Design Methods

Table C.4: Unit Shaft Friction Values for Open-Ended Steel Piles Loaded in Tension (API 2011).

Method	a	b	c	u	v
Simplified ICP	0.1	0.2	0.4	0.016	$4\sqrt{A_r}$
Offshore UWA	0.0	0.3	0.5	0.022	2

methods. The contribution from dilation may be important for piles with a diameter less than 1 m, whereas the contribution is negligible for full-scale offshore piles (Jardine et al. 2005).

For offshore piles, the API (2011) suggests a simplified expression of the ICP-05 and UWA-05 methods for f_s , given by

$$f_s = u \left(\frac{\sigma'_v}{p_a} \right)^a A_r^b \max \left(\frac{h}{D}, v \right)^{-c} \tan(\delta_{cv}) q_c \quad (\text{C.8})$$

where σ'_v is the local vertical effective stress; p_a is a reference stress (100 kPa); $A_r = 1 - (D_i/D)^2$ is the effective area ratio; h is the distance above the pile tip; D and D_i are the outer and inner pile diameters, respectively; δ_{cv} is the interface friction angle; q_c is the local cone resistance; and u , a , b , c , and v are constants with the values given in Table C.4. Equation (C.8) assumes a negligible contribution from dilation, and assumes that the piles are open-ended pipe piles driven unplugged but failing plugged. This expression was used in the following analyses.

Equation (C.8) contains installation effects that were absent from the test results due to the use of the soil preparation procedure. First, the effective area ratio, A_r , accounts for changes in radial stress at the pile tip during installation. This ratio is related to the amount of soil that is displaced during installation and depends on whether the pile is closed-ended ($A_r = 1$), partially plugged ($0.1 < A_r < 1$), or unplugged ($A_r = 0.1$). The very small wall thickness of the test specimen (3 mm) resulted in a factor of 0.0239, which was lower than the unplugged value of $A_r = 0.1$ and indicated a very low disturbance of the soil during installation. As it was assumed that there were no installation effects, this term was included when comparing the test results to the design methods. Second, h/D is the friction fatigue effect that is related to installation. At a given soil horizon, the radial stress decreases as the pile tip moves further into the soil. h/D was ignored in the comparison of the test results, leaving a simplified expression for k_f :

$$k_f = u \left(\frac{\sigma'_v}{p_a} \right)^a A_r^b \tan(\delta_{cv}) \quad (\text{C.9})$$

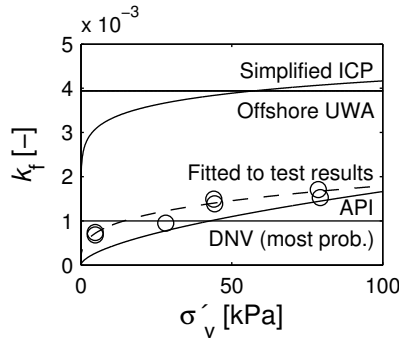


Figure C.10: k_f factors calculated based on the test results, the API method, and the CPT-based methods.

Figure C.10 shows the k_f factors calculated based on the test results, the API method, and the CPT-based methods. The k_f factors for the test results were based on the maximum values of f_s for the plugged calculation. For the unplugged calculation, the k_f factors would decrease by nearly one half. The test results suggested a stress dependency of k_f , which resulted in an expression based on Equation (C.9) with the factor $u = 0.01$ and powers $a = b = 0.3$.

The k_f factors determined by the API method are very different from the ones determined by the simplified ICP and offshore UWA methods. This observation is in agreement with the conclusions of the database study performed by Lehane et al. (2005a), in which the API method seemed to underpredict the capacity of short piles in dense sand. However, for the current test results, the API method gave the best prediction of the unit shaft friction.

In the analysis of the k_f factors, the effects of dilation on the radial effective stress of the pile were not taken into account because the unit skin friction in the simplified ICP-05 and UWA-05 methods has a simpler formulation where the dilation term is excluded. However, because the pile segment used in the tests had a diameter of 0.5 m (i.e., < 1 m), the contribution of dilation-induced changes in the radial effective stress must be examined. The change in radial stress due to dilation is given by (Jardine et al. 2005, Lehane et al. 2005b):

$$\Delta\sigma'_{rd} = 4G \frac{\Delta r}{D} \quad (\text{C.10})$$

where G is the shear modulus of sand, and Δr is the radial displacement in the interface shear zone (assumed to be 0.02 mm for a lightly rusted pile). The UWA-05 and ICP-05 methods calculate the shear modulus differently, although both expressions are based on Baldi et al. (1986). The UWA-05

C.5. t - z Curves

method suggests the following expression for the shear modulus:

$$G_{\text{UWA}} = 185q_c q_{\text{cN1}}^{-0.7} \quad (\text{C.11})$$

$$q_{\text{cN1}} = \frac{q_c / p_a}{(\sigma'_{v0} / p_a)^{0.5}} \quad (\text{C.12})$$

The ICP-05 method gives the following definition:

$$G_{\text{ICP}} = G_0 = q_c \left(0.0203 + 0.00125\eta - 1.21 \cdot 10^{-5}\eta^2 \right)^{-1} \quad (\text{C.13})$$

$$\eta = \frac{q_c}{(\sigma'_{v0} / p_a)^{0.5}} \quad (\text{C.14})$$

where q_c is the average cone resistance at depth z , p_a is the reference stress (100 kPa), and is the effective vertical stress at a given depth.

When dilation effects were included in the calculation of f_s based on the UWA-05 method, the contribution was negligible (approximately 4%). However, for the ICP-05 method, the contribution lay between 7% and 10%, increasing with decreasing effective vertical stress, and should be taken into account. If the contribution is compared directly to the test results, then the UWA method predicts that 10–30% of the unit skin friction stems from dilation effects, which increases with decreasing vertical effective stress. The ICP method predicts contributions of 16–45%. These contributions are substantial; thus, the proposed expression of the k_f factor for the test results should include a term accounting for the dilation effects.

C.5 t - z Curves

Various t - z curve formulations are used to determine the pile-shaft response of axially loaded piles. Some of these formulations are used in this paper in the comparison to the t - z curves obtained from the test results (see Appendix A). The simplest of these formulations is given in API (2011). More advanced formulations include the parabolic function (Randolph & Gourvenec 2011), 80% function (Fellenius 2013), and Zhang function (Zhang & Zhang 2012) that all introduce nonlinear variations in the initial parts of the curves and the possibility of modelling strain-softening.

To compare the methods to the t - z curves obtained from the test results, an average displacement corresponding to the maximum unit skin friction ($z_{t_{\max}} = 3.5$ mm) and an average ratio between the residual and maximum unit skin frictions ($\beta_s = t_{\text{res}}/t_{\max} = 0.81$) were used. The method gave good estimates for most of the test results, except for the two tests conducted with a surcharge of 35 kPa (Figure C.11). For these two tests, however, the 80% function was in good agreement with the strain-softening behavior observed in the tests.

Figure C.12 shows the initial part of the t - z curves. The 80% function and the Zhang function provided the best agreement with the initial part of the test results, whereas the API formulation gave poor predictions of the initial and post-peak parts of the test t - z curves. Of the four presented formulations, the Zhang function had the best fit to the test t - z curves.

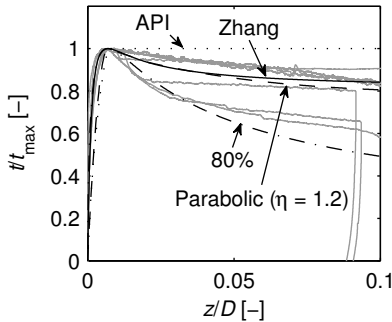


Figure C.11: Various t - z curves compared to the t - z curves obtained from the test results (gray).

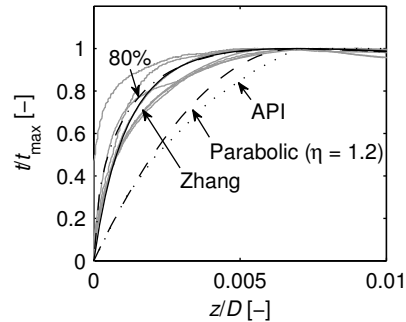


Figure C.12: Initial part of the t - z curves displayed by (Figure C.11).

C.6 Conclusion

This paper presented seven static axial loading tests on a pile segment installed in dense sand in a laboratory setup. To model the pile–soil interface properties to be as close as possible to the properties of full-scale piles, a pile segment diameter of 0.5 m was chosen. To accommodate this diameter in the test setup, the pile segment was 0.96 m long, and the vertical effective stresses in the soil were increased by a vacuum system. Thus, each test simulated a segment of a pile at different overburden pressures. By comparing the test results to PLAXIS models of each test, it was concluded that the sand was highly overconsolidated due to the soil preparation procedure in order to produce the determined pull-out capacities.

C.7. Appendix A

The unit shaft friction was found from the test results by determining the k_f factor linking the CPT cone resistance in the sand to the unit shaft friction. Test results were compared to current design methods. The k_f factor of the test results was dependent on the vertical effective stress. The traditional API method is normally considered to underestimate the shaft capacity of short piles in dense sand. However, compared to the more advanced CPT-based methods, the simplified ICP and offshore UWA, the test results showed better agreement with the predictions of the API method. A formulation of the k_f factor for the test results was suggested.

Due to the short length of the piles, each test was considered to provide a unique t - z curve for each effective stress level. When these curves were compared to current t - z curve formulations, the Zhang formulation, developed from tests on bored piles, gave a good prediction of the initial and post-peak parts of the t - z curves from the test results.

C.7 Appendix A

This appendix presents the four t - z curve formulations used in the analysis. The following symbols are used: t is the mobilized unit skin friction, z is the local axial pile deflection, t_{\max} is the maximum unit skin friction with the corresponding axial pile deflection $z_{t_{\max}}$, t_{res} is the residual unit skin friction over a post-peak displacement Δz_{res} , t_{post} is the residual unit skin friction at a post-peak displacement Δz , and η_{res} is a softening parameter.

C.7.1 API

The API (2011) provides the t - z curve formulation given in Table C.5.

Table C.5: t - z Curve Formulation in API (2011).

z/z_{\max}	t/t_{\max}
0.00	0.00
0.16	0.30
0.31	0.50
0.57	0.75
0.80	0.90
1.00	0.10
2.00	0.10
∞	1.00

C.7.2 Zhang Function

Zhang & Zhang (2012) propose the following formulations for t - z curves from tests on bored piles:

$$t = \frac{z(a + cz)}{(a + bz)^2} \quad (\text{C.15})$$

$$t_{\max} = \frac{1}{4(b - c)} \quad (\text{C.16})$$

$$z_{t_{\max}} = \frac{a}{b - 2c} \quad (\text{C.17})$$

$$a = (b - 2c) z_{t_{\max}} \quad (\text{C.18})$$

$$b = \frac{1 - \sqrt{1 - \beta_s}}{2\beta_s} \frac{1}{t_{\max}} \quad (\text{C.19})$$

$$c = \frac{2 - \beta_s - 2\sqrt{1 - \beta_s}}{4\beta_s} \frac{1}{t_{\max}} \quad (\text{C.20})$$

$$\beta_s = \frac{t_{\text{res}}}{t_{\max}} \quad (\text{C.21})$$

C.7.3 80% Function

Fellenius (2013) gives the following formulation for the 80% function:

$$t = \frac{\sqrt{z}}{C_1 z + C_2} \quad (\text{C.22})$$

$$C_1 = \frac{1}{2t_{\max}\sqrt{z_{t_{\max}}}} \quad (\text{C.23})$$

$$C_2 = \frac{\sqrt{z_{t_{\max}}}}{2t_{\max}} \quad (\text{C.24})$$

C.7.4 Parabolic Function

Randolph & Gourvenec (2011) suggest a parabolic function for t - z curves:

$$t_{\text{ini}} = t_{\text{max}} \left(2 \frac{z}{z_{\text{tmax}}} - \left(\frac{z}{z_{\text{tmax}}} \right)^2 \right) \quad (\text{C.25})$$

$$t_{\text{post}} = t_{\text{max}} - 1.1 (t_{\text{max}} - t_{\text{res}}) \left(1 - \exp \left(-2.4 \left(\frac{\Delta z}{\Delta z_{\text{res}}} \right)^{\eta_{\text{res}}} \right) \right) \quad (\text{C.26})$$

C.8 Acknowledgments

This research was funded by the Danish Advanced Technology Foundation via the program “Cost-effective deep water foundations for large offshore wind turbines”. The funding is sincerely appreciated.

References

- API (2011), *Geotechnical and Foundation Design Considerations*, API RP 2GEO, 1. ed. edn, American Petroleum Institute.
- Baeßler, M., Rücker, W., Cuéllar, P., Georgi, S. & Karbeliov, K. (2013), ‘Large-scale testing facility for cyclic axially loaded piles’, *Steel Construction* 6(3), 200–206.
- Baldi, G., Belotti, R., Ghionna, V., Jamiolkowski, M. & Pascalini, E. (1986), Interpretation of CPTs and CPTUs; 2nd part; drained penetration of sands, in ‘Proceedings of the 4th International Geotechnical Seminar’, p. 143–156.
- Boulon, M. (1989), ‘Basic features of soil structure interface behaviour’, *Computers and Geotechnics* 7, 115–131.
- Boulon, M. & Foray, P. (1986), Physical and numerical simulation of lateral shaft friction along offshore piles in sand, in ‘Proceedings of the 3rd International Conference on Numerical Methods in Offshore Piling’, Institut Français du Pétrole, Laboratoire Central des Ponts et Chaussées, p. 127–147.
- Clausen, C., Aas, P. & Karlsrud, K. (2005), Bearing capacity of driven piles in sand, the NGI approach, in S. Gourvenec & M. Cassidy, eds, ‘Proceedings of the International Symposium on Frontiers in Offshore Geotechnics (ISFOG 2005)’, Taylor & Francis Group, p. 677–681.

- DNV (1992), *Foundations. Classification notes No. 30.4*, Det norske Veritas Classification A/S.
- Fellenius, B. (2013), 'Discussion on Zhang, Q.Q. and Zhang, Z.M. (2012). "A simplified non-linear approach for single pile settlement analysis."', *Canadian Geotechnical Journal* **50**(6), 685–687.
- Foray, P. (1991), Scale and boundary effects on calibration chamber pile tests, in 'Proceeding of the 1st International Symposium on Calibration Chamber Testing (ISOCCT1)', Elsevier, p. 147–160.
- Gaydazhiev, D., Puscasu, I., Vaitkunaite, E. & Ibsen, L. (2015), Investigation of dense sand properties in shallow depths using CPT and DMT, in 'Proceedings of the 3rd International Conference on the Flat Dilatometer', International Society for Soil Mechanics and Geotechnical Engineering, p. 223–230.
- Ghionna, V. & Jamiolkowski, M. (1991), A critical appraisal of calibration chamber testing of sands, in 'Proceedings of the 1st International Symposium on Calibration Chamber Testing/ISOCCT1', Elsevier, p. 13–39.
- Hedegaard, J. & Borup, M. (1993), *Klassifikationsforsøg med Baskarp Sand No. 15*, Aalborg University, Denmark.
- Ho, T., Jardine, R. & Anh-Minh, N. (2011), 'Large-displacement interface shear between steel and granular media', *Géotechnique* **61**(3), 221–234.
- Huang, A.-B. & Hsu, H.-H. (2005), 'Cone penetration tests under simulated field conditions', *Géotechnique* **55**(5), 345–354.
- Ibsen, L., Hanson, M., Hjort, T. & Thaarup, M. (2009), *MC-Parameter Calibration of Baskarp Sand No. 15.*, DCE Technical Report No. 62, Department of Civil Engineering, Aalborg University, Denmark.
- Jardine, R., Chow, F., Overy, R. & Standing, J. (2005), *ICP design methods for driven piles in sands and clays*, Thomas Telford.
- Jardine, R., Lehane, B. & Everton, S. (1992), Friction coefficients for piles in sands and silts, in 'Proceedings of the International Conference on Off-shore Site Investigation and Foundation Behaviour', Society for Underwater Technology, Springer Netherlands, p. 661–677.
- Jardine, R. & Standing, J. (2012), 'Field axial cyclic loading experiments on piles driven in sand', *Soils and Foundations* **52**(4), 723–736.
- Le Kouby, A., Dubla, J., Canou, J. & Francis, R. (2013), 'Pile response in sand: experimental development and study', *International Journal of Physical Modelling in Geotechnics* **13**(4), 122–137.

References

- Lehane, B., Jardine, R., Bond, A. & Frank, R. (1993), 'Mechanisms of shaft friction on sand from instrumented pile tests', *Journal of Geotechnical Engineering* **119**(1), 19–35.
- Lehane, B., Schneider, J. & Xu, X. (2005a), *A Review of Design Methods for Offshore Driven Piles in Siliceous Sand*, The University of Western Australia.
- Lehane, B., Schneider, J. & Xu, X. (2005b), The UWA-05 method for prediction of axial capacity of driven piles in sand, in S. Gourvenec & M. Cassidy, eds, 'Proceeding of the International Symposium on Frontiers in Offshore Geotechnics (ISFOG 2005)', Taylor & Francis Group, p. 661–667.
- Mortara, G., Mangiola, A. & Ghionna, V. (2007), 'Cyclic shear stress degradation and post-cyclic behaviour from sand-steel interface direct shear tests', *Canadian Geotechnical Journal* **44**, 739–752.
- Prai-ai, S. (2013), *Behaviour of soil-structure interfaces subjected to a large number of cycles. Application to piles*, PhD Thesis, University of Grenoble.
- Randolph, M. & Gourvenec, S. (2011), *Offshore Geotechnical Engineering*, Spon Press.
- Salgado, R., Mitchell, J. & Jamiolkowski, M. (1998), 'Calibration chamber size effects on penetration resistance in sand', *Journal of Geotechnical and Geoenvironmental Engineering* **124**(9), 878–887.
- Schnaid, F. & Houlsby, G. (1991), 'An assessment of chamber size effects on the calibration of in situ tests in sand', *Géotechnique* **41**(3), 437–445.
- Uesugi, M. & Kishida, H. (1986), 'Influential factors of friction between steel and dry sand', *Soils and Foundations* **26**(2), 33–46.
- Zhang, Q. & Zhang, Z. (2012), 'A simplified non-linear approach for single pile settlement analysis', *Canadian Geotechnical Journal* **49**(11), 1256–1266.

Appendix D

Axial Cyclic Loading Tests on Pile Segments in Sand

Kristina Thomassen
Lars Vabbersgaard Andersen
Lars Bo Ibsen

The paper has been submitted to
International Journal of Offshore and Polar Engineering
Januar, 2016

The layout has been revised.

Abstract

This paper presents one-way cyclic tension tests on a pile segment installed in dense sand in a laboratory test setup. The test setup allowed application of surcharges to increase the vertical effective stress. The open-ended pipe pile segment was 0.5 m in diameter and 1 m in length. The test results showed that cyclic loading with small amplitudes can increase the shaft capacity, but increase of the cyclic amplitude can result in large accumulated displacements and decreased cyclic reloading stiffness. The test results are compared to an exciting interaction diagram.

D.1 Introduction

Undesirable permanent tilt of offshore wind turbines on jacket foundations can occur as result of accumulated upwards displacements of foundation piles loaded in tension during a storm. To prevent this from happening and avoid load cases resulting in large accumulated displacements of the foundation piles in the future, it is necessary to analyze the effect of cyclic loading on axially loaded piles in tension.

Field tests and small-scale tests with idealized data series of one-way or two-way cyclic loading have been carried out (Chan & Hanna 1980, Al Douri & Poulos 1994, Chin & Poulos 1998, Le Kouby et al. 2004, Tsuha et al. 2012, Silva et al. 2013). These tests analyze the effects of mean load levels and cyclic amplitudes on the pile capacity (Tsuha et al. 2012, Jardine et al. 2006, Le Kouby et al. 2004). Moreover, researchers analyzed the local stress paths in the soil adjacent to the pile (Tsuha et al. 2012) as well as the behavior in the pile-soil interface e.g. (Tsuha et al. 2012, Prai-ai 2013, Mortara et al. 2007).

Field tests are expensive and researchers often conduct laboratory tests instead, even though this suffers from the disadvantage of small-diameter pile specimens with incorrectly modeled pile-soil interface. The one-way cyclic tension tests presented in this paper are conducted in a laboratory test setup but with an open-ended pile segment with a diameter of 0.5 m and a length of 1 m. By increasing the vertical effective stresses in the sand by means of a surcharge, different soil depths are simulated and the test results provide the capacity of 1 m pile segment at a given soil depth.

This paper will provide a short description of the test setup and present the chosen test program. The test program is based on the aim of analyzing the effect of one-way cyclic tests with the mean load in tension and on the interaction diagram by Jardine & Standing (2012). This paper will also include analysis of the effects of the chosen mean load level and cyclic load amplitude

on the accumulated displacement and post-cyclic capacity.

D.2 Methodology

To minimize the scaling effects in the laboratory tests, the objective was to model the pile–soil interface correctly. Therefore, it was desired to have a pile diameter approximating full-scale pile diameters and to make the pile specimen of steel to obtain the lightly rusted surface seen for full-scale piles. The test facilities at Aalborg University Geotechnical Laboratory could not accommodate a full-scale pile, and it was chosen to use an open-ended 1 m long pile segment with a diameter of 0.5 m. The tests were conducted in a sandbox with the possibility of increasing the effective vertical stresses in the sand. Thus, 1 m pile segments at different soil depths could be simulated in the tests. Thomassen et al. (2015) provide a detailed description of the test setup while the following sections provide a short description.

D.2.1 Sandbox

Figure D.1 shows the test setup which consisted of a large circular box with a diameter of 2.5 m and a height of 1.5 m. The vertical boundaries and the bottom boundary were rigid. A drainage system at the bottom of the sand box made it possible to saturate and loosen the sand by means of a hydraulic gradient. The sand layer was 1.2 m thick and consisted of Aalborg University Sand No. 1 with the properties given in Table D.1.

Hydraulic load systems were used to install and load the pile. The hydraulic piston to the right was used when installing the pile while the other piston was used for the tests. Tension loading, Q_T , and upward displacement of the pile segment, w , are defined negative.

The vertical effective stresses were increased by placing an elastic rubber membrane on the sand surface and sealing it along the edge of the sand box and at the pile. Suction was then applied to the sandbox by connecting a vacuum pump to the membrane through five quick-couplings. The maximum applicable suction level was a pressure of -70 kPa, corresponding to a surcharge of 70 kPa. During the tests with applied suction, the water was sucked out of the sand box leaving the sand with a small degree of saturation. In the tests with no suction applied, the sand was fully saturated.

D.2.2 Test Segment

Figure D.2 shows the pile specimen that was a segment of an open-ended steel pipe pile. The length was 1 m, and the embedded length in the tests was

D.2. Methodology

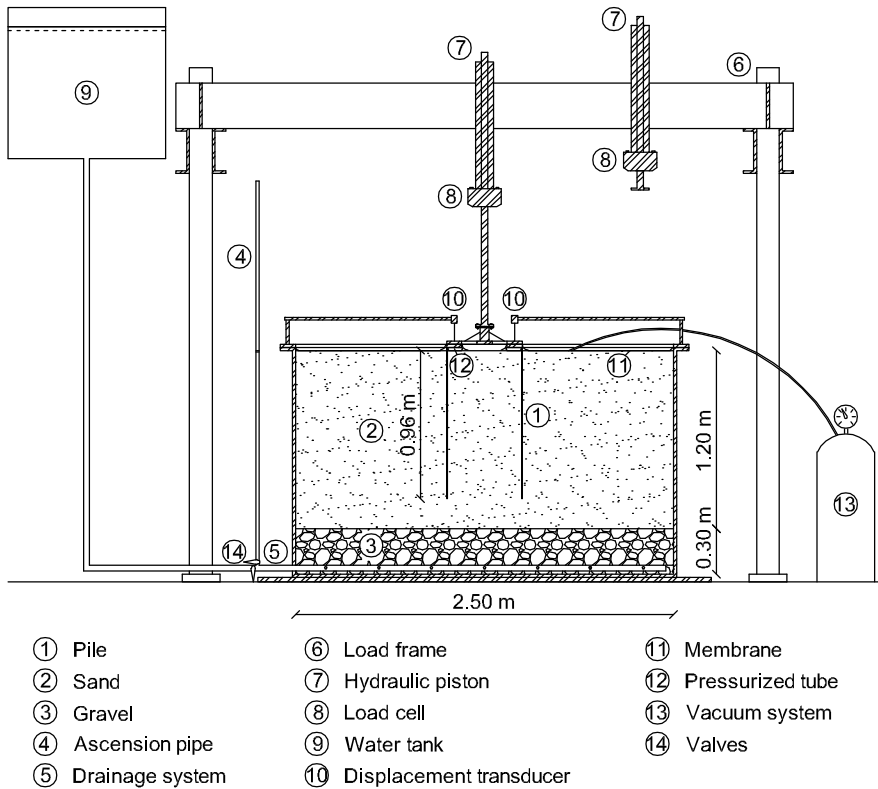


Figure D.1: Concept illustration of the test setup.

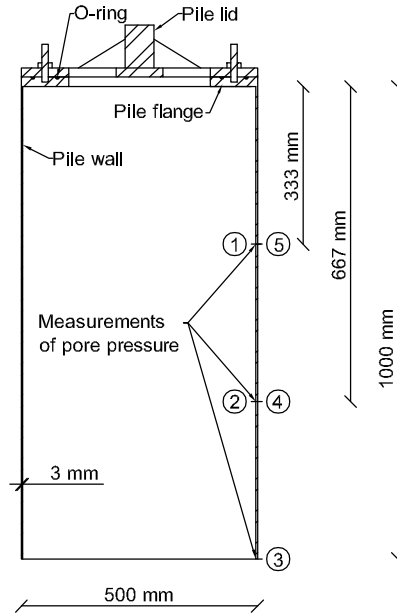
0.96 m. The outer diameter was 0.5 m and the wall thickness was 0.003 m. The small wall thickness minimized the tip resistance. As shown in Figure D.1, two displacement transducers placed opposite each other on the pile top measured the vertical displacement of the pile segment. In the tests with no suction applied to the saturated sand, five transducers measured the pore pressure at three depths: one-third and two-thirds down along the pile segment, inside and outside the pile wall, and at the pile tip, cf. Figure D.2.

D.2.3 Preparation Procedure

After each test, the pile segment was removed from the sand box and the sand was loosened by applying a hydraulic gradient of $i = 0.9i_{crit}$. The pile segment was installed and the sand was vibrated around and inside the pile segment with a rod vibrator. To ensure that the sand was homogeneously compacted to a relative density of around 80 %, CPTs were conducted at different places in the sandbox after vibration. From the measured cone resis-

Table D.1: Material properties for Aalborg University Sand No. 1 (Hedegaard & Borup 1993).

d_s [g/cm ³]	e_{\max} [-]	e_{\min} [-]	d_{50} [-]	$c_u = d_{60}/d_{10}$ [-]
2.64	0.854	0.549	0.14	1.78

**Figure D.2:** Dimensions of the pile segment and position of pore pressure measurements.

tance, the relative density was determined as described by Ibsen et al. (2009).

During cyclic loading tests, the sand grains in the pile-soil interface may be crushed. Nevertheless, the sand was not replaced between each test because of the assumption that the described preparation procedure displaces the sand grains from the pile-soil interface prior to a new test and, thus, the sand characteristics at the interface are the same for all tests. Due to the post-installation vibration procedure, the test results are unaffected by the installation. Thus, the test results are comparable to the results of a storm sequence a period of time after installation.

D.3 Test Program

A typical storm sequence consists of a wave series of increasing magnitude, but decreasing number, and a peak design load usually occurring only once. A complete load series is rarely modeled in field or laboratory tests; instead

D.3. Test Program

a number of cycles of the peak design load are used to represent the cumulative damage that occurs under the full sequence. Four different cyclic loading types are normally used to model a storm sequence: (i) symmetric two-way, (ii) asymmetric two-way, (iii) ideal one-way, or (iv) biased one way.

The effect of cyclic loading is commonly defined as a reduction in shear strength and, thus, a reduction in capacity (API 2000). However, for some designs the cumulative deformations under cyclic loading can be critical—for instance for an offshore wind turbine on a jacket pile foundation where accumulated displacements of a single pile can lead to tilt of the wind turbine. The main objective of the test program was to examine the effect of cyclic loading on axially loaded piles in tension. The described test setup and pile segment could only accommodate one-way cyclic loading tests with the mean load in tension to avoid any influence of the pile tip resistance.

The factors influencing the axial pile capacity during cyclic loading are as follows (Chan & Hanna 1980, API 2000): (i) Mean load and cyclic amplitude relative to the static capacity, (ii) number of cycles, (iii) cycle frequency, (iv) loading history, (v) sand properties, and (vi) pile characteristics.

Several researchers studied the influence of the mean load and the cyclic amplitude on the axial pile capacity for one-way as well as two-way cyclic loading—one-way cyclic loading being the least damaging of the two (Randolph 2012).

Two-way cyclic loading leads to decrease of the radial stresses and, thus, decrease of the shear strength and increase of displacements (Thomas & Kempfert 2011). Large cyclic amplitudes lead to severe local stress reductions at the interface and reductions of the dilatant response resulting in decreased pull-out capacity (Silva et al. 2013). Increasing the mean load will decrease the number of load cycles before failure (Thomas & Kempfert 2011).

Analyzing one-way cyclic tension loading tests, Rimoy (2013) observed that the cyclic stiffness varies with cyclic loading amplitude and remains constant until beginning of failure. Small amplitudes are found to increase the pile capacity (Jardine & Standing 2012, Thomas & Kempfert 2011). Shaft capacity gains emerge from densification at the pile–soil interface leading to marked interface dilation during further loading (Silva et al. 2013). Thomas & Kempfert (2011), Chan & Hanna (1980) found that increasing the cyclic amplitudes resulted in a decreasing number of load cycles to failure.

Based on the observations of a variety of cyclic loading tests, a number of so-called interaction diagrams have been proposed. These diagrams define

the result of a given cyclic loading sequence based on the size of the mean load and the cyclic loading amplitude relative to the static axial capacity of the pile (Jardine & Standing 2012, 2000, Poulos 1988).

The aim of the current test program was to analyze the effect of the mean load, Q_{mean} , and the cyclic amplitude, Q_{cyclic} , defined in Figure D.3, on the pile capacity and the accumulated displacements. To cover different load conditions, Q_{mean} and Q_{cyclic} were chosen based on the interaction diagram proposed by Jardine & Standing (2012). This interaction diagram is based on ten OW cyclic tension tests and three TW cyclic tests performed on seven open-ended steel pipe piles with a diameter of 0.457 m and lengths of 10 and 19 m installed in dense to very dense marine sand. Tsuha et al. (2012) performed seven OW cyclic tension and seven TW cyclic tests on the mini Imperial College Pile installed in dense sand in a calibration chamber. The embedded length of the test pile was 1.05 m and the diameter was 36 m. The results of these tests were comparable to the interaction diagram proposed by Jardine & Standing (2012). The interaction diagram defines three types of cyclic load responses based on the ratio between Q_{mean} and the maximum static load, $Q_{\text{max static}}$, and the ratio between Q_{cyclic} and $Q_{\text{max static}}$:

$$\chi_m = \frac{Q_{\text{mean}}}{Q_{\text{max static}}} \quad , \quad \chi_c = \frac{Q_{\text{cyclic}}}{Q_{\text{max static}}} \quad (\text{D.1})$$

The three cyclic load responses are as follows:

- Stable: Failure does not occur within 1000 cycles and no accumulated displacements take place. Shaft capacity gain due to cyclic loading.
- Meta-stable: Pile head displacements accumulated at moderate rates over 100 to 1000 cycles without stabilizing, resulting in either an increase or a decrease in pile capacity. Or failure develops within $1000 > N > 100$ cycles.
- Unstable: Failure before 100 cycles. Loss of capacity.

To cover both stable and unstable conditions and to accommodate three different surcharge levels in the test setup, the test program given in Table D.2 was chosen. $Q_{\text{max static}}$ was chosen as the average value of the maximum loads recorded in the static tests, $Q_{\text{max,avg}}$, for each surcharge level given in Figure D.4. Thomassen et al. (2015) give a thorough analysis of these tests.

Most laboratory tests on axially loaded piles are conducted in dry sand and, thus, pore pressure considerations are avoided. The general assumption is that excess pore pressure is not expected in saturated sand. Some calibration-chamber penetration tests (Bellotti et al. 1988) and one-way cyclic loading

D.3. Test Program

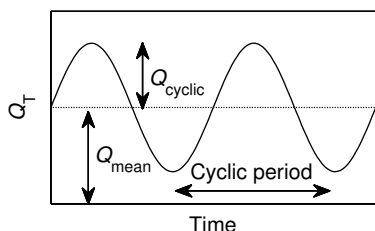


Figure D.3: Definition of Q_{cyclic} and Q_{mean} .

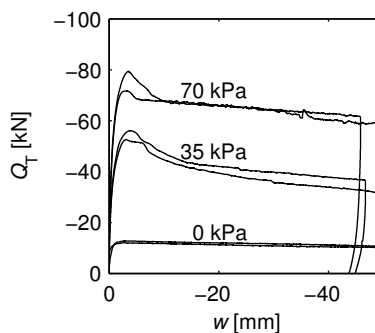


Figure D.4: Test results of six static tension tests.

Table D.2: Test program.

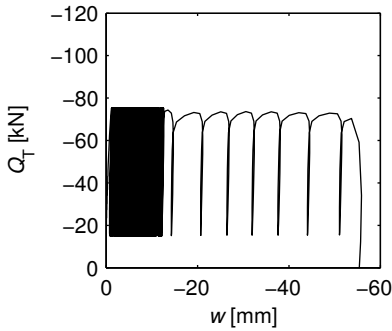
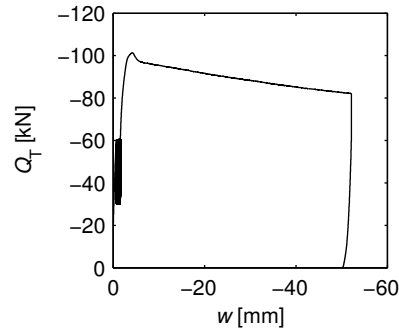
Test no.	χ_m [-]	χ_c [-]	Q_{mean} [kN]	Q_{cyclic} [kN]	Surcharge [kPa]	Expected type
T11C0	0.4	0.4	-4.84	-4.84	0	Unstable
T12C70	0.4	0.4	-30.12	-30.12	70	Unstable
T13C0	0.4	0.2	-4.84	-2.42	0	Stable
T14C35	0.4	0.4	-21.66	-21.66	35	Unstable
T15C35	0.4	0.2	-21.66	-10.83	35	Stable
T16C70	0.4	0.2	-30.12	-15.06	70	Stable
T17C0	0.4	0.2	-4.84	-2.42	0	Stable
T18C70	0.6	0.4	-45.18	-30.12	70	Unstable
T19C70	0.6	0.2	-45.18	-15.06	70	Unstable
T20C70	0.8	0.2	-60.24	-15.06	70	Unstable
T21C70	0.8	0.3	-60.24	-22.59	70	Unstable

compression pile tests (Thomas & Kempfert 2011) show a reduction in sleeve friction for saturated compared to unsaturated sand. However, by using a cyclic frequency of 0.1 Hz in the present tests, it is assumed that pore pressure build-up will not happen, meaning that the effect of running most of the tests in nearly dry sand will not affect the test results.

Idealized cyclic load sequences lasting for two days during which Q_{mean} and Q_{cyclic} are held constant are used in the analyses. A literature study reveals that the number of load cycles is normally limited to few thousands if not less. However, Chan & Hanna (1980) observed that a stable test can eventually become unstable after several thousands of cycles; hence, the number of cycles is relevant for the pile capacity. In the tests presented here, a cyclic period of 10 s results in 17,280 cycles over a period of two days.

Table D.3: Test results for the eleven cyclic loading tests.

Test no.	χ_m	χ_c	Surcharge	N	Observed type	w_{acc}	$Q_{max\ pc}$	$Q_{max,pc}/Q_{max,avg}$
	[-]	[-]	[kPa]	[-]		[mm]	[kN]	[kN]
T11C0	0.4	0.4	0	177	Meta-stable	-60.0	-	-
T12C70	0.4	0.4	69-75	17280	Meta-stable	-10.3	-101.5	1.35
T13C0	0.4	0.2	0	17280	Stable	-0.2	-12.4	1.02
T14C35	0.4	0.4	34.3-36.5	17280	Meta-stable	-29.7	-57.2	1.06
T15C35	0.4	0.2	33.8-35.0	17280	Stable	-0.7	-64.8	1.20
T16C70	0.4	0.2	70.7-71.3	17280	Stable	-0.1	-104.3	1.39
T17C0	0.4	0.2	0	17280	Stable	-0.4	-13.7	1.13
T18C70	0.6	0.4	70.7-72.5	5230	Meta-stable	-60.0	-	-
T19C70	0.6	0.2	69.7-71.2	17280	Stable	-1.5	-101.6	1.35
T20C70	0.8	0.2	69.9-70.3	17280	Stable	-4.3	-87.56	1.16
T21C70	0.8	0.3	68.5-70.3	554	Meta-stable	-60.0	-	-

**Figure D.5:** Total capacity versus displacement for Test T19C70.**Figure D.6:** Total capacity versus displacement for Test T18C70.

D.4 Test Results

Table D.3 shows the test results for the eleven cyclic loading tests. The following data is displayed in the table: The actual surcharge during the tests; the number of cycles, N , that was run; whether the test turned out to be stable, meta-stable or unstable; the accumulated displacements during the cyclic loading part, w_{acc} ; the peak load of the post-cyclic static loading test, $Q_{max\ pc}$; and the ratio between peak load of the post-cyclic static loading and the peak load of the static tests performed without pre-cyclic loading. As representative results, Figure D.5 shows the load–displacement curve for the stable test T19C70 while Figure D.6 shows the load–displacement curve for the meta-stable test T18C70.

D.4. Test Results

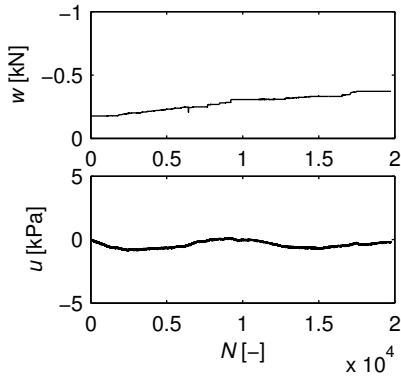


Figure D.7: Pore pressure measured during the stable test T17C0 conducted without surcharge.

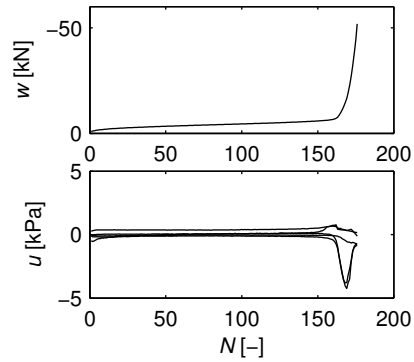


Figure D.8: Pore pressure measured during the meta-stable test T11C0 conducted without surcharge.

D.4.1 Surcharge and Pore Pressure Build-up

A pressure transducer connected to the membrane via a quick-coupling measured the suction applied to the sand box. Except for test T12C70, the maximum variation of the surcharge during a test was 2 kPa. Thus, the surcharge was considered constant during the tests, and variations in the surcharges did not have an effect on the test results.

The pore pressure could only be measured in the tests without surcharge where the sand was fully saturated. Figure D.7 shows the pore pressure measured in a stable test, T17C0, and Figure D.8 illustrates the result of a meta-stable test with pull-out after only 176 cycles, T11C0. As assumed the variations of the measured pore pressures due to the cyclic loading are negligible for the stable test. For the meta-stable test, the pore pressure outside the pile wall shows a negative pore pressure build-up during the last cycles where large displacements take place in each load cycle. The pore pressure build up is large enough to have an effect on the test result. A negative pore pressure would probably build up in full scale tests as well. Thus, for meta-stable and unstable tests a more correct pile response appears for tests performed in saturated sand than for tests performed in dry sand.

D.4.2 Accumulated Displacements and Cyclic Stiffness

Figure D.9 displays the accumulated displacements during the cyclic load sequences of tests T12C70, T16C70, T18C70, and T19C70. Varying the mean load has a small effect on the accumulated displacement. Thus, an increase of the mean load results in a small increase of the accumulated displacement.

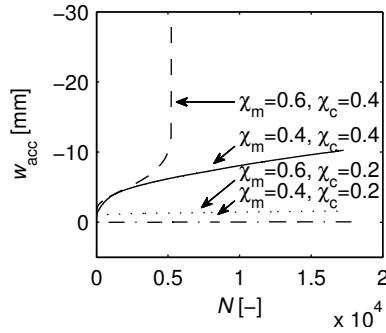


Figure D.9: Accumulated displacements during the cyclic load sequences of tests T12C70 ($\chi_m = 0.4$, $\chi_c = 0.4$), T16C70 ($\chi_m = 0.4$, $\chi_c = 0.2$), T18C70 ($\chi_m = 0.6$, $\chi_c = 0.4$) and T19C70 ($\chi_m = 0.6$, $\chi_c = 0.2$).

However, an increase of the cyclic loading amplitude has a much greater effect on the accumulated displacements. Moreover, when the mean load plus the cyclic amplitude approach the static peak load, it may lead to pull-out of the pile segment before the cyclic loading sequence is over. These trends are apparent for all the tests not only for the four tests given as examples in Figure D.9. The findings are consistent with observations of Thomas & Kempfert (2011), Chan & Hanna (1980).

The cyclic unloading stiffness, k_{un} , and reloading stiffness, k_{re} , defined by Figure D.10 as the secant stiffness of each load cycles, is found. The tangent stiffness tends to infinity for all load cycles and is not used in the analysis. Figure D.11 displays k_{un} and k_{re} for the tests T18C70 and T19C70 as examples of the general observations of all tests. Except for the initial load cycles where the unloading stiffness is higher than the reloading stiffness and the last few cycles of the meta-stable tests, k_{un} and k_{re} are almost identical. For the last few cycles of the meta-stable tests with large permanent displacements, k_{re} reduces significantly while the unloading stiffness remains constant. The stiffness is lower for the meta-stable tests than for the stable tests, and the general observation is that when the amplitude increases, the stiffness decreases. This corresponds to the observations of Rimoy (2013) of the cyclic stiffness depending on the cyclic amplitude. Figure D.11 displays the representative results of k_{un} for the stable test T19C70 and the meta-stable test T18C70. Figure D.10 also defines hysteresis for each load cycles. Comparing hysteresis found for T18C70 and T19C70 in Figure D.11 shows that it generally is low when the stiffness is high. In both tests the hysteresis is high in the beginning where there are almost no permanent displacements. That the hysteresis varies with the stiffness is also evident when looking at T18C70 alone where the hysteresis varies with the oscillations in the stiffness

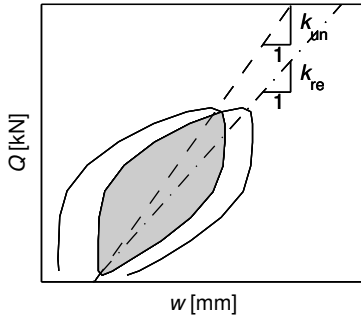


Figure D.10: Definition of cyclic unloading stiffness, k_{un} , reloading stiffness, k_{re} , and hysteresis (gray area between curves).

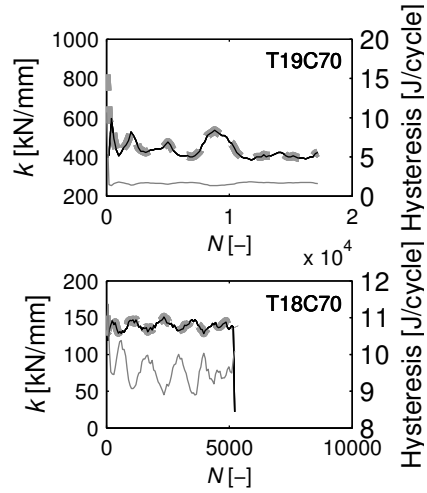


Figure D.11: Unloading stiffness, k_{un} , (dashed gray line), reloading stiffness, k_{re} , (solid black line), and hysteresis (solid gray line) for the stable test T19C70 and the meta-stable test T18C70.

but increases as these oscillations becomes smaller at the end of the test.

D.4.3 Post-cyclic Static Loading

Figure D.12 displays the post-cyclic static loading tests. The maximum value of the post-cyclic static loading test, $Q_{max,pc}$, is higher than the maximum load found in the static tests conducted without pre-cyclic loading. This is the case for all the tests (both stable and meta-stable) where a post-cyclic static test was performed. For some of the tests, the increase is rather small, but for others the increase is as much as 35 %. The capacity increase found in the presented tests corresponds to the findings of Jardine & Standing (2012), Thomas & Kempfert (2011).

The initial and peak stiffness, k_{ini} and k_{peak} , of the static tests without pre-cyclic loading and of the post-cyclic static loading tests are found. k_{ini} is defined as the secant stiffness corresponding to 10 % of the peak load, cf. Figure D.13, whereas k_{peak} is the secant stiffness at the peak. Figure D.14 shows that the initial stiffness, in general, is greater than the peak stiffness. The spread is a bit wider for the post-cyclic tests; however, they are in the same order of magnitude.

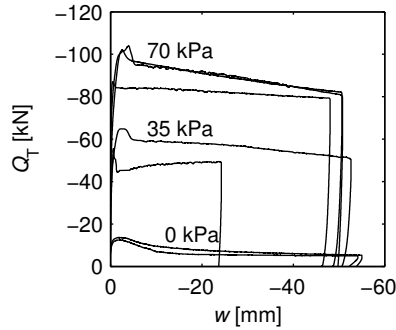
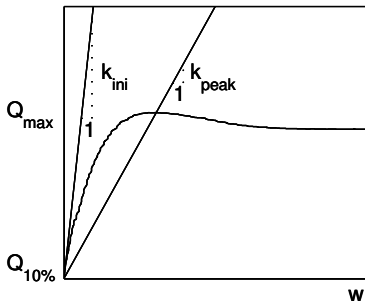
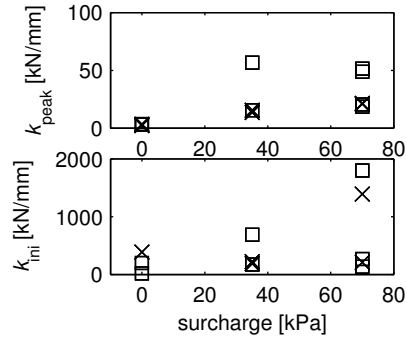


Figure D.12: Post-cyclic static loading.

Figure D.13: Definition of initial and peak stiffness, k_{ini} and k_{peak} .Figure D.14: Peak stiffness, k_{peak} , and initial stiffness, k_{ini} , for the static tests with no pre-cyclic sequence (\square) and post-cyclic static tests (\times).

D.4.4 Interaction Diagrams

The test results are compared to Figure D.15. As described previously, the static loads were chosen as the average of the peak loads found from the static tests, $Q_{max,avg}$. However, Table D.3 shows that the observed type of behavior of the tests that should have been unstable turned out to be meta-stable and in some cases even stable. Figure D.15 shows the interaction diagrams for all eleven cyclic tests. The black circles and triangles in the plot show the results of the tests if $Q_{max,static} = Q_{max,avg}$ is used. As displayed, the meta-stable tests are placed in the unstable zone and some even beyond the possible boundary ($N = 1$). This indicates that the choice of $Q_{max,static} = Q_{max,avg}$ may not be appropriate. Especially for the static tests conducted with a surcharge of 70 kPa, there was a distinct difference between the peak loads for the two static tests. Choosing the larger of the two, $Q_{max,high}$, instead of $Q_{max,avg}$ for

D.4. Test Results

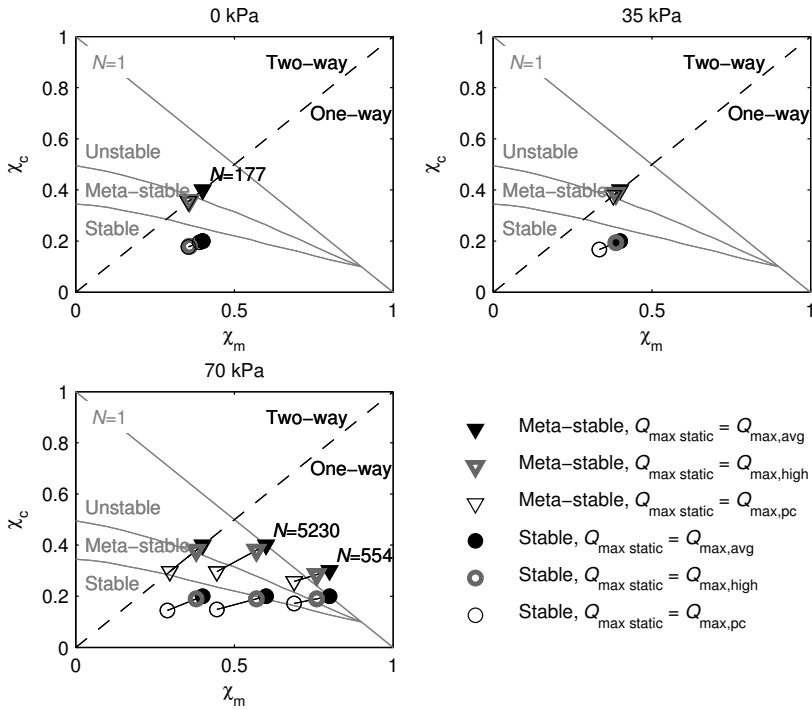


Figure D.15: Interaction diagrams for the three surcharge levels. Three different values of $Q_{\max \text{ static}}$ were used in the analysis for each test: $Q_{\max, \text{avg}}$, $Q_{\max, \text{high}}$, $Q_{\max, \text{pc}}$. The results for the same test with different $Q_{\max \text{ static}}$ are connected by a line.

$Q_{\max \text{ static}}$ gives a better fit to the boundaries proposed by Jardine and Standing (2012); still, it is not a perfect match, cf. Figure D.15.

In the attempt to find an explanation, the post-cyclic static peak load, $Q_{\max, \text{pc}}$, is used as $Q_{\max \text{ static}}$. For the tests without a post-cyclic static sequence (T18C70 and T21C70), $Q_{\max, \text{pc}}$ of the tests with the same Q_{mean} is used (T19C70 and T20C70). By doing so, the test results lie within the boundaries of the stable, meta-stable and unstable zones given by the interaction diagrams cf. Figure D.15. On this revelation, it might have been suitable to conduct a pre-cyclic loading sequence with small mean loads and load amplitudes prior to all the tests including the static loading tests. Thus, the effect of operating conditions of a wind turbine could be simulated providing results closer to full-scale test results. Based on these observations, an interesting study would be to analyze the effect of the number of cycles on the pull-out capacity.

D.5 Summary and Conclusions

The paper presented one-way cyclic loading tests on a 1 m long pile segment with a diameter of 0.5 m loaded in tension. The objective of the tests was to analyze the effect of mean load and cyclic loading amplitude on the pile capacity and on the accumulated displacements.

The tests showed that small cyclic amplitudes result in post-cyclic capacity gain and negligible accumulated displacements. By increasing the load amplitude, the accumulated displacements increases and will eventually lead to an unstable condition. Unstable conditions are also the consequence of increasing the mean load. However, an identical increase in the cyclic amplitude will more rapidly lead to unstable conditions. This is consistent with findings of Jardine & Standing (2012), Thomas & Kempfert (2011), Chan & Hanna (1980). The stable as well as the meta-stable tests—not experiencing pull-out—lead to shaft capacity gains compared to static loading tests made without pre-cyclic loading.

The cyclic unloading and reloading stiffness, defined as tangent stiffness, proved to be equal to each other and constant throughout the tests, except for the first few loading cycles of all tests and the last cycles of the meta-stable tests where the reloading stiffness decreased drastically. The hysteresis was high in the beginning of each test though the permanent displacements were small. The general observation was that the hysteresis decreased when the stiffness increased.

The test results were compared to the limits of the interaction diagram proposed by Jardine & Standing (2012). The tests results lay within the proposed limits of the stable, meta-stable and unstable conditions if the post-cyclic static peak load was used in the comparison instead of the peak load found in the static tension tests conducted without pre-cyclic loading. This implies that in order to get conditions in the laboratory setup resembling serviceability mode in the field, pre-cycling with small mean loads and load amplitudes may be necessary. Nevertheless, based on the test results it is recommended to design future foundation piles in jacket structures for offshore wind turbines in such a way that they will stay within the stable conditions suggested by Jardine & Standing (2012). Thereby, both pull-out and large accumulated displacements can be avoided.

D.6 Acknowledgments

The research is funded by the Danish Advanced Technology Foundation via the program “Cost-effective deep water foundations for large offshore wind turbines”. The financial support is sincerely acknowledged.

References

- Al Douri, R. & Poulos, H. (1994), ‘Cyclic behavior of pile groups in calcareous sediments’, *Soils and Foundations* **34**, 49–59.
- API (2000), *Recommended Practice for Planning, Designing and Constructing Fixed Offshore Platforms – Working Stress Design*, American Petroleum Institute.
- Bellotti, R., Crippa, V., Pedroni, S. & Ghionna, V. N. (1988), Saturation of sand specimen for calibration chamber tests, in ‘Proceedings of the International Symposium on Penetration Testing (ISOPT-1)’, pp. 661–672.
- Chan, S.-F. & Hanna, T. (1980), ‘Repeated loading on single piles in sand’, *Journal of the Geotechnical Engineering Division* **106**(2), 171–188.
- Chin, J. & Poulos, H. (1998), ‘Test on model jacked piles in calcareous sand’, *Geotechnical Testing Journal* **19**(2), 164–180.
- Hedegaard, J. & Borup, M. (1993), *Klassifikationsforsøg med Baskarp Sand No. 15*, Aalborg University, Denmark.
- Ibsen, L., Hanson, M., Hjort, T. & Thaarup, M. (2009), *MC-Parameter Calibration of Baskarp Sand No. 15.*, DCE Technical Report No. 62, Department of Civil Engineering, Aalborg University, Denmark.
- Jardine, R. & Standing, J. (2000), *Pile load testing performed for HSE cyclic loading study at Dunkirk, France. Volume 1 & 2.*, Offshore Technology Report OTO 2000 007, Health and Safety Executive, London, UK.
- Jardine, R. & Standing, J. (2012), ‘Field axial cyclic loading experiments on piles driven in sand’, *Soils and Foundations* **52**(4), 723–736.
- Jardine, R., Standing, J. & Chow, F. (2006), ‘Some observations of the effect of time on the capacity of piles driven in sand’, *Géotechnique* **56**(4), 227–244.
- Le Kouby, A., Canou, C. & Dupla, J. (2004), Behaviour of model piles subjected to cyclic axial loading, in ‘Proceedings of the International Conference Cyclic Behaviour of Soils and Liquefaction Phenomena’, Taylor & Francis Group, London, UK, p. 159–166.

- Mortara, G., Mangiola, A. & Ghionna, V. (2007), 'Cyclic shear stress degradation and post-cyclic behaviour from sand-steel interface direct shear tests', *Canadian Geotechnical Journal* **44**, 739–752.
- Poulos, H. (1988), 'Cyclic stability diagram for axially loaded piles', *Journal of Geotechnical and Geoenvironmental Engineering* **114**(8), 877–895.
- Prai-ai, S. (2013), *Behaviour of soil-structure interfaces subjected to a large number of cycles. Application to piles*, PhD Thesis, University of Grenoble.
- Randolph, M. (2012), Offshore design approaches and model tests for sub-failure cyclic loading of foundations, in C. Di Prisco & D. Wood, eds, 'Mechanical Behaviour of Soils Under Environmentally Induced Cyclic Loads', Springer Wien New York, pp. 441–480.
- Rimoy, S. (2013), *Ageing and Axial Cyclic Loading Studies of Displacement Piles in Sand*, PhD Thesis, Imperial College London.
- Silva, M., Foray, P., Rimoy, S., Jardine, R., Tshusa, C. & Yang, Z. (2013), Influence of cyclic axial loads on the behaviour of piles driven in sand, in 'Proceedings of TC 209 Workshop – 18th ICSMGE, Paris September 4th 2013, Design for cyclic loading: Piles and other foundations', Paris, France, pp. 81–84.
- Thomas, S. & Kempfert, H.-G. (2011), 'Untersuchung des Pfahltragverhaltens infolge zyklisch axialer Einwirkungen in einer Spannungszelle', *Pfahl-Symposium 2011* **94**, 139–158.
- Thomassen, K., Ibsen, L. & Andersen, L. (2015), 'Laboratory test setup for cyclic axially loaded piles in sand', *Submitted for publication in Geotechnical Testing Journal*.
- Tsuha, C., Foray, P., Jardine, R., Yang, Z., Silva, M. & Rimoy, S. (2012), 'Behaviour of displacement piles in sand under cyclic axial loading', *Soils and Foundations* **52**(3), 393–410.

Appendix E

Force Sensors

To get an optimal outcome of the pile tests, measurements of the changes in radial effective stresses at the pile–soil interface and in the surrounding sand during pile loading were desirable. The aim was to get a minimum of disturbance of the properties of the pile–soil interface and as the wall thickness is too small (3 mm) to embed a normal force sensor in the pile wall, an alternative was sought by using very thin force sensors. The intention was to glue the small and thin force sensors of the type FlexiForce Sensor A201 (Tekscan 2010) to the side of the pile. Table E.1 shows the specifications for the sensor.

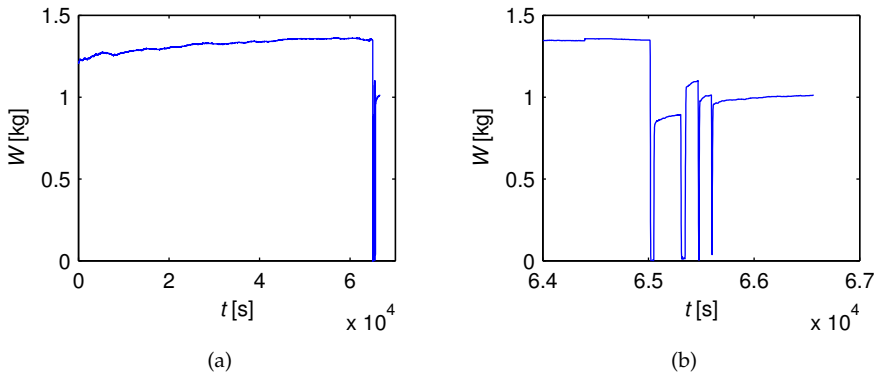
E.1 Calibration FlexiForce Sensor

An attempt was made to calibrate a FlexiForce sensor. The sensor was conditioned as described in the manual (Tekscan 2010) by loading the sensor for three seconds with 110 % of the maximum load that should be applied through the tests and then unload it. This was repeated five times. Hereafter, a weight of 4 kg was applied to the sensor and the potentiometer was adjusted so that 4 kg corresponded to an output of approximately 5 V.

After the calibration, a weight 1 kg was applied for 18.5 hours to monitor the drift of the sensor, which should follow a logarithmic trend with time. Figure E.1a shows the evolution with time. First of all it can be seen that despite of the calibration, the sensor gave an output of 1.2 kg instead of the 1 kg when the weight was first applied. Hereafter, the force kept increasing and even though the increment decreased with time, the output was not stable after 18 hours. After 18 hours of constant loading, the 1 kg weight was removed and reapplied four times. Figure E.1b shows, that the load was not repeatable. The output for the 1 kg weight is 0.8, 1.1, 1.0 and 0.9, respectively.

Table E.1: Specifications of the FlexiForce sensor A201 (Tekscan 2010).

Physical Properties	
Thickness	0.203 mm
Length	51 mm
Diameter	9.53 mm
Typical Performance	
Linearity Error	$<\pm 3\%$
Repeatability	$<\pm 2.5\%$ of full scale
Hysteresis	$<4\%$ of full scale
Drift	$<5\%$ per logarithmic time scale
Response Time	$<5 \mu\text{s}$
Operating Temperature	$-40\text{--}60^\circ\text{C}$
Temperature sensitivity	$\leq 0.2\%$ per $^\circ\text{F}$

**Figure E.1:** (a) Variation of force output of sensor with time with 1 kg applied. (b) Re-applied weight after the 18 hours of constant loading.

The sensor was tested once again where just the voltage output for different weights were registered. Table E.2 shows the results of this test again indicating the low repeatability of the sensor especially for the higher weights. The specifications of the sensors suggest a repeatability error of $<\pm 2.5\%$ of full scale, however, this error was exceeded for the 2.5 kg and 4 kg weights.

E.1.1 Test of Force Sensors on Bar

Despite the discouraging results of the calibration, six sensors were mounted at different levels on a bar, cf. Figure E.2. Figure E.3 shows the bar installed in the middle of the sand box and the membrane placed on the sand surface with suction applied. This was done to get an idea of the horizontal stress levels in the sand with various amount of suction applied. The sensors were

E.1. Calibration FlexiForce Sensor

Table E.2: Results for repeatability test of FlexiForce sensor.

Applied weight [kg]	Output [V]	Output [V]	Output [V]	Error of full scale (5.0 V) [%]
0.0	0.080	0.065	–	0.3%
0.5	0.560	0.600	0.590	0.2%
2.5	1.790	1.860	1.720	2.6%
4.0	3.660	3.900	3.900	4.8%

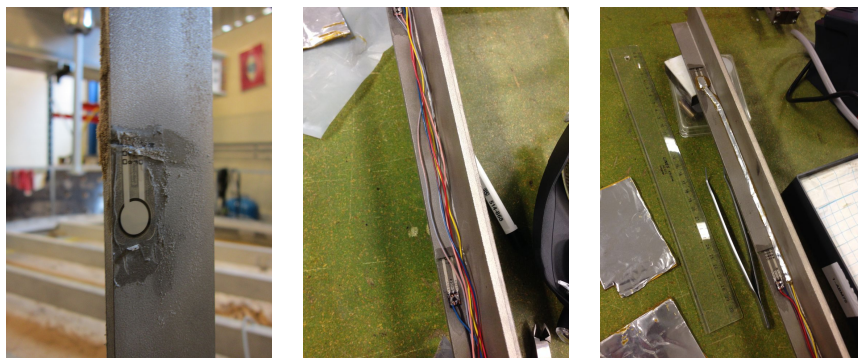


Figure E.2: FlexiForce sensor mounted on the steel bar with the wiring led to the backside of the bar.

reset after installation. Thus, the results of the test did not give total forces on the bar but only changes in the soil stresses due to the applied suction on the membrane.

Figure E.4 shows the results of the test. The upper graph shows the suction increased from 0–20–40–60 kPa and decreased to 0 kPa. The middle graph shows the voltage changes of sensors which revealed the following:

- The voltage output seems to slightly increase when the suction is increased. However, at the end of the test, the suction was removed from the membrane but instead of decreasing to the starting point, the voltage output increases. No explanation to this phenomenon is found.
- Figure E.1a shows that the output of a sensor should increase with time in a logarithmic manner. However, Figure E.4 shows that the voltage output did increase when the suction increases but afterward it decreased instead of increased while the suction was constant. The output signals of the six sensors were identical. So the question is whether this means, that the sensor register the exact same increase or decrease of the stresses in the sand or electrical noise is the source of the variations.

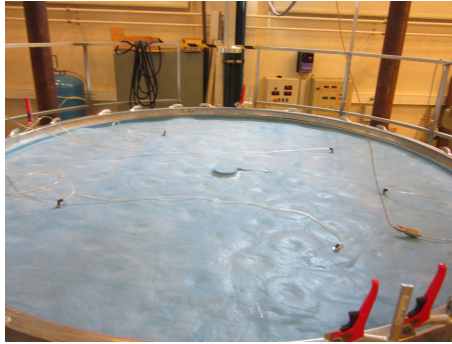


Figure E.3: The bar installed in the middle of the sand box while suction is applied to the sand.

E.2 Conclusion

Due to the difficulties of calibrating the force sensors and the unstable outputs, the idea of using these sensors to register the changes in radial effective stresses was abandoned.

References

Tekscan (2010), *Tekscan FlexiForce® Sensor User Manual*, Tekscan.

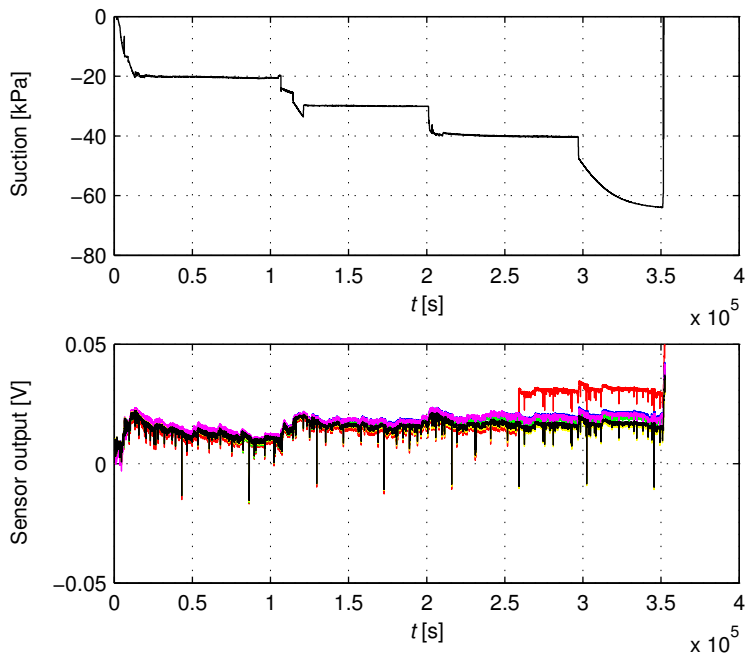


Figure E.4: Suction applied to the membrane and the output of the five FlexiForce sensors on the bar.

Appendix F

Static Test Results

This appendix shows the results of the ten conducted static tests. Table F.1 gives the specifications of the CPTs and the tests, while Table F.2 gives the chosen test program and the maximum force, $Q_{\max \text{ static}}$, applied during the test. Table F.3 shows the average values of the soil properties found for each test based on the conducted CPTs.

Table F.1: Specifications of the CPTs and the static tests.

CPT specifications		
Penetration rate	5	mm/s
Cone area	$1.767 \cdot 10^{-4}$	m ²
Test specifications		
Displacement rate	0.002	mm/s
Sample rate	1	Hz

Table F.2: Test program for the static tests and resulting maximum force applied.

Test	P_0 [kPa]	$Q_{\max \text{ static}}$ [kN]
T1S0	0.0	9.8
T2S0	0.0	13.5
T3S0	0.0	11.6
T4S20	20.0	33.0
T5S70	70.0	–*
T6S0	0.0	11.2
T7S35	35.9	56.0
T8S70	70.5	79.3
T9S70	71.2	71.3
T10S35	36.2	52.3
* Test did not succeed		

Electrical noise in the laboratory interrupted the signal of the load cell. The

load-output is, therefore, modified, cf. Figure F.1. The modified load and not the originally recorded load is displayed in the following appendix.

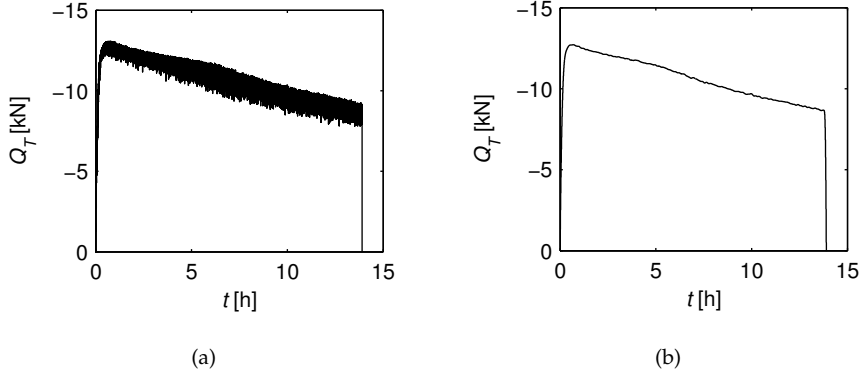


Figure F.1: (a) Original load-signal of the static test T2S0. (b) Modified load-signal of the static test T2S0.

Table E.3: Soil properties determined from the CPTs conducted before each static test.

Test	φ	ψ	γ	D_r
1	53.9	19.7	10.3	87.1
2	54.3	20.0	10.4	88.5
3	54.3	20.0	10.4	88.1
4	53.6	19.2	10.3	84.1
5	54.8	20.7	10.5	92.0
6	53.6	19.3	10.3	84.7
7	53.9	19.6	10.3	86.4
8	53.9	19.6	10.3	86.5
9	53.5	19.2	10.3	84.1
10	53.6	19.3	10.3	84.8

F.1 T1S0

Installation and soil preparation:

- Loosening of the soil with the hydraulic gradient and subsequent vibration was done prior to the pile installation. Thus the results are affected by the installation procedure.
- During installation the pile plugged and it was necessary to stop the installation and pull the pile approximately 1 cm up before continuing the installation process. This procedure was repeated four times, before the pile reached the wanted installation depth.
- Due to a mistake in Catman 6.0, two of the CPT outputs were given in percentage instead of Newtons and were unreliable.

Test:

- The test ran without problems.
- After the pull-out test, the pile segment was pushed back to its initial position.
- The measurements of the pore pressures does not seem reliable.

Observations after tests:

- The soil surface inside the pile segment is raised approximately 3 cm compared to the outside soil surface.

F.1.1 CPT results

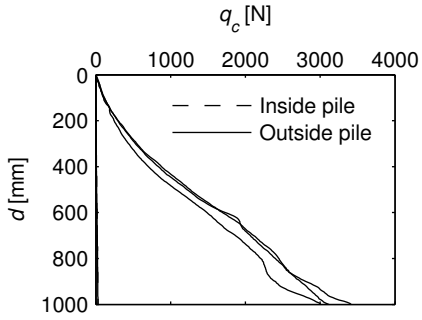


Figure F.2: CPT cone resistance in N.

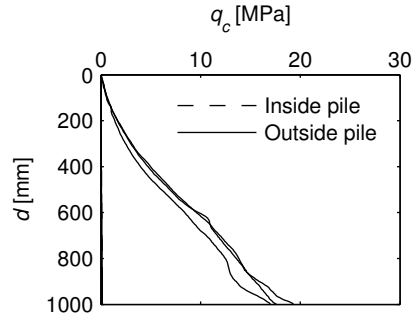


Figure F.3: CPT cone resistance in MPa.

Table F.4: Soil properties determined from CPT results.

Friction angle	φ	53.9°
Dilation angle	ψ	19.7°
Relative density	D_r	87.1%

F.1.2 Test results

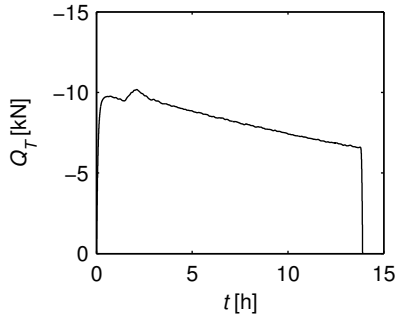


Figure F4: Measured force versus time.

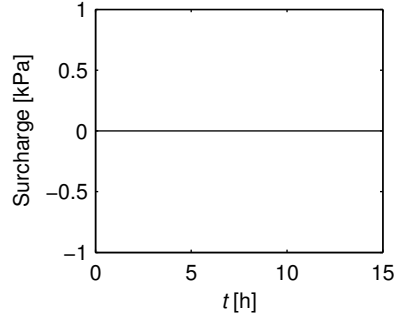


Figure F5: Suction applied to the sand box versus time.

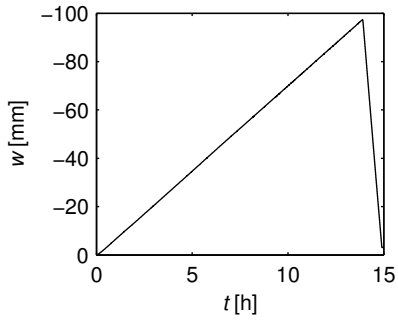


Figure F6: Measured pile displacement versus time.

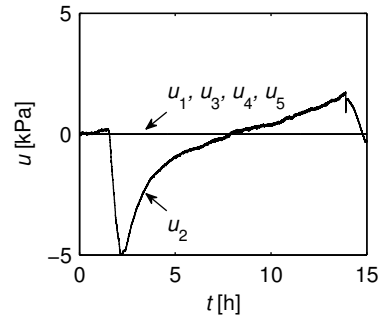


Figure F7: Pore pressure measurements versus time.

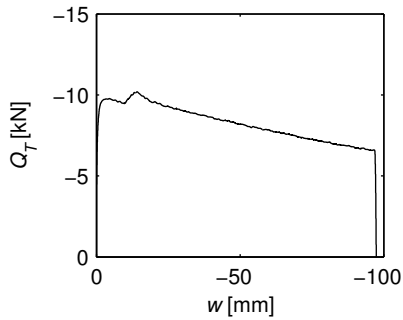


Figure F8: Measured force versus measured pile displacement.

F.2 T2S0

Installation and soil preparation:

- Loosening of the soil with the hydraulic gradient and subsequent vibration was done prior to the pile installation. Thus the results are affected by the installation procedure.
- During installation the pile plugged and it was necessary to stop the installation and pull the pile approximately 1 cm up before continuing the installation process. This procedure was repeated four times, before the pile reached the wanted installation depth.

Test:

- The test ran without problems.
- After the pull-out test, the pile segment was pushed back to its initial position.

Observations after tests:

- The soil surface inside the pile segment is raised a little compared to the outside soil surface.
- The measurements of the pore pressures does not seem reliable.

F.2.1 CPT results

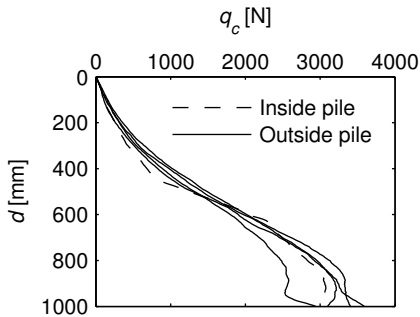


Figure F.9: CPT cone resistance in N.

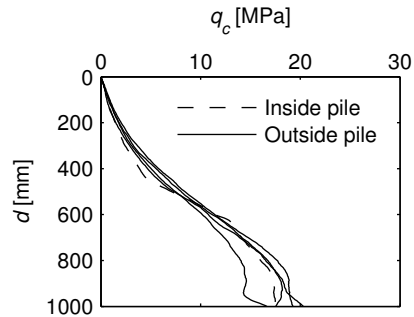


Figure F.10: CPT cone resistance in MPa.

Table F.5: Soil properties determined from CPT results.

Friction angle	φ	54.3°
Dilation angle	ψ	20.0°
Relative density	D_r	88.5%

F.2.2 Test results

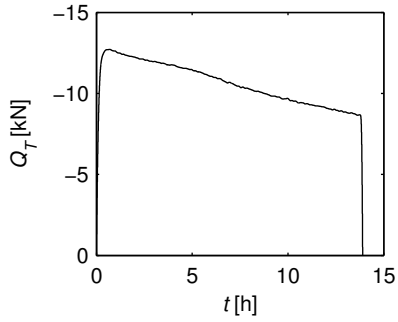


Figure F.11: Measured force versus time.

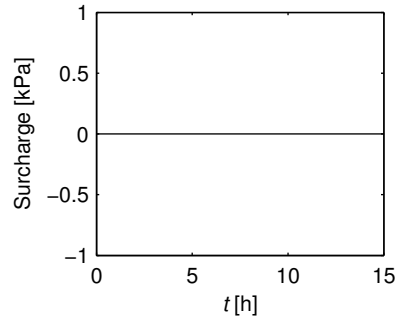


Figure F.12: Suction applied to the sand box versus time.

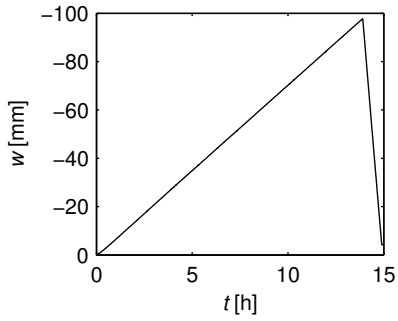


Figure F.13: Measured pile displacement versus time.

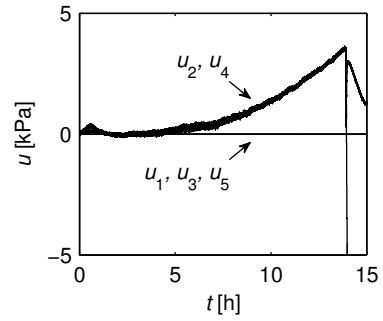


Figure F.14: Pore pressure measurements versus time.

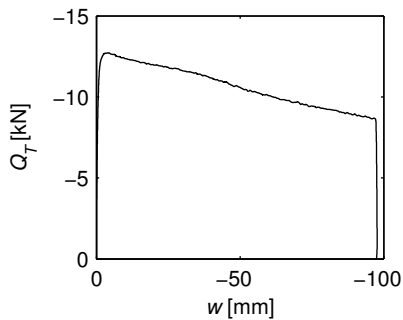


Figure F.15: Measured force versus measured pile displacement.

F.3 T3S0

Installation and soil preparation:

- Loosening of the soil with the hydraulic gradient and subsequent vibration was done prior to the pile installation. Thus the results are affected by the installation procedure.
- During installation the pile plugged and it was necessary to stop the installation and pull the pile approximately 1 cm up before continuing the installation process. This procedure was repeated four times, before the pile reached the wanted installation depth.

Test:

- The test ran without problems.
- After the pull-out test, the force was decreased to 0 kN. Thus, the pile segment did not return to its original position.

Observations after tests:

- The measurements of the pore pressures does not seem reliable.

F.3.1 CPT results

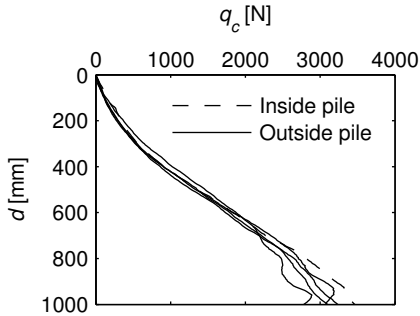


Figure F.16: CPT cone resistance in N.

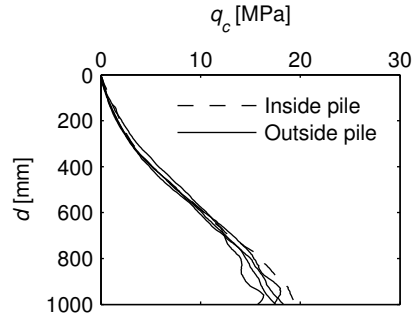


Figure F.17: CPT cone resistance in MPa.

Table F.6: Soil properties determined from CPT results.

Friction angle	φ	54.3°
Dilation angle	ψ	20.0°
Relative density	D_r	88.1%

F.3.2 Test results

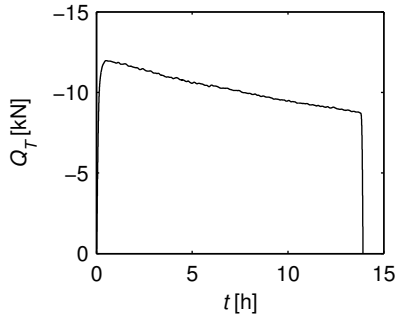


Figure F.18: Measured force versus time.

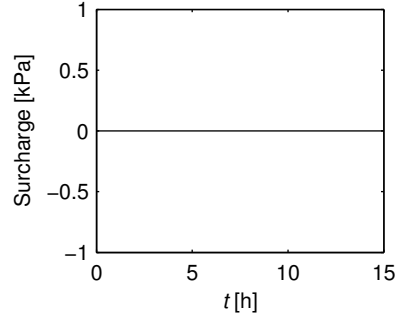


Figure F.19: Suction applied to the sand box versus time.

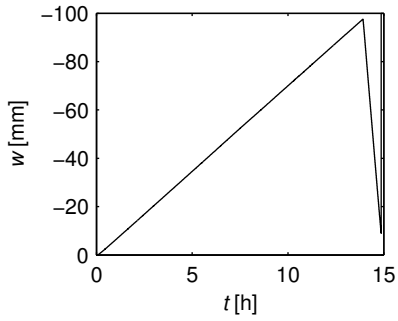


Figure F.20: Measured pile displacement versus time.

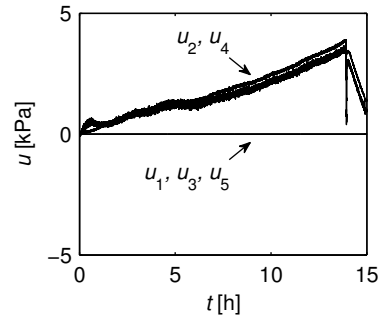


Figure F.21: Pore pressure measurements versus time.

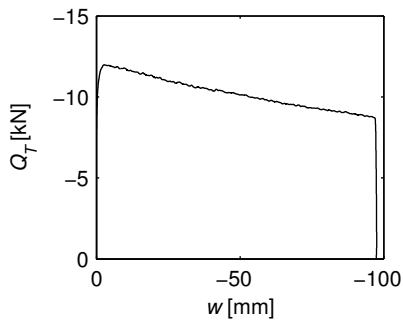


Figure F.22: Measured force versus measured pile displacement.

F.4 T4S20

Installation and soil preparation:

- During installation the pile plugged and it was necessary to stop the installation and pull the pile approximately 1 cm up before continuing the installation process.
- To place the membrane on the soil surface, it was necessary to disconnect the pore pressure transducers from the pipes along the pile shaft in order to remove the pile lid and place the membrane between the pile lid and the pile flange. An attempt was made to re-saturate the pipes to the pore pressure transducers by applying suction to the pipes and suck water from the sand box into the pipes.

Test:

- The test ran without problems.
- After the pull-out test, the force was decreased to 0 kN. Thus, the pile segment did not return to its original position.

Observations after tests:

- When opening the ascension pipe after the test, the water column showed that the water level in the sand box was 80 cm below the sand surface. Due to air in the water and sand prior to the test and probably because the system is not a 100% airtight the water was sucked out of the system prior to the tests. It is assumed that the remaining water was distributed evenly in the sand box during the test and, thus, the sand had a rather low degree of saturation during the test.
- Instead of water, the re-saturation methods of the pore pressure transducers introduced sand in the pipes. However, as the sand was not fully saturated, the pore pressure measurements would not have provided any useful results.

F.4.1 CPT results

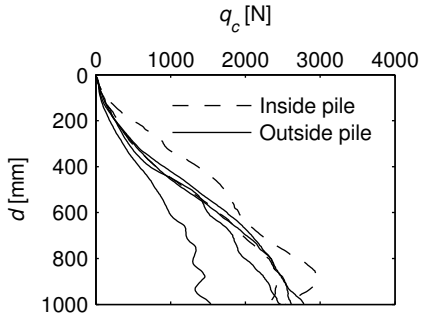


Figure F.23: CPT cone resistance in N.

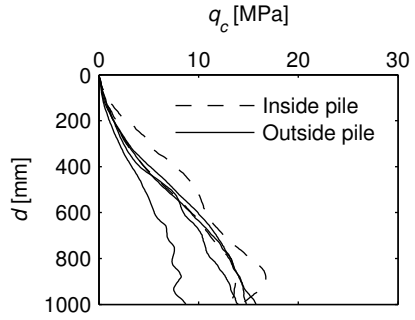


Figure F.24: CPT cone resistance in MPa.

Table E.7: Soil properties determined from CPT results.

Friction angle	φ	53.6°
Dilation angle	ψ	19.2°
Relative density	D_r	84.1%

F.4.2 Test results

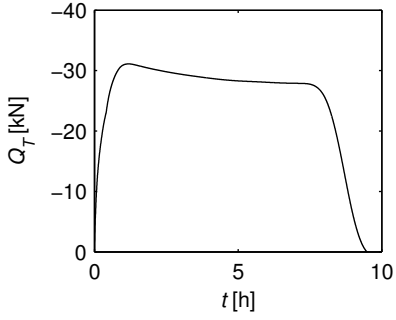


Figure F.25: Measured force versus time.

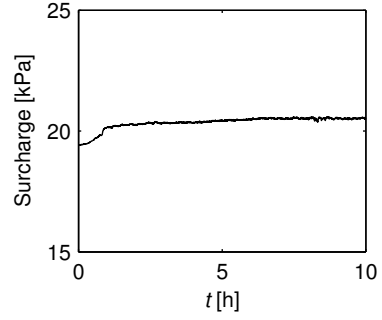


Figure F.26: Suction applied to the sand box versus time.

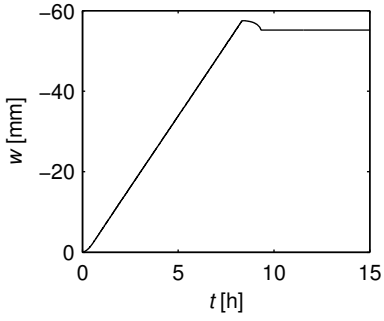


Figure F.27: Measured pile displacement versus time.

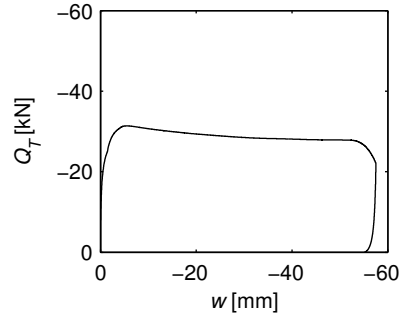


Figure F.28: Measured force versus measured pile displacement.

F.5 T5S70

Installation and soil preparation:

- The pile was installed prior to the soil preparation procedure to avoid installation effects.
- In order to prevent the membrane to get sucked underneath the pile flange, a hose was placed under the pile flange after installation. When the suction was applied to the sand box, the hose was filled with air to a pressure state corresponding to the suction level.
- Another approach of saturating the pore pressure transducers after placing the membrane was tried. Valves were placed between the pipes on the pile wall and the pressure transducers on the pile lid. The pore pressure tubes were saturated prior to installation and the valves were closed keeping the water in the pipes while disconnecting the pore pressure transducers from the pipes after installation. After assembling the pile lid and pile flange the pore pressure transducers were saturated from above while they were reconnected to the pipes and the valves were the reopened. Even though this approach was better compared to the method tried prior to test T4S20, it was not entirely successful as air was trapped in the pipes.

Test:

- The test was not conducted because the membrane broke prior to the test, during stabilization of the suction level. A gap between the sand surface and the pile flange was left after the installation and as suction was applied, the membrane was sucked underneath the pile flange and was torn when in contact with the sharp edges on a bolt underneath the pile flange.

Observations after tests:

- No observations.

F.5.1 CPT results

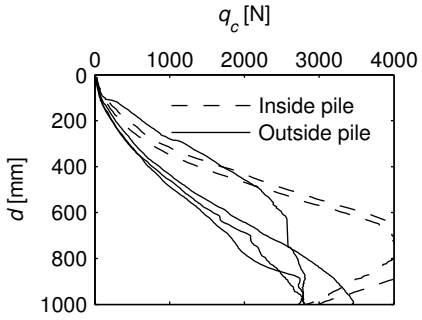


Figure F.29: CPT cone resistance in N.

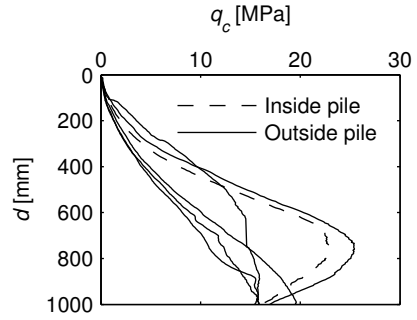


Figure F.30: CPT cone resistance in MPa.

Table E.8: Soil properties determined from CPT results.

Friction angle	φ	54.8°
Dilation angle	ψ	20.7°
Relative density	D_r	92.0%

F.6 T6S0

Installation and soil preparation:

- The pile was installed prior to the soil preparation procedure to avoid installation effects.

Test:

- The test ran without problems.

Observations after tests:

- Due to a mistake, the sampling rate in Catman 6.0 was set to 50 Hz instead of 1 Hz. The chosen procedure of saving data in Catman 6.0 introduces a maximum number of measurements to be recorded in the file. Due to the very high sampling rate, the file ran out of space and only a few minutes of the measurements were recorded in Catman 6.0. As the real displacement of the pile segment is only recorded through Catman 6.0, the results cannot be used for further analysis.

F.6.1 CPT results

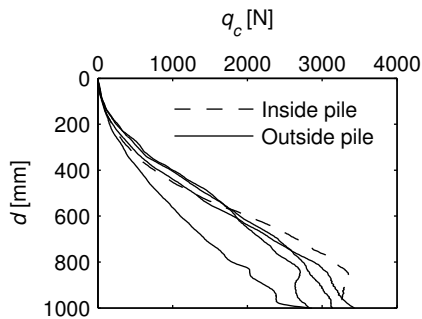


Figure F.31: CPT cone resistance in N.

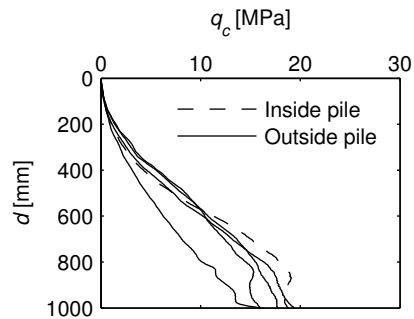


Figure F.32: CPT cone resistance in MPa.

Table F.9: Soil properties determined from CPT results.

Friction angle	φ	53.6°
Dilation angle	ψ	19.3°
Relative density	D_r	84.7%

F.6.2 Test results

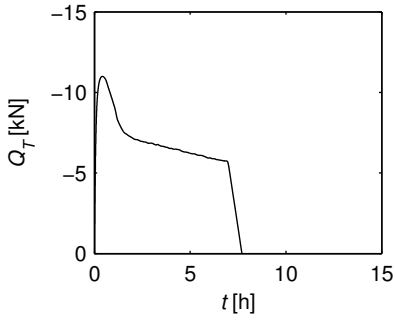


Figure E.33: Measured force versus time.

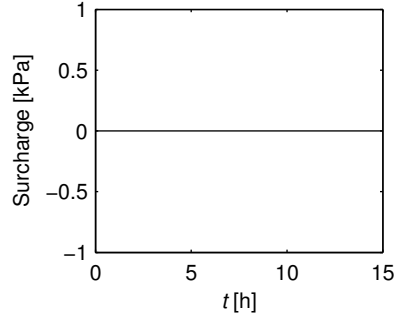


Figure E.34: Suction applied to the sand box versus time.

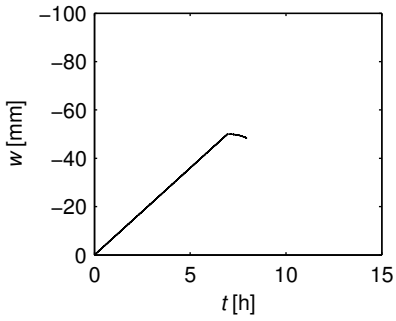


Figure E.35: Measured pile displacement versus time.

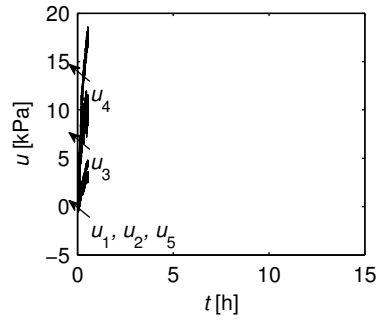


Figure E.36: Pore pressure measurements versus time.

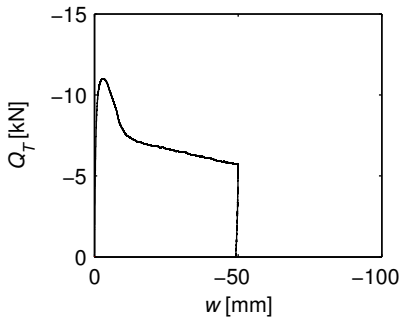


Figure E.37: Measured force versus measured pile displacement.

F.7 T7S35

Installation and soil preparation:

- The pile was installed prior to the soil preparation procedure to avoid installation effects.
- The pore pressure transducers were saturated as described for test T5S70.

Test:

- The test ran without problems.

Observations after tests:

- The water was sucked out of the sand box during stabilization of the suction level and the pore pressure measurements could not be used.
- The pile plugged during loading.
- By mistake the valves under the pore pressure transducers were closed during the tests. Thus, no pore pressure measurements during the test.

F.7.1 CPT results

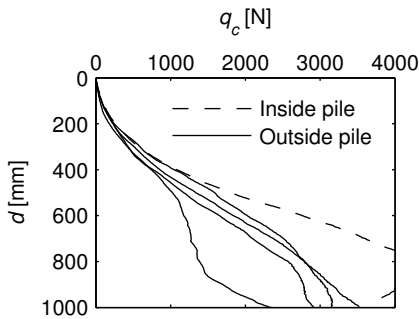


Figure F.38: CPT cone resistance in N.

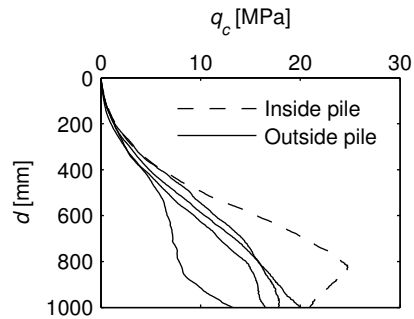


Figure F.39: CPT cone resistance in MPa.

Table F.10: Soil properties determined from CPT results.

Friction angle	φ	53.9°
Dilation angle	ψ	19.6°
Relative density	D_r	86.4%

F.7.2 Test results

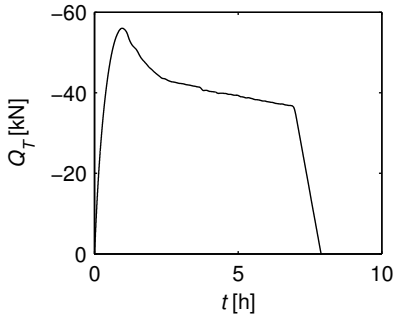


Figure F.40: Measured force versus time.

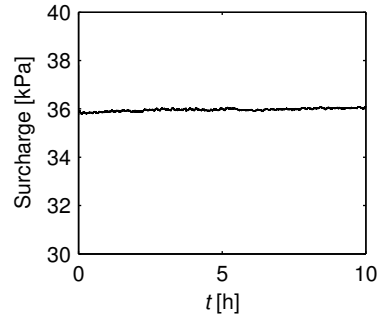


Figure F.41: Suction applied to the sand box versus time.

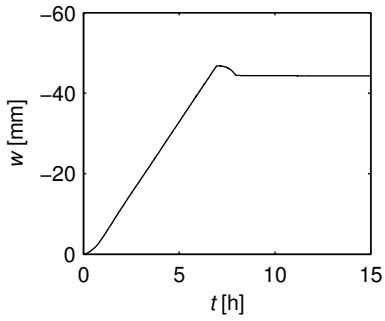


Figure F.42: Measured pile displacement versus time.

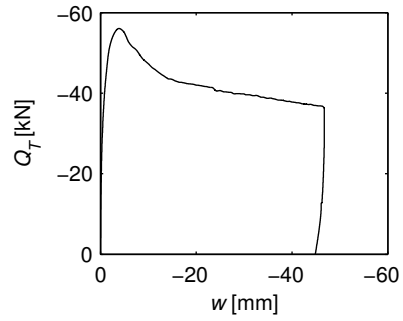


Figure F.43: Measured force versus measured pile displacement.

F.8 T8S70

Installation and soil preparation:

- The pile was installed prior to the soil preparation procedure to avoid installation effects.

Test:

- The test ran without problems.

Observations after tests:

- The pile plugged during loading, approximately 3 cm.
- On the outside of the pile wall, an approximately 5 mm of sand moved up along the side of the pile and was stuck under the membrane.
- The water was sucked out of the sand box when stabilizing the suction level.

F.8.1 CPT results

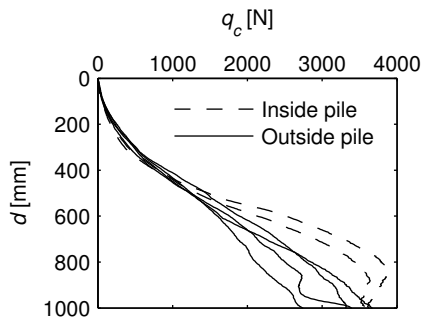


Figure F.44: CPT cone resistance in N.

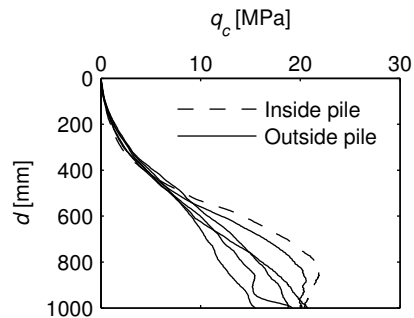


Figure F.45: CPT cone resistance in MPa.

Table F.11: Soil properties determined from CPT results.

Friction angle	φ	53.9°
Dilation angle	ψ	19.6°
Relative density	D_r	86.5%

F.8.2 Test results

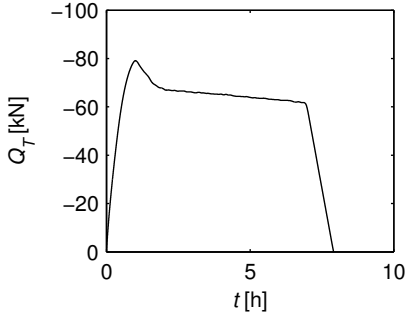


Figure F.46: Measured force versus time.

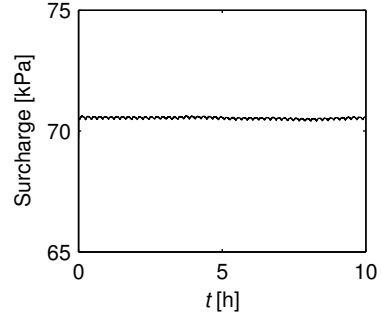


Figure F.47: Suction applied to the sand box versus time.

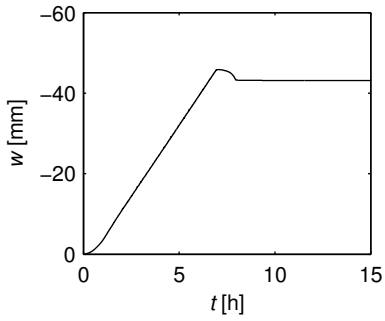


Figure F.48: Measured pile displacement versus time.

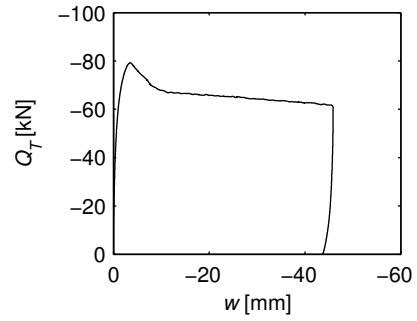


Figure F.49: Measured force versus measured pile displacement.

F.9 T9S70

Installation and soil preparation:

- The pile was installed prior to the soil preparation procedure to avoid installation effects.

Test:

- The test ran without problems.

Observations after tests:

- The water was sucked out of the sand box when stabilizing the suction level.

F.9.1 CPT results

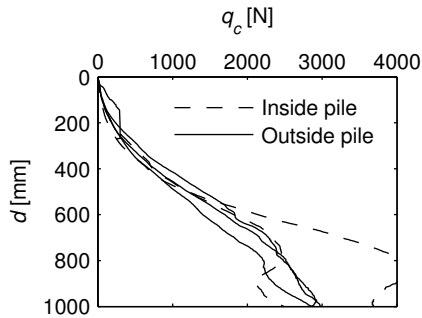


Figure F.50: CPT cone resistance in N.

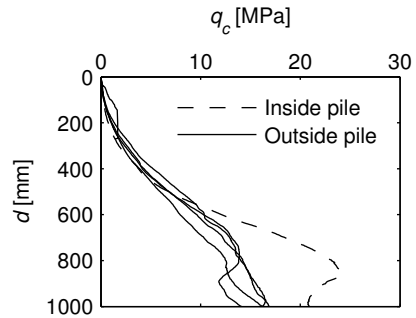


Figure F.51: CPT cone resistance in MPa.

Table F.12: Soil properties determined from CPT results.

Friction angle	φ	53.5°
Dilation angle	ψ	19.2°
Relative density	D_r	84.1%

F.9.2 Test results

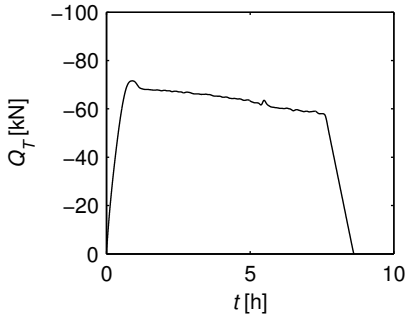


Figure E.52: Measured force versus time.

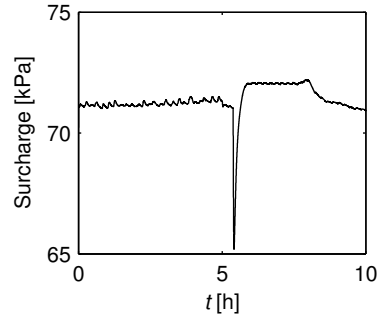


Figure E.53: Suction applied to the sand box versus time.

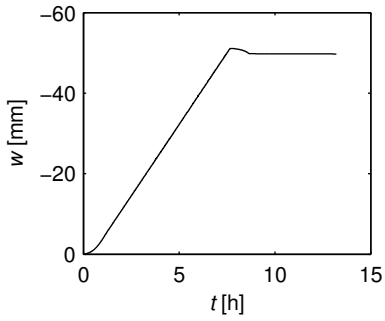


Figure E.54: Measured pile displacement versus time.

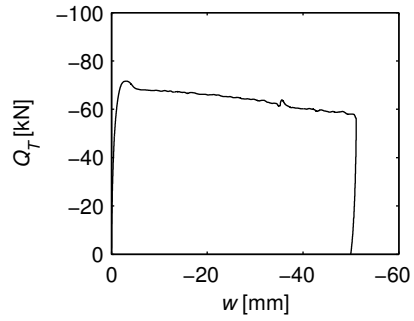


Figure E.55: Measured force versus measured pile displacement.

F.10 T10S35

Installation and soil preparation:

- The pile was installed prior to the soil preparation procedure to avoid installation effects.

Test:

- The suction level dropped at the end of the test, however, this did not have any affect on the initial load–displacement curve or on the use of the results in the analyses.

Observations after tests:

- The water was sucked out of the sand box when stabilizing the suction level.

F.10.1 CPT results

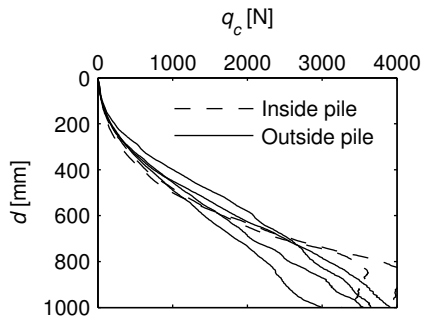


Figure F.56: CPT cone resistance in N.

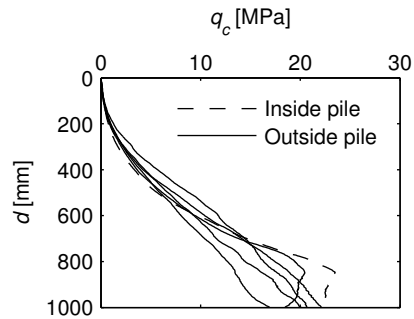


Figure F.57: CPT cone resistance in MPa.

Table F.13: Soil properties determined from CPT results.

Friction angle	φ	53.6°
Dilation angle	ψ	19.3°
Relative density	D_r	84.8%

F.10.2 Test results

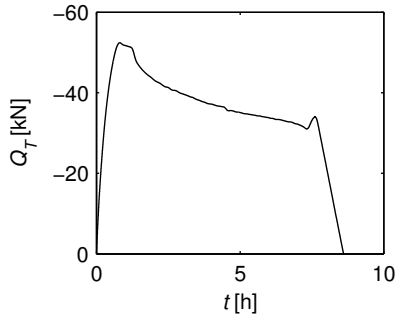


Figure E.58: Measured force versus time.

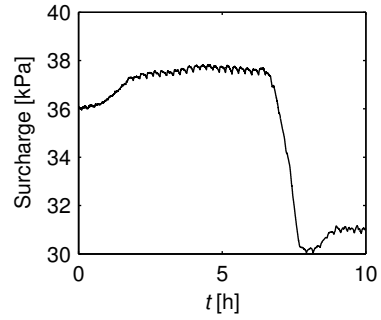


Figure E.59: Suction applied to the sand box versus time.

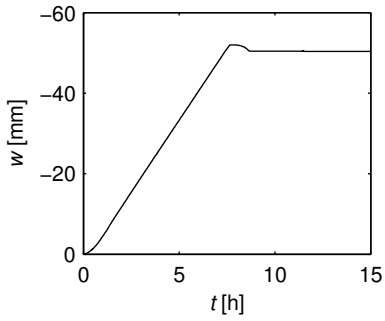


Figure E.60: Measured pile displacement versus time.

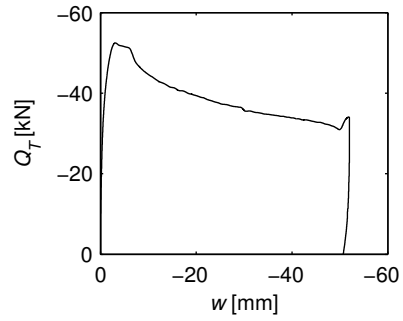


Figure E.61: Measured force versus measured pile displacement.

Appendix G

Cyclic Test Results

This appendix shows the results of the ten conducted static tests. Table G.1 gives the specifications of the CPTs and the tests, while Table G.2 gives the chosen test program and the maximum force, $Q_{\max \text{ static}}$, applied during the test. Table G.3 shows the average values of the soil properties found for each test based on the conducted CPTs.

Table G.1: Specifications of the CPTs and the static tests.

CPT specifications		
Penetration rate	5	mm/s
Cone area	$1.767 \cdot 10^{-4}$	m ²
Test specifications		
Loading frequency (cyclic part)	0.1	Hz
Displacement rate (static part)	0.002	mm/s
Sample rate	2	Hz

The test results for the cyclic test have been altered in order to use them in the analyses. The resulting load was recorded both in the program MooG Test Suite and in Catman 6.0 located at separate computers. No attention was paid to the fact that the time on the two computers differed. Thus, even though the sample rate was 2 Hz in both recordings, the sampling did not take place at the exact same time, resulting in wrong recordings of the load in Catman 6.0 during the cyclic loading. MooG Test Suite did not record the pile head displacement, hence it was necessary to alter the load recordings from Catman 6.0 to get simultaneous recordings of the applied load and the pile head displacement (Figure G.1. Like for the static tests, the curve of the post-cyclic static loading was interrupted by electrical noise, and the curves are smoothed. Figure G.2 shows the definition of the cyclic unloading stiffness, k_{un} , reloading stiffness, k_{re} , and hysteresis found for each test.

Table G.2: Test program for the cyclic tests, the resulting number of cycles and the maximum force applied in the post-cyclic static tests.

Test	$Q_{\text{mean}}/$ $Q_{\text{max static}}$ [-]	$Q_{\text{cyclic}}/$ $Q_{\text{max static}}$ [-]	Q_{mean} [kN]	Q_{cyclic} [kN]	Surcharge [kPa]	N [-]	Post-cyclic $Q_{\text{max,pc}}$ [kN]
T11C0	0.4	0.4	4.84	4.84	0	177	-
T12C70	0.4	0.4	30.12	30.12	69.0–75.0	17280	101.5
T13C0	0.4	0.2	4.84	2.42	0	17280	12.4
T14C35	0.4	0.4	21.66	21.66	34.3–36.5	17280	57.2
T15C35	0.4	0.2	21.66	10.83	33.8–35.0	17280	64.8
T16C70	0.4	0.2	30.12	15.06	70.7–71.3	17280	104.3
T17C0	0.4	0.2	4.84	2.42	0	17280	13.7
T18C70	0.6	0.4	45.18	30.12	70.7–72.5	5230	-
T19C70	0.6	0.2	45.18	15.06	69.7–71.2	17280	101.6
T20C70	0.8	0.2	60.24	15.06	69.9–70.3	17280	87.6
T21C70	0.8	0.3	60.24	22.59	68.5–70.3	554	-

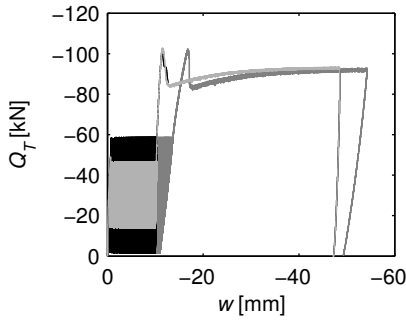
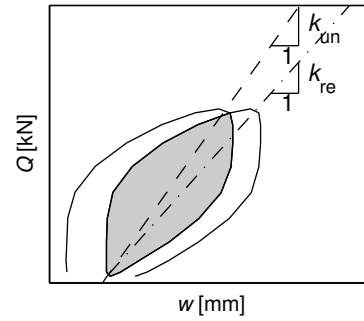

Figure G.1: Altering the load recorded in Catman 6.0. (Light gray: Catman-data. Dark gray: MOOG-data. Black: Altered Catman-data.)

Figure G.2: Definition of cyclic unloading stiffness, k_{un} , reloading stiffness, k_{re} , and hysteresis (gray area between curves).

Table G.3: Soil properties determined from the CPTs conducted before each cyclic test.

Test	φ	ψ	γ	D_r
11	53.8	19.4	10.3	85.6
12	54.2	20.0	10.4	88.4
13	53.5	19.1	10.3	83.7
14	53.4	19.0	10.3	83.3
15	53.4	19.0	10.3	83.5
16	53.5	19.1	10.3	83.8
17	52.9	18.3	10.2	79.4
18	53.0	18.4	10.2	80.3
19	52.9	18.4	10.2	80.0
20	52.2	17.5	10.1	75.4
21	53.2	18.7	10.2	81.8

G.1 T11C0

Installation and soil preparation:

- The pile was installed prior to the soil preparation procedure to avoid installation effects.
- The pore pressure transducers were saturated as described for test T5S70.

Test:

- The pile was pulled out before the test finished.

Observations after tests:

- No comments.

G.1.1 CPT results

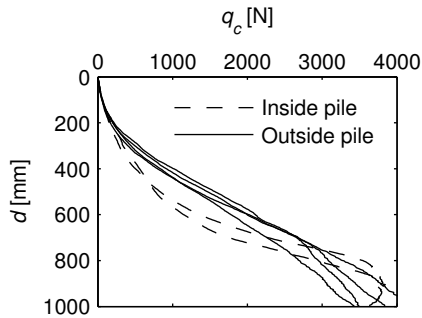


Figure G.3: CPT cone resistance in N.

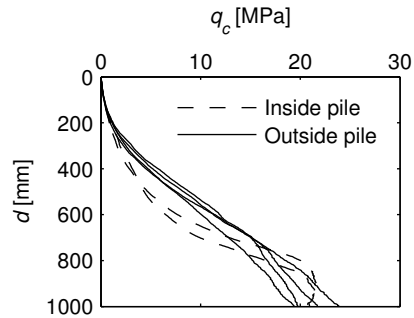


Figure G.4: CPT cone resistance in MPa.

Table G.4: Soil properties determined from CPT results.

Friction angle	φ	53.8°
Dilation angle	ψ	19.4°
Relative density	D_r	85.6%

G.1.2 Test results

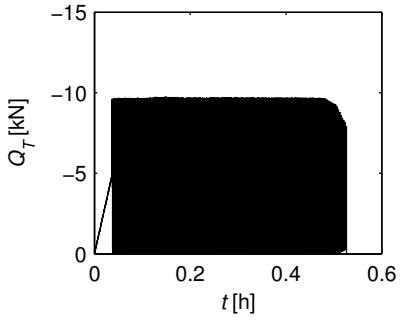


Figure G.5: Measured force versus time.

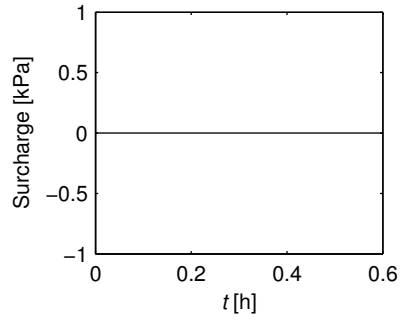


Figure G.6: Suction applied to the sand box versus time.

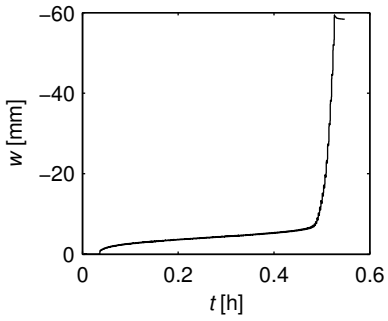


Figure G.7: Measured pile displacement versus time.

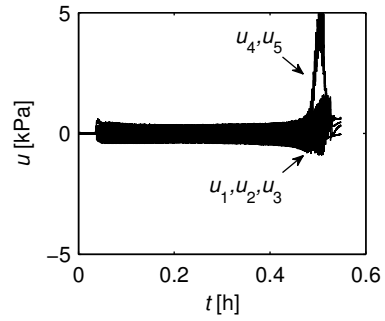


Figure G.8: Pore pressure measurements versus time.

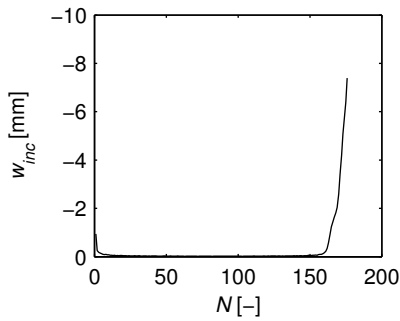


Figure G.9: Incremental pile displacement versus Number of cycles.

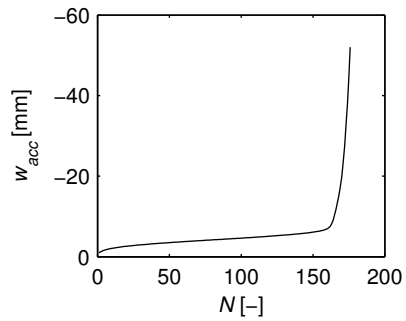


Figure G.10: Accumulated pile displacement versus Number of cycles.

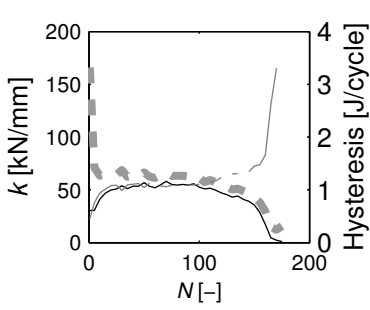


Figure G.11: Unloading stiffness, k_{un} , (dashed gray line), reloading stiffness, k_{re} , (solid black line), and hysteresis (solid gray line).

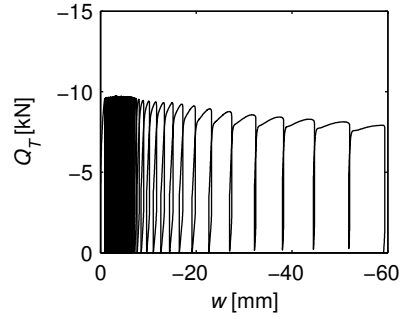


Figure G.12: Measured force versus measured pile displacement.

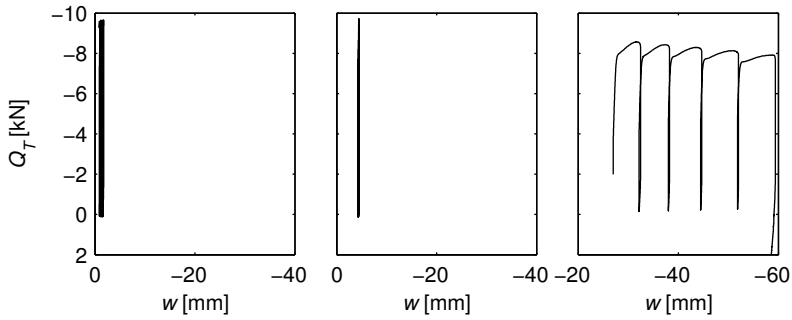


Figure G.13: Load cycles in the beginning, middle and end of the cyclic part of the test.

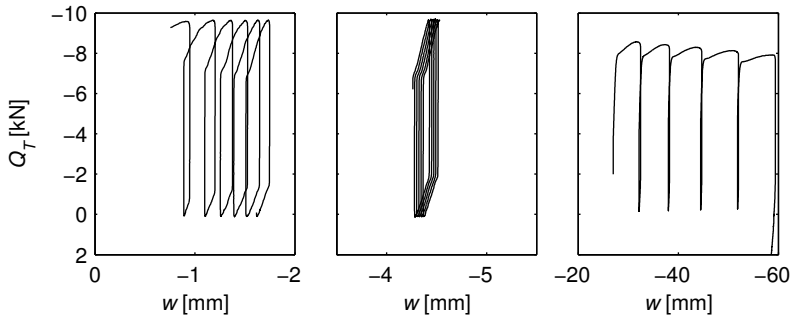


Figure G.14: Load cycles in the beginning, middle and end of the cyclic part of the test.

G.2 T12C70

Installation and soil preparation:

- The pile was installed prior to the soil preparation procedure to avoid installation effects.
- The CPT device bend during the CPTs and had to be straightened up prior to each penetration. It showed quiet high cone resistance but due to the defect, the results may not be trustworthy.

Test:

- The suction increased from 69 kPa to 75 kPa during the test.
- The test was assumed to be unstable or meta-stable however, it showed to be stable.

Observations after tests:

- The pile plugged during the test. The soil surface inside the pile was raised approximately 4.5 cm compared to the outside soil surface.
- The water was sucked out of the sand box.

G.2.1 CPT results

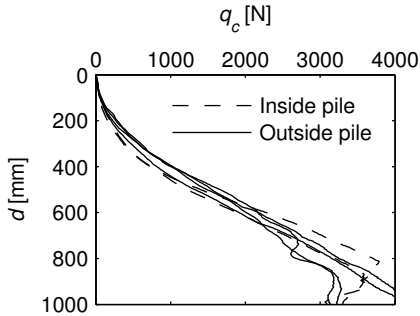


Figure G.15: CPT cone resistance in N.

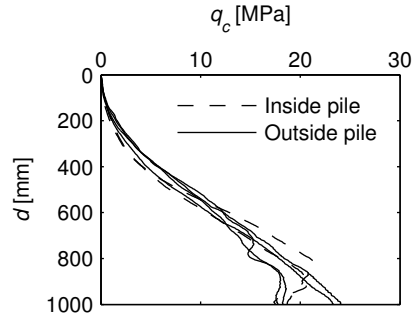


Figure G.16: CPT cone resistance in MPa.

Table G.5: Soil properties determined from CPT results.

Friction angle	φ	54.2°
Dilation angle	ψ	20.0°
Relative density	D_r	88.4%

G.2.2 Test results

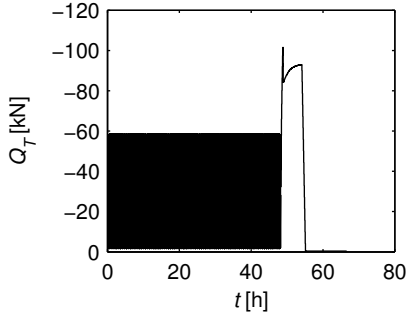


Figure G.17: Measured force versus time.

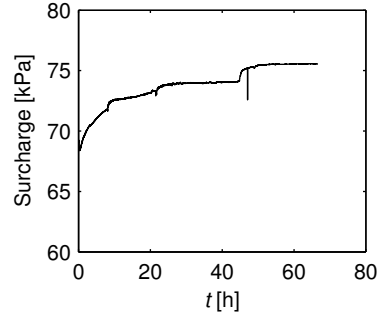


Figure G.18: Suction applied to the sand box versus time.

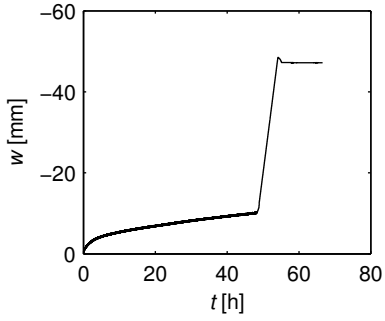


Figure G.19: Measured pile displacement versus time.

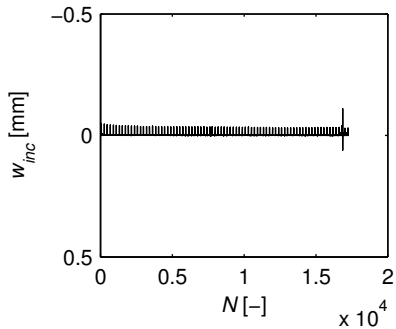


Figure G.20: Incremental pile displacement versus Number of cycles.

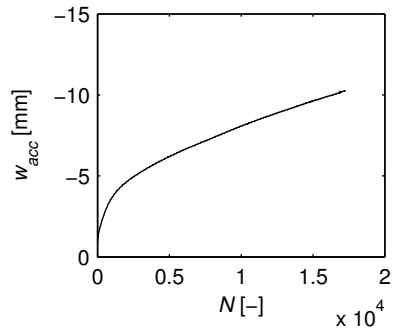


Figure G.21: Accumulated pile displacement versus Number of cycles.

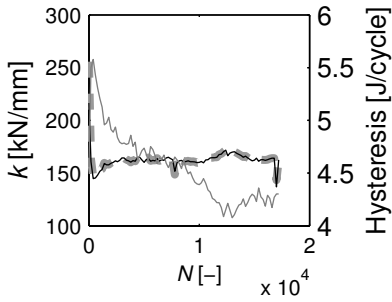


Figure G.22: Unloading stiffness, k_{un} , (dashed gray line), reloading stiffness, k_{re} , (solid black line), and hysteresis (solid gray line).

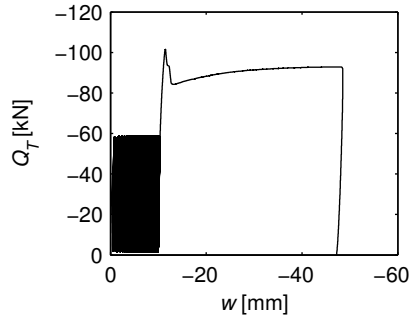


Figure G.23: Measured force versus measured pile displacement.

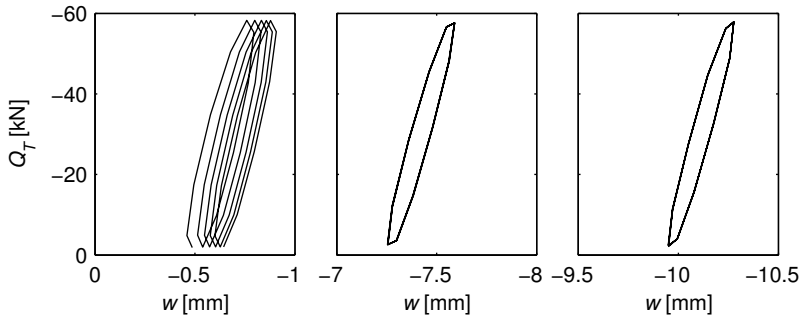


Figure G.24: Load cycles in the beginning, middle and end of the cyclic part of the test.

G.3 T13C0

Installation and soil preparation:

- The pile was installed prior to the soil preparation procedure to avoid installation effects.
- After test T12C70, the pile was uninstalled prior to re-saturation of the sand to observe how the sand was stuck to the pile. This caused a large amount of disturbance of the sand near the pile. Prior to Test T13C0, the sand in the middle of the sand box was, therefore, vibrated before the pile installation to ensure a homogeneous compaction of the sand. However, the CPTs conducted after installation and vibration showed that the cone resistance near the pile was considerably lower than in previous tests. The vibration procedure should have been conducted prior to the test but, unfortunately, the vibrator broke and it was decided to continue the test after all.

Test:

- Test ran without problems.

Observations after tests:

- No comments.

G.3.1 CPT results

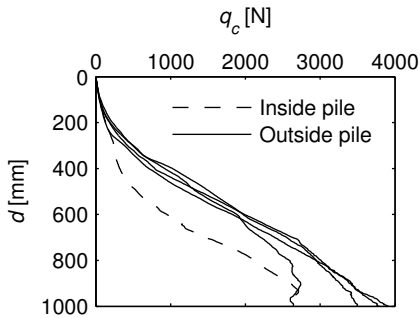


Figure G.25: CPT cone resistance in N.

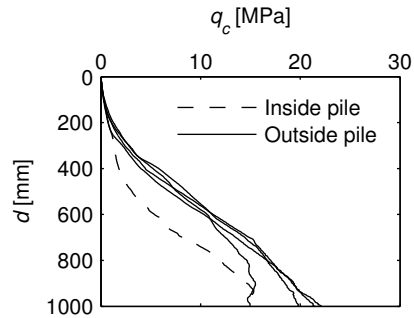


Figure G.26: CPT cone resistance in MPa.

Table G.6: Soil properties determined from CPT results.

Friction angle	φ	53.5°
Dilation angle	ψ	19.1°
Relative density	D_r	83.7%

G.3.2 Test results

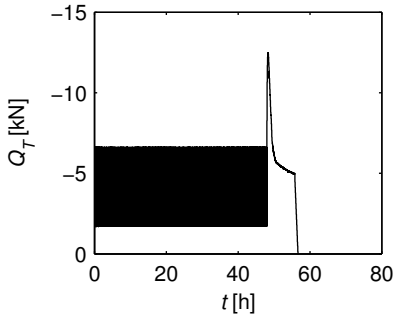


Figure G.27: Measured force versus time.

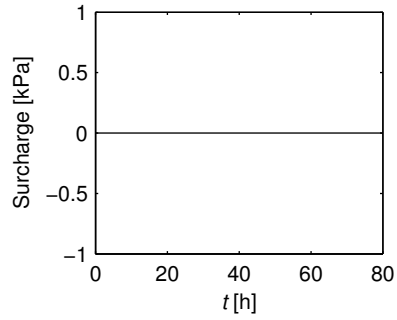


Figure G.28: Suction applied to the sand box versus time.

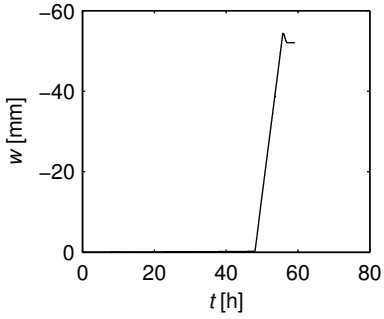


Figure G.29: Measured pile displacement versus time.

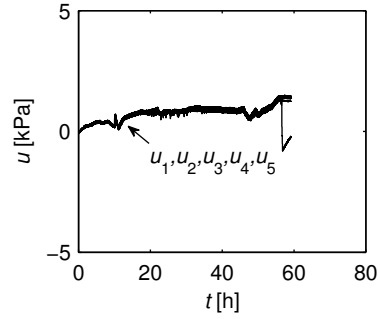


Figure G.30: Pore pressure measurements versus time.

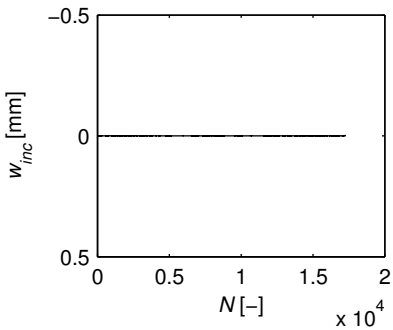


Figure G.31: Incremental pile displacement versus Number of cycles.

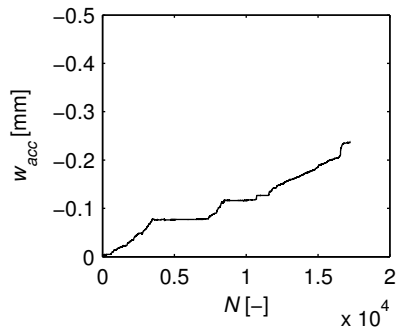


Figure G.32: Accumulated pile displacement versus Number of cycles.

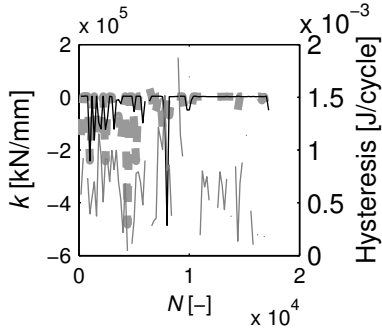


Figure G.33: Unloading stiffness, k_{un} , (dashed gray line), reloading stiffness, k_{re} , (solid black line), and hysteresis (solid gray line).

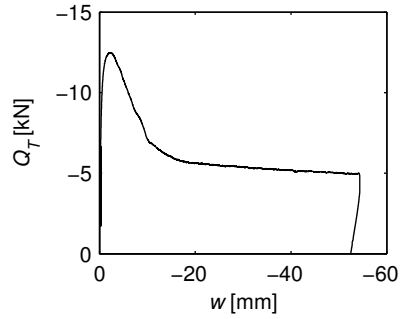


Figure G.34: Measured force versus measured pile displacement.

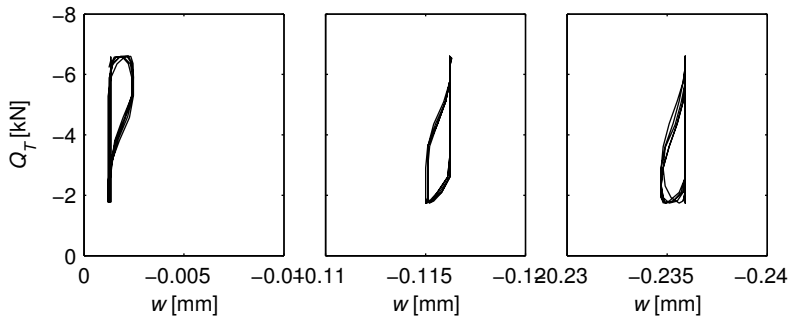


Figure G.35: Load cycles in the beginning, middle and end of the cyclic part of the test.

G.4 T14C0

Installation and soil preparation:

- The pile was installed prior to the soil preparation procedure to avoid installation effects.
- The CPTs inside the pile showed very high cone resistances.

Test:

- The load sequence was not computed correctly in MOOG instead of cyclic loads of 0–43 kN, cycles of -2–39 kN was applied. Thus the test was stopped after 1 h to correct this. The soil was not re-vibrated prior the new load sequence.
- The test was assumed to be unstable or meta-stable however, it showed to be stable.

Observations after tests:

- The pile plugged during the test. The soil surface inside the pile was raised approximately 2 cm compared to the outside soil surface.
- The water was sucked out of the sand box.

G.4.1 CPT results

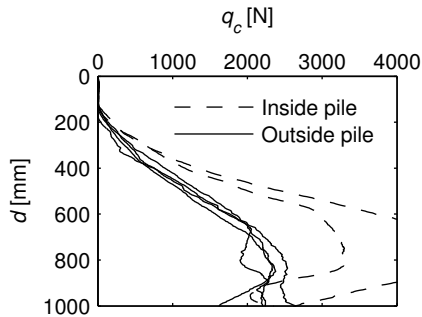


Figure G.36: CPT cone resistance in N.

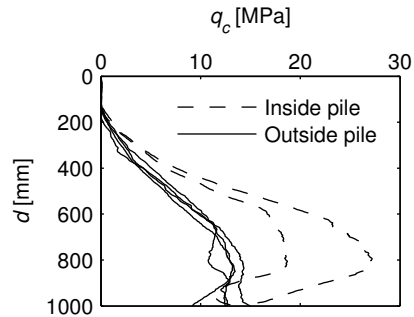


Figure G.37: CPT cone resistance in MPa.

Table G.7: Soil properties determined from CPT results.

Friction angle	φ	53.4°
Dilation angle	ψ	19.0°
Relative density	D_r	83.3%

G.4.2 Test results

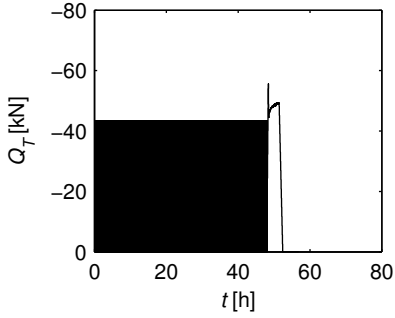


Figure G.38: Measured force versus time.

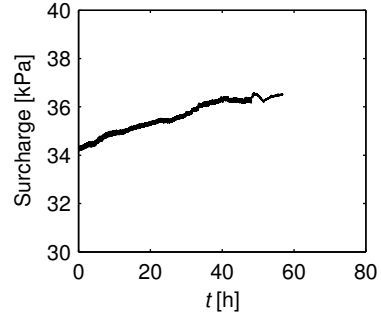


Figure G.39: Suction applied to the sand box versus time.

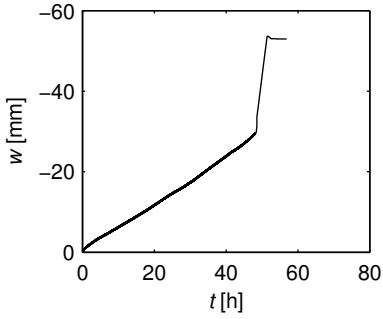


Figure G.40: Measured pile displacement versus time.

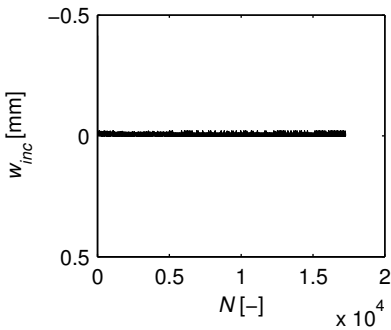


Figure G.41: Incremental pile displacement versus Number of cycles.

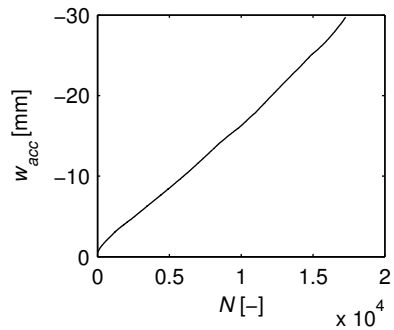


Figure G.42: Accumulated pile displacement versus Number of cycles.

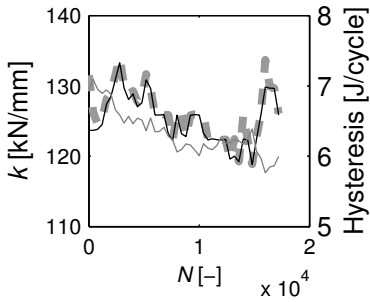


Figure G.43: Unloading stiffness, k_{un} , (dashed gray line), reloading stiffness, k_{re} , (solid black line), and hysteresis (solid gray line).

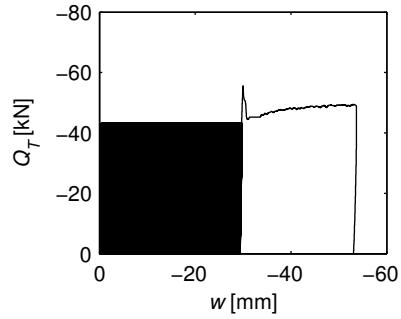


Figure G.44: Measured force versus measured pile displacement.

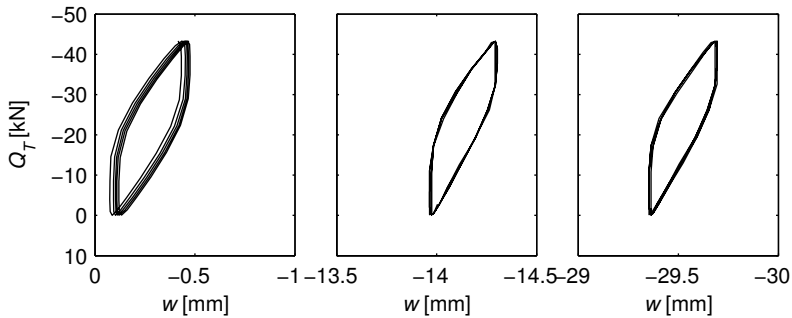


Figure G.45: Load cycles in the beginning, middle and end of the cyclic part of the test.

G.5 T15C35

Installation and soil preparation:

- The pile was installed prior to the soil preparation procedure to avoid installation effects.

Test:

- The test ran without problems.

Observations after tests:

- No plugging observed.
- The water was sucked out of the sand box.

G.5.1 CPT results

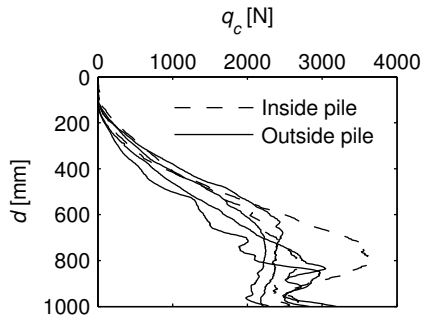


Figure G.46: CPT cone resistance in N.

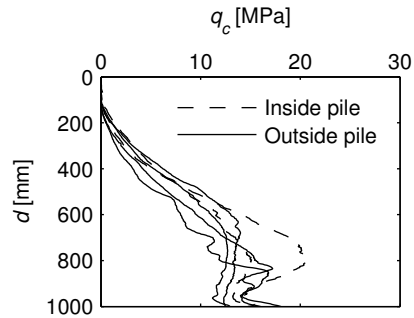


Figure G.47: CPT cone resistance in MPa.

Table G.8: Soil properties determined from CPT results.

Friction angle	φ	53.4°
Dilation angle	ψ	19.0°
Relative density	D_r	83.5%

G.5.2 Test results

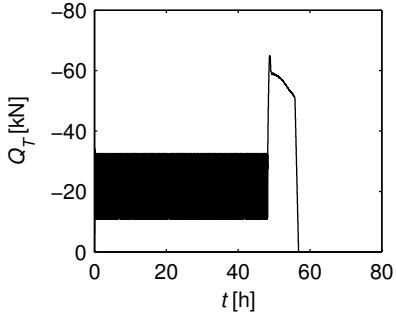


Figure G.48: Measured force versus time.

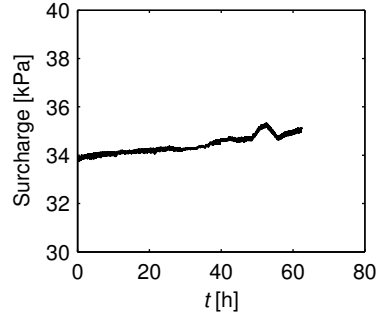


Figure G.49: Suction applied to the sand box versus time.

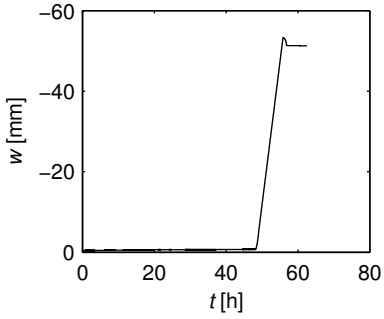


Figure G.50: Measured pile displacement versus time.

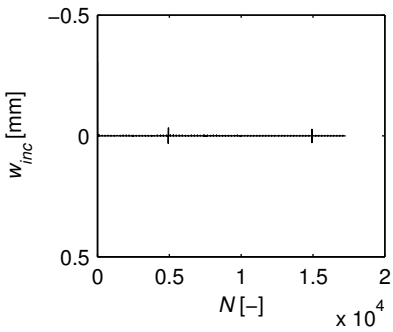


Figure G.51: Incremental pile displacement versus Number of cycles.

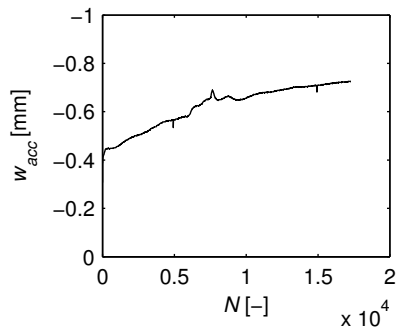


Figure G.52: Accumulated pile displacement versus Number of cycles.

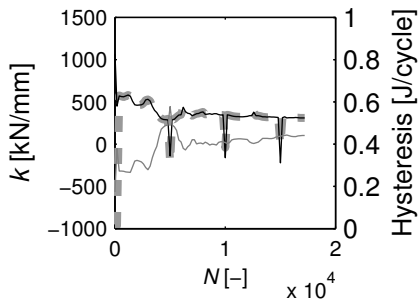


Figure G.53: Unloading stiffness, k_{un} , (dashed gray line), reloading stiffness, k_{re} , (solid black line), and hysteresis (solid gray line).

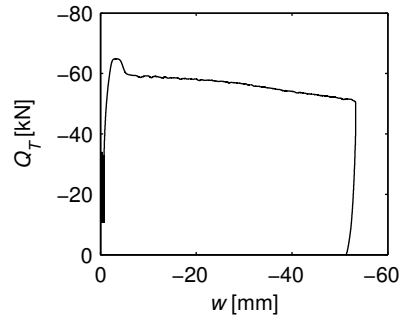


Figure G.54: Measured force versus measured pile displacement.

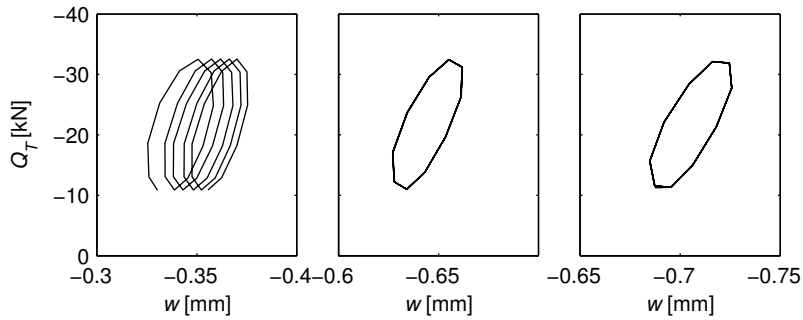


Figure G.55: Load cycles in the beginning, middle and end of the cyclic part of the test.

G.6 T16C70

Installation and soil preparation:

- The pile was installed prior to the soil preparation procedure to avoid installation effects.

Test:

- The test ran without problems.
- The first twelve hours of the test was not recorded in Catman 6.0.

Observations after tests:

- Pile plugging observed ca. 4 cm.
- The water was sucked out of the sand box.

G.6.1 CPT results

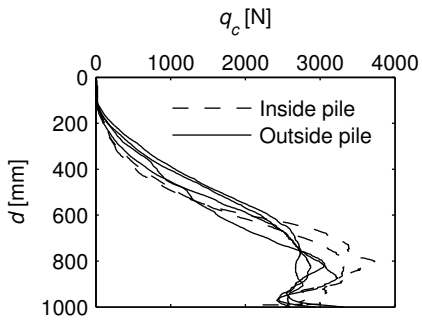


Figure G.56: CPT cone resistance in N.

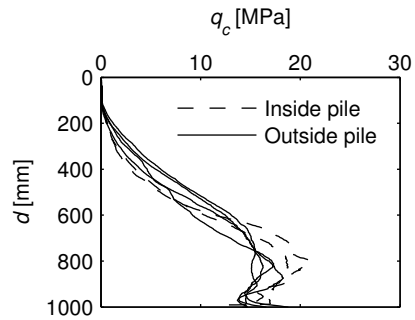


Figure G.57: CPT cone resistance in MPa.

Table G.9: Soil properties determined from CPT results.

Friction angle	φ	53.5°
Dilation angle	ψ	19.1°
Relative density	D_r	83.8%

G.6.2 Test results

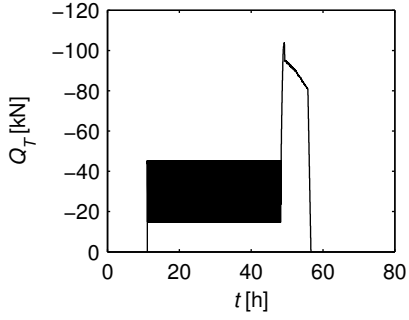


Figure G.58: Measured force versus time.

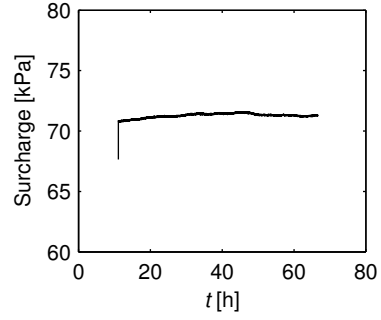


Figure G.59: Suction applied to the sand box versus time.

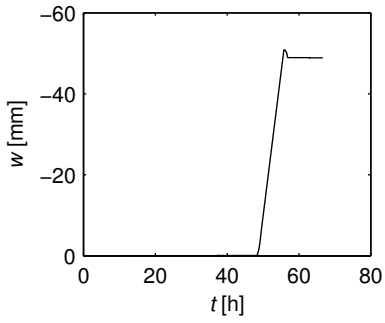


Figure G.60: Measured pile displacement versus time.

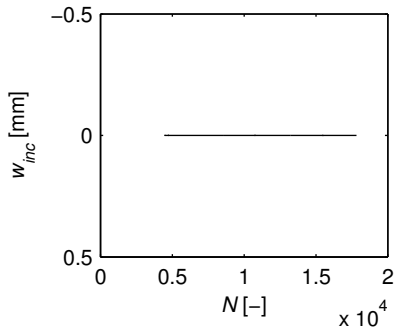


Figure G.61: Incremental pile displacement versus Number of cycles.

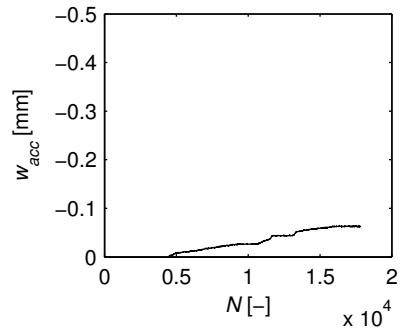


Figure G.62: Accumulated pile displacement versus Number of cycles.

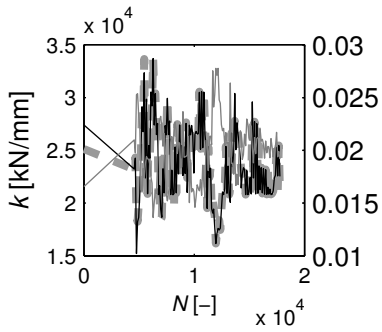


Figure G.63: Unloading stiffness, k_{un} , (dashed gray line), reloading stiffness, k_{re} , (solid black line), and hysteresis (solid gray line).

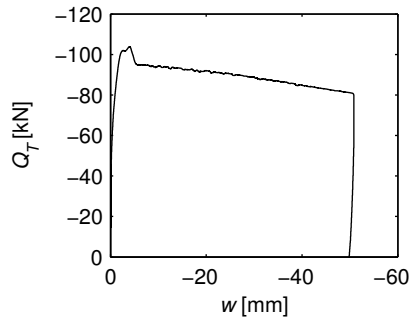


Figure G.64: Measured force versus measured pile displacement.

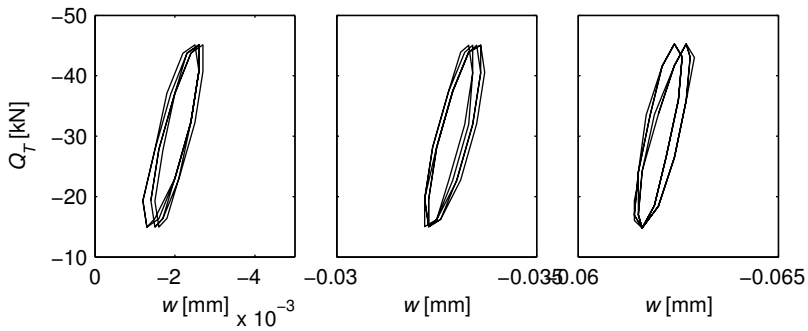


Figure G.65: Load cycles in the beginning, middle and end of the cyclic part of the test.

G.7 T17C0

Installation and soil preparation:

- The pile was installed prior to the soil preparation procedure to avoid installation effects.

Test:

- When the test had been running for eleven hours, the MOOG Test Suite interface froze, however, the hydraulics went on. To ensure that the correct load sequence was applied, the test was stopped by pressing the emergency button. This resulted in a drop in load from 2 kN to -2 kN. Afterwards the load was slowly increased to 0 kN and the test restarted from the point where it was stopped.

Observations after tests:

- No comments.

G.7.1 CPT results

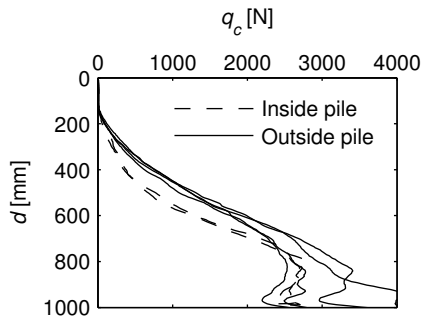


Figure G.66: CPT cone resistance in N.

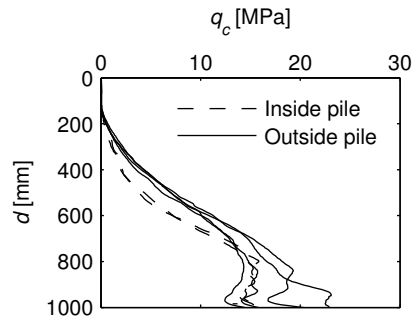


Figure G.67: CPT cone resistance in MPa.

Table G.10: Soil properties determined from CPT results.

Friction angle	φ	52.9°
Dilation angle	ψ	18.3°
Relative density	D_r	79.4%

G.7.2 Test results

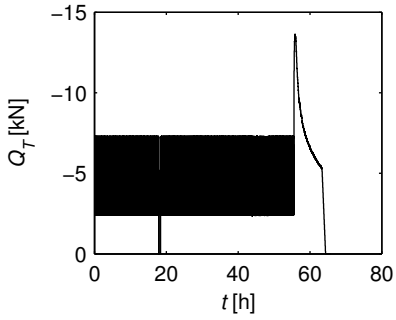


Figure G.68: Measured force versus time.

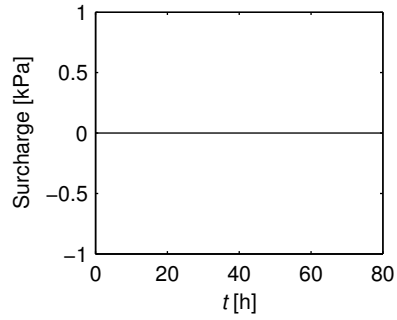


Figure G.69: Suction applied to the sand box versus time.

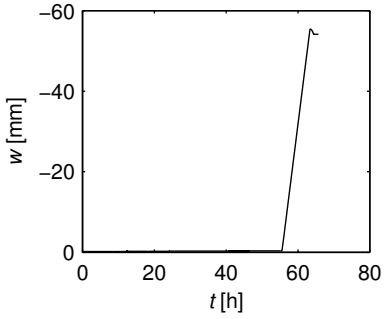


Figure G.70: Measured pile displacement versus time.

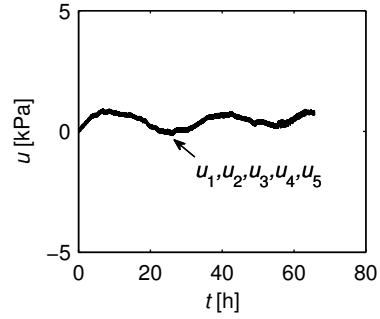


Figure G.71: Pore pressure measurements versus time.

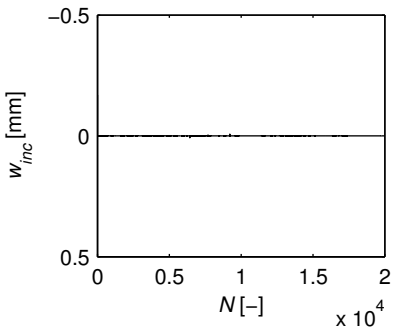


Figure G.72: Incremental pile displacement versus Number of cycles.

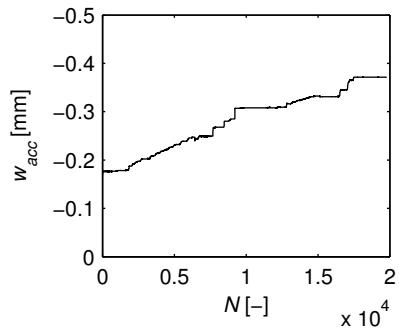


Figure G.73: Accumulated pile displacement versus Number of cycles.

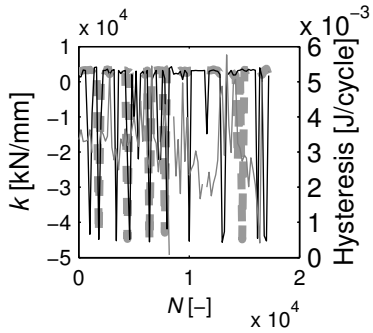


Figure G.74: Unloading stiffness, k_{un} , (dashed gray line), reloading stiffness, k_{re} , (solid black line), and hysteresis (solid gray line).

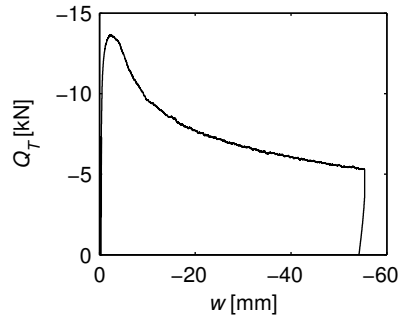


Figure G.75: Measured force versus measured pile displacement.

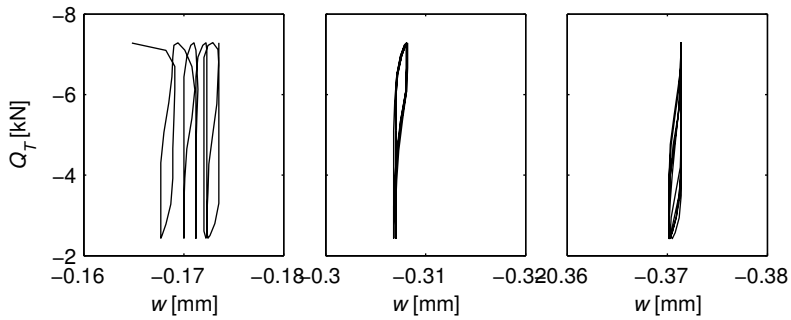


Figure G.76: Load cycles in the beginning, middle and end of the cyclic part of the test.

G.8 T18C70

Installation and soil preparation:

- The pile was installed prior to the soil preparation procedure to avoid installation effects.

Test:

- The maximum allowed displacement (60 mm) was reached before the cyclic loading sequence had ended.

Observations after tests:

- Pile plugging (4 cm).
- The water was sucked out of the sand box.

G.8.1 CPT results

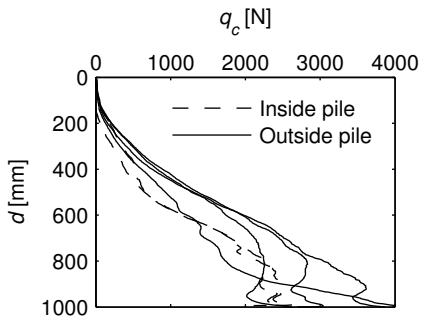


Figure G.77: CPT cone resistance in N.

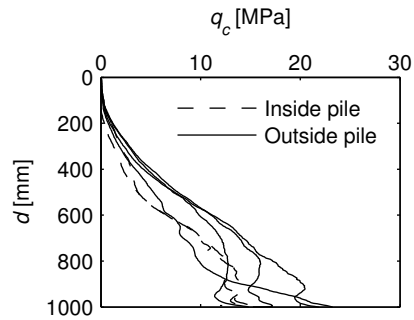


Figure G.78: CPT cone resistance in MPa.

Table G.11: Soil properties determined from CPT results.

Friction angle	φ	53.0°
Dilation angle	ψ	18.4°
Relative density	D_r	80.3%

G.8.2 Test results

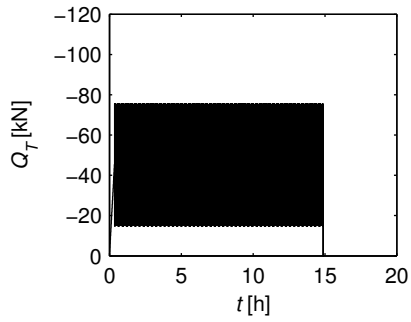


Figure G.79: Measured force versus time.

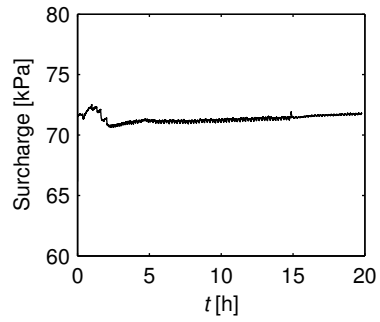


Figure G.80: Suction applied to the sand box versus time.

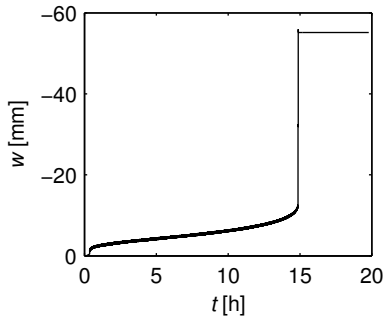


Figure G.81: Measured pile displacement versus time.

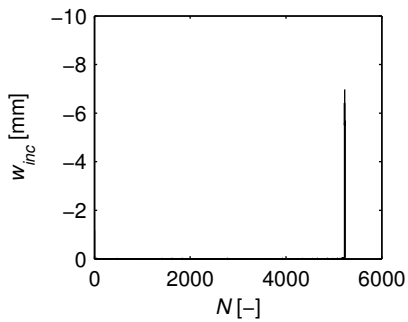


Figure G.82: Incremental pile displacement versus Number of cycles.

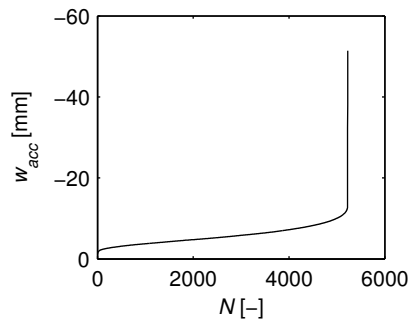


Figure G.83: Accumulated pile displacement versus Number of cycles.

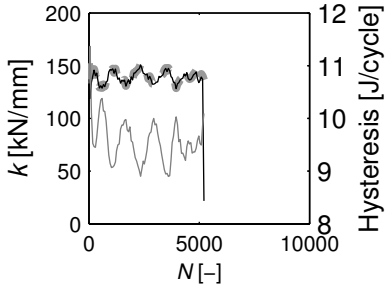


Figure G.84: Unloading stiffness, k_{un} , (dashed gray line), reloading stiffness, k_{re} , (solid black line), and hysteresis (solid gray line).

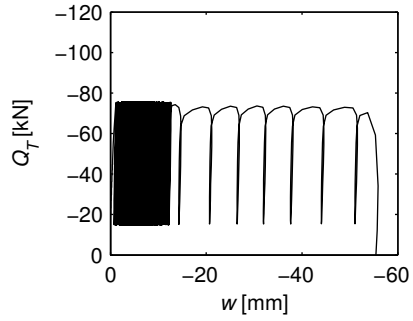


Figure G.85: Measured force versus measured pile displacement.

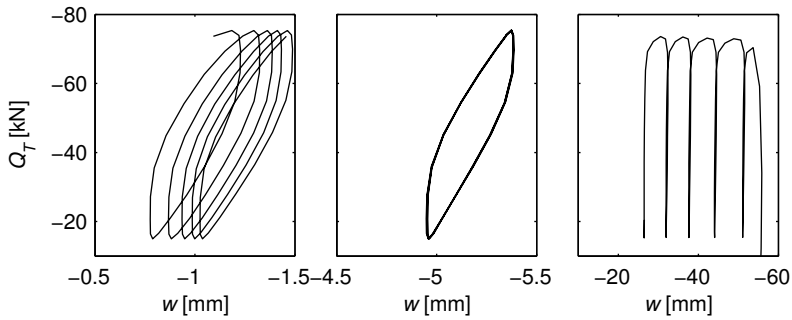


Figure G.86: Load cycles in the beginning, middle and end of the cyclic part of the test.

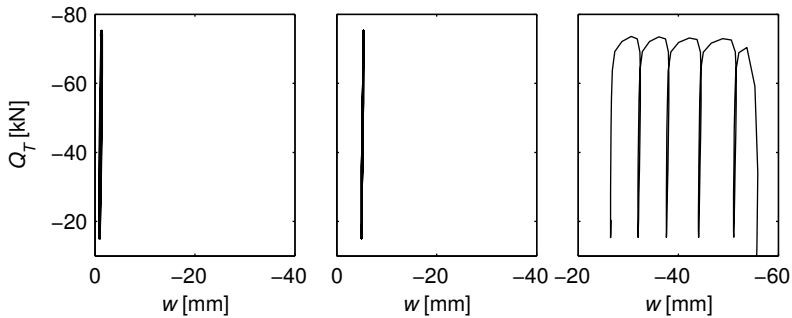


Figure G.87: Load cycles in the beginning, middle and end of the cyclic part of the test.

G.9 T19C70

Installation and soil preparation:

- The pile was installed prior to the soil preparation procedure to avoid installation effects.

Test:

- The ran without problems.

Observations after tests:

- Pile plugging.
- The water was sucked out of the sand box.

G.9.1 CPT results

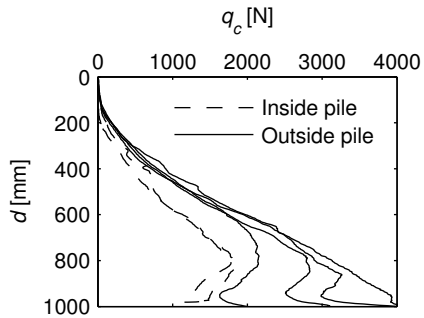


Figure G.88: CPT cone resistance in N.

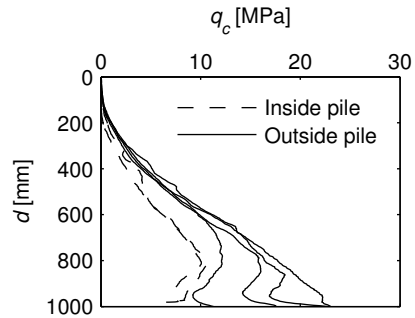


Figure G.89: CPT cone resistance in MPa.

Table G.12: Soil properties determined from CPT results.

Friction angle	φ	52.9°
Dilation angle	ψ	18.4°
Relative density	D_r	80.0%

G.9.2 Test results

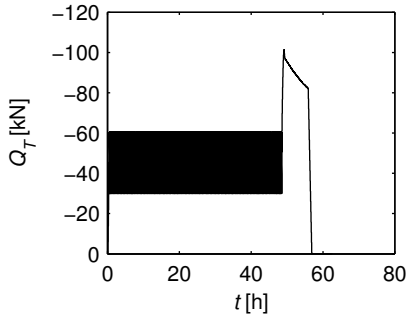


Figure G.90: Measured force versus time.

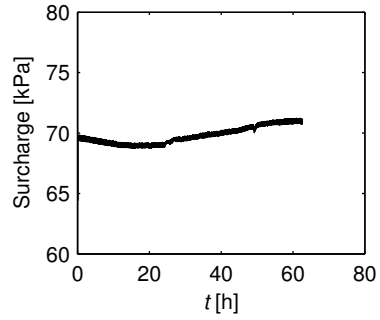


Figure G.91: Suction applied to the sand box versus time.

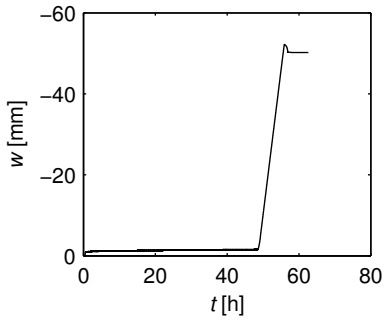


Figure G.92: Measured pile displacement versus time.

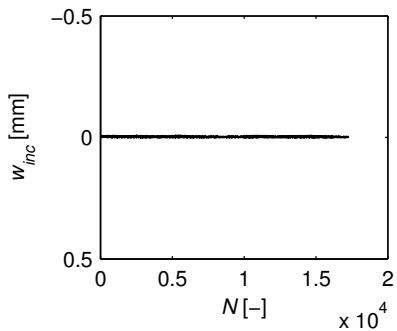


Figure G.93: Incremental pile displacement versus Number of cycles.

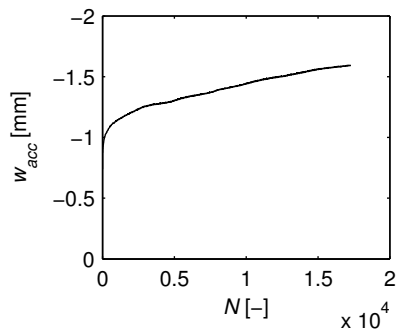


Figure G.94: Accumulated pile displacement versus Number of cycles.

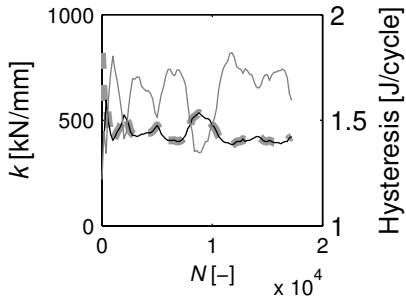


Figure G.95: Unloading stiffness, k_{un} , (dashed gray line), reloading stiffness, k_{re} , (solid black line), and hysteresis (solid gray line).

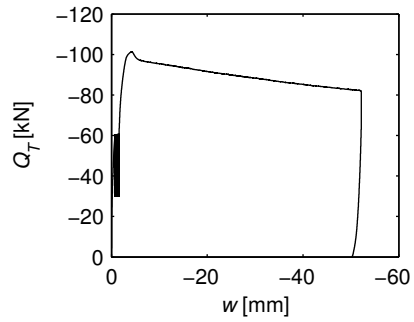


Figure G.96: Measured force versus measured pile displacement.

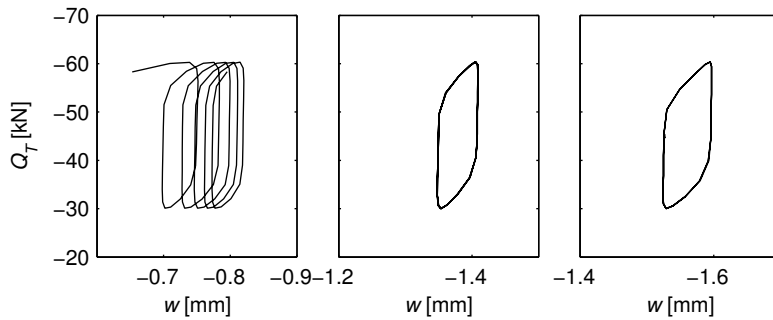


Figure G.97: Load cycles in the beginning, middle and end of the cyclic part of the test.

G.10 T20C70

Installation and soil preparation:

- The pile was installed prior to the soil preparation procedure to avoid installation effects.

Test:

- The ran without problems.

Observations after tests:

- The water was sucked out of the sand box.

G.10.1 CPT results

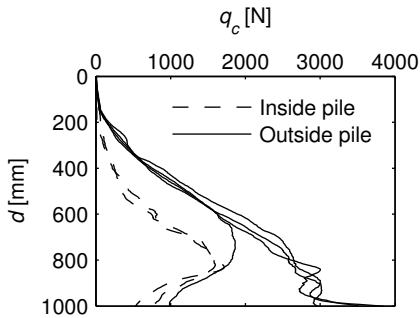


Figure G.98: CPT cone resistance in N.

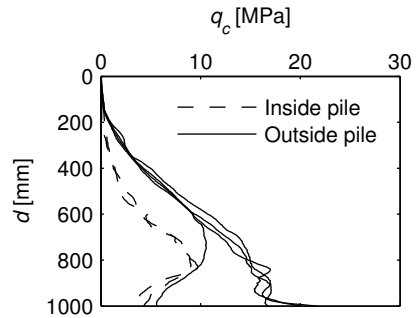


Figure G.99: CPT cone resistance in MPa.

Table G.13: Soil properties determined from CPT results.

Friction angle	φ	52.2°
Dilation angle	ψ	17.5°
Relative density	D_r	75.4%

G.10.2 Test results

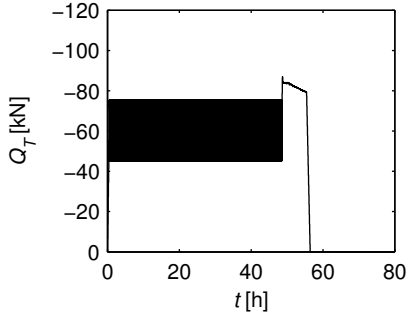


Figure G.100: Measured force versus time.

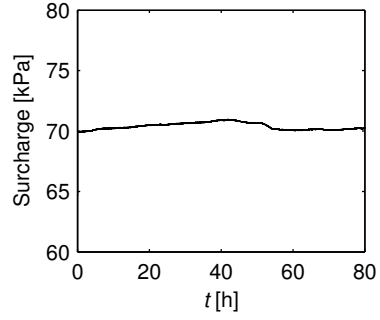


Figure G.101: Suction applied to the sand box versus time.

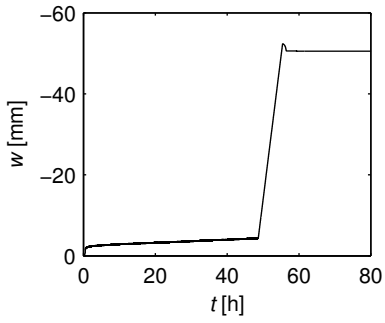


Figure G.102: Measured pile displacement versus time.

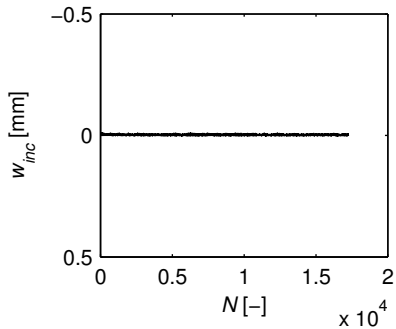


Figure G.103: Incremental pile displacement versus Number of cycles.

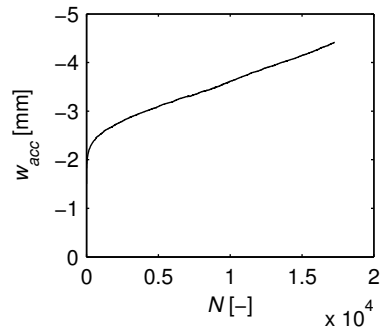


Figure G.104: Accumulated pile displacement versus Number of cycles.

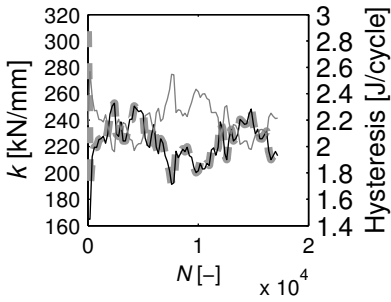


Figure G.105: Unloading stiffness, k_{un} , (dashed gray line), reloading stiffness, k_{re} , (solid black line), and hysteresis (solid gray line).

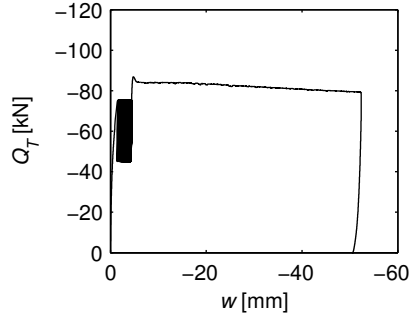


Figure G.106: Measured force versus measured pile displacement.

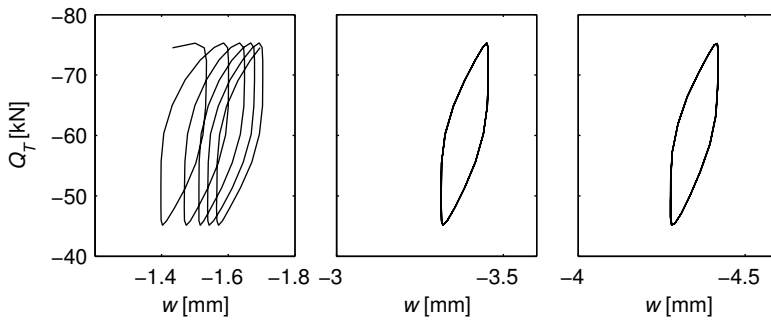


Figure G.107: Load cycles in the beginning, middle and end of the cyclic part of the test.

G.11 T21C70

Installation and soil preparation:

- The pile was installed prior to the soil preparation procedure to avoid installation effects.

Test:

- The maximum allowed displacement was reached before the cyclic load sequence ended.

Observations after tests:

- Pile plugging (1 cm).
- The water was sucked out of the sand box.

G.11.1 CPT results

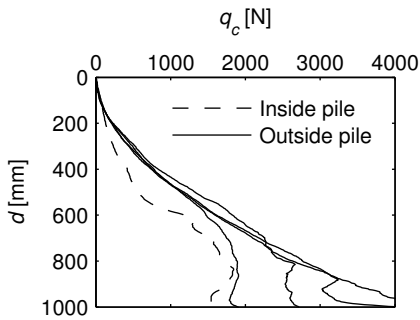


Figure G.108: CPT cone resistance in N.

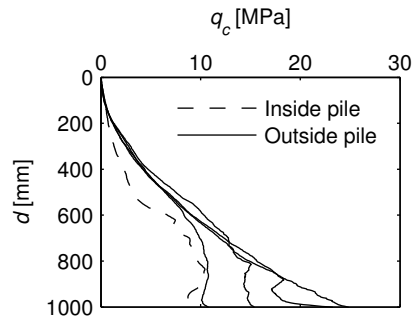


Figure G.109: CPT cone resistance in MPa.

Table G.14: Soil properties determined from CPT results.

Friction angle	φ	53.2°
Dilation angle	ψ	18.7°
Relative density	D_r	81.8%

G.11.2 Test results

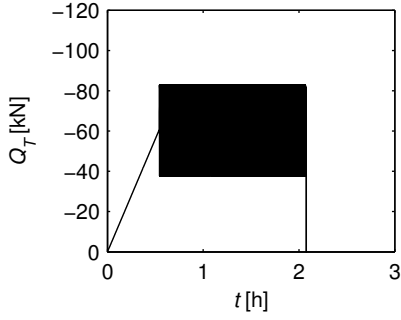


Figure G.110: Measured force versus time.

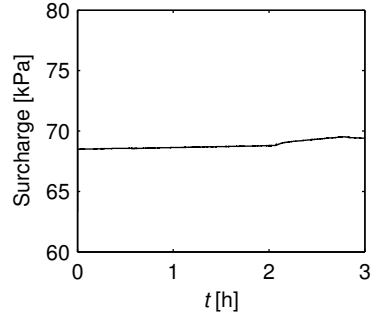


Figure G.111: Suction applied to the sand box versus time.

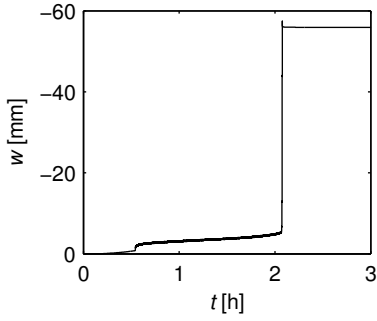


Figure G.112: Measured pile displacement versus time.

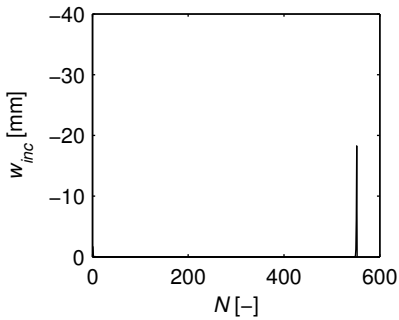


Figure G.113: Incremental pile displacement versus Number of cycles.

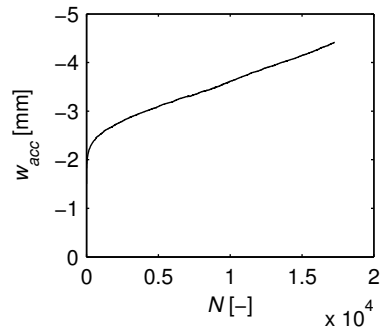


Figure G.114: Accumulated pile displacement versus Number of cycles.

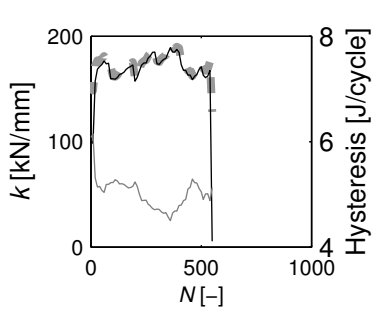


Figure G.115: Unloading stiffness, k_{un} , (dashed gray line), reloading stiffness, k_{re} , (solid black line), and hysteresis (solid gray line).

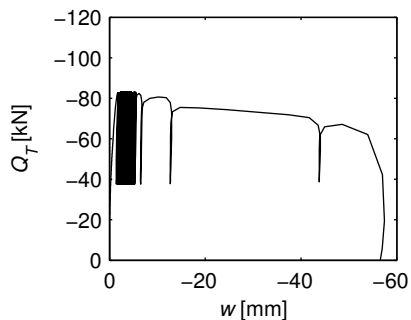


Figure G.116: Measured force versus measured pile displacement.

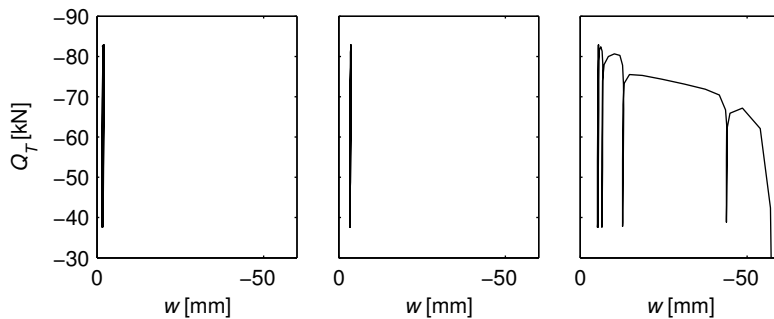


Figure G.117: Load cycles in the beginning, middle and end of the cyclic part of the test.

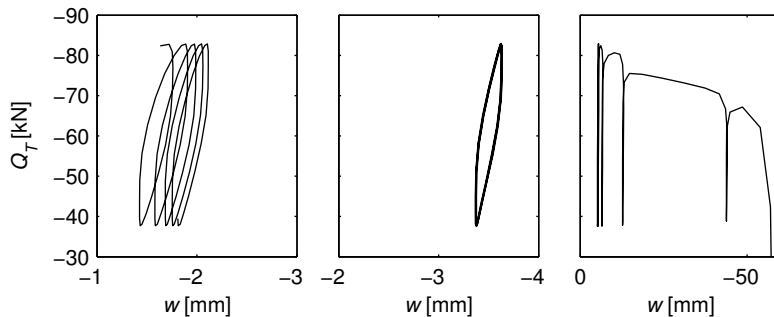


Figure G.118: Load cycles in the beginning, middle and end of the cyclic part of the test.

SUMMARY

The present thesis regards the behavior of the piles in jacket pile foundations used for offshore wind turbines. The piles are often loaded in tension because of the combination of wind and wave conditions and the low self-weight of the wind turbine. The repeated cyclic loading can lead to accumulated upwards displacement of the piles and, thus, undesired deflection of the wind turbine structure.

This study concerns the effect of cyclic loading on a pile installed in dense sand and loaded in tension. A new laboratory test setup was constructed to make these pile load tests. The thesis discusses the advantages and disadvantages of the test setup. The results of cyclic loading tests showed that the loading conditions are very important for the behavior of piles. Some wind and wave conditions can be beneficial and increase the pile capacity while other conditions can be damaging and reduce the pile capacity and result in large permanent displacement of the piles. Hence, it is vital to account for the cyclic load conditions at the site of an offshore wind farm when designing the wind turbines.